Techno-Economic Analysis of the Carbon Dioxide Capture Process in Pre-Combustion Applications

by

Husain E. Ashkanani

B.S. in Chemical Engineering, Kuwait University, 2014

M.S. in Chemical Engineering, University of Florida, 2016

Submitted to the Graduate Faculty of the

Swanson School of Engineering in partial fulfillment

of the requirements for the degree of

Doctor of Philosophy

University of Pittsburgh

2021

UNIVERSITY OF PITTSBURGH

SWANSON SCHOOL OF ENGINEERING

This dissertation was presented

by

Husain E. Ashkanani

It was defended on

July 19, 2021

and approved by

George E. Klinzing, PhD, Professor Emeritus, Department of Chemical and Petroleum
Engineering

Hseen O. Baled, PhD, Assistant Professor, Department of Chemical and Petroleum Engineering

Joaquin Rodriguez Alonso, PhD, Assistant Professor, Department of Chemical and Petroleum
Engineering

Nicholas S. Siefert, PhD, Research Mechanical Engineer, U.S. Department of Energy, NETL

Omar M. Basha, PhD, Senior Process Engineer, Anellotech Inc.

Dissertation Director: Badie I. Morsi, PhD, Professor, Department of Chemical and Petroleum
Engineering

Techno-Economic Analysis of the Carbon Dioxide Capture Process in Pre-Combustion Applications

Husain E. Ashkanani, PhD

University of Pittsburgh, 2021

Aspen Plus v.8.8 was used to perform techno-economic analysis (TEA) of the CO_2 capture process in pre-combustion applications. The capital expenditure (CAPEX), operating expenditure (OPEX), and levelized cost of CO_2 captured (LCOC) were calculated to assess the feasibility of the process. 35 physical solvents (11 ionic liquids, 5 hydrocarbons, 7 oxygenated-hydrocarbons, 2 nitrogenized-hydrocarbons, 5 cyclic-hydrocarbons, 3 polymers, and 2 subcooled) were used for CO_2 capture from actual shifted fuel gas at 54.1 bar in 543 MW power plant. The CO_2 capture process included a countercurrent packed-bed absorber containing random or structured packing, followed by three flash drums for solvent regeneration, and multi-stage compressors for CO_2 sequestration. The key process constraints were 90% CO_2 capture from the shifted gas and less than 0.5 mol% fuel gas and maximum 600 ppm water in the CO_2 sequestration stream. The PC-SAFT Equation-of-State was used to model the solvent density and VLE of the gas-liquid systems used, while other physico-chemical properties were acquired from experimental data, literature, and Aspen Plus database.

Aspen Plus calculated results indicated that (1) structured packing, Mellapak 250Y, of large specific surface area improved gas-liquid mass transfer, which lowered LCOC; (2) operating at low temperatures increased CO_2 solubility and decreased solvent loss, which lowered LCOC; (3) volatile solvents exhibited significant solvent loss; (4) ionic liquids with negligible vapor pressure have high viscosity and would be suitable for warm/hot temperature CO_2 capture; (5) the

CAPEX and OPEX decreased with decreasing plant power capacity, however, LCOC increased due to the small mass of CO_2 captured; and (6) among the 35 solvents used, diethyl sebacate provided the lowest LCOC at $7.14 per ton CO_2 captured.

An artificial neural network (ANN) was developed using the Aspen Plus calculated CAPEX, OPEX, and LCOC of the CO_2 capture process. 320 randomly selected cases were used for training and 481 cases were used for testing the ANN. The input to the ANN included plant power capacity, operating temperature, solvent properties, and packing specific surface area. The ANN was able to predict the calculated CAPEX, OPEX, and LCOC with high coefficient of determination (R^2) of 0.9961, 0.9994, 0.9995, respectively.

Table of Contents

List of Tables

List of Figures

Nomenclature

a	Specific surface area, m^2/m^3
$AARE$	Absolute average relative error
a_w	Specific wetted area, m^2/m^3
b	Bias
C	Concentration, mol/m^3
C^*	Equilibrium concentration, mol/m^3
$CAPEX$	Capital expenditure, $
$CAPEX_{solv}$	Solvent cost, $/L
C_D	Drag coefficient
$CEPI$	Chemical engineering plant cost index
COP	Coefficient of performance
c_P	Specific heat capacity, J/kg.K
C_{power}	Cost of electricity, $/MWh
D	Diameter, m
D_{AL}	Diffusivity, m^2/s
d_p	Packing diameter, m
E	Sum of the squared error
f_c	Capacity factor
f_{CR}	Capital recovery factor, $year^{-1}$
f_{mat}	Material factor
F_p	Packing factor, ft^{-1}
f_{pres}	Pressure factor
Fr	Froude number
g	Acceleration due to gravity, m/s^2
H	Height, m
h	Specific enthalpy, J/kg
h_d	Developed head, m
He	Henry's law constant, $mol/m^3.bar$
$h_{H,C}$	Heat transfer coefficient, $W/m^2.K$
h_L	Liquid holdup
i	Annual discount rate, $year^{-1}$
k_B	Boltzmann constant, J/K
k_G	Gas mass transfer coefficient, $mol/m^2.bar.s$

K_G	Overall gas mass transfer coefficient, mol/m^2.bar.s
k_{ij}	Binary interaction parameter
k_L	Liquid mass transfer coefficient, m/s
K_L	Overall liquid mass transfer coefficient, m/s
k_{th}	Thermal conductivity, W/m.K
$LCOC$	Levelized cost of CO_2 captured, \$/ton CO_2
$LMTD$	Log mean temperature difference, K
M	Superficial mass velocity, kg/m^2.s
m	Number of segments
$\dot{m}$	Mass flow rate, kg/s
MWt	Molecular weight, kg/kmol
N	Plant lifetime, year
n	number of moles, mol
N_A	Molar flux, mol/m^2.s
N_{AV}	Avogadro's number
$N_{i,j}$	Node of j of hidden layer i
$OPEX$	Operating expenditure, \$/year
P	Pressure, bar
P^*	Equilibrium pressure, bar
P_c	Critical pressure, bar
P^{vap}	Vapor pressure, Pa
$\dot{Q}$	Heat transferred, W
$Q_{L,G}$	Volumetric flow rate, m^3/s
R	Universal gas constant, J/mol.K
R^2	Coefficient of determination
Re	Reynolds number
S	Corrugartion length, m
Sc	Schmidt's number
Sh	Sherwood number
t	Time, s
T_c	Critical temperature, K
t_e	Exposure time, s
t_w	Wall thickness, m
U	velocity, m/s
U_{HT}	Overall heat transfer coefficient, W/m^2.K
V	Volume, m^3
W	Work, W
w	Weight
x	mole fraction

Z	Compressibility factor

Greek Letters

μ	Dynamic viscosity, Pa.s
α	Damping coefficient
β	Damping coefficient
γ	Minimum number of parameters
ε	Void fraction
ϵ	Segment energy, J
ϵ^{AB}	Association energy, J
η	Efficiency
κ^{AB}	Association volume
ν	Kinematic viscosity, m^2/s
ξ	Rate of surface renewal, s^{-1}
ρ	Density, kg/m^3
σ	Segment diameter, Å
σ_L	Surface tension, N/m

Subscripts

amb	ambient
C	Cold
G	Gas
H	Hot
in	Inlet
L	Liquid
max	maximum
min	minimum
norm	Normalized
out	Outlet

Ionic Liquids

[aPy]	Allyl-pyridinium
[BF_4]	tetrafluoroborate
[bmim]	1-Butyl-3-methylimidazolium
[bmPyr]	1-Butyl-1-methylpyrrolidinium
[$(C_2F_5)_3PF_3$]	tris(pentafluoroethyl) trifluorophosphate
[emim]	1-Ethyl-3-methylimidazolium
[hmim]	1-Hexyl-3-methylimidazolium

[MeSO$_4$]	methylsulfate
[omim]	1-Octyl-3-methylimidazolium
[PF$_6$]	hexafluorophosphate
[Tf$_2$N]	bis(trifluorosulfonyl)imide

Acronyms

AGR	Acid gas removal
AMP	2-Amino-2-methyl-propanol
ANN	Artificial neural network
ASU	Air separation unit
CycHC	Cyclic-hydrocarbon
DEA	Diethanolamine
DES	Diethyl sebacate
DMF	n,n-Dimethyl formamide
EOS	Equation of state
EPA	Environmental Protection Agency
GPDC	Generalized Pressure Drop Correlation
HC	Hydrocarbon
HP	High pressure
IGCC	Integrated Gasification combined cycle
IL	Ionic liquids
IMTP	Intalox metal tower packing
LP	Low pressure
LRST	Leidos Research Support Team
MEA	Monoethanolamine
ML	Machine learning
MNPh	1-methylnaphthalene
MP	Medium pressure
NAM	n-Acetyl-morpholine
NBAc	n-Butyl acetate
NETL	National Energy Technology Laboratory
NFM	n-Formyl-morpholine
NHC	Nitrogenized-hydrocarbon
NMP	n-Methyl-2-pyrrolidone
NPAc	n-Propyl acetate
OHC	Oxygenated-hydrocarbon
PC	Propylene carbonate
PCC	Pulverized coal combustion
PC-SAFT	Perturbed Chain Statistical Association Fluid Theory
PEGDME	Polyethylene glycol dimethyl ether

PEGPDMS	Polyethylene glycol polydimethylsiloxane
PN	Propionitrile
TBP	Tributyl phosphate
TEA	Techno-economic analysis
THF	Tetrahydrofuran
VLE	Vapor-liquid equilibria
WGS	Water-gas-shift

Acknowledgement

I would like to express my utmost gratitude to Dr. Badie I. Morsi for being an inspiring mentor and guiding me throughout my progress. I would also like to thank Dr. George E. Klinzing, Dr. Hseen O. Baled, Dr. Joaquin Rodriguez Alonso, Dr. Nicholas S. Siefert, and Dr. Omar M. Basha for serving at my committee and for providing helpful comments and suggestions.

In addition, I would like to particularly thank Dr. Omar M. Basha for helping me get through my initial year at the Reactor and Process Engineering Laboratory and Pittsburgh and I would like to thank Mr. Rui Wang for enriching my work with our discussions and I would like to acknowledge Mr. Jacob Goodwin for his assistance in completing some of the simulations conducted in this dissertation.

I would like to thank Kuwait University for their financial support throughout my studies. Also, I would like to thank the National Energy Technology Laboratory (NETL) for supporting this research and providing constructive comments and key data for some of the solvents used.

Finally, I would like to thank my parents, siblings, wife, and sons for providing the emotional support throughout my progress towards my completion of this dissertation.

Disclaimer

1.0 Introduction

In 2019, the global CO_2 emission reached 34.2 Gtons with China emitting 9.83 Gtons, followed by the USA 4.96 Gtons [1]. Figure 1.1 shows the top ten countries, which have the highest CO_2 emission totaling more than two thirds of the worldwide emissions.
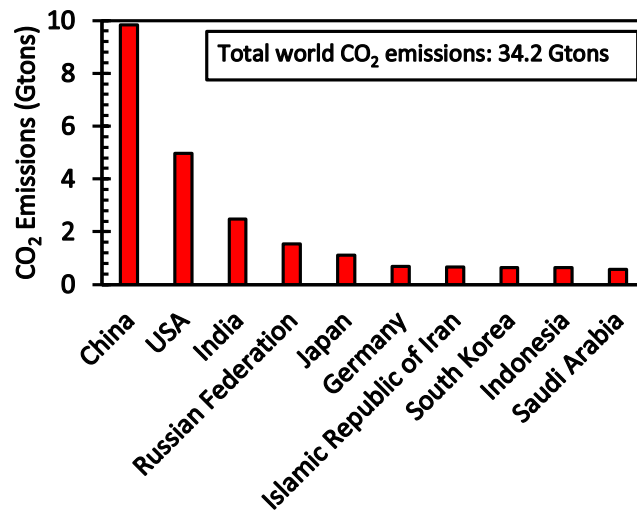
Figure 1.1. Top ten countries in terms of highest CO_2 emissions in 2019 [1]

According to the EPA, the highest source of CO_2 emissions in the USA was from transportation followed by power plants [2]. Coal, which produces the most CO_2 among fossil fuels [3], is used to generate electricity in three different venues: (1) pulverized coal combustion (PCC), (2) integrated gasification combined cycle (IGCC) and (3) Oxy-combustion [4]. In PCC, coal is combusted to flue gas in a boiler to generate high-pressure steam, which is sent to a turbine to produce electricity. The concentration of CO_2 in the flue gas at atmospheric pressure varies typically between 10 and 14 vol% [5]. In an IGCC, solid carbonaceous feedstocks (coal, biomass, municipal solid waste, plastics, heavy residue, etc.) are gasified with steam and air (or oxygen) to

produce fuel gas, which is used for generating electricity and/or for the production of clean transportation fuels and high-value chemicals [6, 7]. If oxygen is used in the IGCC plant, an expensive air separation unit (ASU) is required. Raw syngas often contains solid particulates and its H_2 to CO ratio (H_2/CO) is low. To increase the H_2/CO ratio in the syngas, the solid particulates are first removed, and the syngas is then shifted in a conventional or sour water-gas-shift (WGS) reactor [8]. In the shift reactor, CO reacts with steam to produce H_2 and CO_2, increasing their concentrations in the shifted gas [9]. The concentration of CO_2 in the fuel gas is typically between 15 and 50 vol% [10] at higher pressures up to 70 bar [5]. Also, the temperatures of the fuel gas is up to 520 °C depending on the steam/CO ratio of the shift reactor [8]. Typically, the shifted gas is cooled and H_2S is removed and sent to Claus plants before sending it to the CO_2 capture facility. The IGCC is considered more advantageous than PCC due to the following: (1) IGCC has a higher thermal efficiency, (2) the release of solid by-products and waste is lower, (3) the emissions of NO_x, SO_x and trace pollutants such as mercury (Hg) are lower, and (4) the CO_2 capture is more efficient because the CO_2 concentration in the fuel gas is much greater than that in the flue gas.

In oxy-combustion, coal is combusted in high-purity oxygen (up to 97%) instead of air to produce flue gas containing highly concentrated CO_2 since air is not used in the process [4]. The steam is condensed and separated from the flue gas and the remaining CO_2 could be sent to sequestration sites. However, this process is expensive due to the need for an ASU and other technical difficulties associated with separating incondensable gases [4]. Typically, CO_2 can be removed from flue gas streams using chemical methods and from fuel gas steams using physical methods.

1.1 Chemical Methods

Chemical methods involve using a reactive solvent, such as monoethanolamine (MEA), diethanolamine (DEA), triethanolamine, and 2-amino-2-methyl-1-propanol (AMP), to chemically react with CO_2 from post-combustion flue gas streams. The overall reaction with MEA can be represented as follows [11]:

$$CO_2 + 2HOCH_2CH_2NH_2 \rightleftharpoons HOCH_2CH_2NH_3^+ + HOCH_2CH_2NHCO_2^- \qquad (1.1)$$
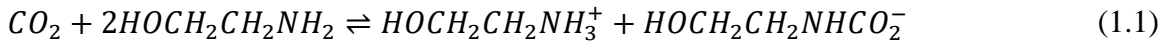
This reaction is reversible, which means that the solvent can be regenerated by forcing the backward reaction to take place. Increasing the temperature will achieve this objective as it will dissociate the carbamates back to MEA and CO_2 [12].

Other solvents used for CO_2 chemical absorption include aqueous-ammonia, potassium carbonate, and sodium glycinate [13-15]. The advantages of using aqua-ammonia to capture CO_2 are (1) ammonia does not corrode the process units, (2) there is no degradation due to the O_2 present in the flue gas [16], and (3) useful products can be obtained, such as ammonium sulfate (gypsum) and ammonium nitrate, a fertilizer [13]. The drawback of this process, however, is related to the loss of ammonia in the flue gas due to its volatility [17, 18]. This led Kozak *et al.* [19] to propose and build a chilled ammonia pilot-plant capable of capturing 15,000 ton of CO_2 per year. Potassium carbonate has been used as a solvent for CO_2 capture in the Benfield process [20], which has been studied and modeled by other authors [21-23]. The overall reaction of the process is as follows [24, 25]:

$$CO_2 + H_2O + K_2CO_3 \rightarrow 2KHCO_3 \qquad (1.2)$$
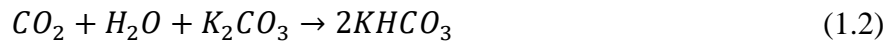
Sodium glycinate, which is the product of glycine amino acid reaction with sodium hydroxide salt, has been extensively studied as a potential chemical solvent for CO_2 capture [14, 15, 26-34]. The amino acid forms a zwitterion by transferring the hydrogen ion from the carboxylic

acid group to the amine group. In 2019, Wang *et al*. [15] developed a model for CO_2 capture using sodium glycinate as the chemical solvent. The model predictions were validated using CO_2-AMP experimental data by Tontiwachwuthikul *et al.* [35].

1.2 Physical Methods

Unlike chemical methods, physical methods employ solvents with high affinity and capacity to absorb CO_2 from fuel gas streams without any chemical reactions. Some processes and their corresponding physical solvents are given in Table 1.1 and some commercial plants are summarized in Table 1.2. In general, physical solvents have similar features for acid gas removal (AGR), including (1) higher H_2S and COS selectivity when compared to that of CO_2, (2) high loading when the acid gas partial pressure is high, (3) they are chemically and thermally stable, and (4) their heat of solution is low. This means that heating the solvent is not required to regenerate the solvent, whereas decreasing system pressure is sufficient [36, 37]. A physical process with high H_2S over CO_2 selectivity can be configured into two-stages, where H_2S is captured in the first stage and then CO_2 is captured in the second stage [38, 39].

When the partial pressure of CO_2 in the fuel gas streams is high, physical solvents become more favorable than chemical methods due to the increased concentration difference between the CO_2 in the gas-phase and its mole fraction in the solvent, which is the driving force. This is why physical absorption is more favorable in pre-combustion applications such as in an IGCC power plant because the fuel gas exits the WGS reactor at a high pressure.

Table 1.1. Conventional physical solvents used in AGR processes[22, 40]

Solvent (Major Component) Manufacturer	Operating Requirements	Comments
Rectisol (Chilled Methanol) Linde AG/Lurge AG	• Refrigeration required. • High vapor pressure. • Water washing of effluent streams to prevent high solvent losses.	• Exhibits higher selectivity for H_2S over CO_2.
Selexol (Dimethylether of polyethyleneglycol) Norton/Dow/UOP	• Exhibits a high CO_2 solubility among physical solvents. • Operates at temperature range 0 to 40 ºC.	• Higher viscosity than most physical solvents, particularly at low temperatures, resulting in low mass transfer and high packing requirements.
Sepasolv-MPE (Mixture of polyethylene glycol dialkyl ethers) BASF	• Similar in performance and operation to Selexol process.	• No longer licensed.
Fluor Solvent (Propylene carbonate) Fluor	• Has been in use since the late 1950s. • A higher vapor pressure than Selexol, although solvent losses are still low.	• Not recommended if more than trace levels of H_2S are present. • Reacts irreversibly with water. • Unstable at high temperatures (> 65 °C).
Purisol (n-Methyl-2-pyrrolidone (NMP)) Lurgi GmbH	• Water washing of treated and rejected acid gas required for solvent recovery. • Higher vapor pressure than Selexol and Fluor solvent and therefore operates at ambient temperatures or below.	• Exhibit higher selectivity for H_2S over CO_2.
Morphysorb (n-Formyl-morpholine (NFM) and n-Acetyl-morpholine (NAM)). ThyssenKrupp	• Specialty solvent first used industrially in 2002. • It was developed for its high selectivity of acid gases over heavier hydrocarbons.	

Table 1.2: Commercial plants in the USA [41]

Name	Year started	Solvent used
Terrell	1972	Fluor solvent
Shute Creek	1986	Selexol
Great Plains	2000	Rectisol
Century	2010	Selexol
Lost Cabin	2013	Selexol
Coffeyville	2013	Selexol

The most commonly used physical solvents are Selexol and Rectisol. Selexol is a mixture of dimethylether polyethyleneglycol and Rectisol is a chilled methanol. The properties of the two solvents are listed in Table 1.3. As can be seen Selexol is approximately ten times more viscous

than methanol at 298 K, which makes Selexol less favorable if the two processes were operated at the same temperature. Selexol, however, has a much lower vapor pressure making it a better solvent at 298 K. The solubility indices of some gases in Selexol are shown in Table 1.4; and as can be observed, Selexol is more selective to acid gases (H_2S and CO_2) than other fuel gases, such as H_2 and CO. For a solvent to be economically feasible, it should have the following criteria: (1) low vapor pressure to ensure minimal solvent losses, (2) low viscosity to minimize pumping costs, (3) thermal and chemical stability to avoid its degradation, (4) non-corrosivity to prevent corrosion of the process units, and (5) high selectivity to acid gases compared to fuel gases, such as H_2 and CO. Unfortunately, commercially available solvents could possess some but not all of these criteria.

Table 1.3. Properties of solvents used in the Selexol and Rectisol processes [42]

Process	Selexol	Rectisol
Solvent Name	Dimethylethers of Polyethyleneglycol	Methanol
Formula	$CH_3(CH_2CH_2O)_nCH_3$ $3 \leq n \leq 9$	CH_3OH
MWt (kg/kmol)	280	32.04
Density at 298 K (kg/m^3)	1,030	753
Viscosity at 298 K (Pa.s)	0.0059	0.000539
Melting point (K)	244-251	175.62
Boiling point at 1.013 bar (K)	NA	321.25
c_p at 298 K (J/kg.K)	2090	2498
Thermal conductivity at 298 K (W/m.K)	0.19	0.2011
Vapor pressure at 298 K (Pa)	0.093	16678.4

Table 1.4. Component index solubility in Selexol relative to methane [42]

Component	Component index solubility
CH_4	1.0
H_2	0.2
CO	0.8
CO_2	15
COS	35
H_2S	134
CH_3SH	340
C_6H_6	3,800
H_2O	11,000
HCN	38,000

It should be noted, however, there remain significant problems associated with using physical solvents, such as difficulty in meeting fuel gas specifications and high solvent viscosities. Therefore, ongoing research efforts are focusing on the development of physical solvents with extremely low vapor pressure, high thermal stability, low flammability, low toxicity and high selectivity to CO_2 over H_2.

2.0 Research Objective

The objective of this research is to perform a detailed techno-economic analysis (TEA) using Aspen Plus of the CO_2 capture process in pre-combustion applications using numerous selected physical solvents. More specifically, the capital expenditure (CAPEX), operating expenditure (OPEX) and the levelized cost per ton of CO_2 captured (LCOC) will be obtained for each physical solvent under typical process conditions of an actual IGCC power plant. The overall goal is to screen many physical solvents and design the corresponding proper CO_2 capture process based on the given fuel gas flow rate of the IGCC power plant in order to obtain the most economically feasible process for CO_2 capture. In order to achieve this goal, the following steps are followed:

1. Identify a potential physical solvent for pre-combustion CO_2 capture.

2. Obtain the physico-chemical properties of the solvent and regress and model these properties for Aspen Plus.

3. Obtain the experimental solubilities of the fuel gas species in the solvent and select a proper Equation-of-State (EOS) in Aspen Plus to model these solubility data for vapor-liquid equilibria (VLE) calculations.

4. Design a complete CO_2 capture process with solvent regeneration for the identified solvent.

5. Simulate the complete CO_2 capture process at various, solvent flow rates, operating temperatures, packing type, and power generated.

6. Make sure the constraints imposed on the simulation process in Aspen Plus are met. These constraints include (1) 90% CO_2 captured, (2) no flooding in the

8

countercurrent packed-bed absorber, (3) Height to diameter ratio (H/D) of the absorber is greater than or equal to 6, (4) minimum water concentration level ($\leq$ 600 ppm) in the CO_2 stream destined for sequestration [43], and (5) the sum of fuel gas (CO, H_2 and CH_4) mole fractions in the CO_2 stream destined for sequestration should be less than or equal to 0.5 mol%.

7. Perform a TEA of the CO_2 capture process.

8. Chose another potential solvent and repeat steps 2 through 7.

9. Compare the TEA results and determine which solvent is the most economically feasible for CO_2 capture.

After testing enough solvents, machine learning (ML) is used to develop a model, which will predict the TEA parameters from physico-chemical properties of the solvents, the solubility of CO_2 and fuel gas in the solvent, operating conditions, and the size of the power plant.

3.0 Background

3.1 Theories of Gas Absorption into Liquids

In gas absorption, the gas diffuses through the liquid interface and continues through the liquid film to dissolve into the liquid bulk until equilibrium is reached. At equilibrium, there is no concentration gradient, and the net rate of mass transfer becomes nil. Since there is no gas accumulation at the gas-liquid interface, the rate of mass transfer at both sides of the interface should be equal, and as such the concentration gradient in each phase will adjust so that the aforementioned condition is met [44]. There are many theories for gas absorption into liquids, such as two-film theory, penetration theory and surface renewal theory.

3.1.1 Two-Film Theory

The two-film theory by Whitman in 1924 [45] states that gas mass transfer into a liquid takes place through two films, a gas film and a liquid film, separated by an interface. The gas transfer follows these steps: (1) gas transfer from the gas bulk to the gas-film boundary, (2) gas transfer through the gas-film to the gas-liquid interface, (3) gas transfers through the interface, (4) gas transfer through liquid-film to the liquid-film boundary, and (4) gas transfer from the liquid film boundary into the liquid bulk. These steps are schematically shown in Figure 3.1. The theory assumes the following: (1) the rate of mass transfer between the two phases is controlled by gas diffusion rate, (2) there is no mass transfer resistance at the gas-liquid interface [46], (3) the flow at the gas-liquid interface is laminar, and (4) if any turbulence exists, it would be only outside the

gas-liquid interface [47]. It should be noted that the two-film theory treats the mass transfer process as steady-state and hence the time it takes to form the concentration gradients is small [44].
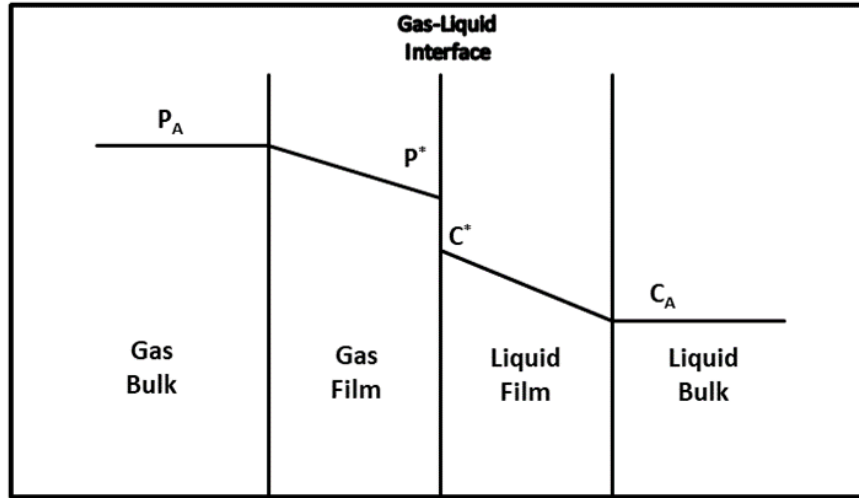
Figure 3.1. Concentration profile of a gas transferring into a liquid

In the two-film theory, the mass flux for equimolar counter-diffusion for the gas and liquid phases is expressed by Equations (3.1) and (3.2) and if the equilibrium relation between the two phases is linear, Henry's Law can be expressed as in Equation (3.3):

$$N_A = k_G(P_{Ab} - P_A^*) \tag{3.1}$$

$$N_A = k_L(C_A^* - C_{Ab}) \tag{3.2}$$

$$He_A P_A^* = C_A^* \tag{3.3}$$

k_G and k_L are the gas-side and liquid-side mass transfer coefficients, respectively, P_{Ab} and P_A^* are the bulk and interface equilibrium partial pressure of component A in the gas-phase, and C_{Ab} and C_A^* are the bulk and interface equilibrium concentration of component A in the liquid phase. Since it is not possible to determine the concentration at the gas-liquid interface, the overall mass transfer coefficients (K_G and K_L) are introduced to enable computing the mass flux based on the driving

force between the bulk compositions of the two phases. The mass flux in the gas and liquid phases is given by Equations (3.4) and (3.5), respectively.

$$N_A = K_G\left(P_{Ab} - \tilde{P}_A\right) \tag{3.4}$$

$$N_A = K_L\left(\tilde{C}_A - C_{Ab}\right) \tag{3.5}$$

$\tilde{P}_A$ and $\tilde{C}_A$ are the equilibrium partial pressure and concentration in the gas and liquid bulk. Again, if the equilibrium relation between the two phases is linear, Henry's Law can be used as in Equation (3.7):

$$He_A P_{Ab} = \tilde{C}_A \tag{3.6}$$

$$He_A \tilde{P}_A = C_{Ab} \tag{3.7}$$

Combining Equations (3.1) to (3.7) gives the following relations:

$$\frac{1}{K_G} = \frac{1}{k_G} + \frac{1}{He_A k_L} \tag{3.8}$$

$$\frac{1}{K_L} = \frac{He_A}{k_G} + \frac{1}{k_L} \tag{3.9}$$

In general, the partial pressure of the solvent in the gas-phase is so small that its resistance in the gas-phase can be neglected making the overall mass transfer dependent only on the liquid-side mass transfer coefficient.

3.1.2 Penetration Theory

The penetration theory by Higbie in 1935 [47, 48] assumes that the gas diffuses or penetrates into the liquid through the gas-liquid interface through a film of thickness (dz) and it accumulates within the film in unsteady-state. No convective mass transfer takes place during the gas diffusion. The general mass balance of a component, A, diffusing through the interface is:

$$\frac{\partial C_A}{\partial t} = D_{AL} \frac{\partial^2 C_A}{\partial z^2} \qquad (3.10)$$

where D_{AL} is the gas diffusivity into the liquid. This equation is valid for an equimolar counter-diffusion with a small concentration of component A [44]. The initial and boundary conditions for the gas absorption are:

$$t = 0, \quad 0 < z < \infty \qquad C_A = C_{Ab} \qquad (3.11)$$

$$t > 0, \qquad z = 0 \qquad C_A = C_A^* \qquad (3.12)$$

C_{Ab} is the concentration in the liquid bulk, and C_A^* is the concentration at the gas-liquid interface. Assuming constant concentrations at the bulk and surface, Equation (3.10) can be integrated to yield:

$$\frac{C_A^* - C_A}{C_A^* - C_{Ab}} = erf\left(\frac{z}{2\sqrt{tD_{AL}}}\right) \qquad (3.13)$$

$$erf\left(\frac{z}{2\sqrt{tD_{AL}}}\right) = \frac{2}{\sqrt{\pi}} \int_0^{z/(2\sqrt{tD_{AL}})} e^{-\tau^2} d\tau \qquad (3.14)$$

Neglecting convective mass transfer, the flux at the interface can be calculated by:

$$N_A = -D_{AL} \left(\frac{\partial C_A}{\partial z}\right) \qquad (3.15)$$

Using Equation (3.13) gives:

$$N_A = (C_A^* - C_{Ab}) \sqrt{\frac{D_{AL}}{\pi t}} \qquad (3.16)$$

Equation (3.16) provides the rate of mass transfer at a time t. The average rate of mass transfer at an exposure time (t_e) can be obtained using:

$$\overline{N}_A = (C_A^* - C_{Ab}) \sqrt{\frac{4D_{AL}}{\pi t_e}} \qquad (3.17)$$

13

Equation (3.17) shows that shorter exposure times results in higher mass transfer rates. Similar to the two-film theory (Equation (3.2)), the rate of mass transfer is proportional to the driving force with a different proportionality constant.

3.1.3 Surface Renewal Model

The surface renewal model by Danckwerts in 1951 states that each element of the interface does not have the same exposure time to the gas [49] and the exposure time is random. It is assumed that the probability of an element surface to be exchanged with the bulk of the fluid is independent of the age of the element at the interface. The distribution of the surface age is assumed to follow the following function:

$$f(t) = \xi e^{-\xi t} \tag{3.18}$$

where ξ is the rate of surface renewal per unit surface area. Therefore, when the surface is randomly renewed, the overall mass flux becomes:

$$N_A = (C_A^* - C_{Ab}) \sqrt{\frac{D_{AL}}{\pi}} \int_0^\infty \frac{\xi e^{-\xi t}}{\sqrt{t}} dt \tag{3.19}$$

Integrating the right-hand side of Equation (3.19) gives:

$$N_A = (C_A^* - C_{Ab}) \sqrt{D_{AL} \xi} \tag{3.20}$$

Since there is a finite limit to the age of the surface, Equation (3.20) most likely underestimates the rate of mass transfer. However, if the amount of old surface elements is small relative to other ages, the overall rate should not be affected. As the fluid flow becomes more turbulent the value of the surface renewal rate (ξ) will become greater, however, estimating its value might be challenging. Gas absorption usually takes place in a unit operation where an

14

intimate contact between the gas and liquid is achieved. There are many types of unit operations used for gas absorption, nonetheless, this study is focusing on packed-bed absorbers. A brief discussion of these gas-liquid absorbers is given in the following section.

3.2 Packed-Bed Gas Absorbers

Packed-bed absorbers are columns containing different packings of various types, shapes, and sizes which are mainly used to increase the turbulence and spread the liquid over their surfaces thereby increasing the contact area between the gas and liquid phases increasing the gas-liquid mass transfer. Packed-beds can be operated in a co-current or a countercurrent mode. Conventionally, gas absorption is carried out in a countercurrent mode and therefore the focus of this study is on countercurrent gas absorbers. The design and scaleup of these absorbers require, among others, precise knowledge of the hydrodynamics and heat as well as mass transfer under the actual gas absorption process conditions.

3.2.1 Packing Used

The packings used in gas absorption operations can be random or structured, which are physically different [50]. Table 3.1 gives the void fraction and specific surface area of some industrial packings, where the oldest packing was Raschig rings, named after the German chemist Friedrich Raschig [51].

Table 3.1. Types of packing and their properties. [52-56]

Packing	Void fraction	Specific surface area (m^2/m^3)
Raschig rings	0.64 – 0.74	92 – 364
Berl saddles	0.62 – 0.68	105 – 466
Pall rings	0.94 – 0.96	102 – 207
Metal Intalox (IMTP)	0.97 – 0.98	98 – 230
Nor-Pac	0.92 – 0.94	102 – 180
Hy-Pak	0.92 – 0.97	95 – 180
Mellapak 250Y	0.95 – 0.99	249 – 499
Flexipac	0.93 – 0.98	223
Gempak	0.91 – 0.93	220 – 452
Norton Intalox	0.97	177 – 213

3.2.2 Hydrodynamics in Packed-Beds

The hydrodynamics of the gas-liquid systems in the packed-beds include flow regimes, pressure drop and liquid (solvent) holdup. There is no flow regime map for packed-beds operating in a countercurrent mode. Table 3.2 shows literature correlations for pressure drop in packed-beds; and as can be observed, these empirical correlations are primarily developed for an air-water system. Thus, using these correlations for different gas-liquid systems with properties different from air-water could be misleading.

Also, Figure 3.2 shows the Generalized Pressure Drop Correlation (GPDC) graph for a packed-bed developed by Eckert in 1961 [57] and modified by Strigle [55]. This graph is based on the flow rates and density of the liquid and gas phases. In 1992, Leva [58] improved the GPDC graph by adding more packings and more gas-liquid systems as shown in Figure 3.3. In this study, all graph lines (pressure drop per unit length) were translated in the modified GPDC into equations, which are presented in Table 3.3.

Table 3.2. Litertutre correlations for pressure drop in packed-beds

Ref no.	Author, Year	Packing	System	Correlation	Notes
[59]	Stichlmair *et al.*, 1989	Gempak Mellapak 250Y Montz Raschig rings Pall rings Reflux rings Hiflow rings Intalox saddles Berl saddles Torus saddles	Air/water Oil Syrup	$$\frac{\Delta P}{\Delta z} = \frac{3}{4} f_0' \left(\frac{1-\varepsilon'}{\varepsilon'^{4.65}}\right)\left(\frac{\rho_G U_G^2}{d_P'}\right)$$	$\varepsilon' = \varepsilon - h_L$ $d_P' = d_P \left(\frac{1-\varepsilon'}{1-\varepsilon}\right)^{\frac{1}{3}}$ $f_0' = f_0 \left(\frac{1-\varepsilon'}{1-\varepsilon}\right)^{\frac{c}{3}}$ $f_0 = \frac{C_1}{Re_G} + \frac{C_2}{Re_G^{\frac{1}{2}}} + C_3$ $c = \frac{1}{f_0}\left(\frac{C_1}{Re_G} + \frac{C_2}{Re_G^{\frac{1}{2}}}\right)$ $Re_G = \frac{\rho_G U_G d_p}{\mu_G}$
[60]	Kister *et al.*, 2007	Random packing Structured packing	Air/water	$$Y = \frac{C_1 \left(\frac{\Delta P}{\Delta z}\right)^{C_2}[1 - \exp(C_6 \cdot X^{C_7})]}{1 + C_3 \left(\frac{\Delta P}{\Delta z}\right)^{\left(\frac{C_2}{C_4}\right)} X^{C_5}}$$ $$Y = U_G \left[\frac{\rho_G}{(\rho_L - \rho_G)}\right]^{0.5} F_P^{0.5} \nu_L^{0.05}$$ $$X = \left(\frac{\dot{m}_L}{\dot{m}_G}\right)\left(\frac{\rho_G}{\rho_L}\right)^{0.5}$$ $$\left(\frac{\Delta P}{\Delta z}\right)_{flood} = 0.12 F_P^{0.7}$$	ν_L is in cSt Equation developed by Tsai [61] C_1 to C_7 are constants found in [62] for structured and random packing Results more consistent for structured packing
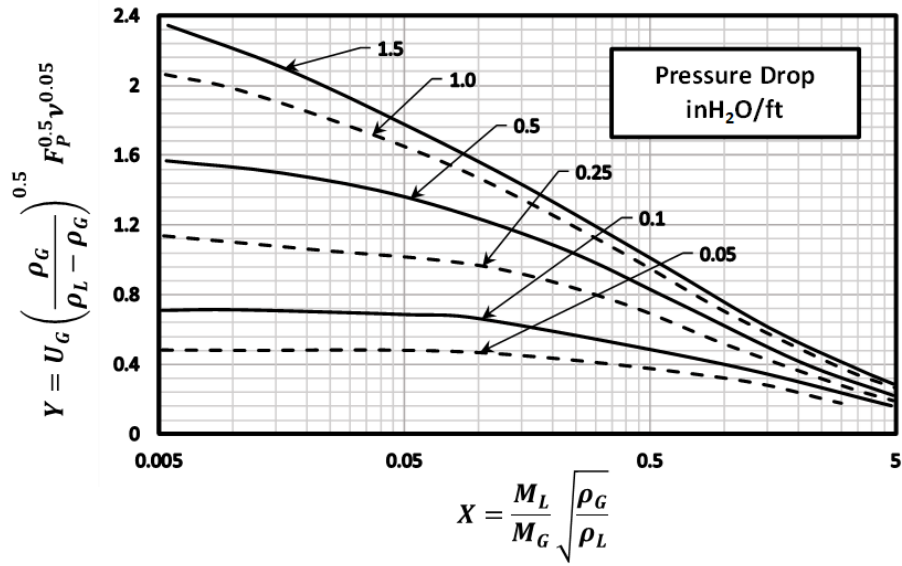
Figure 3.2. GPDC for packed-beds developed by Eckert [57] and modified by Strigle [55]
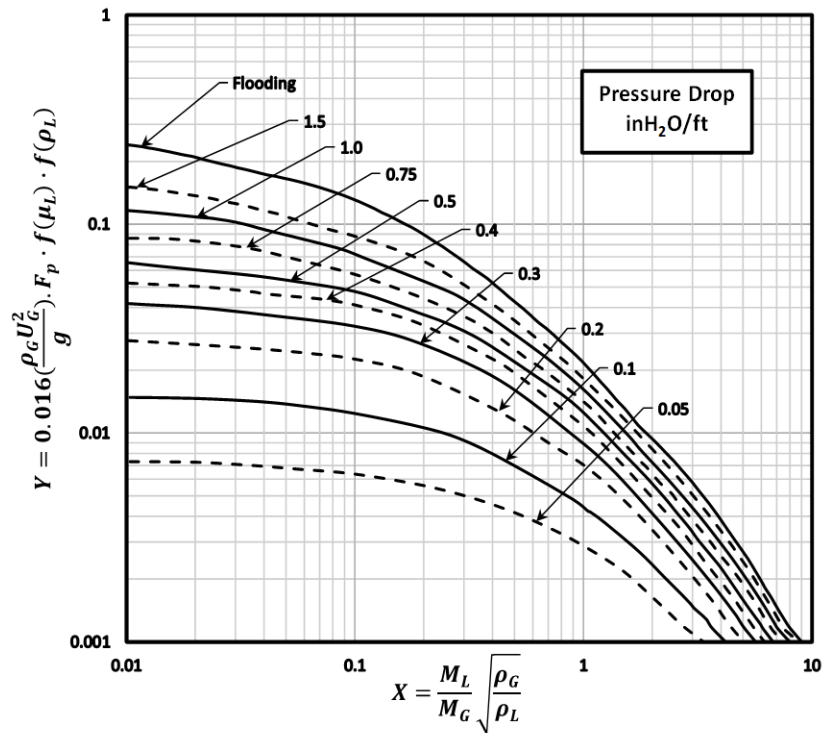
Figure 3.3. GPDC as modified by Leva [58]

18

Table 3.3. Parameters and limitations of the GPDC graph modified by Leva

Author	Systems	Correlation	Constraints
Piche *et al.* [63]	4% solution of NaOH/air + CO_2 Water/air $CaCl_2$ solution/air Methanol/ethanol	*Flooding* $\log(Y) = -0.29[\log_{10}(X)]^2 - 1.075[\log_{10}(X)] - 1.636$ $$X = \frac{M_L}{M_G}\sqrt{\frac{\rho_G}{\rho_L}}$$ $$Y = 0.016\left(\frac{\rho_G U_G{}^2}{g}\right) \cdot F_p \cdot f(\mu_L) \cdot f(\rho_L)$$ For $d_p < 1$ in $\log[f(\mu_L)] = 0.0591 \cdot log^3(\mu_L) + 0.0226 \cdot log^2(\mu_L) + 0.1701 \cdot log(\mu_L) - 0.0135$ For $d_p > 1$ in $\log_{10}[f(\mu_L)] = 0.1839 \cdot \log(\mu_L) - 0.011$ $$f(\rho_L) = 1.5052 \cdot \ln\left(\frac{\rho_{H2O}}{\rho_L}\right) + 1.1883$$	$0.01 < X < 10$ $700 < \rho_L < 1400$ kg/m³ $0.2 \leq \mu_L \leq 20\ cP$
This study	4% solution of NaOH/air + CO_2 Water/air $CaCl_2$ solution/air Methanol/ethanol	$$\log(Y) = a[\log_{10}(X)]^2 + b[\log_{10}(X)] + c$$ $$a = -0.3525P_{log}^5 - 0.9796P_{log}^4 - 0.8232P_{log}^3 - 0.0538P_{log}^2 + 0.1077P_{log} - 0.299$$ $$b = -0.2893P_{log}^5 - 0.8153P_{log}^4 - 0.772P_{log}^3 - 0.0763P_{log}^2 - 0.0634P_{log} - 1.0086$$ $$c = 0.514P_{log}^5 + 1.3853P_{log}^4 + 0.9824P_{log}^3 - 0.1339P_{log}^2 + 0.3157P_{log} - 1.824$$ $$P_{log} = log_{10}\frac{\Delta P}{\Delta z}$$	$0.01 < X < 10$ $700 < \rho_L < 1400$ kg/m³ $0.2 \leq \mu_L \leq 20\ cP$ $0.05 \leq \frac{\Delta P}{\Delta z} \leq 2.5\ in\ H_2O/ft$

The liquid holdup (h_L), known as dynamic holdup, represents the liquid retained in the packed-bed during the two-phase flow. Static holdup is the liquid retained by capillary forces in the contact points between the packing elements [64]. Table 3.4 shows some liquid holdup correlations available in the literature, and as can be seen, these correlations include dimensionless numbers.

Table 3.4. Literature correlations for the liquid holdup in a packed-beds

Ref no.	Author, Year	Packing	Correlation	Notes
[59]	Stichlmair *et al.*, 1989	Gempak Mellapak 250Y Montz Raschig rings Pall rings Reflux rings Hiflow rings Intalox saddles Berl saddles Torus saddles	$h_L = 0.555 Fr_L^{\frac{1}{3}}$	$Fr_L = \dfrac{U_L^2 a}{g \varepsilon^{4.65}}$
[65]	Billet and Schultes, 1993		$\dfrac{a_h}{a} = C_h Re_L^{0.15} Fr_L^{0.1}, Re_L < 5$ $\dfrac{a_h}{a} = 0.85 C_h Re_L^{0.25} Fr_L^{0.1}, Re_L \geq 5$ $h_L = \left(12 \cdot \dfrac{Fr_L}{Re_L}\right)^{1/3} \left(\dfrac{a_h}{a}\right)^{2/3}$ a_h is the hydraulic specific surface area	$800 < \rho_L < 1800 \; kg/m^3$ $0.00059 \leq \mu_L \leq 0.185$ cP $20.8 \leq \sigma_L \leq 86.3 \; dyne/cm$ $Re_L = \dfrac{U_L \rho_L}{a \mu_L}$ $Fr_L = \dfrac{U_L^2 a}{g}$

3.2.3 Mass Transfer in Packed-Beds

Table 3.5 shows available literature correlations reported for predicting the mass transfer coefficients (k_L) for random packing, whereas Table 3.6 show different correlations for structured packing.

From these tables, the following remarks can be made:

1. In general, these correlations are empirical in nature and cover a wide range of gases and solvents with different physico-chemical properties and packings of different characteristics.

2. Some of these correlations, however, are gas and liquid specific and using them for other systems could be risky.

3.   The experiments used to develop these correlations were carried under ambient pressure and temperature. This could raise doubt about the validity of using such correlations under different operating conditions.

4.   Some of these correlations include may dimensionless numbers, such as Reynolds, Weber, Schmidt, Froude, and Sherwood numbers. Dimensionless numbers can mask the true impact of a variable such as velocity as it appears in both Reynolds number and Froude number. The proper approach is to use Froude number to highlight the effect of velocity (inertia) whereas Reynolds number should be used to amplify the effect of viscosity (viscous force). Another important issue is the choice of the characteristic length in these numbers. For instance, Reynolds number based on the packing size is much smaller than that based on the column diameter.

Table 3.5. Literature correlations for the mass transfer coefficient in random packing

Ref no.	Author, Year	Packing	System	k_L	Notes
[66]	Sherwood and Holloway, 1940	Raschig rings	CO_2/water	$\dfrac{k_L a}{D_A} = 550 \left(\dfrac{\mu_L}{\rho_L D_{AL}}\right)^{0.5} \left(\dfrac{L}{\mu_L}\right)^{0.54}$	
[67]	Van Krevelen and Hoftijzer, 1948		CO_2/MEA CO_2/DEA	$\dfrac{k_L \left(\dfrac{\mu_L^2}{\rho_L^2 g}\right)^{1/3}}{D_{AL}} = 0.015 \left(\dfrac{L}{a_e \mu}\right)^{2/3} \left(\dfrac{\mu}{\rho D_{AL}}\right)^{1/3}$	
[68]	Shulman et al., 1955	Raschig rings Berl saddles	Air/water	$\dfrac{k_L d_p}{D_{AL}} = 25.1 \left(\dfrac{d_p M_L}{\mu_L}\right)^{0.45} \left(\dfrac{\mu_L}{\rho_L D_{AL}}\right)^{0.5}$	T= 20 – 23 ºC Gas flow rate = 100 – 1000 lb/hft^2
[69]	Wilson and Geankoplis, 1966	spheres	Benzoic acid/water Benzoic acid/propylene glycol	$\dfrac{k_L}{M_L} Sc^{\frac{2}{3}} \epsilon = 1.09 Re^{-\frac{2}{3}}$ for $0.0016 < Re < 55$ and $0.35 < \epsilon < 0.75$ $\dfrac{k_L}{M_L} Sc^{\frac{2}{3}} \epsilon = 0.250 Re^{-0.31}$ for $55 < Re < 1500$	$950 < Sc < 70,600$
[70]	Onda et al., 1968	Raschig rings Berl Saddle Sphere Rods	CO_2/water CO_2/CCl_4 CO_2/CH_3OH	$k_L \left(\dfrac{\rho_L}{\mu_L g}\right)^{\frac{1}{3}} = 0.0051 \left(\dfrac{M_L}{a_w \mu_L}\right)^{\frac{2}{3}} \left(\dfrac{\mu_L}{\rho_L D_{AL}}\right)^{-\frac{1}{2}} (a d_p)^{0.4}$	This was originally tested with water and then the organic solvents agreed with the correlation
[71]	Mohunta et al., 1969	Raschig rings		$k_L a = 25 \times 10^{-4} \left(\dfrac{g \rho_L}{a \mu_L}\right)^{0.66} \left(\dfrac{g^2 \rho_L}{\mu_L}\right)^{\frac{1}{9}} \left(\dfrac{\mu_L M_L^3 a^3}{g^2 \rho_L^4}\right)^{0.25} \left(\dfrac{\mu_L}{\rho_L D_{AL}}\right)^{-0.5}$	
[72]	Akita and Yoshida, 1973	Berl saddles	Water/O_2 Glycerol solution/O_2 30% Vol glycol solution/O_2 Methanol/O_2 0.15 M Na_2SO_3 solution/O_2	$k_L a = c_2 D_{AL}^{0.5} \nu_L^{-0.12} \left(\dfrac{\gamma}{\rho_L}\right)^{-0.62} d_p^{0.17} g^{0.93} \epsilon_G^{1.1}$	
[73]	Fukushima and Kusaka, 1978	spheres	Air/sulfite	$\dfrac{k_L d_p}{D_{AL}} = 5 \cdot 10^2 \phi^{0.3} Re_L^{\frac{1}{3}} Re_G^{\frac{1}{5}} Sc^{\frac{1}{2}} \left(\dfrac{d_p}{T}\right)^{2.2}$	Not valid for foam flow region $T = 20$ ºC $Re_L = 138$ $Re_G = 500$
[74]	Mangers and Ponter, 1980	Raschig rings	CO_2/Glycerol-water	$\dfrac{k_L a}{D_{AL}} = 2.03 \left(\dfrac{M_L}{\mu_L}\right)^{1.44} \left(\dfrac{\mu_L}{\rho_L D_{AL}}\right)^{0.50} \left(\dfrac{\rho_L^2 g d_p^3}{\mu_L^2}\right)^{-0.183}$	
[75]	Echarte et al., 1984	Raschig rings	CO_2/water CO_2/water-glycerol	$k_L = \sqrt{\dfrac{4 D_{AL} \nu_L}{\Pi l}}$	$6 < \dfrac{H}{D} < 36$ $300 < Sc < 10,000$ $6 \times 10^7 < Ga < 230 \times 10^7$ $30 < Re < 800$

Table 3.5 continued.

Ref no.	Author, Year	Packing	System	k_L	Notes
[76]	Billet and Schultes, 1993	Pall rings Ralu rings NOR PAC rings Hiflow rings Hiflow rings Super TOP-Pac rings Raschig rings VSP rings Envi Pac rings Bialecki rings Tellerettes Spheres Berl saddles Intalox saddles	CO_2/methanol CO_2/buffer solution 1 CO_2/buffer solution 2 CO_2/1.78 molal NaCl solution CO_2-water/air CO_2-air/water O_2-water/air Chlorine-air/water	$k_L a_w = C_L \left(\dfrac{g}{v_L}\right)^{1/6} \left(\dfrac{D_{AL}}{d_h}\right)^{1/2} a^{2/3} U_L^{1/3} \left(\dfrac{a_w}{a}\right)$	$\dfrac{a_w}{a}$ $= 1.5(ad_h)^{-0.5}\left(\dfrac{u_L d_h}{v_L}\right)^{-0.2}\left(\dfrac{u_L^2 \rho_L d_h}{\sigma_L}\right)^{0.75}\left(\dfrac{u_L^2}{gd_h}\right)^{-0.45}$ C_L is a constant that is dependent on packing Mean deviation = 8.3%
[77]	Potnis and Lenz, 1996	Raschig rings Berl saddles Pall rings Spheres Rods	Humid Air/liquid-desiccant	Regenerator $Sh = 0.46Re^{1.2}Sc^{0.5}$ Dehumidifier $Sh = 0.8ReSc^{0.5}$	Exponent of Sc is set to 0.5
[78]	Shetty and Cerro, 1997			$k_L = \left(\dfrac{0.4185D_{AL}}{b}\right)\left(\dfrac{\sin\alpha}{l_{ratio}}\right)^{0.5}\left(\dfrac{4\rho_L q}{\mu_L}\right)^{1/3}\left(\dfrac{\rho_L^2 gb^3}{\mu_L^2}\right)^{1/6}Sc_L^{0.5}$	
[79]	Yuan et al., 2004	spheres	N_2-air/water	$\dfrac{k_L a d_1}{a_t D_{AL}} = 0.428\left(\dfrac{4\rho_L u_L}{a_b \mu_L (1-F)}\right)^{0.8748}\left(\dfrac{\mu_L}{\rho_L D_{AL}}\right)^{0.5}$	Error = 11.38% $u_L = 0.0018 - 0.0072\ m/s$ $u_G = 0.14 - 0.57\ m/s$ normal temperature atmospheric pressure
[80]	Longo and Gasparella, 2005	Pall rings	H_2O/LiCl H_2O/LiBr H_2O/KCOOH	$k_L = 25.1\left(\dfrac{D_{AL}}{d_s}\right)\left(\dfrac{d_s L'}{\mu_L}\right)^{0.45}Sc_L^{0.5}$	Vapor flow rate = 0 – 5 kg/h $L' = 0.1 - 1.39\ kg/m^2 s$
[81]	Krupiczka et al., 2015	Raschig rings	CO_2/[emim][Ac] CO_2/[bmim][Ac] CO_2/MEA	$k_L = 3.76Re^{-\frac{1}{3}}\ for\ Re^{\frac{2}{3}}Sc^{\frac{1}{2}}\left(\dfrac{d_z}{h}\right)^{\frac{1}{2}} < 5.17$ $k_L = 0.725Re^{\frac{1}{3}}Sc^{\frac{1}{2}}\left(\dfrac{d_z}{h}\right)^{\frac{1}{2}}\ for\ Re^{\frac{2}{3}}Sc^{\frac{1}{2}}\left(\dfrac{d_z}{h}\right)^{\frac{1}{2}} > 5.17$	$T = 40 - 60\ ^oC$ $Q_L = 0.05 - 0.5\ L/min$

23

Table 3.6. Literature correlations for the mass transfer coefficient for structured packing

Ref no.	Author, Year	Packing	System	k_L	Notes
[82]	Kanak, 1980	Goodloe	Krypton gas/freon	$Sh_L a = 8.0 Re_G^{0.605} Re_L^{0.45} Sc_L^{0.5}$	
[83]	Bravo *et al.*, 1985	Flexipac 2 Gempak 2AT Intalox 2T Maxpak Sulzer BX Mellapak 250Y Mellapak 350Y Mellapak 500Y	Cyclohexane/n-hexane o/p-xylenes chlorobenzene/ethylbenzene i-butane/n-butane	$k_L = 2\sqrt{\dfrac{D_{AL} U_{LE}}{\pi S}}$	
[84]	Henriques de Brito *et al.*, 1992	Mellapak 250Y Mellapak 250Y 500Y		$k_L = 2\sqrt{\dfrac{D_{AL}}{C_1 \pi l \cos\alpha}} u_L^{\frac{1-C_2}{2}}$	
[85]	Weiland *et al.*, 1993	Goodloe A2 Montz	SO$_2$/caustic soda CO$_2$/NaOH	$Sh_L = 3.4 Re_L^{-0.08} Sc_L^{0.5}$ for Goodloe packing $Sh_L = 5.2 Re_L^{-0.04} Sc_L^{0.5}$	
[86]	Rocha *et al.*, 1993	Flexipac 2 Gempak 2A Gempak 2AT Intalox 2T Maxpak Sulzer BX	Cyclohexane/n-hexane	$k_L = 2\left(\dfrac{D_{AL} C_E U_{LE}}{\pi S}\right)^{0.5}$	$C_E = 0.9$ $U_{LE} = \dfrac{U_L}{\varepsilon h_L \sin\theta}$
[87]	Hanley *et al.*, 1994		Air/Isopar	$k_L = \dfrac{D_{AL}}{d_{eq}}\left(\dfrac{d_{eq} u_L \rho_L}{\epsilon \mu_L}\right)^{0.5} Sc_L^{0.5}$	
[88]	Brunazzi *et al.*, 1995	Mellapak 250Y	1,1,1-trichloroethane/Genosorb 300	$k_L = 2\sqrt{\dfrac{D_{AL} U_{LE}}{0.9\pi d_h}}$	
[77]	Potnis and Lenz, 1996	Munters CELDEK	Humid Air/liquid-desiccant	Regenerator $Sh = 0.01 Re Sc^{0.5}$ (30 cm packing size) $Sh = 0.02 Re Sc^{0.5}$ (55 cm packing size) Dehumidifier $Sh = 0.04 Re^{0.9} Sc^{0.5}$ (30 cm packing size) $Sh = 0.03 Re Sc^{0.5}$ (55 cm packing size)	Exponent of *Sc* is set to 0.5
[89]	Brunazzi and Paglianti, 1997	Mellapak 250Y Sulzer BX	CO$_2$-water/air Gensorb 300/air Gensorb 1843/air	$\dfrac{k_L d}{D_{AL}} = A\dfrac{Gz^B}{Ka^C}$	$Ka = \dfrac{\sigma^3 \rho_L}{\mu_L^4 g}$ $Gz = Re_L Sc_L \dfrac{\delta}{H}$ *A, B, C* are constants Liquid flow rates = 1.2 – 21.6 m^3/(m^{2}h) Gas flow rates = 0.44 – 1.4 m^3/(m^{2}h)

Table 3.6 continued.

Ref no.	Author, Year	Packing	System	k_L	Notes
[90]	Gualito *et al.*, 1997	Flexipac Flexiramic Mellapak 250Y	Chlorobenzene/ethylbenzene Methanol/ethanol Air/water Cyclohexane/n-heptane Isobutene/n-butane	$k_L = 2\sqrt{\dfrac{D_{AL}U_{LE}}{\pi S}}$	
[91]	Xu *et al.*, 2000	Gempak 2.5A, AW7, AW12	Methanol/isopropanol Water/acetic acid Methanol/water	$k_L = \sqrt{\dfrac{4D_{AL}U_L}{\pi l \left(\dfrac{4F_t}{s}\right)^{2/3}\left(\dfrac{3\mu_L U_L}{\rho_L \varepsilon g_{eff}\sin\alpha}\right)^{1/3}}}$	Packing height = 2.15 m P = 710 and 260 mmHg
[92]	Raynal *et al.*, 2004	Mellapak 250Y	CO_2/NaOH	$k_L = 2\sqrt{\dfrac{D_{AL}U_{LE}}{\pi l}}$	
[93]	Haroun *et al.*, 2010			$\dfrac{k_L e}{D_{AL}} = K\left(\dfrac{e}{\lambda}\right)^{0.5} Re_L^{0.5} Sc_L^{0.5}$	Simulations K=0.65 Re_L = 65 Re_G = 180 Sc_L = 23 Sc_G = 0.03
[94]	Hanley and Chen, 2012	Sheet metal Gauze in X configuration		$k_L = A Re_L Sc_L^{1/3}\left(\dfrac{c_L D_{AL}}{d_{eq}}\right)$	*A* is a constant Exponents are assumptions based on previous studies

3.3 Techno-Economic Analysis

To perform a TEA of the CO_2 capture process using Aspen Plus, a complete layout of the process, including all process equipment are needed. The simulations are helpful in determining the viability of a potential solvent in capturing CO_2 from the fuel gas stream. Table 3.7 shows some literature CO_2 capture simulations. In this table, Field and Brasington [38] simulated a CO_2 capture process using Selexol in Aspen Plus. The Perturbed Chain Statistical Association Fluid Theory (PC-SAFT) EOS was used to perform vapor-liquid equilibrium calculations and added three flash units to regenerate the solvent rated at 20.7, 11, and 1.5 bar, respectively. They also added a sequestration stream with the conditions 153 bar and 50 °C. Padurean et al. [95] ran simulations for three different physical solvents for pre-combustion applications using three solvents, Selexol, Rectisol, and Purisol. Their work shows Selexol was the better solvent of the three as it had the simplest configuration along with the lowest energy required to regenerate the solvent.

Basha et al. [96, 97] used Aspen Plus to develop a process to capture CO_2 using ionic liquids (ILs). A modified Peng-Robinson EOS was used along with the Span-Wagner EOS for VLE calculations. Their work is considered unique among the others presented in Table 3.7 because the fuel gas is kept at a high temperature rather than cooling it down leading to some energy savings and potentially more economic benefits. In addition, Basha et al. [96, 97] showed that ILs have great potential for capturing CO_2 even at such elevated temperatures due to their thermal stability and extremely low vapor pressure at the simulation temperatures.

Similar to Padurean *et al.* [95], Park *et al.* [98] simulated the CO_2 capture process using Selexol, Rectisol, and Purisol using Aspen Plus. They used the PC-SAFT EOS for the VLE calculations and they found Selexol to be the more energy efficient of the three followed by Purisol and then Rectisol being the least efficient. Dave *et al.* [99] used ProTreat software to design the process of capturing CO_2 using Selexol. Thermodynamic properties were calculated using a package within the software while the Peng-Robinson EOS was used for the gas-phase. The simulations showed that there is some H_2 being absorbed along with the CO_2 and a sensitivity study was conducted for the recovery of the absorbed H_2.

Siefert *et al.* [100] used Aspen Plus to simulate for three solvents including one IL. The PC-SAFT EOS was used to simulate for two of the solvents, while the ENRTL method was used for the IL. They found that PEGPDMS-1 performed similarly to Selexol while the IL [aPy][Tf$_2$N] could potentially better the other two solvents. Zhai and Rubin [101] performed simulations of the CO_2 capture process using the IL [hmim][Tf$_2$N] as the solvent. The Redlich-Kwong EOS was used for VLE calculations. Their study found that the main concerns when using [hmim][Tf$_2$N] are the pumping cost of the solvent and compression of the CO_2. Roussanaly *et al.* [102] used Aspen Plus to simulate the CO_2 capture process using Rectisol. The Peng-Robinson EOS was used for VLE calculations and H_2S was removed from the fuel gas stream before the process.

Table 3.7: Literature simulations of the CO$_2$ capture process

Ref no.	Author, year	Solvents	Solvent temperature (ºC)	Solvent Flow rate (kg/s)	Gas temperature (ºC)	Gas flow rate (kg/s)	CO$_2$ capture efficiency (%)
[38]	Field and Brasington, 2011	Selexol	10	1,939	17	227	90
[95]	Padurean et al., 2012	Selexol Rectisol Purisol	-40 – 40		-40 – 40	125	90.6 – 91.4
[96]	Basha et al., 2013	[hmim][Tf$_2$N]	24.9	1,038	227	102.4	95
[97]	Basha et al., 2014	TEGO IL K5 TEGO IL P51P	24.9	250 – 900	227	102.4	92
[98]	Park et al., 2015	Selexol Rectisol Purisol	-40 – -10	96.25 – 166			90
[99]	Dave et al., 2016	Selexol	20	1,604	26	163	90
[100]	Siefert et al., 2016	Selexol PEGPDMS-1 [aPy][Tf$_2$N]	10 – 40	1,514 – 3,154	40	147	90
[101]	Zhai and Rubin, 2018	[hmim][Tf$_2$N]	29.4	2,439.2	29	1,734	90
[102]	Roussanaly et al., 2020	Rectisol	-19.7	0.99	30	68	85

Table 3.8 shows literature TEA parameters used for the CO_2 capture process and as can be seen, the values of the parameters are very similar with the exception of Roussanaly *et al.* [102] where they used the internal utility of the plant for the electricity. The cost of the solvents also varied depending on the solvents. Siefert *et al.* [100] found that the IL [aPy][Tf$_2$N] could have better economics than the other two solvents provided that its cost becomes low. However, at the higher end of the cost, the IL becomes less economically favorable compared to the other two solvents. In addition, Selexol and PEGPDMS-1 had similar performances and therefore similar economics. Zhai and Rubin [101] compared their TEA of [hmim][Tf$_2$N] to that of Selexol. They found that Selexol was more favorable than the IL due to the latter higher cost and have determined for the IL to be more favorable, its CO_2 solubility would have to be 10% better. In addition, they concluded that there is a need to improve the CO_2 compression technology to further reduce costs. Roussanaly *et al.* [102] found that adding the CO_2 capture process raised the cost of the plant by 40% and that lowering the CO_2 capture ratio increased the CO_2 avoidance cost. Avoidance cost is the minimum CO_2 tax required to make CO_2 capture in a plant more economically favorable [103].

Table 3.8: Literature TEA parameters of the CO_2 capture process

Ref no.	Author, year	Solvents	Plant lifetime (year)	Annual discount rate (%)	Cost of electricity ($/MWh)	Capacity factor	Operating and maintenance cost (% of CAPEX/year)	Solvent cost ($/L)
[100]	Siefert *et al.*, 2016	Selexol PEGPDMS-1 [aPy][Tf$_2$N]	30	7	50	0.8	4	4 4 40 – 400
[101]	Zhai and Rubin, 2018	[hmim][Tf$_2$N]		7.09	50	0.75	5	13.78
[102]	Roussanaly *et al.*, 2020	Rectisol	25	10	0 (internal utility of plant)	0.85	4.5	

4.0 Research Approach

The research approach is described in the following steps:

1. Obtain the fuel gas flow rate, composition, pressure, and temperature based on the plant power. Make sure the fuel gas stream is sulfur-free because sulfur compounds could be removed using a bed of zinc oxide sorbent [104-107].

2. Select the packing type (structured or random) to be used in the absorber and obtain its specifications, (voidage, specific surface area, etc.)

3. Select a physical solvent and obtain its experimental physico-chemical properties (density, viscosity, and surface tension) from literature or from measurements.

4. In Aspen Plus (equilibrium-based model), select an appropriate EOS and determine the minimum solvent flow rate to achieve 90% CO_2 removal.

5. Set the pressure of the high-pressure (HP) flash drum.

6. Calculate the absorber diameter and height. Make sure the height/diameter ratio of the absorber is greater than or equal to 6 to avoid any channeling and wall effects in the absorber.

7. Assume a flow rate of the selected solvent.

8. Select equations for mass transfer coefficients (k_L and k_G) and specific wetted area of the packing (a_w).

9. Run Aspen Plus (rate-based model) with the selected EOS to check 90% CO_2 capture and obtain the compositions of the fuel gas species in the solvent and the molar densities of the liquid and gas phases.

10. Check for flooding in the countercurrent absorber.

11. Obtain the two-phase pressure drop and the corresponding liquid (solvent) holdup.

12. Check if the fuel gas content in the CO_2 stream destined for sequestration is below the target.

13. Check if the water content in the CO_2 stream destined for sequestration is below the target.

14. If the solvent is highly hydrophilic, add a tray distillation column in Aspen Plus to separate the water from the solvent.

15. Size the process equipment and calculate the CAPEX, OPEX, and LCOC.

A flowchart of the LCOC calculations is illustrated Figure 4.1.
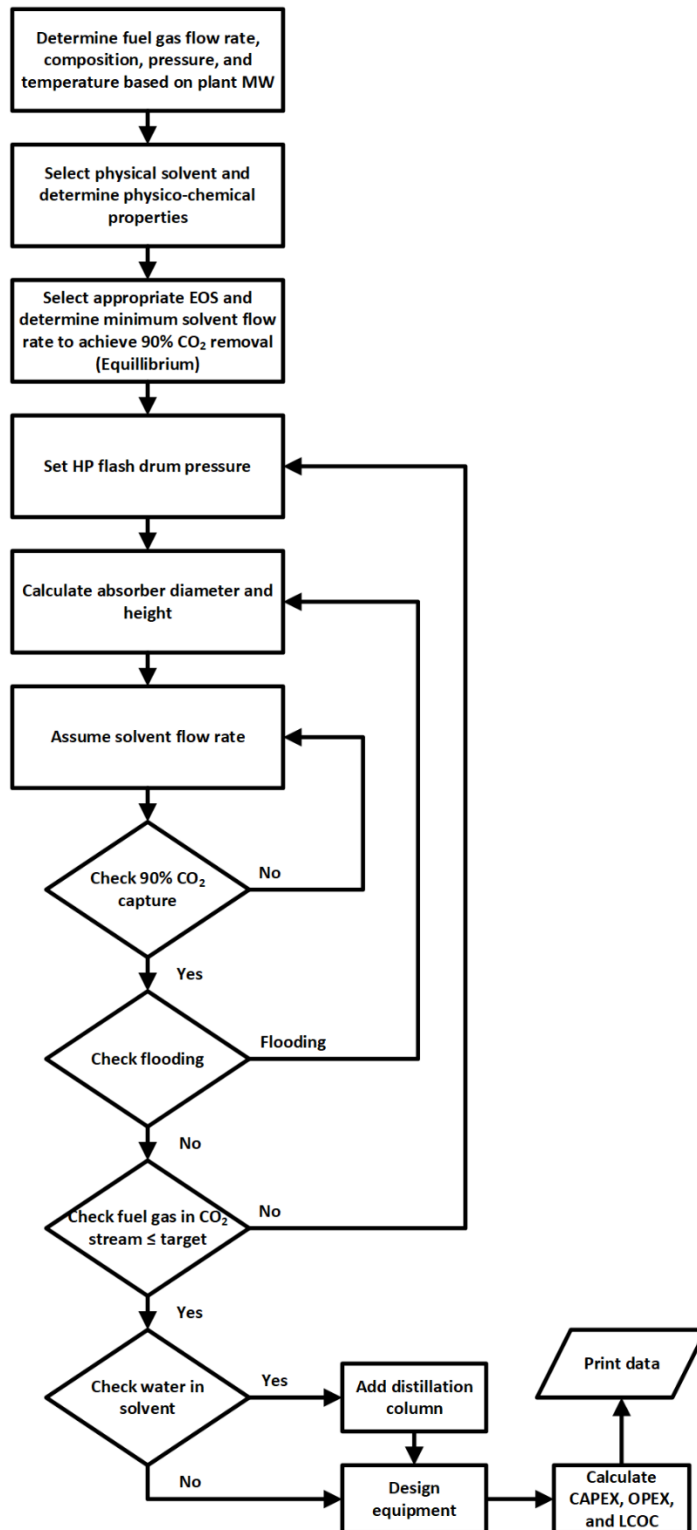
Figure 4.1: Flowchart for TEA calculations

5.0 Details of the Developed CO_2 Capture Process

The fuel gas composition used was based on Case B5B, GEE IGCC with CO_2 capture found in "Cost and Performance Baseline for Fossil Energy Plants Volume 1b: Bituminous Coal (IGCC) to Electricity Revision 2b - Year Dollar Update" by the NETL [108]. The only exception was that sulfur-containing compounds were removed from the fuel gas composition. This was because these compounds can be removed from the fuel gas using zinc oxide sorbents [104-107] and accordingly this study was focusing on CO_2 capture from a sulfur-free fuel gas. The fuel gas flow rate was maintained at 155 kg/s and Table 5.1 shows the composition of the fuel gas used in the 543 MW IGCC plant.

Table 5.1: Fuel gas composition used [108]

Component	Mol%
Ar	0.7144
CH_4	0.0906
CO	0.815
CO_2	40.7829
H_2	56.8223
H_2O	0.1208
N_2	0.654
H_2S	0.000

The CO_2 capture process included a countercurrent packed-bed absorber operating under high pressure over a wide range of temperatures and one structured packing (Mellapak 250Y) and one random packing (IMTP50) were used in the absorber. The properties of the two packings are given in Table 5.2.

Table 5.2: Properties of the packing used [56, 109-111]

Packing type	Mellapak 250Y	IMTP50
Images		
Vendor	Sulzer	KOCH
S, d_p	11.1 mm	50 mm
Material	Metal	Metal
Void fraction	0.987	0.98
Specific surface area (m^{-1})	256	102
Packing factor (ft^{-1})	20	18

The equilibrium solubilities of the fuel gas components in each solvent and the molar densities of the liquid and gas phases were modeled using the PC-SAFT EOS, developed by Gross and Sadowski [112, 113] as given in 8.0. The PC-SAFT parameters for the gaseous species used in this study are given in Table 5.3.

Table 5.3: PC-SAFT parameters for the gases used [38, 114, 115]

Component	PC-SAFT parameter				
	m	σ	ϵ/k_B (K)	κ^{AB}	ϵ^{AB}/k_B (K)
CO_2	2.6037	2.555	151.04	0	0
CO	1.2751	3.342	93.038	0	0
CH_4	1.00	3.704	150.03	0	0
H_2	0.487	4.24	33.85	0	0
N_2	1.2053	3.313	90.96	0	0
Ar	0.9285	3.4784	122.23	0	0
H_2O	1.9599	2.362	279.42	0.034868	2500.7

where the parameters m, σ, ϵ, κ^{AB}, and ϵ^{AB} used in the PC-SAFT EOS were obtained either from the literature or from regressing experimental data [113].

5.1 Process Flow Diagram for Techno-Economic Analysis

The CO_2 capture process flow diagram developed in Aspen Plus is illustrated in Figure 5.1 and Figure 5.2 shows the modified process for hydrophilic solvents which require further treatment for regeneration.

1	Packed absorber
2	Gas expander
3	HP flash tank
4	MP flash tank
5	LP flash tank
6	Solvent recycle pump
7	Solvent recycle cooler
8	LP multistage compressor with intercooling
9	MP multistage compressor with intercooling
10	Gas recycle compressor
11	Gas recycle cooler
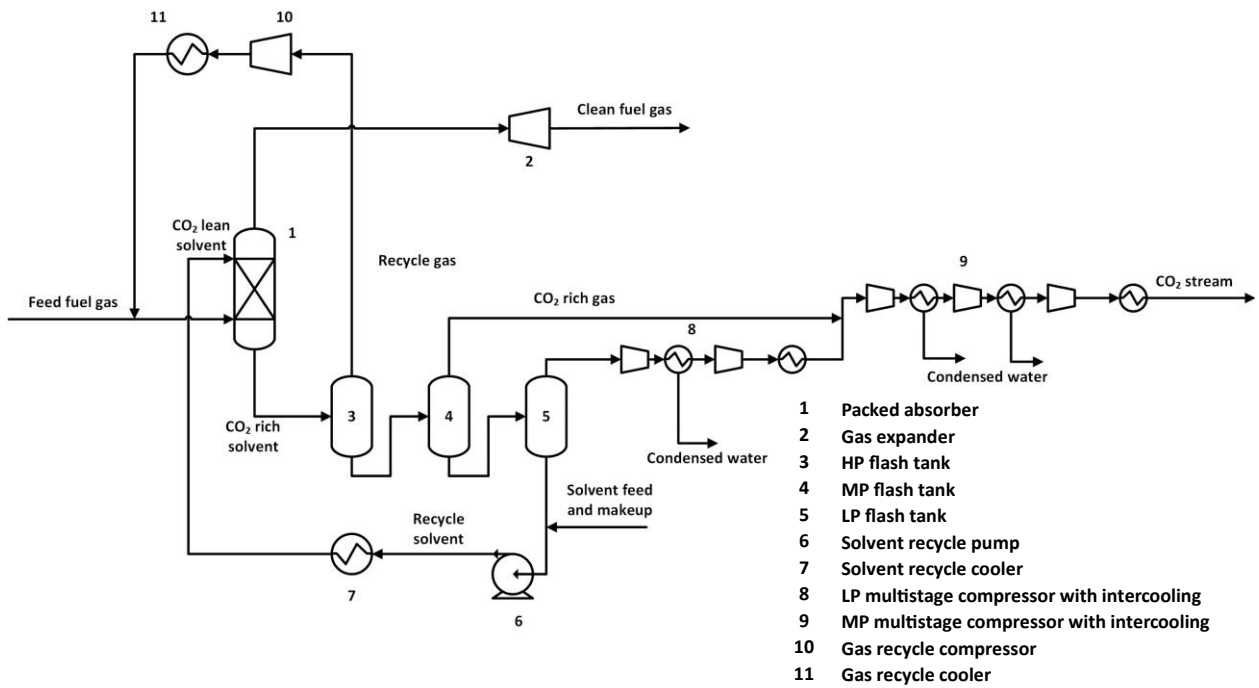
Figure 5.1: Process flow diagram of the CO_2 capture plant

1	Packed-bed absorber
2	HP flash tank
3	MP flash tank
4	LP flash tank
5	Solvent recycle pump
6	Solvent recycle cooler
7	Gas expander
8	Gas recycle compressor
9	Gas recycle cooler
10	LP multistage compressor with Intercooling
11	MP multistage compressor with Intercooling
12	Distillation column with condenser and reboiler
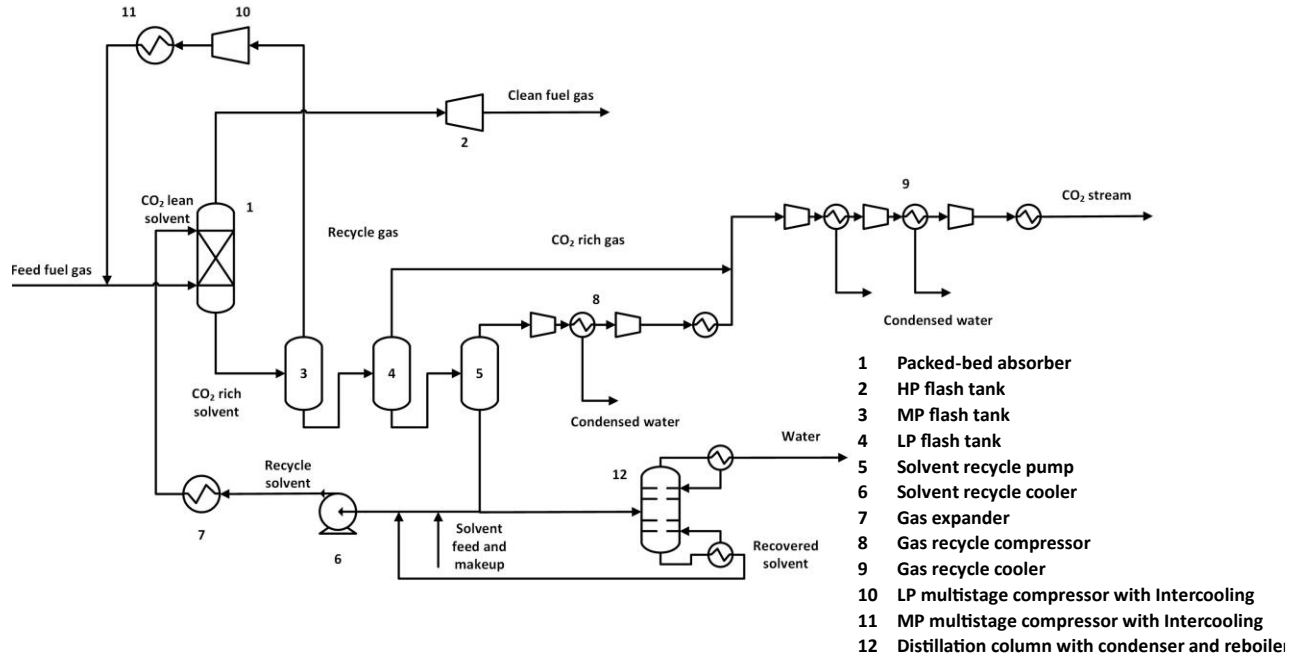
Figure 5.2: Process flow diagram of the CO_2 capture plant for hydrophilic solvents

The constraints imposed on the process are: (1) no flooding in the absorber and minimum irrigated pressure drop, (2) minimum CO_2 capture efficiency of 90%, (3) minimum fuel gas (H_2, CH_4 and CO) loss ($\leq$ 0.5 mole%) in the CO_2 steam destined to sequestration sites, (4) the height (*H*) to the internal diameter (*D*) ratio of the packing in the absorber should be greater than or equal to 6 to avoid channeling of the gas and solvent in the absorber, and (5) the H_2O content in the CO_2 stream destined to sequestration sites should be less than or equal to 600 ppm [43] to avoid CO_2 hydrates formation in the CO_2 pipelines. To meet the process constraints, the solvent flow rate and the absorber internal diameter were adjusted to avoid flooding and achieve minimum 90% CO_2 capture efficiency from the fuel gas stream. In Aspen Plus, the absorber dimensions were calculated using a rate-based model containing the mass transfer correlations developed by Onda *et al.* [70] for random packing and by Bravo *et al.* [83] for structured packing, which are given in Tables 3.5 and 3.6, respectively. The diameter of the absorber was varied depending on flooding

36

occurrence. For all diameters, the packing height to diameter ratio was maintained to at least 6. The check for flooding occurrence in the countercurrent absorber was carried out using the GPDC modified by Leva [58]. Also, the pressure drop was calculated using Leva's graph.

In the process flow diagram, the fuel gas enters from the bottom of the absorber at a total molar flow rate of 28,182 kmol/h and a pressure of 51.4 bar for the 543 MW plant. The solvent enters the process from the top of the absorber. The "clean" fuel gas exiting the absorber goes through a gas expander to reduce the pressure to 30 bar just to ensure that the pressure drop across the absorber is considered. The CO_2-rich solvent goes through three flash drums to obtain a lean solvent for recycling. The first flash drum is a high pressure (HP) flash drum. The pressure is lowered and the liberated gas from the top of the HP flash drum is recycled back to the absorber to minimize fuel gas losses (≤ 0.5 mol%). The liquid from the bottom of the first flash drum goes through the medium pressure (MP) flash drum where the pressure is set to 10.5 bar. The liquid from the bottom of the second flash drum then enters a third low pressure (LP) flash drum set at 1 bar. The liquid from the bottom of the third flash drum is then mixed with a fresh make-up solvent to account for any solvent losses (if needed) and the pressure and temperature of the recycle solvent stream are set to the pre-absorber conditions using a pump and a heat exchanger. The gas from the top of the LP flash drum, which consists mainly of CO_2 is compressed to 10.5 bar using multi-stage compressors with intercooling heat exchangers. This is done so that this gas stream can be mixed with the gas from the top of the MP flash drum. After mixing the two gas streams, the resultant gas is compressed to 152.7 bar using multi-stage compressors with intercooling for sending to sequestration sites. Between compression stages, the condensed water is removed from the gas stream. It was assumed that an unlimited supply of water at ambient conditions (298.15 K

and 1 bar) was available and the cooling fluid temperature is set as to have a temperature difference between the cold and hot fluids be 10 °F ($\approx$6 K) [116].

5.2 Cost Calculations

5.2.1 Capital Expenditure

5.2.1.1 Design and Cost Estimation of the Absorption Column

In sizing of the packed-bed absorber to handle high fuel gas flow rates, the flow rate of the selected solvent was adjusted in two steps. Firstly, the equilibrium model of Aspen Plus was used to capture 90% of the CO_2 in the fuel gas stream, and secondly, the rate-based model of Aspen Plus along with the PC-SAFT EOS was used to refine the column size while maintaining the height to internal diameter ratio at 6 ($H/D = 6$) in order to avoid gas and liquid channeling and wall effects in the absorber.

Brown [117] proposed Equation (5.1) to calculate the cost of the column based on its volume (V) using carbon steel as the construction material.

$$CAPEX_{2017} = 10,600 \left(\frac{V}{1000}\right)^{0.7} \tag{5.1}$$

where V is in gallons. Brown [117] added a pressure factor (f_{pres}) and a material factor (f_{mat}) to adjust the cost for operating pressures and different materials rather than carbon steel. The pressure factor is expressed in Equation (5.2) and the material factor is given in Table 5.4.

$$f_{pres} = 0.0023P + 0.66 \tag{5.2}$$

where P is in psi.

Material	Material factor (f_{mat})
Carbon steel	1.0
Stainless steel	1.4
Titanium	2.0

Thus, after including the pressure and material factors, Equation (5.1) becomes:

$$CAPEX_{2017} = 10{,}600 \left(\frac{V}{1000}\right)^{0.7} (f_{pres})(f_{mat}) \tag{5.3}$$

5.2.1.2 Design of Flash Drums

There are three methods to design a flash drum:

(1) First method: it is based on the disengagement theory to calculate the gas terminal velocity as:

$$U_T = \sqrt{\frac{4gD_P(\rho_L - \rho_G)}{3C_D\rho_G}} \tag{5.4}$$

where g is the acceleration due to gravity, D_P is the liquid droplet diameter, ρ_L and ρ_G are the densities of the liquid and gas phases, respectively, and C_D is the drag force coefficient. Reynolds number is defined as:

$$Re_G = \frac{\rho_G U_T D_P}{\mu_G} \tag{5.5}$$

The relation between the drag force coefficient and Reynolds number depends on the prevailing flow regime in the flash drum [54] as follows:

Stokes' regime $\qquad\qquad Re_G < 1 \qquad\qquad C_D = \dfrac{24}{Re_G}$ $\qquad\qquad$ (5.6)

Intermediate regime $\quad 1 < Re_G < 1000 \quad C_D = \dfrac{24}{Re_G}(1 + 0.14(Re_G)^{0.7})$ $\quad$ (5.7)

Newton's regime $\qquad Re_G > 1000 \qquad\qquad C_D = 0.44 \qquad\qquad$ (5.8)

The calculated terminal velocity is then compared with the gas superficial velocity to determine whether the flashing occurs, and if the gas and liquid will separate without dragging liquid droplets in the gas moving upward.

(2) Second method: it is based on using the Sounders-Brown [118] method to determine the terminal gas velocity using Equation (5.9).

$$U_T = K \sqrt{\frac{\rho_L - \rho_G}{\rho_G}} \qquad\qquad (5.9)$$

This equation includes an empirical constant (K) defined as:

$$K = a + bP + cP^2 + dP^3 \qquad\qquad (5.10)$$

where K is in m/s and the pressure (P) is in kPa. The values of the coefficients a, b, c, and d are given in Table 5.5 for a constant droplet size of 300 μm.

Table 5.5: Coefficients in Equation (5.10) [118]

Constant	Value
a	0.015996
b	1.21×10^{-5}
c	-1.4×10^{-9}
d	5.41×10^{-14}

Combining Equations (5.4) and (5.9) gives Equation (5.11), which shows the dependency of K on the droplet size and the drag force coefficient.

$$K = \sqrt{\frac{4gD_P}{3C_D}} \qquad\qquad (5.11)$$

In this study, the diameter of the liquid droplet used was 300 µm. Once the terminal gas velocity was determined, the cross-sectional area and diameter of the flash drum were calculated using Equations (5.12) and (5.13).

$$A_{flash} = \frac{Q_G}{U_T}$$

(5.12)

$$D_{flash} = \sqrt{\frac{4A_{flash}}{\pi}}$$

(5.13)

Then, based on the flash drum pressure, the appropriate height to diameter ratios of the flash drum provided in Table 5.6 can be calculated.

Table 5.6: Height to diameter ratio of flash drums at different pressures [64]

Pressure (bar)	H/D
<10	2 − 3
~20	3 − 4
~40	4
>80	5+

(3) Third method: it is based on the method outlined by Rodwell and Riazi [64], which requires the knowledge of liquid holdup time (t_H) and surge time (t_S). The liquid holdup time is the time at which the liquid level inside the flash drum increases from a normal operation level to a high level. The surge time is the time required for the liquid level in the flash drum to fall to a low level from the normal operation level. The surge time is usually set as 25% of the holdup time [64]. Typical holdup times and calculated surge times are given in Table 5.7. Figure 5.3 shows a schematic of a flash drum.

Table 5.7: Typical holdup times and claculted surge times of flash drums [64]

Equipment in process unit	Holdup time (minutes)	Calculated Surge time (minutes)
Feed to another column	5	1.25
Feed to series of distillation columns	10	2.50
Liquid knockout drums	5	1.25
Refrigerant and reboilers	2	0.50
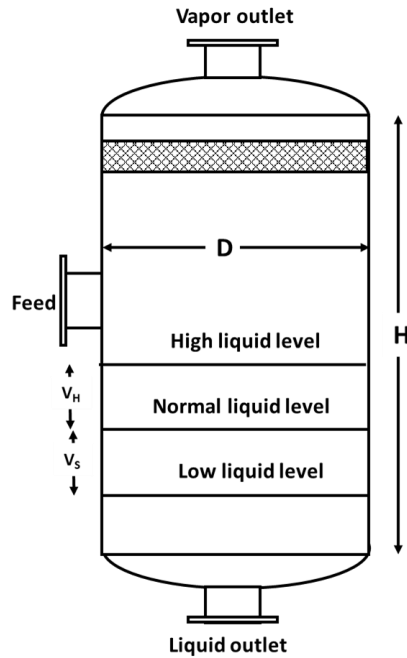
Figure 5.3: Schematic of a flash drum

The total volume covered by the holdup and surge times ($V_H + V_S$) is set to 40% of the flash drum volume. V_H and V_S are calculated using the liquid flow rate as.

$$V_H = t_H Q_L \tag{5.14}$$

$$V_S = t_s Q_L \tag{5.15}$$

Once the holdup and surge volumes are determined, the cross-sectional area and inside diameter of the flash drum are calculated using Equations (5.16) and (5.17), respectively.

$$V_H + V_S = 0.4 \, (A_{flash} H) \tag{5.16}$$

$$D_{flash} = \left(\frac{10(V_H + V_S)}{\pi(H/D)}\right)^{1/3} \tag{5.17}$$

Therefore, knowing the (*H/D*) value at a given pressure from Table 5.6, the diameter of the flash drum can be calculated using Equation (5.17). Then, the height is calculated from the ratio (*H/D*). To satisfy both the maximum gas velocity and minimum liquid holdup and surge times, the method that produces the larger diameter is used. The CAPEX of the flash drums was obtained using Equation (5.3), which is the same as that used for the absorber column cost estimates.

5.2.1.3 Total Capital Expenditure of Equipment

Table 5.8 compiles the equations to calculate the total CAPEX of the equipment used, including heat exchangers, compressors, pumps and the gas expander [117, 119, 120]. The installation factors for equipment are given in Table 5.9.

Table 5.8: Calculation of the total CAPEX of equipment [117, 119, 120]

Equipment	Equation	Comments
Heat Exchanger	$$\dot{Q} = \dot{m}c_P\Delta T$$ $$A_{HT} = \frac{\dot{Q}}{U_{HT} \cdot LMTD}$$ *LMTD*: Log mean temperature difference $$LMTD = \frac{(T_{Hin} - T_{Cout}) - (T_{Hout} - T_{Cin})}{\ln\left(\frac{T_{Hin} - T_{Cout}}{T_{Hout} - T_{Cin}}\right)}$$ $$\frac{1}{U_{HT}} = \frac{1}{h_C} + \frac{t_w}{k_{th}} + \frac{1}{h_H}$$ $$CAPEX_{2017} = 1000(0.4587A_{HT}^{0.67})(f_{pres})(f_{mat})$$	$\dot{m}$ is the mass flow rate in kg/s c_p is the specific heat capacity in J/kg.K ΔT is the temperature difference in K U_{HT} is the overall heat transfer coefficient in J/m^2.K.s A_{HT} needs to be in ft^2 to calculate the cost $CAPEX_{2017}$ f_{pres} is 1.06, 1.26, and 1.44 for pressures 200, 600, and 1000 psig respectively f_{mat} is 1 for carbon steel, and 1.4 for stainless steel
Compressors	$$W = \frac{\dot{m}(h_{out} - h_{in})}{\eta}$$ $$CAPEX_{2006} = (8400 + 3100W^{0.6})(f_{mat})$$	W is power in kW $\dot{m}$ is the mass flow rate in kg/s h is the specific enthalpy in kJ/kg f_{mat} is 1 for carbon steel and 1.3 for stainless steel η is the efficiency set to 72%
Pumps	$$W = \frac{Q_L\Delta P}{\eta}$$ $$h_d = \frac{P_{out} - P_{in}}{\rho g}$$ $$CAPEX_{2017} = 1000\left[0.683\left(\frac{Q_L \times h_d}{1000}\right)^{0.62}\right](f_{mat})$$	h_d is the developed head in ft Q_L is the solvent flow rate in gal/min f_{mat} is 1 for carbon steel and 1.8 for stainless steel η is the efficiency set to 86%
Gas Expander	$$W = \dot{m}(h_{out} - h_{in})$$ $$\log_{10} CAPEX_{2002} = (0.602 \log_{10} W + 3.49) + \log_{10} f_{mat}$$	W is power in kW $\dot{m}$ is the mass flow rate in kg/s h is the specific enthalpy in kJ/kg f_{mat} is 1 for carbon steel and 2 for stainless steel

Table 5.9. Installation factor for equipment [119]

Unit	Installation factor
Compressors	2.5
Heat exchangers	3.5
Pumps	4.0
Pressure vessels	4.0
Distillation columns	4.0

5.2.1.4 Solvent and Packing Costs

The initial cost of solvent used is estimated using Equation (5.18).

$$CAPEX_{2020} = CAPEX_{solv} \times \left(0.15V_{abs} + 0.3V_{flash}\right) \qquad (5.18)$$

where *CAPEX$_{solv}$* is the solvent cost in \$/L and *V$_{abs}$* and *V$_{flash}$* are the volumes of the absorber and flash drums in L, respectively.

5.2.1.5 Cost Adjustment

The costs calculated in previous years are adjusted to the present-day value, since the value of money could be affected by inflation and other unpredictable factors. This adjustment was made using the Chemical Engineering Plant Cost Index (CEPI) as in Equation (5.19). Table 5.10 gives the CEPI values since the year 2002.

$$CAPEX_{2020} = CAPEX_{year} \left(\frac{CEPI_{2020}}{CEPI_{year}}\right) \qquad (5.19)$$

Table 5.10. CEPI for different years [117, 119-121]

Year	CEPI
2002	390.4
2006	478.6
2012	584.6
2017	570
2020	593.6

5.2.2 Operating Expenditure

The OPEX includes the power required to operate the equipment and making up any solvent losses in the process. In addition, the annual maintenance cost is assumed to be 4% of the total CAPEX.

5.2.2.1 Power Required for Each Equipment

To calculate the power required for each equipment, an energy balance was applied on a control volume containing the equipment as given in Equation (5.20):

$$\dot{Q} + W = \dot{m}\Delta h \qquad (5.20)$$

where $\dot{Q}$ is the heat provided to the control volume, W is the work done on the control volume, $\dot{m}$ is the mass flow rate, and Δh is the change in specific enthalpy of the system.

5.2.2.2 Cost of the Chiller

In addition, for heat exchangers, a chiller was sometimes required to cool the solvent to temperatures below ambient temperatures. Based on the CO_2 capture process, the cost of a chiller was calculated knowing the energy required to reduce the coolant temperature using Equation (5.21).

$$W = \frac{2\dot{Q}}{COP} \qquad (5.21)$$

where $\dot{Q}$ is the heat transferred from the fluid to the coolant, COP is the coefficient of performance of the refrigeration cycle and the safety factor, 2, is to account for the chiller efficiency. The COP is defined by Equation (5.22) as:

$$COP \leq \frac{T_{Cin}}{T_{amb} - T_{Cin}} \qquad (5.22)$$

where T_{Cin} is the required cooling temperature and T_{amb} is the ambient temperature, which was assumed to be 298.15 K [122].

5.2.2.3 Cost of Solvent Make-Up

The cost of the solvent make-up is calculated by finding the difference between the volume of solvent required for CO_2 absorption and the recycled volume. This difference is then multiplied by the cost of the solvent in \$/L to obtain the solvent make-up cost.

$$OPEX_{solv2020} = CAPEX_{solv} \left(Q_{Lrequired} - Q_{Lrecycled} \right) \tag{5.23}$$

The total OPEX is then calculated by multiplying the total power required by the cost (\$50 per MWh) and adding the cost of make-up solvent and the annual maintenance and operating cost.

$$OPEX_{2020} = \left(C_{power} \sum W \right) + OPEX_{solv2020} + 0.04 CAPEX_{2020} \tag{5.24}$$

5.2.3 Levelized Cost of CO_2 Captured

The levelized cost of CO_2 captured (LCOC), including the total capital and operating costs per ton of CO_2 captured, was used to provide a fair quantification of the CO_2 capture process [100]. LCOC was also dependent on other factors, such as plant lifetime ($N = 30$ years), discount rate ($i = 10\%$/year), capacity factor ($f_c = 0.8$), and the capital recovery factor (f_{CR}). The capital recovery factor can be calculated using Equation (5.25). The LCOC was computed using Equation (5.26).

$$f_{CR} = \frac{i(1+i)^N}{(1+i)^N - 1} \tag{5.25}$$

The LCOC is calculated using Equation (5.26) as:

$$LCOC = \frac{f_{CR} \sum CAPEX_{2020}}{f_c \times \dot{m}_{CO2}} + \frac{\sum OPEX_{2020}}{\dot{m}_{CO2}} \tag{5.26}$$

where $\dot{m}_{CO2}$ is the CO_2 captured in ton/year.

6.0 Fuel Gas Species and Solvents Investigated

The fuel gas species used in this study and their critical properties are given in Table 6.1. The gas enters the absorber at a temperature of 308.15 K and a pressure 51.4 bar.

Table 6.1: Composition and properties of the fuel gas used [108]

Component	Mol%	Mwt (kg/kmol)	T_c (K)	P_c (bar)
CO_2	40.7829	44.0	304.2	73.8
H_2	56.8223	2.0	33.2	13.0
CH_4	0.0906	16.0	190.8	46.4
CO	0.815	28.0	133.2	35.0
Ar	0.7144	39.9	151.2	48.7
H_2O	0.1208	18.0	647.1	220.6
N_2	0.654	28.0	126.2	33.9
H_2S	0.000	34.1	373.4	89.7

35 different solvents were investigated and categorized in Table 6.2. The structures of these solvents are given in Table 6.3. These solvents cover a wide range of functional groups and a wide range of cost, molecular weights, and critical properties as shown in Table 6.4.

All solvents listed in Table 6.2, except NMP, PC, methanol, and THF, were used in the CO_2 capture process schematically shown in Figure 5.1. NMP, PC, methanol, and THF were used in the process schematically shown in Figure 5.2.

Table 6.2: Investigated solvents in their respective categories

Category	Solvent	Name
Ionic Liquids (ILs)	[aPy][Tf$_2$N]	Allyl-pyridinium bis(trifluorosulfonyl)imide
	[bmim][BF$_4$]	1-Butyl-3-methylimidazolium tetrafluoroborate
	[bmim][MeSO$_4$]	1-Butyl-3-methylimidazolium methylsulfate
	[bmim][PF$_6$]	1-Butyl-3-methylimidazolium hexafluorophosphate
	[bmim][Tf$_2$N]	1-Butyl-3-methylimidazolium bis(trifluorosulfonyl)imide
	[bmPyr][Tf$_2$N]	1-Butyl-1-methylpyrrolidinium bis(trifluorosulfonyl)imide
	[emim][BF$_4$]	1-Ethyl-3-methylimidazolium tetrafluoroborate
	[emim][Tf$_2$N]	1-Ethyl-3-methylimidazolium bis(trifluorosulfonyl)imide
	[hmim][(C$_2$F$_5$)$_3$PF$_3$]	1-Hexyl-3-methylimidazolium tris(pentafluoroethyl) trifluorophosphate
	[hmim][Tf$_2$N]	1-Hexyl-3-methylimidazolium bis(trifluorosulfonyl)imide
	[omim][Tf$_2$N]	1-Octyl-3-methylimidazolium bis(trifluorosulfonyl)imide
Hydrocarbons (HCs)	1-Heptene	1-Heptene
	1-Octene	1-Octene
	n-Decane	n-Decane
	n-Octane	n-Octane
	n-Tetradecane	n-Tetradecane
Oxygenated-Hydrocarbons (OHCs)	1-Hexanol	1-Hexanol
	1-Nonanal	1-Nonanal
	1-Octanol	1-Octanol
	DES	Diethyl sebacate
	NBAc	n-Butyl acetate
	NPAc	n-Propyl acetate
	TBP	Tributyl phosphate
Nitrogenized-Hydrocarbons (NHCs)	DMF	n,n-Dimethyl formamide
	PN	Propionitrile
Cyclic-Hydrocarbons (CycHCs)	cis-Decalin	cis-Decalin
	Cyclohexanone	Cyclohexanone
	MNPh	1-methylnaphthalene
	NMP	n-Methyl-2-pyrrolidone
	PC	Propylene carbonate
Polymers	PEGDME	Polyethylene glycol dimethyl ether
	PEGPDMS-1	Polyethylene glycol polydimethyl siloxane-1
	PEGPDMS-3	Polyethylene glycol polydimethyl siloxane-2
Subcooled	Methanol	Methanol
	THF	Tetrahydrofuran

Table 6.3: Structures of the solvents used
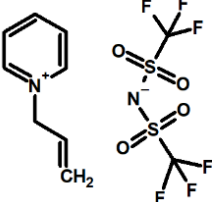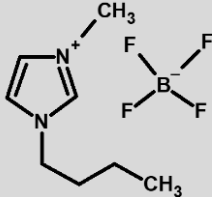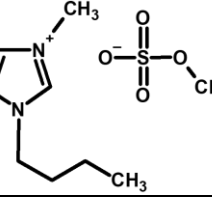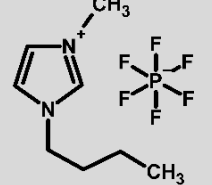
Category	Solvent	Structure
ILs	[aPy][Tf₂N]	
	[bmim][BF₄]	
	[bmim][MeSO₄]	
	[bmim][PF₆]	

Table 6.3 continued.
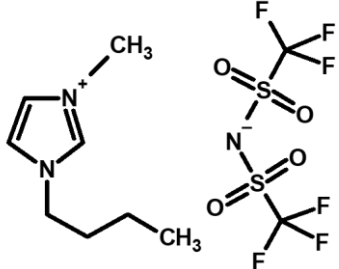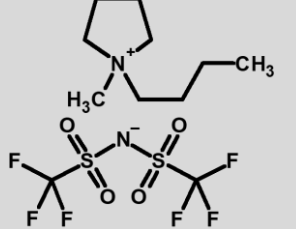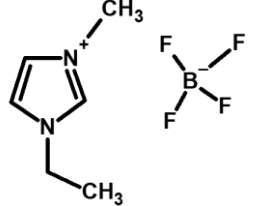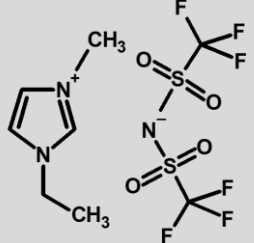
Category	Solvent	Structure
ILs	[bmim][Tf₂N]	
	[bmPyr][Tf₂N]	
	[emim][BF₄]	
	[emim][Tf₂N]	

Table 6.3 continued.
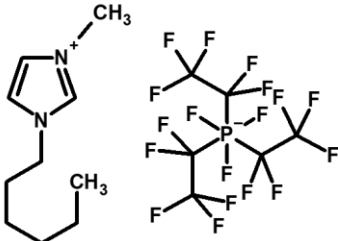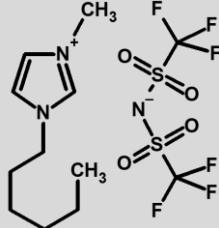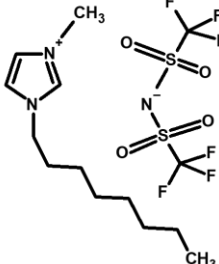
Category	Solvent	Structure
ILs	[hmim][(C₂F₅)₃PF₃]	
	[hmim][Tf₂N]	
	[omim][Tf₂N]	

Table 6.3 continued.
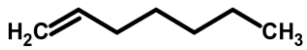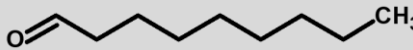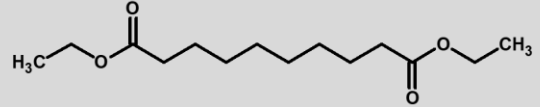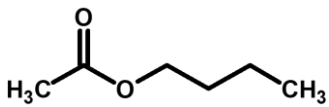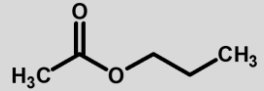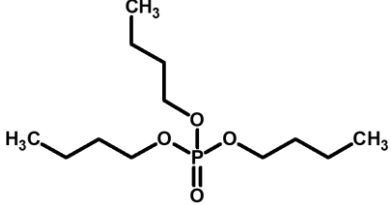
Category	Solvent	Structure
HCs	1-Heptene	
	1-Octene	
	n-Decane	
	n-Octane	
	n-Tetradecane	
OHCs	1-Hexanol	
	1-Nonanal	
	1-Octanol	
	DES	
	NBAc	
	NPAc	
	TBP	

Table 6.3 continued.
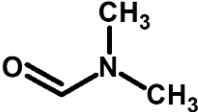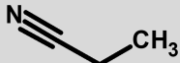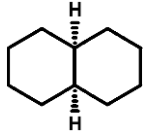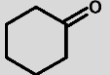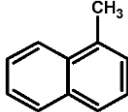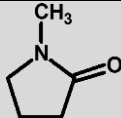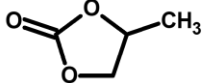
Category	Solvent	Structure
NHCs	DMF	
	PN	
CycHCs	cis-Decalin	
	Cyclohexanone	
	MNPh	
	NMP	
	PC	

Table 6.3 continued.
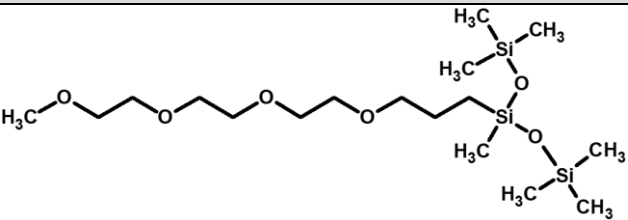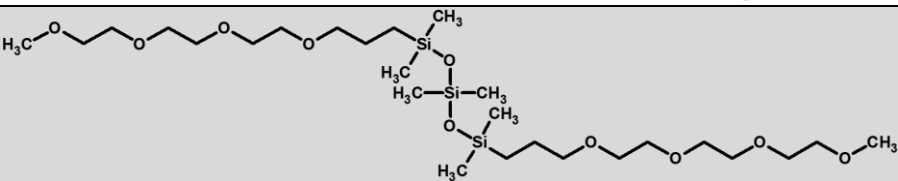
Category	Solvent	Structure
Polymers	PEGDME	
	PEGPDMS-1	
	PEGPDMS-3	
Subcooled	Methanol	H₃C—OH
	THF	

Table 6.4: Costs, molecular weights, and critical properties of the solvents used

Category	Solvent	CAPEX$_{solv}$ ($/L)	MWt (kg/kmol)	T_c (K)	P_c (bar)
ILs	[aPy][Tf$_2$N]*	40.00	401.33	1297.48	30.89
	[bmim][BF$_4$]*	18.11	226.02	643.18	20.38
	[bmim][MeSO$_4$]*	18.14	250.32	1081.64	36.10
	[bmim][PF$_6$]*	14.65	284.18	719.39	17.28
	[bmim][Tf$_2$N]*	14.37	419.38	1269.93	27.65
	[bmPyr][Tf$_2$N]*	32.17	422.42	1209.16	24.84
	[emim][BF$_4$]*	17.34	197.98	596.23	23.59
	[emim][Tf$_2$N]*	30.38	391.32	1249.31	32.65
	[hmim][(C$_2$F$_5$)$_3$PF$_3$]*	34.16	612.30	861.54	8.87
	[hmim][Tf$_2$N]*	41.50	448.43	815.00	16.11
	[omim][Tf$_2$N]*	26.44	475.48	1317.82	20.98
HCs	1-Heptene	1.39	98.19	537.47	28.52
	1-Octene	2.13	112.22	566.58	26.76
	n-Decane	0.73	142.29	618.05	21.04
	n-Octane	0.70	114.23	568.78	24.86
	n-Tetradecane	0.76	198.39	692.49	15.67
OHCs	1-Hexanol	0.82	102.18	610.40	34.13
	1-Nonanal	6.62	142.24	658.50	26.81
	1-Octanol	0.82	130.23	651.33	28.19
	DES	0.96	258.36	731.00	15.35
	NBAc	0.88	116.16	575.44	31.61
	NPAc	0.88	102.13	549.69	33.95
	TBP	1.96	266.32	751.00	15.09
NHCs	DMF	0.76	73.10	649.60	44.09
	PN	0.78	55.08	561.26	42.60
CycHCs	cis-Decalin	0.45	138.25	702.22	30.43
	Cyclohexanone	0.94	98.15	664.90	44.40
	MNPh	1.02	142.20	770.72	35.40
	NMP	2.00	99.13	721.74	45.32
	PC	0.60	102.09	762.70	40.85
Polymers	PEGDME	4.00	280.00	605.00	51.86
	PEGPDMS-1^	4.00	426.77	713.77	9.44
	PEGPDMS-3^	4.00	617.01	497.72	6.89
Subcooled	Methanol	0.18	32.04	512.68	80.65
	THF	0.62	72.11	539.99	52.80

*Critical properties predicted using group contribution by Valderrama and Rojas [123]

^ Critical properties predicted using group contribution by Lydersen [124]

6.1 Properties of the Solvents Used

6.1.1 Density and Vapor Pressure

The parameters of the PC-SAFT EOS for the pure solvents used, given in Table 6.5, were regressed using the corresponding density and vapor pressure experimental data available in the literature. The average absolute relative error (ARRE), defined by Equation (6.1), is presented in the table. As can be seen in this table, the PC-SAFT EOS is able to predict the density of the pure solvents with AARE values ranging from 0.010 to 0.455%.

$$AARE = \frac{1}{N} \sum_{i=1}^{N} \left| \frac{Predicted\ Value_i - Experimental\ Value_i}{Experimental\ Value_i} \right| \times 100\% \qquad (6.1)$$

Table 6.5: PC-SAFT parameters of the solvents investigated

Category	Solvent	m	σ	ϵ/k_B (K)	κ^{AB} ($\times 10^4$)	ϵ^{AB}/k_B (K)	Temperature range (K)	Density AARE (%)	Experimental data references
ILs	[aPy][Tf$_2$N]	4.306	4.552	367.249	900	4,800	293.15 – 328.15	0.01	[100]
	[bmim][BF$_4$]	3.594	4.394	523.717	127.27	5,000	293.15 – 353.15	0.039	[125]
	[bmim][MeSO$_4$]	2.751	4.974	591.083	3,634.73	5,000	283.15 – 333.15	0.106	[126-128]
	[bmim][PF$_6$]	3.411	4.614	503.833	70.07	6,000	283.15 – 353.15	0.021	[125, 129]
	[bmim][Tf$_2$N]	4.195	4.745	375.589	2,995.84	7,000	273.15 – 363.15	0.054	[130]
	[bmPyr][Tf$_2$N]	4.515	4.675	361.696	3,000	7,000	283.15 – 393.15	0.173	[131-133]
	[emim][BF$_4$]	4.237	3.915	530.741	482.87	4,259.41	278.15 – 343.15	0.243	[134-137]
	[emim][Tf$_2$N]	2.235	5.133	549.789	30	2,006.32	278.15 – 391.29	0.084	[138, 139]
	[hmim][(C$_2$F$_5$)$_3$PF$_3$]	7.207	4.379	342.579	3,000	5,000	267.25 – 359.73	0.048	[140-142]
	[hmim][Tf$_2$N]	3.114	5.526	508.025	1,000	5,000	258.15 – 373.15	0.148	[143-146]
	[omim][Tf$_2$N]	5.192	4.65	280.667	2,000	7,500	273.15 – 473.15	0.145	[147-149]
HCs	1-Heptene	3.298	3.814	243.197	0	0	173.16 – 360.03	0.261	[150-154]
	1-Octene	3.663	3.838	246.024	0	0	173.16 – 511.41	0.3	[152, 155-158]
	n-Decane	4.58	3.854	246.42	0	0	273.15 – 333.12	0.136	[159-165]
	n-Octane	4.245	3.66	178.131	10,000	1,400	273.15 – 343.12	0.021	[166-168]
	n-Tetradecane	7.782	3.552	218.423	0	0	273.15 – 333.13	0.137	[169-174]
OHCs	1-Hexanol	3.168	3.806	255.37	97.8	2,800	273.15 – 358.15	0.059	[172, 175-184]
	1-Nonanal	5.406	3.498	239.727	0	0	288.15 – 318.15	0.455	[185-189]
	1-Octanol	4.246	3.732	243.169	100	2,950	273.15 – 333.15	0.115	[190-197]
	DES	8.865	3.482	223.678	1,500	2,400	291.44 – 358.92	0.017	
	NBAc	3.438	3.735	244.647	2,588.22	32.41	273.15 – 393.15	0.169	[198-204]
	NPAc	3.088	3.696	237.773	1.86	1,816.97	273.10 – 503.16	0.308	[205-209]
	TBP	5.927	4.034	258.823	1,500	1,500	288.04 – 357.20	0.066	[210-215]
NHCs	DMF	2.91	3.333	320.599	0.68	1,843.59	263.15 – 333.15	0.069	[216-223]
	PN	1.601	3.767	160.175	900	3,000	273.15 – 368.17	0.166	[224-227]

Table 6.5 continued.

Category	Solvent	m	σ	ϵ/k_B (K)	κ^{AB} (×10^4)	ϵ^{AB}/k_B (K)	Temperature range (K)	Density AARE (%)	Experimental data references
CycHCs	cis-Decalin	3.138	4.102	321.945	0	0	273.15 – 388.13	0.096	[169, 228-233]
	Cyclohexanone	2.442	3.907	350.276	0	0	281.35 – 364.62	0.159	[234-238]
	MNPh	3.176	3.986	359.921	0	0	273.15 – 473.15	0.373	[239-243]
	NMP	4.055	3.195	231.67	19,616.21	1,445.05	275.15 – 373.15	0.199	[244-254]
	PC	4.002	3.091	240.009	24,945.4	1,768.62	273.00 – 392.97	0.083	[255-260]
Polymers	PEGDME*	11.605	3.095	169.758	2,254.60	2,500	273.00 – 392.97	0.083	[38]
	PEGPDMS-1	40.606	2.482	199.17	0	0	293.15 – 323.15	0.012	[100]
	PEGPDMS-3	42.069	2.76	231.078	0	0	288.15 – 353.15	0.072	[261]
Subcooled	Methanol	2.244	2.842	182.561	652.89	2,580.08	203.15 – 340.00	0.22	[262-285]
	THF	2.162	3.689	289.256	0	0	213.20 – 323.15	0.237	[286-292]

*Field and Brasington [38] is based on Aspen Plus simulations.

6.1.2 Viscosity

The viscosities of the solvents used were modeled as a function of temperature using the experimental data found in the literature. Equation (6.2) shows the general form in which the viscosity is calculated, while the constants *a* through *e* for each solvent are given in Table 6.6 along with the AARE and temperature range. As can be seen in the table, the viscosity can be calculated with low AARE values ranging from 0.10 to 8.12%.

$$\ln \mu_L = a + \frac{b}{T} + c \ln T + d\, T^e \tag{6.2}$$

Table 6.6: Constants for Equation (6.2) to calculate the solvent viscosity

Category	Solvent	a	b	c	d	e	Temperature range (K)	Viscosity AARE (%)	Experimental data references
ILs	[aPy][Tf$_2$N]	5.28	0	0	-0.0297	1	293.15 – 323.15	1.4	[100]
	[bmim][BF$_4$]	-142.7	10,000	18.76	0	0	293.15 – 353.15	4.94	[125, 293]
	[bmim][MeSO$_4$]	-168.3	11,544	22.45	0	0	283.15 – 333.15	8.12	[294-296]
	[bmim][PF$_6$]	-130.7	10,000	16.83	0	0	283.15 – 363.15	2.84	[125, 297]
	[bmim][Tf$_2$N]	-194.8	11,851	26.69	0	0	273.15 – 353.15	0.647	[130]
	[bmPyr][Tf$_2$N]	-196.1	12,165	26.8	0	0	273.15 – 363.15	1.8	[133, 298]
	[emim][BF$_4$]	-146.1	9,217	19.64	0	0	278.15 – 343.15	4.13	[134, 135, 137]
	[emim][Tf$_2$N]	-49.29	4,492.2	5.411	0	0	293.39 – 388.19	1.93	[139]
	[hmim][(C$_2$F$_5$)$_3$PF$_3$]	-183.8	11,965	24.79	0	0	293.15 – 343.15	0.305	[141]
	[hmim][Tf$_2$N]	-213	13,009	29.27	0	0	286.15 – 370.15	4.46	[145]
	[omim][Tf$_2$N]	-145.7	10,000	19.27	0	0	278.00 – 358.00	2.72	[147, 299]
HCs	1-Heptene	-10.943	900.64	0	0	0	298.15 – 360.03	0.308	[154]
	1-Octene	-10.871	963.85	0	0	0	283.10 – 386.52	1.44	[158, 300]
	n-Decane	-11.503	1,320.1	0	0	0	273.15 – 333.12	0.978	[159, 160, 301, 302]
	n-Octane	-11.225	1,084.8	0	0	0	273.38 – 395.20	0.588	[303]
	n-Tetradecane	-12.358	1,844.1	0	0	0	283.10 – 335.13	1.83	[171, 304-306]
OHCs	1-Hexanol	-14.509	2,718.2	0	0	0	278.15 – 348.13	1.05	[307-309]
	1-Nonanal	-9.935	1,001.4	0	0	0	298.15 – 318.15	0.1	[185]
	1-Octanol	-14.209	2,775.4	0	0	0	283.15 – 460.15	4.24	[310-314]
	DES	-12.305	2,091.5	0	0	0	292.88 – 359.05	1.21	
	NBAc	-11.593	1,277.4	0	0	0	293.15 – 343.15	0.879	[315-317]
	NPAc	-11.325	1,137	0	0	0	273.10 – 373.07	0.606	[318, 319]
	TBP	-12.16	1,925.2	0	0	0	288.15 – 359.05	1.83	[211, 212, 320, 321]

Table 6.6 continued.

Category	Solvent	*a*	*b*	*c*	*d*	*e*	Temperature range (K)	Viscosity AARE (%)	Experimental data references
NHCs	DMF	-10.788	1,101.6	0	0	0	263.15 – 353.15	1.84	[223, 322-324]
	PN	-6.0032	758.72	-0.7604	0	0	293.14 – 353.12	1.12	[227, 325]
CycHCs	cis-Decalin	-11.921	1,823.8	0	0	0	273.15 – 372.02	1.13	[169, 229, 232, 233]
	Cyclohexanone	-12.61	1,913.7	0	0	0	253.00 – 322.99	1.8	[326, 327]
	MNPh	41.329	-2,345	-7.24	2.56×10^{10}	-4.09	273.15 – 473.15	0.767	[239, 328, 329]
	NMP	-11.279	1,457	0	0	0	288.15 – 323.15	1.69	[250, 330-332]
	PC	-11.202	1,551.3	0	0	0	273.00 – 392.97	1.87	[256, 257, 260, 333]
Polymers	PEGDME	-43.324	6,708.3	13.95	-55.31	0.0047	253.91 – 420.48	2.82	[38, 334, 335]
	PEGPDMS-1	14.916	941.77	-4.106	0	0	293.15 – 323.15	3.55	[100]
	PEGPDMS-3	-12.376	2,381.3	0	0	0	288.16 – 323.11	1.23	[261]
Subcooled	Methanol	-25.317	1,789.2	2.069	0	0	203.15 – 340.00	3.15	[267, 336-346]
	THF	-13.705	1,005.2	0.4695	0	0	203.20 – 332.98	1.29	[256, 286, 292]

6.1.3 Surface Tension

The surface tensions of the solvents used were modelled using the Equation (6.3), which is a function of the operating temperature and the solvents critical temperature given in Table 6.7. Experimental data from the literature were used to determine the values of the constants a and b. Table 6.7 shows the values of these constants along with the AARE. As can be seen, the surface tension can be calculated with an AARE ranging from 0.0438 to 2.66%.

$$\sigma_L = a \left(1 - \frac{T}{T_c}\right)^b \qquad (6.3)$$

Table 6.7: Constants for Equation (6.3) to calculate the solvent surface tension

Category	Solvent	a	b	Temperature range (K)	Surface Tension AARE (%)	Experimental data references
ILs	[aPy][Tf$_2$N]	0.051	1.422	298.15 – 353.15	0.33	[100]
	[bmim][BF$_4$]	0.0627	0.5521	293.15 – 323.15	0.121	[347]
	[bmim][MeSO$_4$]	0.0802	1.81	283.00 – 368.10	1.25	[295, 348]
	[bmim][PF$_6$]	0.0657	0.6089	298.00 – 393.00	0.178	[349]
	[bmim][Tf$_2$N]	0.048	1.4	278.75 – 351.56	0.474	[138, 350-352]
	[bmPyr][Tf$_2$N]	0.0468	1.204	288.15 – 323.15	0.0476	[353]
	[emim][BF$_4$]	0.0603	0.2567	278.15 – 338.15	0.113	[354]
	[emim][Tf$_2$N]	0.0562	1.641	278.75 – 328.15	0.346	[138]
	[hmim][(C$_2$F$_5$)$_3$PF$_3$]	0.0501	1.087	267.03 – 360.23	0.225	[142]
	[hmim][Tf$_2$N]	0.0502	1.77	283.17 – 348.15	1.25	[155, 350, 352, 355]
	[omim][Tf$_2$N]	0.0505	2.011	283.15 – 512.60	2.21	[149, 356]
HCs	1-Heptene	0.0527	1.207	273.15 – 353.12	0.295	[357, 358]
	1-Octene	0.0538	1.242	273.15 – 373.12	0.721	[155, 357, 358]
	n-Decane	0.0506	1.027	273.15 – 333.15	0.712	[359-361]
	n-Octane	0.0502	1.152	273.00 – 359.12	1.09	[362-369]
	n-Tetradecane	0.0509	0.8924	273.15 – 333.12	0.135	[359]
OHCs	1-Hexanol	0.0462	0.8924	278.15 – 408.13	2.18	[308, 370, 371]
	1-Nonanal*	0.0620	1.222			
	1-Octanol	0.0478	0.9722	273.15 – 503.16	2.66	[372-375]
	DES	0.0643	1.314	293.24 – 360.22	0.053	
	NBAc	0.0571	1.157	293.14 – 359.52	0.864	[376, 377]
	NPAc	0.0596	1.194	273.25 – 333.22	1.91	[378-380]
	TBP	0.0496	1.171	288.15 – 359.05	0.0438	[381]

Table 6.7 continued.

Category	Solvent	*a*	*b*	Temperature range (K)	Surface Tension AARE (%)	Experimental data references
NHCs	DMF	0.079	1.303	277.85 – 327.89	1.48	[219, 374, 382]
	PN	0.06	1.089	273.15 – 353.15	0.0494	[383]
CycHCs	cis-Decalin	0.0646	1.292	243.07 – 453.14	0.993	[384]
	Cyclohexanone	0.0721	1.258	288.14 – 353.13	0.415	[385, 386]
	MNPh	0.0673	1.188	291.44 – 360.32	0.077	[387]
	NMP	0.0724	1.062	277.84 – 337.88	2.15	[219, 330, 388]
	PC	0.085	1.466	276.67 – 540.37	1.37	[389-391]
Polymers	PEGDME^	0.085	1.466	276.67 – 540.37	1.37	[38]
	PEGPDMS-1	0.0408	1.152	293.15 – 343.15	0.297	[100]
	PEGPDMS-3	0.061	1.12	298.15	0.37	[392]
Subcooled	Methanol	0.0434	0.7738	198.10 – 353.13	1.39	[269, 385, 393-398]
	THF	0.0696	1.184	288.15 – 353.13	0.808	[385, 399-401]

*Brock-Bird Group Contribution method used [402].
^Field and Brasington [38] is based on Aspen Plus simulations.

6.1.4 Carbon Dioxide Solubility

To accurately predict the solubility of CO_2 in each solvent, the PC-SAFT EOS was used for the VLE calculations. Table 6.8 shows the constants of Equation (A.17) used to calculate the binary interaction parameters, k_{ij}, of CO_2 and the solvent. The AARE values of CO_2 solubilities are also given in the table and as can be seen, the PC-SAFT EOS can predict the solubility of CO_2 in the solvents used up to a CO_2 partial pressure of 60 bar with the highest AARE of 24.81% for CO_2-1-octanol system. The AARE values of the other CO_2-solvent systems are lower than that value varying from 2.71 to 16.19%.

Table 6.8: Constants used to calculate binary interaction parameter of CO_2 with solvents

Category	Solvent	a_{ij}	b_{ij}	c_{ij}	d_{ij}	e_{ij}	Temperature range (K)	AARE (%)	Experimental data references
ILs	[aPy][Tf₂N]	0.16	0	0	0	0	298.15 – 313.15	8.19	[100]
	[bmim][BF₄]	0.13	0	0	0	0	283.15 – 323.15	13.46	[403]
	[bmim][MeSO₄]	0.247	0	0	0	0	293.20 – 353.10	2.71	[404]
	[bmim][PF₆]	0.165	0	0	0	0	283.15 – 323.15	5.37	[403]
	[bmim][Tf₂N]	-0.156	0	0	0.677	-0.296	283.15 – 323.15	12	[403]
	[bmPyr][Tf₂N]	-0.0223	0	0	0.305	-0.111	293.10 – 413.20	6.64	[132]
	[emim][BF₄]	0.545	0	0	-0.858	0.364	298.15 – 353.15	9.12	[405, 406]
	[emim][Tf₂N]	0.139	0	0	-0.162	0.114	295.10 – 323.70	12.27	[407]
	[hmim][(C₂F₅)₃PF₃]	0.11	0	0	0	0	298.15 – 333.13	14.34	[408]
	[hmim][Tf₂N]	0.26	0	0	0	0	293.15 – 373.15	4.13	[143]
	[omim][Tf₂N]	0.0718	0	0	0.239	-0.159	303.15 – 353.15	10.94	[409, 410]
HCs	1-Heptene	-0.644	0	0	1.316	-0.556	303.14 – 343.13	8.74	[411]
	1-Octene	0.135	0	0	0	0	313.15 – 353.15	4.27	[412]
	n-Decane	0.481	0	0	-0.605	0.285	277.59 – 323.20	7.75	[413-415]
	n-Octane	0.09	0	0	0	0	298.20 – 333.20	12.47	[416-421]
	n-Tetradecane	8.474	-12.624	-20.8	0.313	3.961	290.00 – 323.20	3.03	[422, 423]
OHCs	1-Hexanol	0.135	0	0	0	0	293.15 – 313.15	12.54	[424]
	1-Nonanal	0.0017	0	0	0.0745	0	313.15 – 333.15	7.71	[412, 425]
	1-Octanol	0.137	0	0	0	0	308.15 – 348.15	24.81	[426-429]
	DES	-0.0494	0	0	0.0994	0	292.88 – 359.05	3.96	
	NBAc	0.03	0	0	0	0	213.20 – 353.20	16.19	[430]
	NPAc	-0.07	0	0	0	0	303.15 – 323.15	9.37	[431]
	TBP	0.1	0	0	0	0	298.15	7.21	[432]

Table 6.8 continued.

Category	Solvent	a_{ij}	b_{ij}	c_{ij}	d_{ij}	e_{ij}	Temperature range (K)	AARE (%)	Experimental data references
NHCs	DMF	0.04	0	0	0	0	293.95 – 338.05	9.88	[433, 434]
	PN	0.005	0	0	0	0	298.15	7.68	[432]
CycHCs	cis-Decalin	0.22	0	0	0	0	292.75 – 352.95	14.8	[435]
	Cyclohexanone	-0.372	0	0	1.0375	-0.561	298.15 – 313.15	5.62	[436-438]
	MNPh	0.178	0	0	0	0	308.19 – 328.19	8.71	[439]
	NMP	-12.534	-4.224	-16.85	20.772	-3.997	273.10 – 313.19	12	[440-444]
	PC	-0.164	0	0	0.408	-0.2334	273.10 – 327.66	5.24	[445-448]
Polymers	PEGDME	0.219	-0.171	0	0	0	298.15 – 333.15	5.27	[38]
	PEGPDMS-1	-0.03	0	0	0	0	298.15 – 313.15	8.46	[100]
	PEGPDMS-3	0.0794	0	0	-0.0994	0	298.15 – 313.15	6.12	[261]
Subcooled	Methanol	0	0.0099	0.0044	0	0	213.15 – 273.15	3.43	[449-453]
	THF	0.0018	0.0195	0.212	0.00204	0.0019	298.15 – 333.00	3.59	[442, 454, 455]

6.1.5 Hydrogen Solubility

The solubility of H_2 in each solvent used was determined using the PC-SAFT EOS. The constants of Equation (A.17) used to calculate the binary interaction parameter between H_2 and the solvents are given in Table 6.9 along with the AARE values. As can be seen, the AARE values for the majority of H_2-solvent used are low ranging from 0.23 to 18.3%. [aPy][Tf$_2$N] showed a higher AARE than the other solvents at 51.85% due to the large deviations in the data.

Table 6.9: Constants used to calculate binary interaction parameter of H₂ with solvents

Category	Solvent	a_{ij}	b_{ij}	c_{ij}	d_{ij}	e_{ij}	Temperature range (K)	AARE (%)	Experimental data references
ILs	[aPy][Tf₂N]	3.649	0	0	-3.379	0	298.15 – 313.15	51.85	[100]
	[bmim][BF₄]	-1.029	0	0	-0.0175	0.2878	314.09 – 342.75	2.12	[456]
	[bmim][MeSO₄]	-1.5064	0	0	1.7336	-0.5556	293.30 – 413.15	1.26	[457]
	[bmim][PF₆]	-2.2938	0	0	2.8559	-1.1112	313.05 – 353.10	0.554	[458]
	[bmim][Tf₂N]	0.73272	0.15517	0	0.14335	0.01184	333.15 – 453.15	3.89	[459]
	[bmPyr][Tf₂N]	-1.2419	0	0	1.6073	-0.5139	293.20 – 413.20	0.668	[132]
	[emim][BF₄]	-1.7432	0	0	0.2982	0	313.20 – 333.20	3.7	[460]
	[emim][Tf₂N]	-1.1915	0	0	1.0544	-0.35	313.15 – 423.15	1.31	[461]
	[hmim][(C₂F₅)₃PF₃]	-2.4281	0	0	4.0571	-2.2223	302.30 – 343.40	9.58	[462]
	[hmim][Tf₂N]	-1.13	0	0	1.3219	-0.4163	293.20 – 413.20	1.3	[463]
	[omim][Tf₂N]	-0.1451	0	0	0.4107	0	303.15 – 332.85	1.7	[464]
HCs	1-Heptene	1.1459	0	0	-1.9735	0.8164	333.18 – 473.16	4.05	[465]
	1-Octene	-0.8196	0	0	0.6261	0	313.15 – 333.15	1.8	[412]
	n-Decane	0.328	0	0	-0.2982	0	328.00 – 428.00	4.09	[47]
	n-Octane	74.557	0	0	-143.27	68.787	295.00 – 323.14	2.09	[466, 467]
	n-Tetradecane	7.3248	0	0	-11.268	4.3558	328.00 – 428.00	1.79	[47]
OHCs	1-Hexanol	-0.1	0	0	0	0	298.15 – 373.15	2.29	[468]
	1-Nonanal	-0.9263	0	0	0.5963	0	313.15 – 333.15	3.17	[412]
	1-Octanol	-0.13	0	0	0	0	273.32 – 317.95	3.27	[467, 469]
	DES	-0.23	0	0	0	0	298.2	1.14	
	NBAc	-0.18	0	0	0	0	291	4.19	[470]
	NPAc	-0.215	0	0	0	0	291	3.91	[470]
	TBP	-0.14	0	0	0	0	313.15	0.235	[471]

Table 6.9 continued.

Category	Solvent	a_{ij}	b_{ij}	c_{ij}	d_{ij}	e_{ij}	Temperature range (K)	AARE (%)	Experimental data references
NHCs	DMF	-1.0877	0	0	1.1668	-0.4741	298.14 – 373.12	2.65	[466]
	PN	0.85	0	0	0	0	298.15	11.7	[432]
CycHCs	cis-Decalin	-0.05	0	0	0	0	303.15	0.76	[472]
	Cyclohexanone	58.79	0	0	-110.54	51.749	303.14 – 333.13	8.35	[473, 474]
	MNPh	-0.1114	0	0	0.0596	0	462.16 – 701.54	8.82	[475]
	NMP	-0.16	0	0	0	0	298.14 – 373.12	1.22	[466]
	PC	-0.41	0	0	0	0	298.15	9.19	[476]
Polymers	PEGDME*	12.128	-11.622	0	0	0			[38]
	PEGPDMS-1	-0.73	0	0	0	0	298.15 – 313.15	6.14	[100]
	PEGPDMS-3	-0.73	0	0	0	0	298.15 – 313.15	4.32	[392]
Subcooled	Methanol	-30.963	0	0	69.113	-38.944	243.06 – 278.01	18.3	[450, 477, 478]
	THF	-0.15	0	0	0	0	298.14 – 373.12	1.14	[466]

*Field and Brasington [38] is based on Aspen Plus simulations.

6.1.6 Water-Solvent Interaction

The interaction between water and the solvents used is an important criterion for determining the hydrophilicity of the solvents. Table 6.10 shows the constants of Equation (A.17) used to calculate the binary interaction between water and the solvents for the PC-SAFT EOS. As can be seen the AARE ranges from 0.114 to 19.13% and the majority of most hydrophilic solvents are the subcooled solvents (methanol and THF) due to the very low temperatures. They are followed by NMP which will also requires an additional distillation column to remove water before recycling the solvent. Solvents with water partial pressures below 0.005 bar are considered hydrophilic and will follow the process presented in Figure 5.2.

Table 6.10: Constants used to calculate the binary interaction parameter of H₂O-solvent systems

Category	Solvent	a_{ij}	b_{ij}	c_{ij}	d_{ij}	e_{ij}	Temperature range (K)	AARE (%)	Experimental data references	P^*_{H2O} for 10 mol% H₂O at 298.15 K (bar)
ILs	[aPy][Tf₂N]	0.300	0	0	0	0				0.035644
	[bmim][BF₄]	0.0906	0	0	0	0				0.0323259
	[bmim][MeSO₄]	0.654	0	0	0	0				0.035644
	[bmim][PF₆]	0.160	0	0	0	0	288.15 – 323.15	18.16	[403]	0.0136668
	[bmim][Tf₂N]	0.400	0	0	0	0				0.035644
	[bmPyr][Tf₂N]	0.400	0	0	0	0				0.035644
	[emim][BF₄]	-0.0428	0	0	0	0	298.15	0.660	[479]	0.0286455
	[emim][Tf₂N]	0.400	0	0	0	0				0.035644
	[hmim][(C₂F₅)₃PF₃]	-0.1826	0	0	0.2485	0	303.40 – 315.10	25.54	[480]	0.0109936
	[hmim][Tf₂N]	0.150	0	0	0	0				0.00917266
	[omim][Tf₂N]	0.400	0	0	0	0				0.035644
HCs	1-Heptene	-0.0566	0	0	0	0	283.14 – 294.34	0.114	[481]	0.1078973
	1-Octene	0.09716	0	0	0	0	310.93 – 539.21	19.13	[482]	0.0356577
	n-Decane	-97.376	0	0	99.982	-25.557	573.20 – 340.05	0.260	[483]	0.0374409
	n-Octane	0.0695	0	0	0	0				0.035669
	n-Tetradecane	0	0	0	0	0				0.0356628
OHCs	1-Hexanol	0.050	0	0	0	0	294.15 – 313.14	15.25	[484]	0.0149932
	1-Nonanal	0	0	0	0	0				0.0361247
	1-Octanol	1.0499	0	0	-2.1094	1.1112	293.15 – 333.13	18.89	[485]	0.0159397
	DES	0.150	0	0	0	0				0.0356441
	NBAc	-0.010	0	0	0	0				0.01963
	NPAc	0	0	0	0	0				0.035668
	TBP	1.6196	0	0	-3.2751	1.6205	313.15	5.15	[484]	0.00692476

Table 6.10 continued.

Category	Solvent	a_{ij}	b_{ij}	c_{ij}	d_{ij}	e_{ij}	Temperature range (K)	AARE (%)	Experimental data references	P^*_{H2O} for 10 mol% H_2O at 298.15 K (bar)
NHCs	DMF	3.486	0	0	-6.2826	2.77779	303.15 – 343.15	23.88	[486]	0.0164448
	PN	0	0	0	0	0				0.027319
CycHCs	cis-Decalin	0	0	0	0	0				0.0324553
	Cyclohexanone	0.005	0	0	0	0	293.14 – 323.13	6.76	[487]	0.030587
	MNPh	0.180	0	0	0	0	573.05 – 673.15	10.83	[488]	0.0357378
	NMP	-0.110	0	0	0	0	343.15 – 380.24	0.476	[251, 489]	0.0019966
	PC	0.080	0	0	0	0	273.15 – 298.14	16.28	[490]	0.0191075
Polymers	PEGDME*	-1.1201	1.0228	0	0	0			[38]	0.00549951
	PEGPDMS-1	0	0	0	0	0				0.029505
	PEGPDMS-3	0	0	0	0	0				0.029006
Subcooled	Methanol	-0.010	0	0	0	0	243.75 – 273.15	8.17	[491, 492]	0.000101 (248.15 K)
	THF	-0.062	0	0	0	0	298.14 – 343.13	8.33	[493, 494]	0.0005307 (248.15 K)

*Field and Brasington [38] is based on Aspen Plus simulations.

7.0 Process Simulation Results

7.1 Ionic Liquids Used

This category includes the following 11 ILs: [aPy][Tf$_2$N], [bmim][BF$_4$], [bmim][MeSO$_4$], [bmim][PF$_6$], [bmim][Tf$_2$N], [bmPyr][Tf$_2$N], [emim][BF$_4$], [emim][Tf$_2$N], [hmim][(C$_2$F$_5$)$_3$PF$_3$], [hmim][Tf$_2$N], and [omim][Tf$_2$N].

7.1.1 Physico-Chemical Properties

Figure 7.1 shows that the density of these ILs ranges from 1,200 to 1,600 kg/m^3, with [hmim][(C$_2$F$_5$)$_3$PF$_3$] has the highest, while [bmim][BF$_4$] and [bmim][MeSO$_4$] have the lowest density. The vapor pressures of these ILs shown Figure 7.1 are the lowest among those of all solvents used. This means that negligible solvent losses are expected in the CO$_2$ capture process.
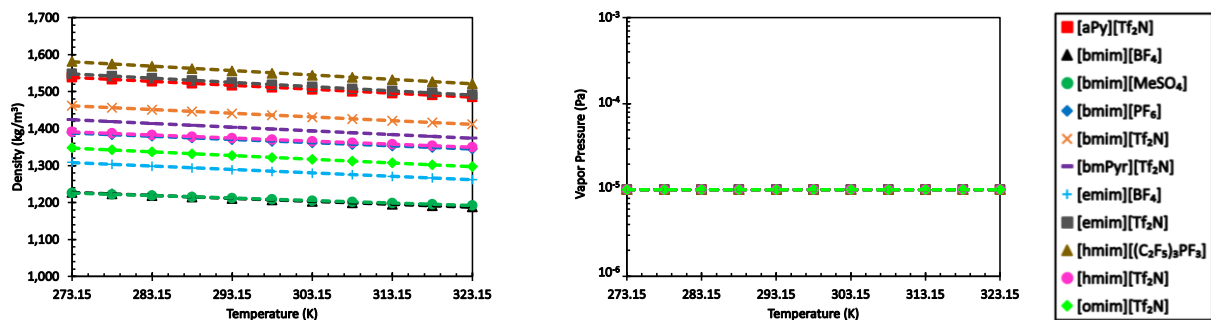
Figure 7.1: Density and vapor pressure of ILs

On the other hand, these ILs have the highest viscosity among all solvents used, which ranges from 0.01 to 1.4 Pa.s as shown in Figure 7.2. The [aPy][Tf$_2$N] has the lowest viscosity while [bmim][PF$_6$] has the highest viscosity. Using a solvent with high viscosity in the CO_2 capture process could be problematic because of the elevated pumping costs and the need for large absorbers to avoid flooding. The surface tension of these ILs presented in Figure 7.2 ranges from 0.028 to 0.055 N/m. Among these solvents, [emim][BF$_4$] exhibits the highest, while [omim][Tf$_2$N] exhibits the lowest surface tension

Figure 7.2: Viscosity and surface tension of ILs

7.1.2 Solubility of Gases

The solubility of CO_2 in the ILs at temperatures 298.15 and 313.15 K are presented in Figure 7.3. The solubility values of CO_2 in all ILs used are close, however, those in [bmim][MeSO$_4$] are lower. The figure also shows that the solubility of CO_2 in these ILs decreases with increasing temperature.

Figure 7.3: Solubility of CO$_2$ in ILs at 298.15 K and 313.15 K

The solubility of H$_2$ in the ILs at 298.15 and 313.15 K are shown in Figure 7.4, where the H$_2$ solubility values in [hmim][(C$_2$F$_5$)$_3$PF$_3$] are the highest, whereas those in [aPy][Tf$_2$N] and [bmim][MeSO$_4$] are the lowest. In addition, unlike those of CO$_2$, the solubility values of H$_2$ in the ILs used increase with increasing temperature.

Figure 7.4: Solubility of H$_2$ in ILs at 298.15 K and 313.15 K

7.1.3 Solvent Flow Rate

The flow rate of ILs required to achieve a 90% CO$_2$ capture increases with operating temperature as shown in Figure 7.5. This is due to the decrease of the solubility of CO$_2$ in the

solvents. [bmim][BF$_4$] shows the lowest, while [bmim][MeSO$_4$] shows the highest flow rate requirement. In addition, using Mellapak 250Y packing leads to a slightly lower solvent flow rate than when using IMTP50, because Mellapak 250Y has higher specific surface area than IMTP50.
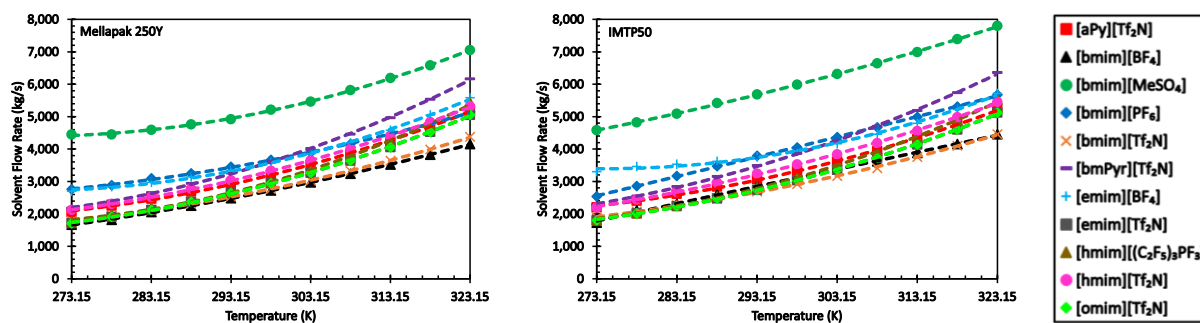
Figure 7.5: Required solvent flow rate using Mellapak 250Y and IMTP50 (ILs)

Figure 7.6 shows the fraction of solvent lost in the process, which has to be made up and as can be seen, due to extremely low vapor pressure of the ILs, the fraction of solvent lost is negligible. This means that there is no need to make up fresh solvent to keep operations going which leads to low operating costs. In addition, there is no significant difference between the fraction of solvent lost using Mellapak 250Y and IMTP50.
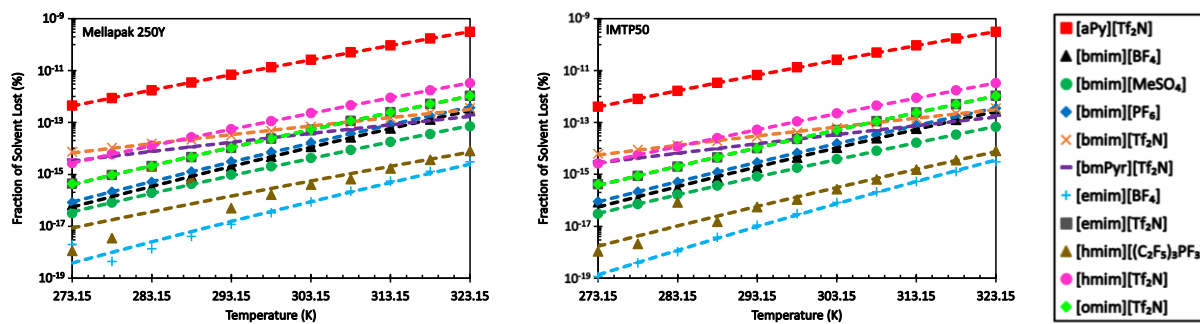
Figure 7.6: Percentage of solvent lost using Mellapak 250Y and IMTP50 (ILs)

78

7.1.4 Absorber

The absorber diameter and height are shown in Figures 7.7 and 7.8, respectively. As can be deduced from these figures, the size of the absorber increases with temperature due to the required high solvent flow rate. The high solvent flow rates require large absorber diameters to avoid flooding and consequently long absorber heights to maintain a *H/D* ratio of greater than 6.
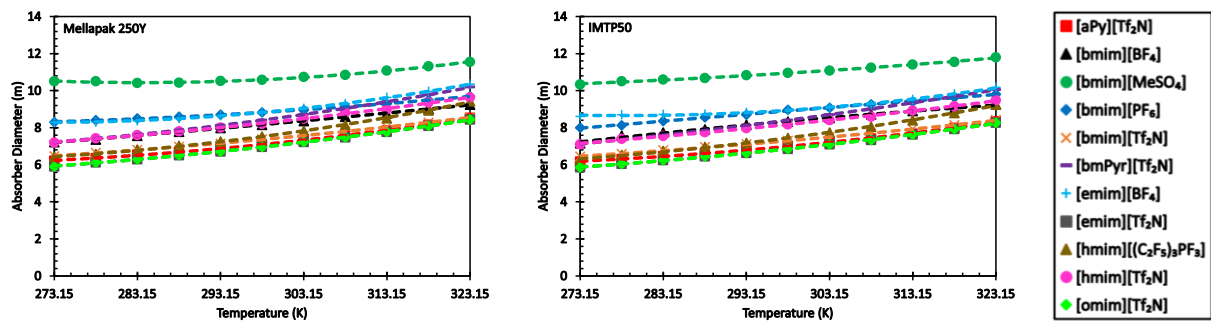
Figure 7.7: Absorber diameter using Mellapak 250Y and IMTP50 (ILs)
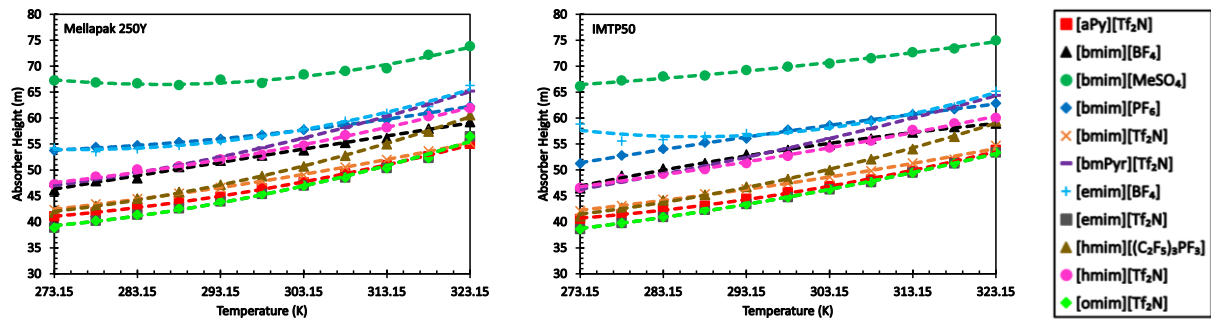
Figure 7.8: Absorber height using Mellapak 250Y and IMTP50 (ILs)

7.1.5 HP Flash Drum Pressure

The pressure of the HP flash drum as a function of temperature is shown in Figure 7.9. In general, the pressure of the HP flash drum decreases with temperature, indicating more fuel gas is absorbed at high temperatures. [bmim][MeSO$_4$], [bmim][PF$_6$], and [emim][BF$_4$], however, show the pressure of the HP flash drum increases when the temperature increases gradually from 273.15 K to 303.15, and 308.15 K, and then decreases. This means that at temperatures up to 308.15 K, less fuel gas was absorbed and beyond this temperature more fuel gas was absorbed. In addition, using IMTP50 showed slightly lower pressure of the HP flash drum due to the use of larger solvent flow rates leading to more fuel gas absorption.
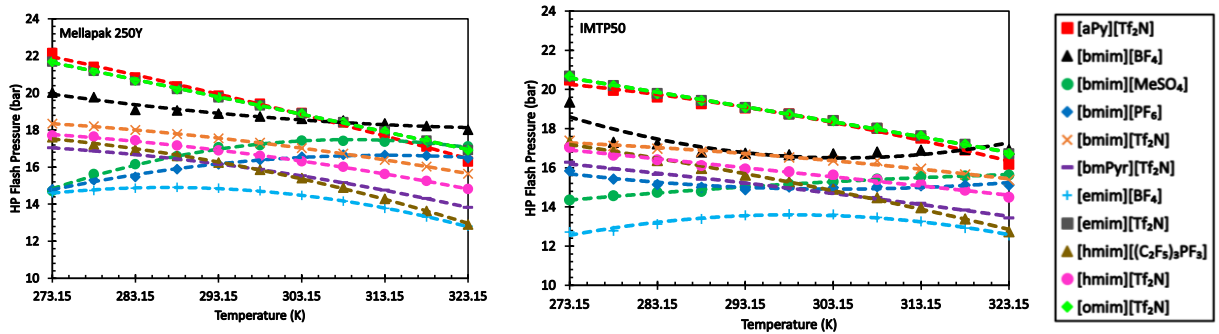
Figure 7.9: Pressure of HP flash drums when using Mellapak 250Y and IMTP50 (ILs)

7.1.6 Power

Figure 7.10 shows the power required to operate the CO$_2$ capture process increases with temperature, which can be attributed to the required higher flow rate of the ILs. In addition, the higher power consumption is associated with the larger flow rate of gas passing through the first set of multi-stage compressors. ILs also have a high viscosity which could contribute to increasing

the pumping cost. Using Mellapak 250Y showed slightly lower power requirements because the flow rate of solvent needed to reach 90% CO_2 capture is lower.
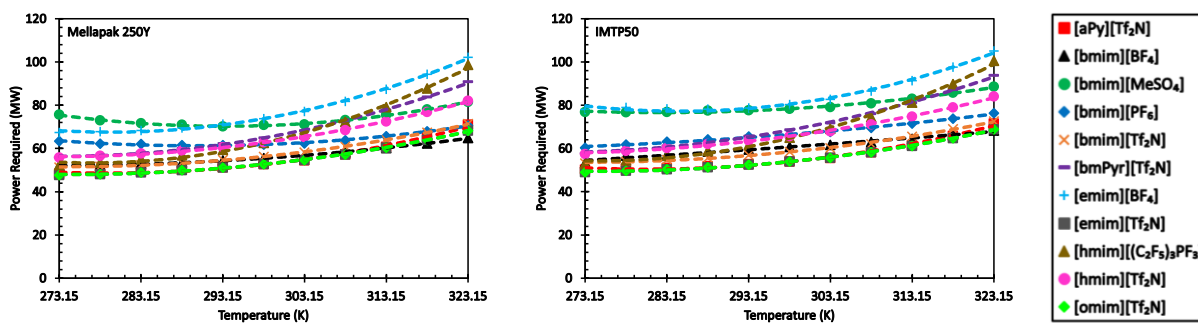
Figure 7.10: Power required to operate plant using Mellapak 250Y and IMTP50 (ILs)

7.1.7 Capital Expenditure

The total CAPEX of the process when using ILs is given in Figure 7.11 as a function of operating temperature. The CAPEX increases with operating temperature due to the large equipment needed to achieve 90% CO_2 capture and to process large flow rates. The cost of the solvent also contributes to the CAPEX and since ILs are the most expensive of the tested solvents, their CAPEX is found to be higher than those of the other solvents used in Aspen Plus simulations. [emim][BF$_4$] showed the largest CAPEX followed by [bmim][MeSO$_4$], making them less likely to be used for CO_2 capture compared to other ILs. On the other hand, [bmim][Tf$_2$N] and [emim][Tf$_2$N] exhibited the lowest CAPEX among the ILs used, making them more favorable than the other ILs for CO_2 capture.
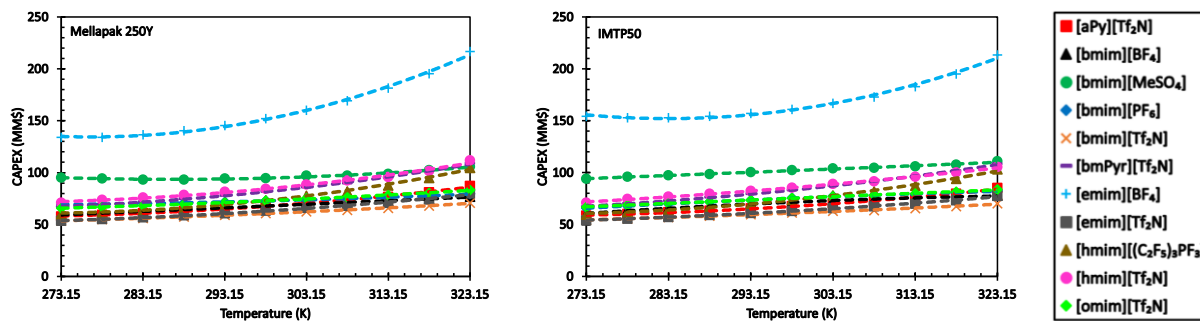
Figure 7.11: CAPEX of capture process using Mellapak 250Y and IMTP50 (ILs)

7.1.8 Operating Expenditure

Figure 7.12 shows the total OPEX increases with temperature due to the increase of the power requirement for the CO_2 capture process (Figure 7.10), and the increasing operating and maintenance cost, which depends on the CAPEX (Figure 7.11). IMTP50 exhibited higher operating costs due to its higher CAPEX and power requirement. Similar to CAPEX, [emim][BF$_4$] and [bmim][MeSO$_4$] showed the highest OPEX, while [aPy][Tf$_2$N], [bmim][BF$_4$], and [emim][Tf$_2$N] showed the lowest.
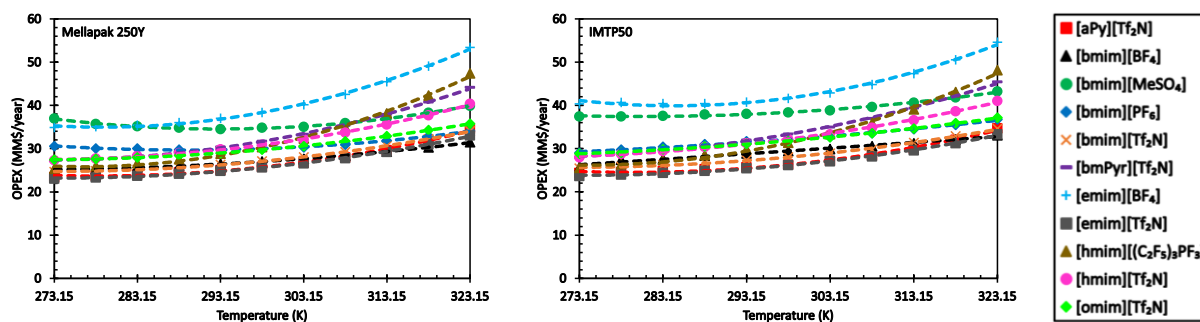
Figure 7.12: OPEX of capture process using Mellapak 250Y and IMTP50 (ILs)

7.1.9 Levelized Cost

Figure 7.13 shows the LCOC when using ILs increases with temperature due to the increase of both the CAPEX and OPEX. Mellapak 250Y showed lower LCOC values than IMTP50 due to the former's lower CAPEX and OPEX. In addition, [emim][BF4] and [bmim][MeSO4] showed highest LCOC values among the ILs used due to their highest CAPEX and OPEX. On the other hand, [aPy][Tf_2N], [bmim][Tf_2N], and [emim][Tf_2N] showed the lowest LCOC values due to their competitive CAPEX and OPEX. Among the ILs used, using [emim][Tf_2N] at 273.15 K with Mellapak 250Y, gives the lowest LCOC of \$7.55/ton CO_2 captured.
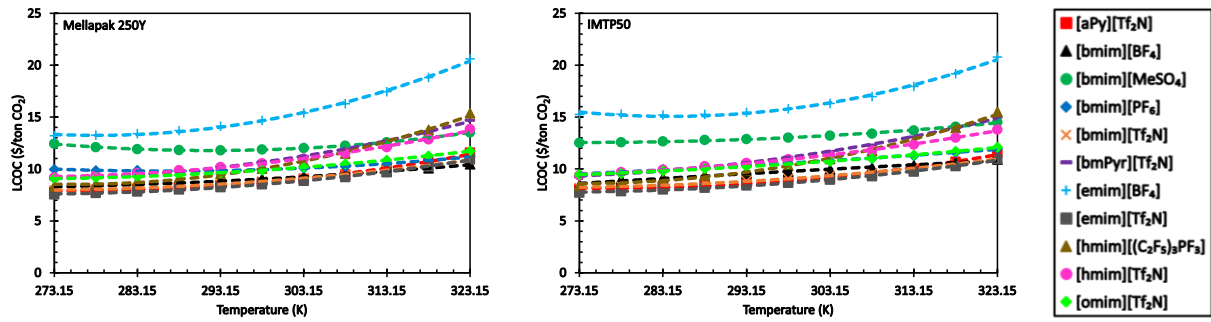
Figure 7.13: LCOC of capture process using Mellapak 250Y and IMTP50 (ILs)

7.2 Hydrocarbons Used

This category includes the following 5 HCs: 1-Heptene, 1-Octene, n-Octane, n-Decane and, n-Tetradecane

7.2.1 Physico-Chemical Properties

Figure 7.14 shows that the density of the HCs used ranges from 660 to 780 kg/m^3. 1-Heptene and n-octane have the lowest density, while n-Tetradecane has the highest density. The vapor pressure of the HCs, shown in Figure 7.14 ranges from 0 to more than 10,000 Pa, indicating that there will be some solvent loss, particularly for the alkenes and n-octane.
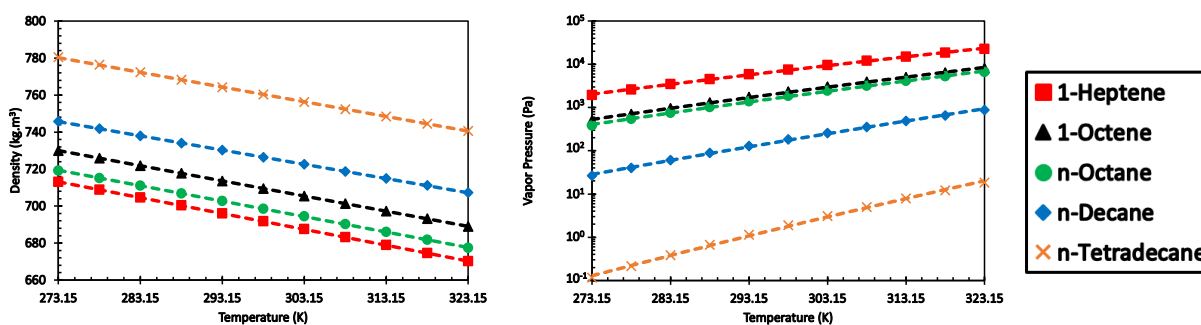
Figure 7.14: Density and vapor pressure of HCs

On the other hand, the viscosity of these HCs ranges from 0.0005 to 0.004 Pa.s as shown in Figure 7.15 with 1-heptene having the lowest and n-tetradecane having the highest viscosity among the HCs. The surface tension of these HCs, presented in Figure 7.15, ranges from 0.017 to 0.028 N/m. The HCs showed close surface tensions with the difference between the highest and the lowest at the same temperature is about 0.007 N/m.
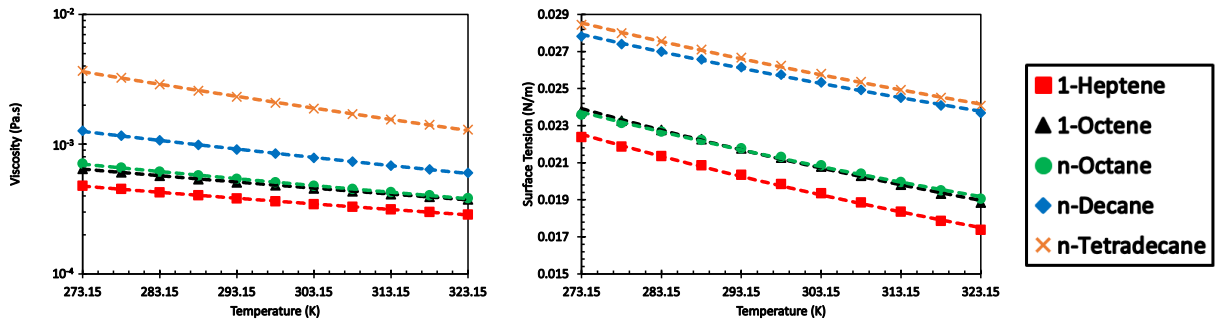
Figure 7.15: Viscosity and surface tension of the HCs

7.2.2 Solubility of Gases

The solubility of CO_2 in these HCs at temperatures 298.15 and 313.15 K are presented in Figure 7.16. The solubility of CO_2 is lower in longer chain HCs than those in shorter HCs. Also, the solubility of CO_2 in these HCs decreases with increasing temperature.
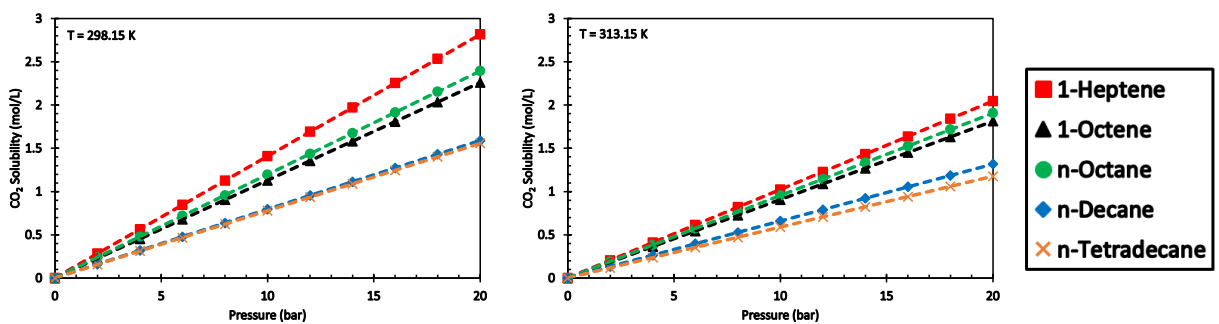
Figure 7.16: Solubility of CO_2 in HCs at 298.15 K and 313.15 K

The solubility of H_2 in these HCs at 298.15 and 313.15 K are shown in Figure 7.17 and similar to the solubility of CO_2, the solubility of H_2 in longer HCs is lower than that in shorter HCs. In addition, the solubility of H_2 in these HCs increases with temperature.
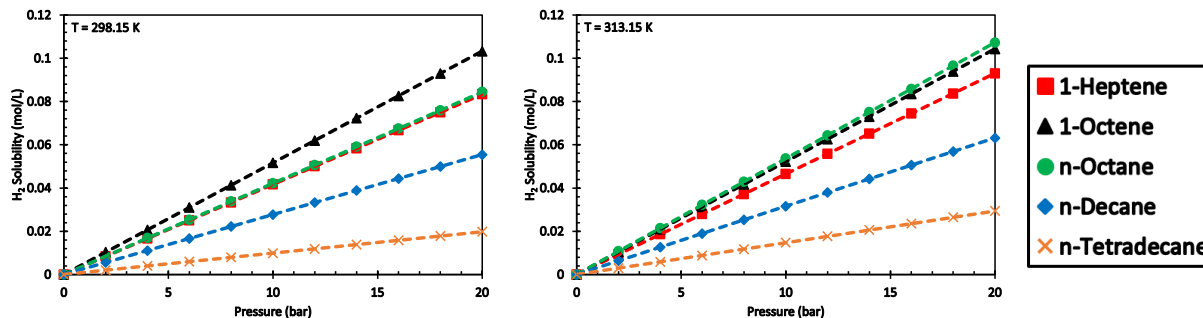
Figure 7.17: Solubility of H_2 in HCs at 298.15 K and 313.15 K

7.2.3 Solvent Flow Rate

The flow rates of the HCs used required to achieve a 90% CO_2 capture are shown in Figure 7.18, and as can be deduced the required HCs flow rate increases with temperature, which could be due to the decrease of the solubility of CO_2 in these solvents. In addition, using Mellapak 250Y packing leads to lower solvent flow rates than those when using IMTP50 because of the former's higher specific surface area, leading to better mass transfer. Shorter structure HCs need lower flow rates than longer HCs because of their better CO_2 solubility, leading to lower flow rate requirement to achieve 90% CO_2 capture.
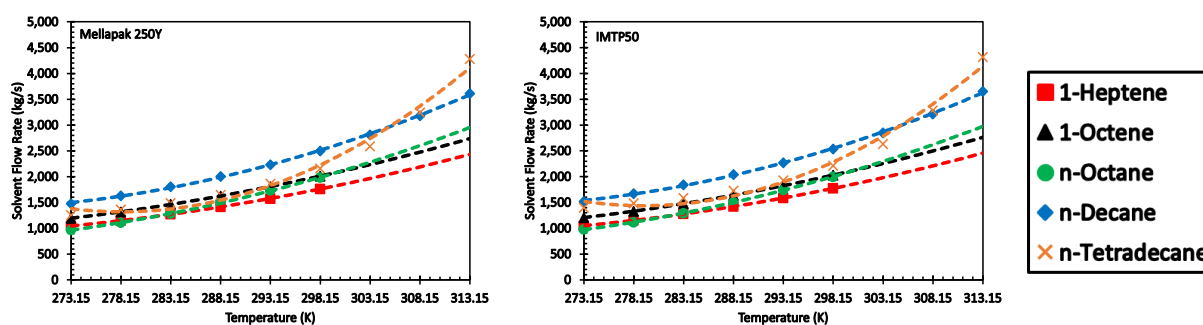
Figure 7.18: Required solvent flow rate using Mellapak 250Y and IMTP50 (HCs)

86

Figure 7.19 shows the fraction of solvent lost in the CO_2 capture process increases with temperature. The solvent loss when using shorter chain HCs is more significant than that when using longer chain HCs. This is because of the significantly higher vapor pressure of short chain HCs than longer chain HCs. This means that more fresh solvent is required for shorter chain HCs, which increases the OPEX. Also, there is no measurable difference between the solvent loss using Mellapak 250Y and IMTP50.
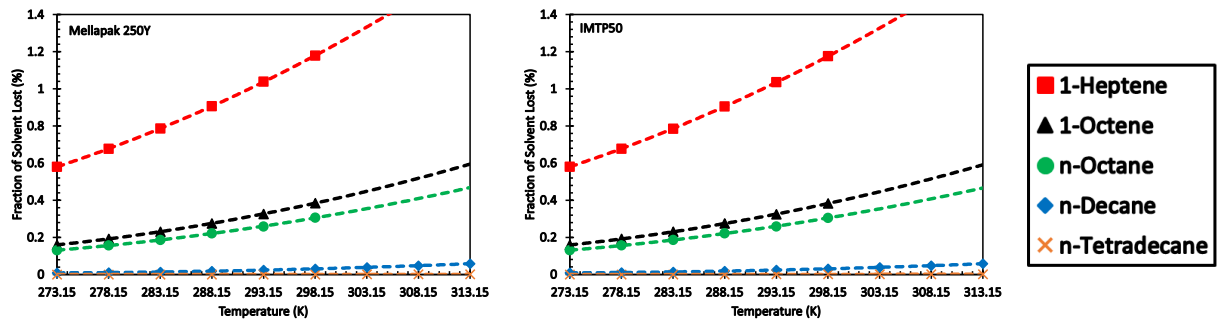
Figure 7.19: Percentage of solvent lost using Mellapak 250Y and IMTP50 (HCs)

7.2.4 Absorber

The absorber diameter and height are presented in Figures 7.20 and 7.21, respectively and as can be seen the size and height of the absorber increase with temperature due to the need for higher solvent flow rate. The higher solvent flow rates require large absorber diameters to avoid flooding and consequently longer absorber height to maintain a *H/D* ratio of greater than 6.
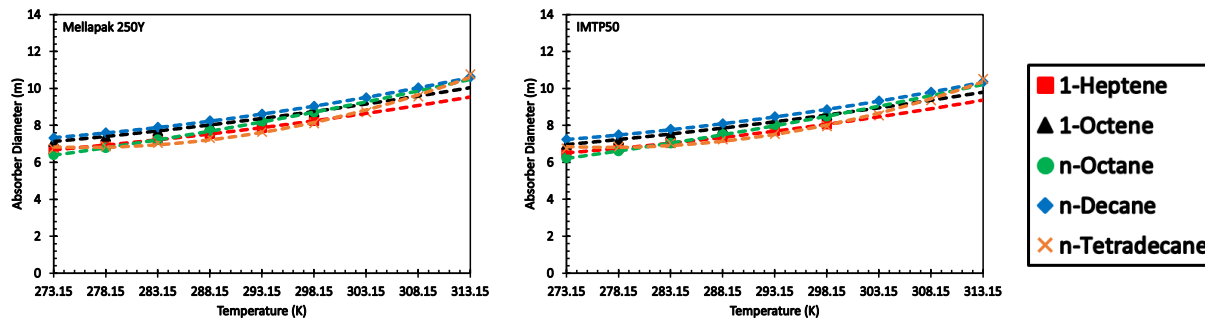
Figure 7.20: Absorber diameter using Mellapak 250Y and IMTP50 (HCs)

Figure 7.21: Absorber height using Mellapak 250Y and IMTP50 (HCs)

7.2.5 HP Flash Drum Pressure

Figure 7.22 illustrates the pressure of the HP flash drum decreases with increasing temperature, indicating that more fuel gas is absorbed at higher temperatures as lower pressures are needed to release the fuel gas and satisfy the fuel gas constraint (≤ 0.5 mol%). Longer chain HCs show higher flash drum pressures than those of shorter chain HCs due to their lower fuel gas solubilities. In addition, using IMTP50 showed slightly lower flash drum pressure than using Mellapak 250Y due to more fuel gas is absorbed as a result of the higher solvent flow rate.

Figure 7.22: Pressure of HP flash drums when using Mellapak 250Y and IMTP50 (HCs)

7.2.6 Power

Figure 7.23 shows the power required for the CO_2 capture process increases with temperature due to the increase of the solvent flow rate, which raises the pumping cost and the increase of the gas flow rate entering the first multi-stage compressors. Using Mellapak 250Y showed lower power requirements because the flow rate of the solvent needed to reach 90% capture is lower and therefore its processing requirements consume less power.

Figure 7.23: Power required to operate plant using Mellapak 250Y and IMTP50 (HCs)

7.2.7 Capital Expenditure

The total CAPEX of the CO_2 capture process when using these HCs is given in Figure 7.24 and as can be seen, the CAPEX increases with temperature due to the large equipment needed to achieve 90% CO_2 removal and to process large solvent flow rates. n-Tetradecane showed the lowest CAPEX due to the small compressors needed as indicated by the power requirements shown above. Other solvents showed similar CAPEX due to their similar power requirements and absorber sizes.

Figure 7.24: CAPEX of capture process using Mellapak 250Y and IMTP50 (HCs)

7.2.8 Operating Expenditure

Figure 7.25 shows the total OPEX when using these HCs increases with temperature, which can be due to the increase of the power requirement and the operating and maintenance cost, which is dependent on the CAPEX. IMTP50 exhibits higher operating costs due to its higher power requirement and higher CAPEX. n-Tetradecane shows lower OPEX values than other solvents due to its lower loss and lower power requirement. 1-Heptene exhibits the highest OPEX among these HCs due to its high vapor pressure and large solvent losses.

90
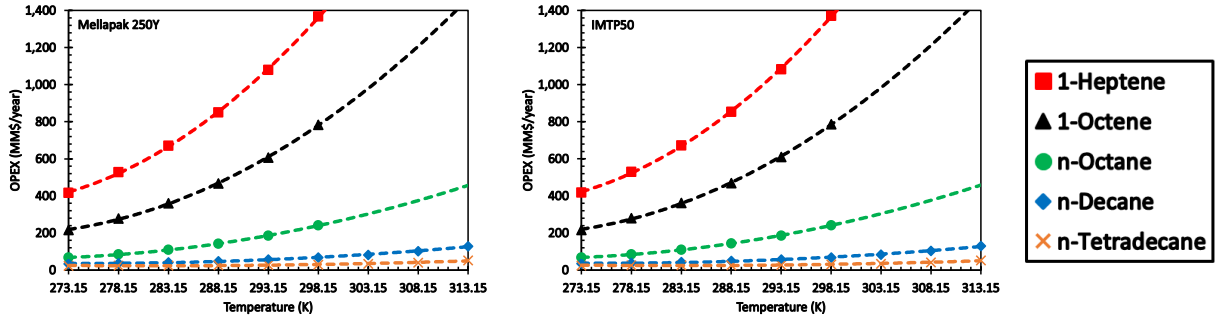
Figure 7.25: OPEX of capture process using Mellapak 250Y and IMTP50 (HCs)

7.2.9 Levelized Cost

Figure 7.26 shows the LCOC values of the CO_2 capture process when using HCs increases with temperature due to the increase of both the CAPEX and OPEX. Mellapak 250Y shows lower LCOC values than IMTP50 due to the former's lower CAPEX and OPEX. In addition, n-tetradecane showed lower LCOC values than the other HCs due to its lower CAPEX and OPEX while 1-heptene showed the highest LCOC. Among the HCs, n-tetradecane operated at 273.15 K using Mellapak 250Y gives the lowest LCOC at \$7.58/ton CO_2 captured.
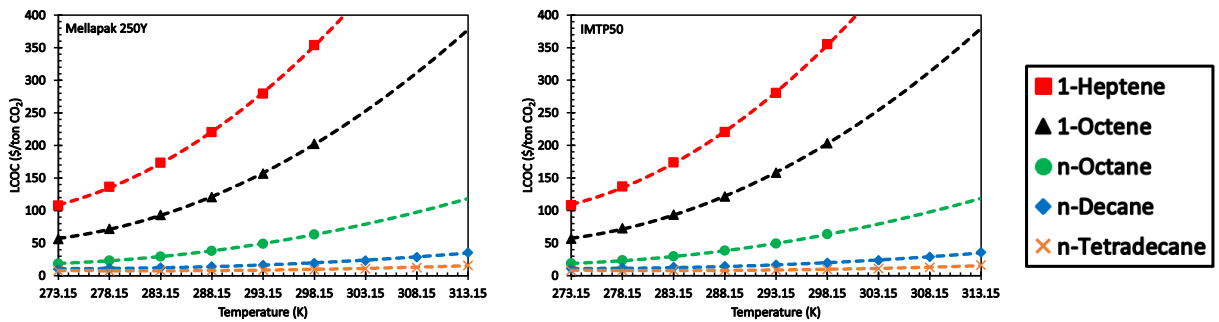
Figure 7.26: LCOC of capture process using Mellapak 250Y and IMTP50 (HCs)

7.3 Oxygenated-Hydrocarbons Used

This category includes the following 7 OHCs: 1-Hexanol, 1-Nonanal, 1-Octanol, DES, NBAc, NPAc, and TBP.

7.3.1 Physico-Chemical Properties

Figure 7.27 shows that the density of the OHCs used ranges from 800 to 1,000 kg/m^3, with alcohols and the aldehyde having the lowest, while TBP and DES having the highest density among these OHCs. The vapor pressure of the OHCs, shown in Figure 7.27 ranges from 0 to more than 15,000 Pa, indicating that there will be some solvent loss, particularly for NPAc and NBAc, which have the highest vapor pressure among these OHCs.
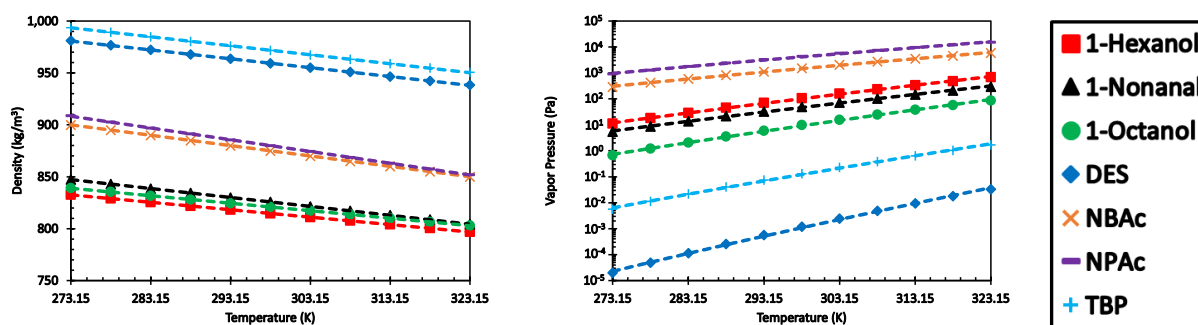
Figure 7.27: Density and vapor pressure of OHCs

On the other hand, the viscosity of the OHCs ranges from 0.0005 to 0.017 Pa.s as shown in Figure 7.28 with NPAc having the lowest and 1-octanol having the highest viscosity among the OHCs. The surface tension of the OHCs, presented in Figure 7.28, ranges from 0.02 to 0.035 N/m. Also, DES shows the highest while NPAc had the lowest surface tension among these OHCs.
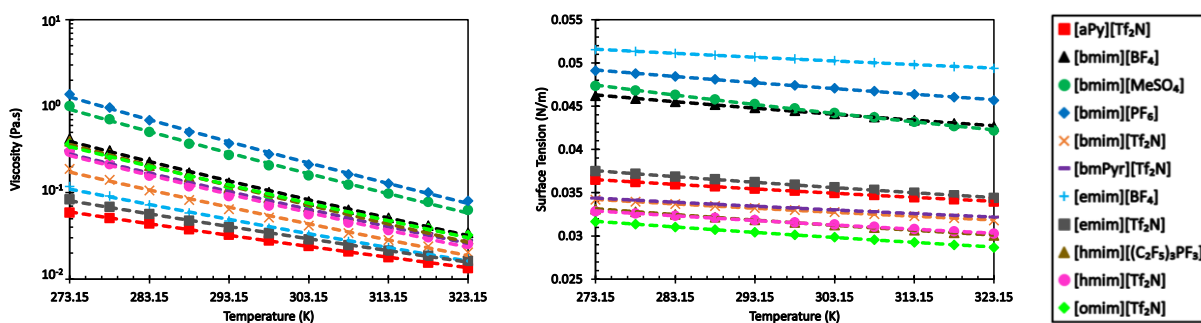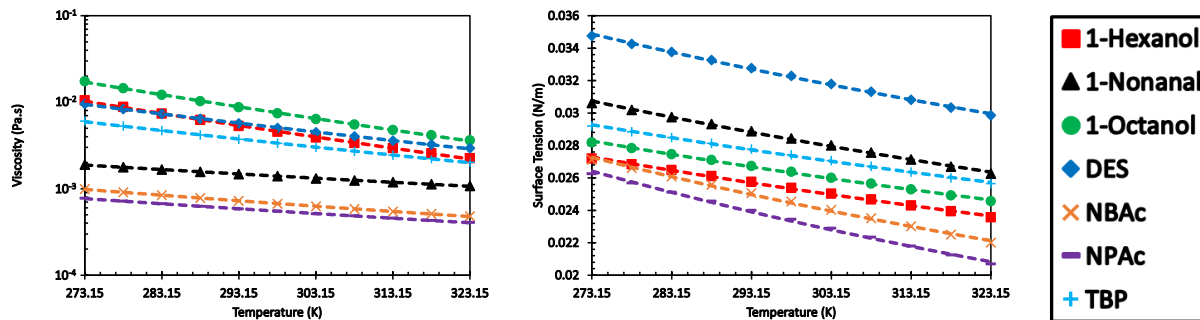
Figure 7.28: Viscosity and surface tension of the OHCs

7.3.2 Solubility of Gases

The solubility of CO_2 in the OHCs at temperatures 298.15 and 313.15 K are presented in Figure 7.29, and as can be observed the solubility of CO_2 is lower for the alcohols and higher for the acetates. Also, the solubility of CO_2 in all OHCs decreases as the temperature increases.
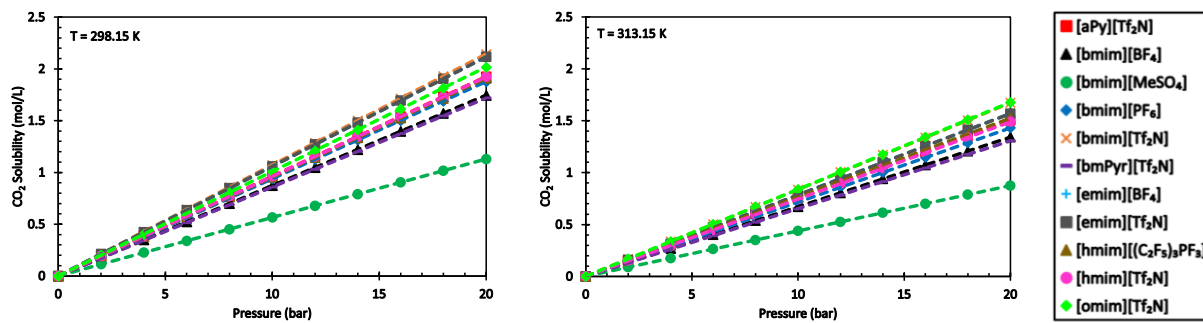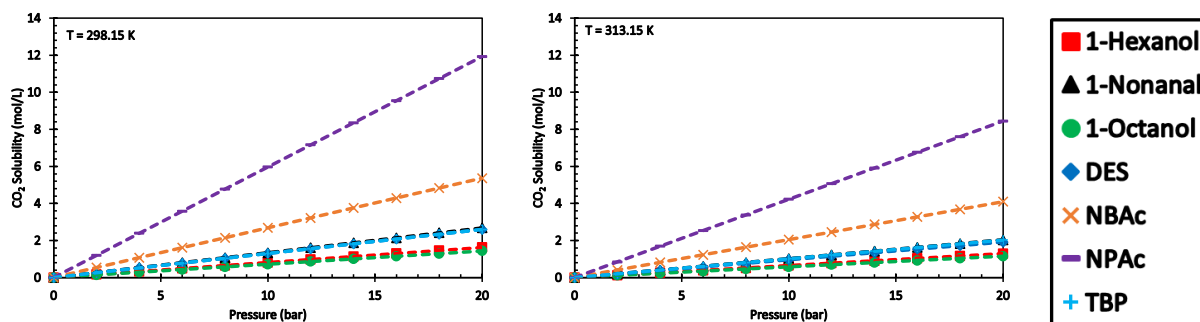

Figure 7.29: Solubility of CO_2 in OHCs at 298.15 K and 313.15 K

The solubility of H_2 in the OHCs at 298.15 and 313.15 K are shown in Figure 7.30, and similar to the solubility of CO_2, the solubility of H_2 is lower in the alcohols and higher for the acetates. In addition, the solubility of H_2 in the OHCs increases with temperature.
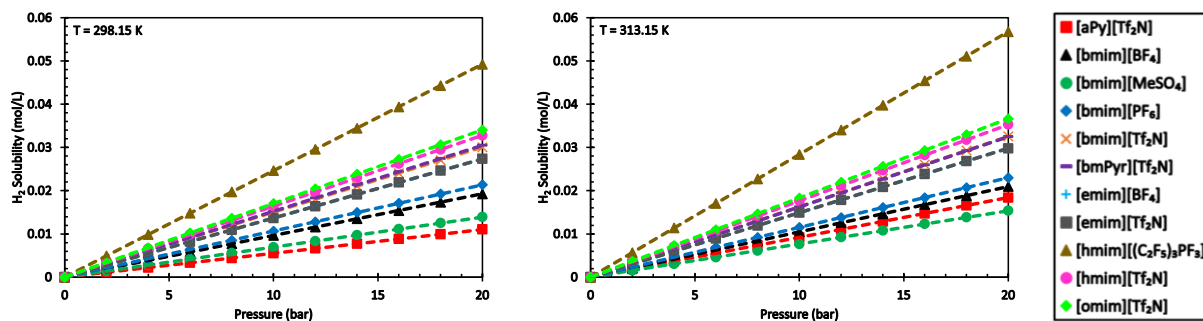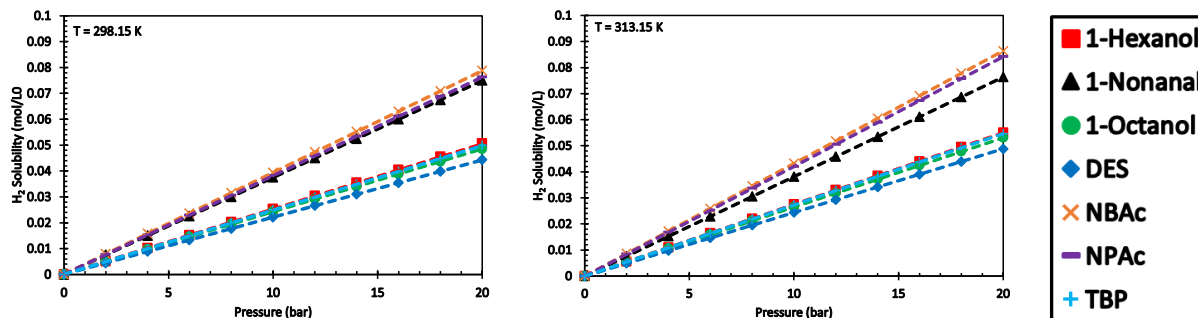
Figure 7.30: Solubility of H$_2$ in OHCs at 298.15 K and 313.15 K

7.3.3 Solvent Flow Rate

The flow rate of OHCs required to achieve a 90% CO$_2$ capture is shown in Figure 7.31 and as can be seen, the required OHCs flow rate increases with temperature due to the decrease of the solubility of CO$_2$ in these solvents. The acetates need the lowest, while alcohols need a higher solvent flow rate among these OHCs because of the higher CO$_2$ solubility in acetates.
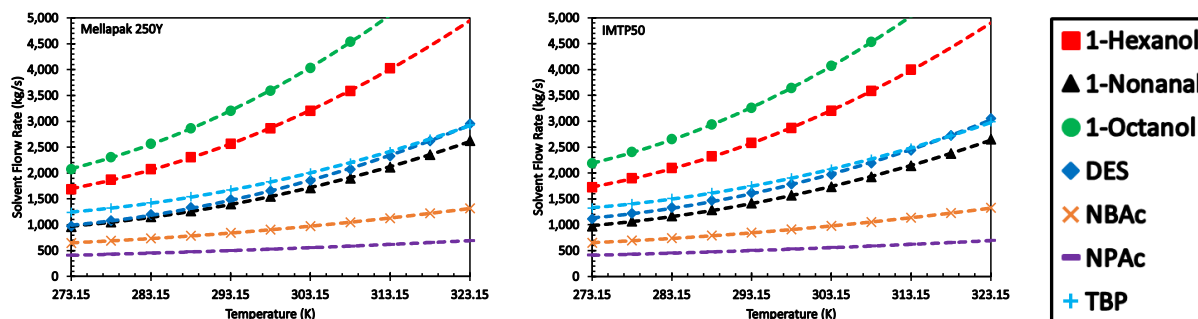
Figure 7.31: Required solvent flow rate using Mellapak 250Y and IMTP50 (OHCs)

Figure 7.32 shows that NPAc loses a large amount of solvent due to its significant vapor pressure and the percentage loss of solvent increases with temperature. This means that the OPEX

94

will be much higher than the others. DES, TBP, and the alcohols have much lower vapor pressures which leads to the low percentage of solvent loss as shown in Figure 7.32. In addition, there is no significant difference between the solvents flow rates using Mellapak 250Y and IMTP50.
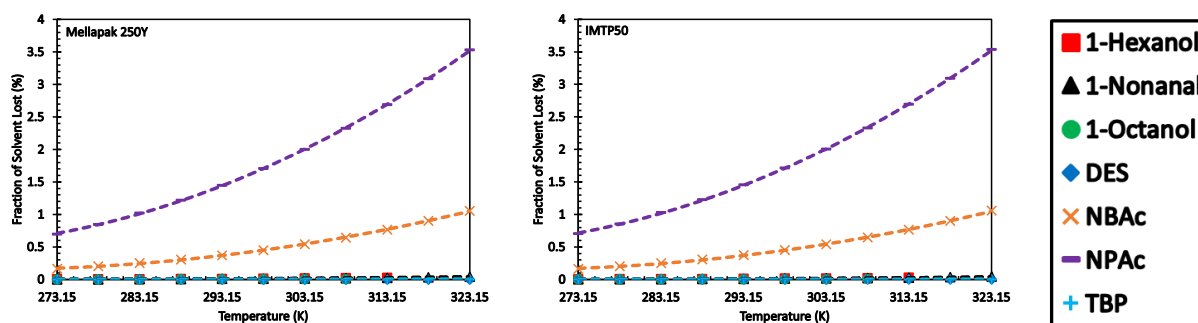
Figure 7.32: Percentage of solvent lost using Mellapak 250Y and IMTP50 (OHCs)

7.3.4 Absorber

Figures 7.33 and 7.34 show that the absorber diameter and height when using OHCs increase with increasing temperature. This is due to the higher flow rate of the solvent needed, which requires larger absorber diameter to avoid flooding and consequently longer absorber height to maintain a *H/D* ratio of greater than 6. Also, using IMTP50 leads to the need for smaller absorbers because as a random packing, it can handle higher flow rates without flooding than the Mellapak 250Y, which is a structured packing.
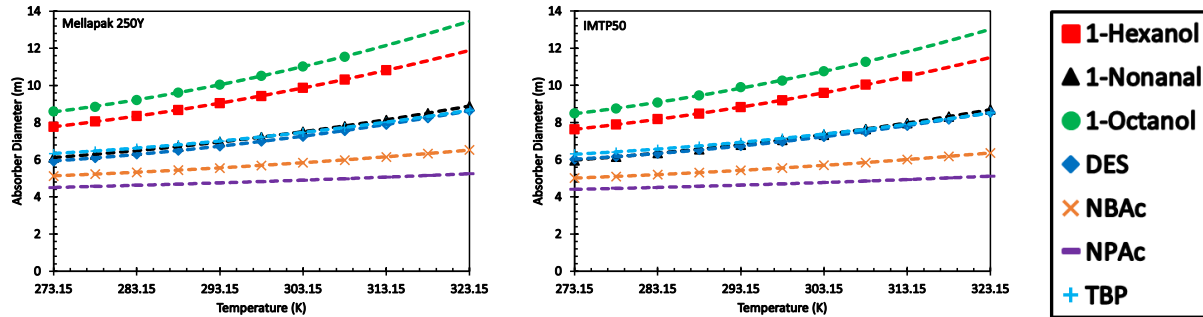
Figure 7.33: Absorber diameter using Mellapak 250Y and IMTP50 (OHCs)
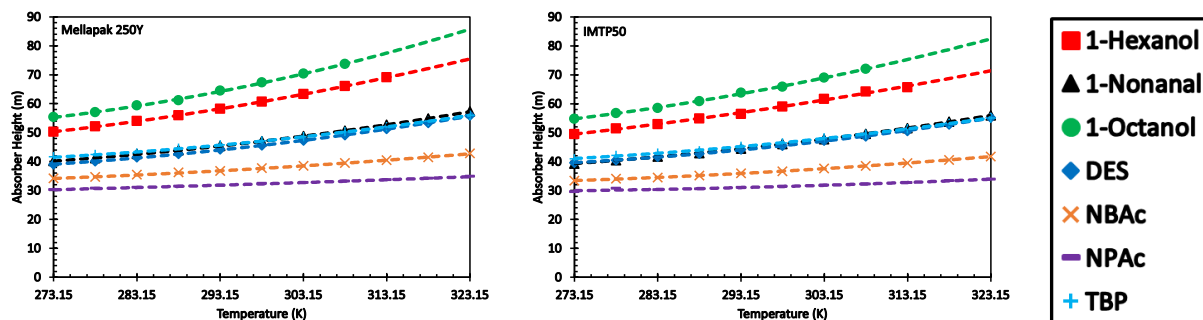
Figure 7.34: Absorber height using Mellapak 250Y and IMTP50 (OHCs)

7.3.5 HP Flash Drum Pressure

Figure 7.35 shows the pressure of the HP flash drum decreases when increasing the operating temperature. This is an indication that more fuel gas is absorbed in the solvents at higher temperatures. Using IMTP50 showed slightly lower flash drum pressure due to more fuel gas is absorbed in the high solvent flow rate.
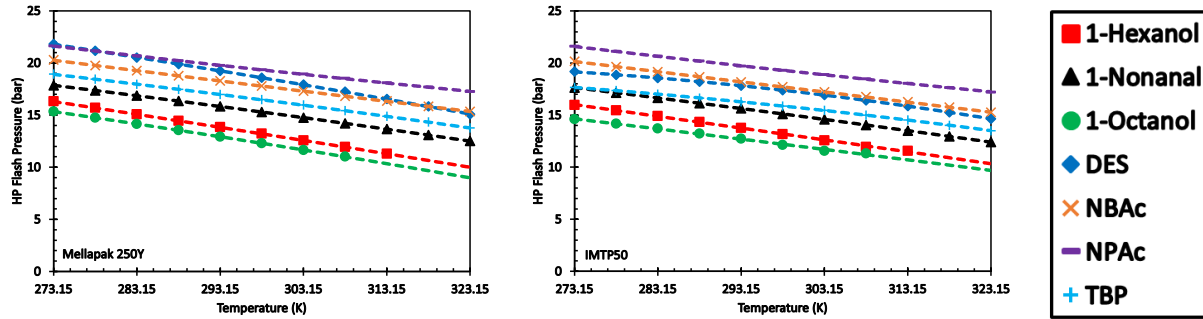
Figure 7.35: Pressure of HP flash drums when using Mellapak 250Y and IMTP50 (OHCs)

7.3.6 Power

Figure 7.36 shows the power consumption of the CO_2 capture process using the OHCs and as can be seen, the power consumed increases with temperature due to the need for higher solvent flow rates and the larger gas flow rate entering the first multi-stage compressors. Using Mellapak 250Y showed lower power requirements because the flow rate of solvent needed to reach 90% capture is lower and therefore process requirements consume less power.
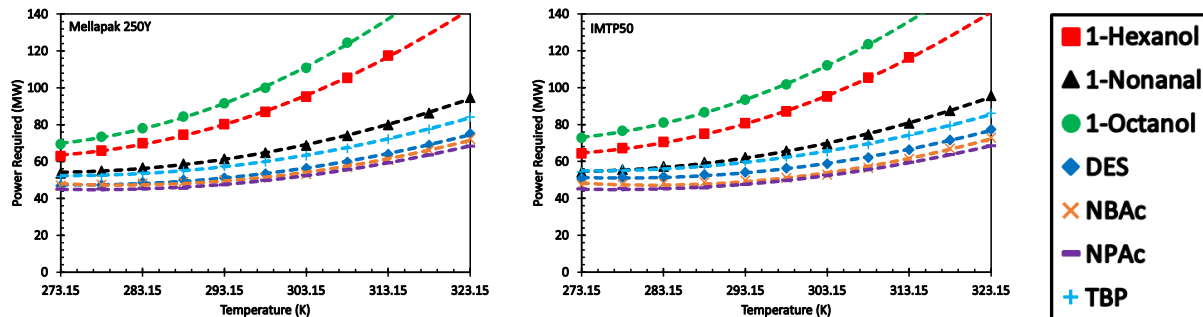
Figure 7.36: Power required to operate plant using Mellapak 250Y and IMTP50 (OHCs)

97

7.3.7 Capital Expenditure

Figure 7.37 shows the total CAPEX of the CO_2 capture process using OHCs increases with temperature due to the large equipment needed to achieve 90% CO_2 capture and to process the large solvent flow rates. NPAc showed the lowest CAPEX due to the small absorber sizes needed, however, the alcohols had the highest CAPEX due to the need for large absorber sizes.
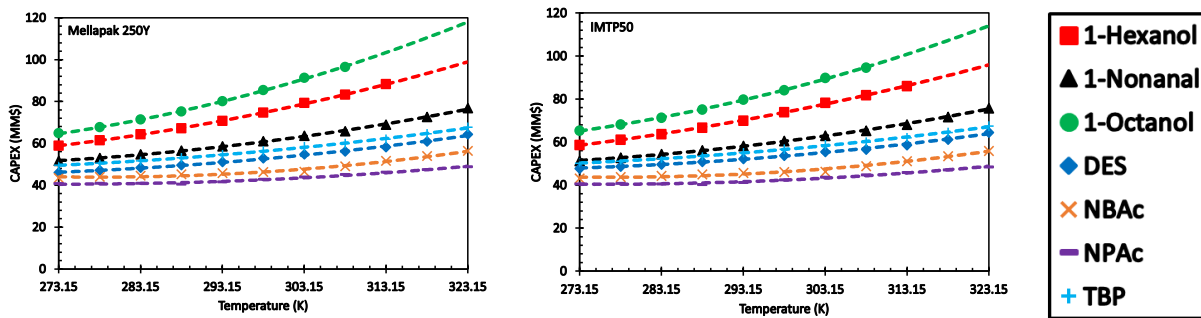
Figure 7.37: CAPEX of capture process using Mellapak 250Y and IMTP50 (OHCs)

7.3.8 Operating Expenditure

Figure 7.38 shows the total OPEX increases with temperature, which can be attributed to the increased power requirement, operating and maintenance cost, and solvent losses. DES shows the lowest OPEX values among OHCs due to its lowest solvent loss and lowest power requirement, whereas NPAc exhibited the highest OPEX because of its high vapor pressure leading to significant solvent losses, which have to be made up.
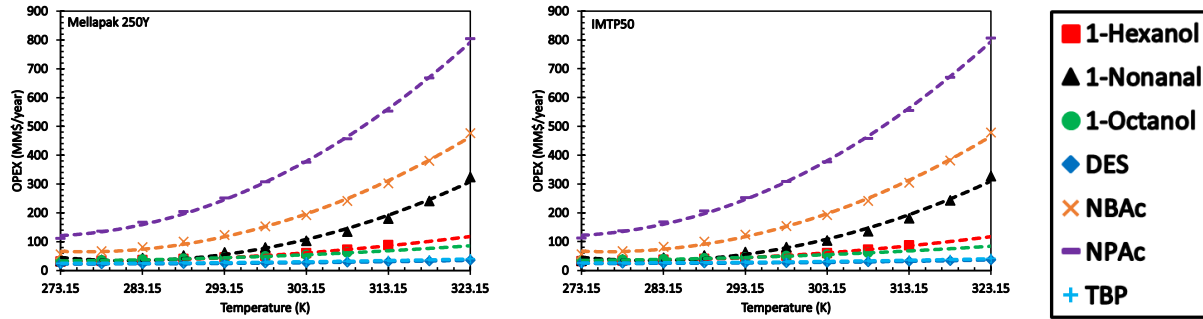
Figure 7.38: OPEX of capture process using Mellapak 250Y and IMTP50 (OHCs)

7.3.9 Levelized Cost

Figure 7.39 shows the LCOC of the CO_2 capture process using OHCs, and as can be observed, LCOC values increase with temperature due to the increase of both the CAPEX and OPEX. Mellapak 250Y showed lower LCOC values than IMTP50 due to the former's lower CAPEX and OPEX. In addition, DES and TBP show lower LCOC values than the other OHCs due to their lower CAPEX and OPEX, while NPAc showed the highest LCOC value. Using DES operated at 273.15 K with Mellapak 250Y, yields the lowest LCOC value at \$7.14/ton CO_2 captured.
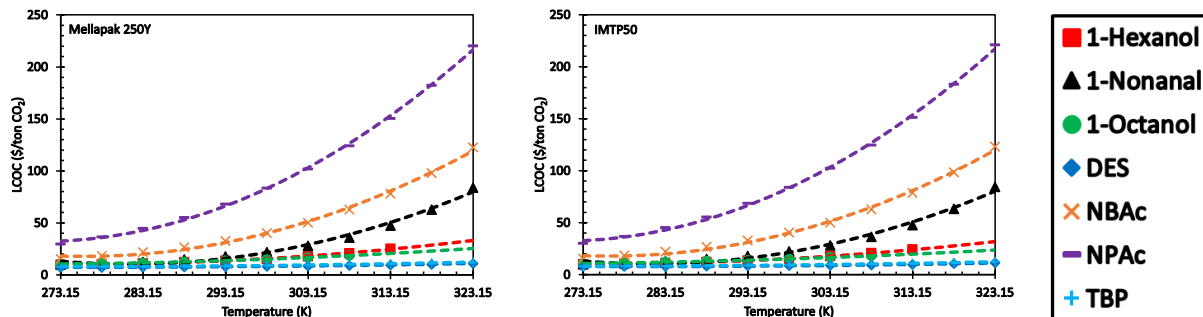
Figure 7.39: LCOC of capture process using Mellapak 250Y and IMTP50 (OHCs)

99

7.4 Nitrogenized-Hydrocarbons Used

This category includes the following 2 NHCs: DMF and PN.

7.4.1 Physico-Chemical Properties

Figure 7.40 shows that the density of the NHCs used ranges from 750 to 970 kg/m^3, with DMF having higher density then PN. The vapor pressure of the NHCs used, shown in Figure 7.40, ranges from 100 to more than 20,000 Pa. PN has higher vapor pressure than DMF, which means that there will be solvent losses using PN, leading to high OPEX.
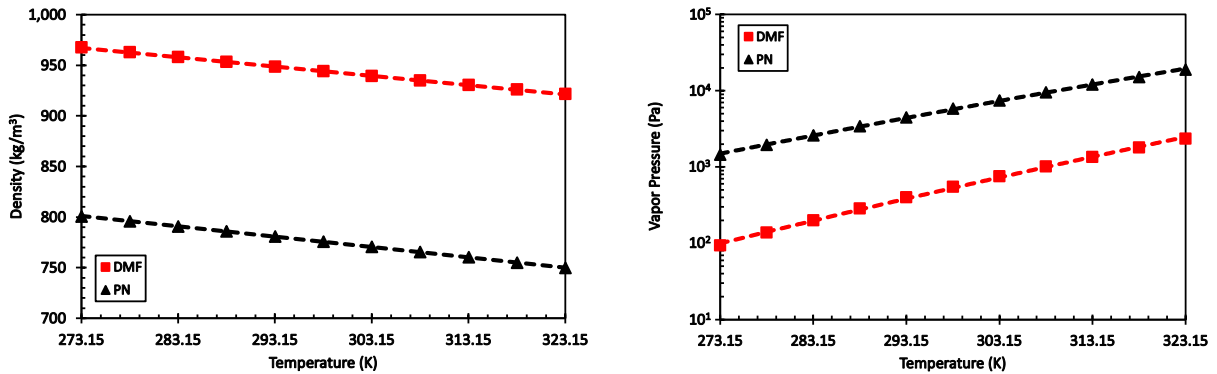
Figure 7.40: Density and vapor pressure of NHCs

Figure 7.41 shows that the viscosities of NHCs are less than 0.002 Pa.s. The surface tension of the NHCs is given in Figure 7.41 and as can be seen, DMF has a higher surface tension than PN within the temperature range studied.

100
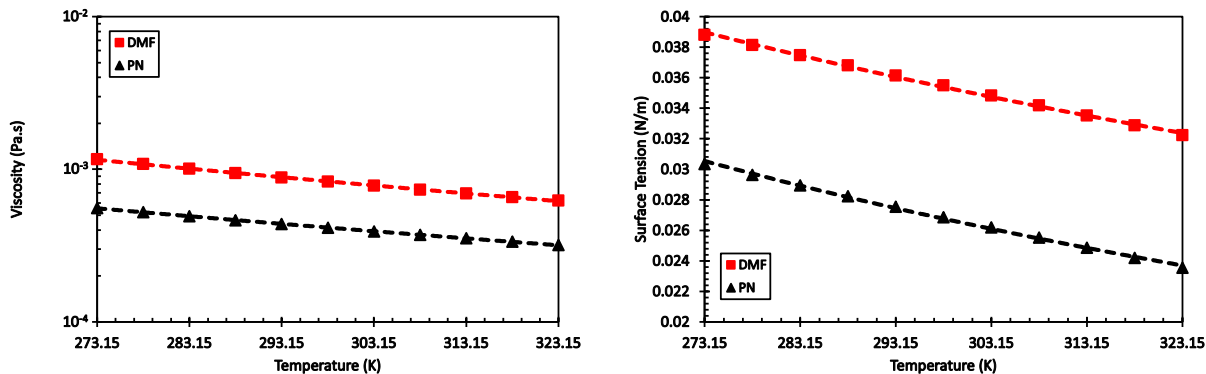
Figure 7.41: Viscosity and surface tension of the NHCs

7.4.2 Solubility of Gases

The solubilities of CO_2 in the NHCs at temperatures 298.15 and 313.15 K are presented in Figure 7.42. The solubility of CO_2 in PN is slightly greater than in DMF within the pressure range from 0 to 20 bar. Also, the solubility of CO_2 in both NHCs decreases with temperature.
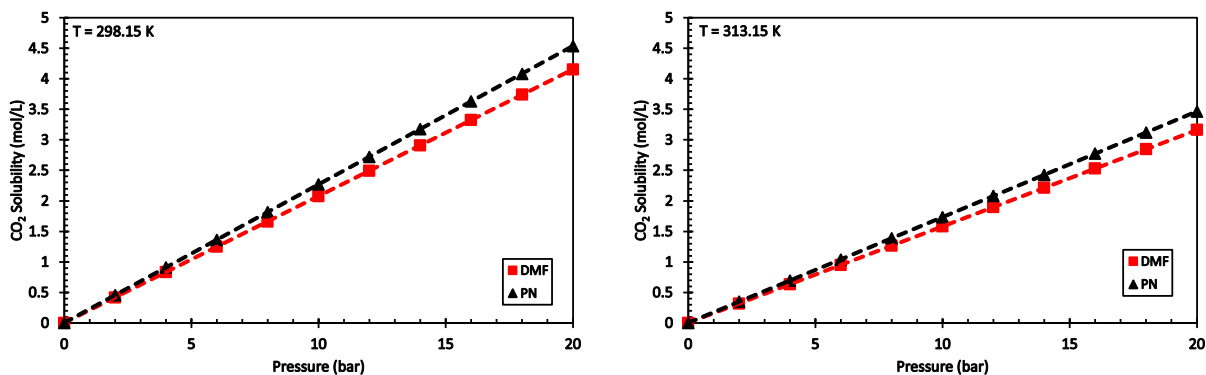
Figure 7.42: Solubility of CO_2 in NHCs at 298.15 K and 313.15 K

The solubilities of H_2 in the NHCs at 298.15 and 313.15 K are presented in Figure 7.43. The solubility of H_2 in PN is slightly greater than in DMF within the pressure range from 0 to 20 bar. Also, the solubility of H_2 in both NHCs increases with temperature.

101
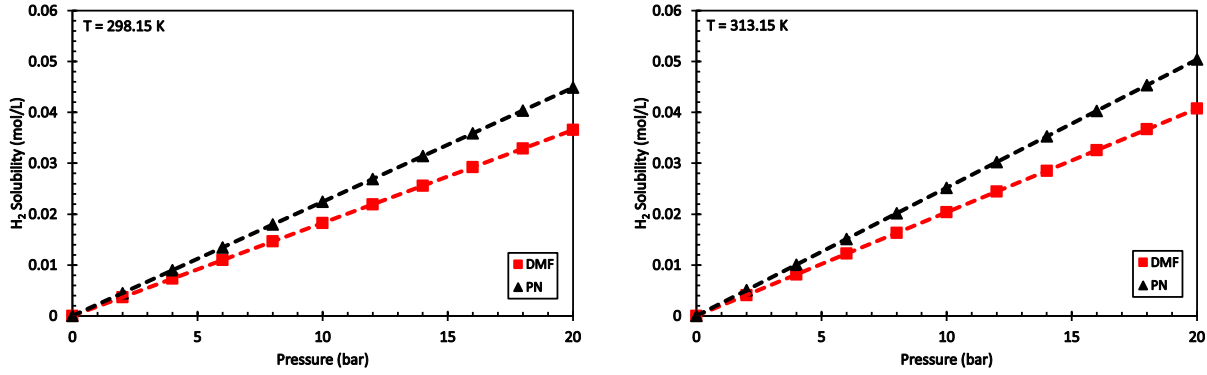
Figure 7.43: Solubility of H₂ in NHCs at 298.15 K and 313.15 K

7.4.3 Solvent Flow Rate

The flow rate of NHCs needed to achieve 90% CO_2 capture is shown in Figure 7.44 and as can be observed, the required NHCs flow rate increases with temperature, due to the decrease of the solubility of CO_2 in the solvents. Both solvents have similar flow rate requirements due to the similarity of CO_2 solubility in the solvents. In addition, there is no significant difference between the solvent flow rates when using both packings.
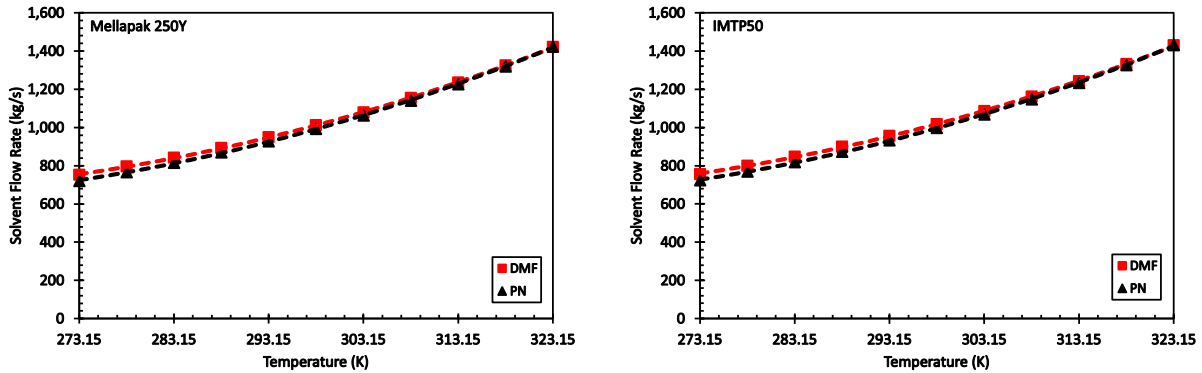
Figure 7.44: Required solvent flow rate using Mellapak 250Y and IMTP50 (NHCs)

102

Figure 7.45 shows that PN loses a large amount of solvent due to its high vapor pressure, and as temperature increases, the percentage loss of solvent increases. This means that the OPEX will be much higher for PN than DMF. In addition, there is no significant difference in solvent loss when using Mellapak 250Y and IMTP50.
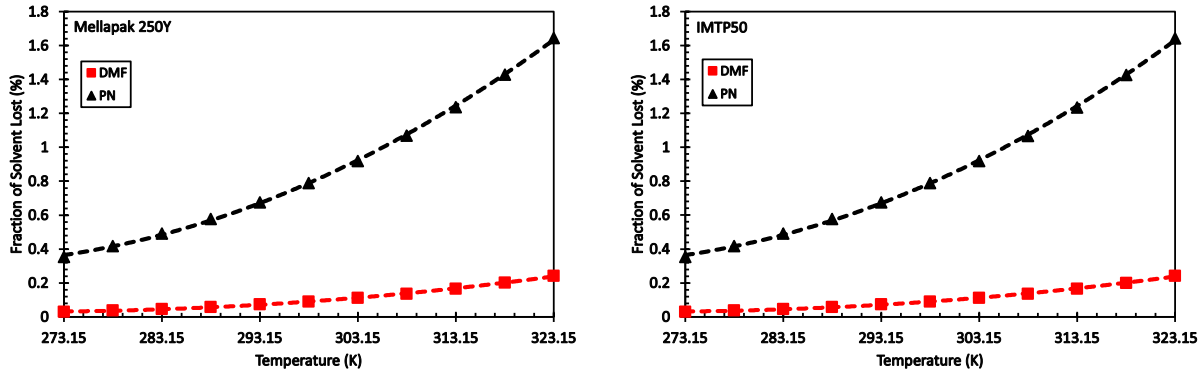
Figure 7.45: Percentage of solvent lost using Mellapak 250Y and IMTP50 (NHCs)

7.4.4 Absorber

The absorber diameter and height are given in Figures 7.46 and 7.47 and as can be seen the size of the absorber increases with temperature due to the need for high solvent flow rate, which requires a large absorber diameter to avoid flooding and consequently a taller absorber. Using IMTP50 leads to needing smaller absorbers than when using Mellapak 250Y because IMTP50 can handle higher flow rates without flooding.
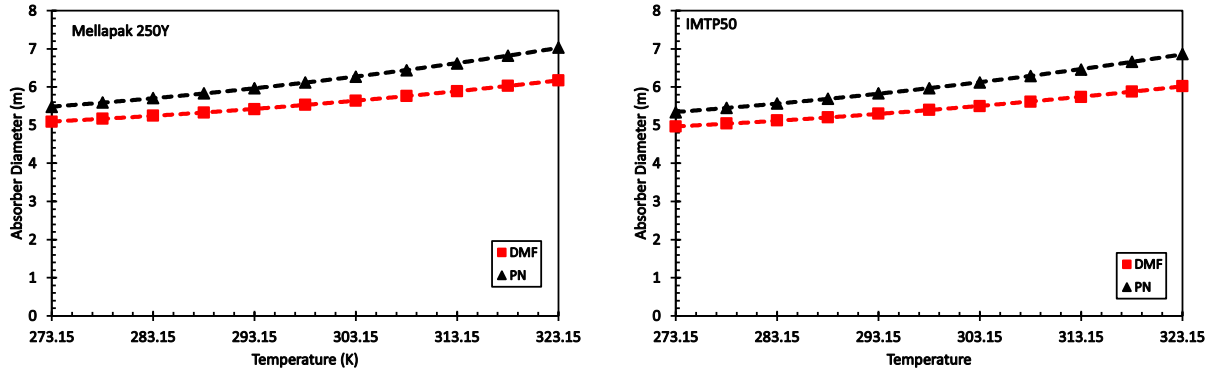
Figure 7.46: Absorber diameter using Mellapak 250Y and IMTP50 (NHCs)
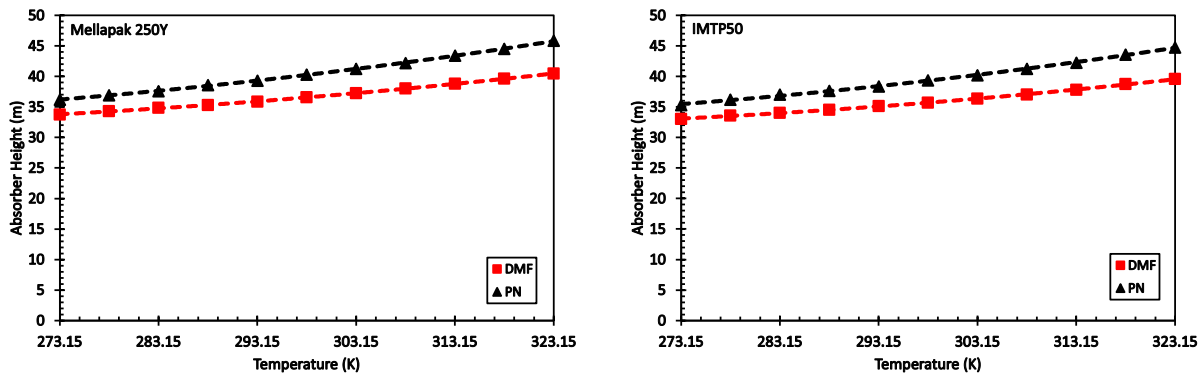
Figure 7.47: Absorber height using Mellapak 250Y and IMTP50 (NHCs)

7.4.5 HP Flash Drum Pressure

Figure 7.48 shows the pressure of the HP flash drum decreases with increasing temperature. DMF shows higher pressures in the flash drum than PN, which indicates that PN absorbs more fuel gas than DMF. Also, Mellapak 250Y or IMTP50 shows similar flash drum pressure.
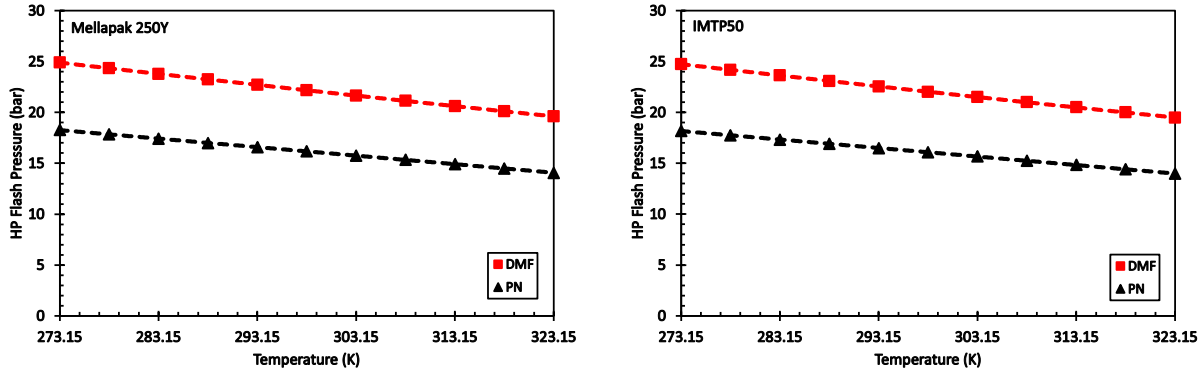
Figure 7.48: Pressure of HP flash drums when using Mellapak 250Y and IMTP50 (NHCs)

7.4.6 Power

Figure 7.49 shows the power requirement for the CO_2 capture process using NHCs increases with temperature due to the need for pumping higher solvent flow rates and processing large gas flow rates entering the first multi-stage compressors. Also, there is no significant difference between the power requirements using Mellapak 250Y and IMTP50 packings.
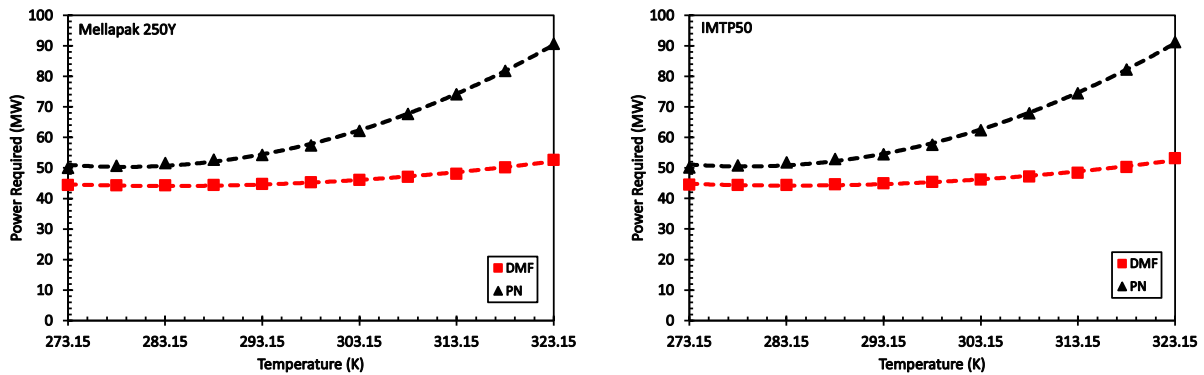
Figure 7.49: Power required to operate plant using Mellapak 250Y and IMTP50 (NHCs)

7.4.7 Capital Expenditure

The total CAPEX of the CO_2 capture process using NHCs is given in Figure 7.50 and as can be seen, the CAPEX values for both solvents increase with temperature due to the need for larger equipment for 90% CO_2 removal and processing large solvent and fuel gas flow rates. DMF showed lower CAPEX than PN due to the need for smaller absorber size.
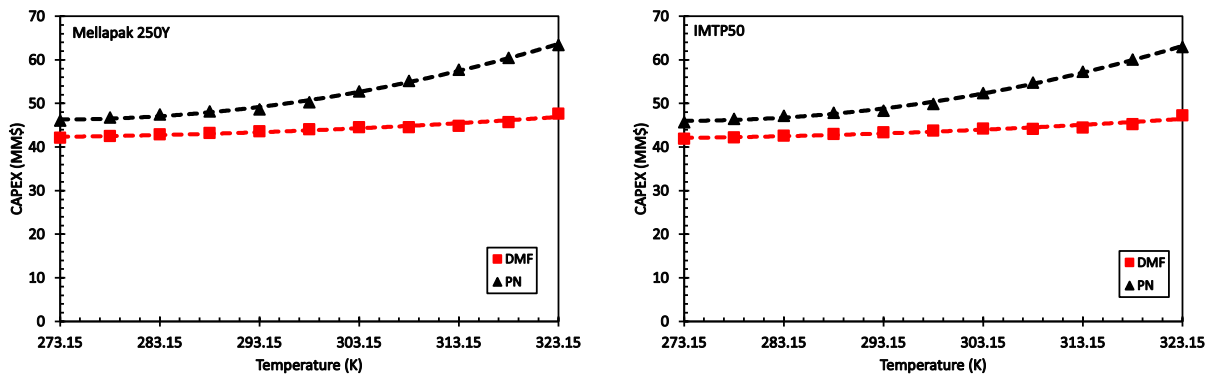
Figure 7.50: CAPEX of capture process using Mellapak 250Y and IMTP50 (NHCs)

7.4.8 Operating Expenditure

Figure 7.51 shows the total OPEX values of the CO_2 capture process increase with temperature due to the increase of the process power consumption, operating and maintenance cost, and solvent losses. The figure also shows DMF has lower OPEX than PN, which means that DMF is a more favorable than PN for CO_2 capture.
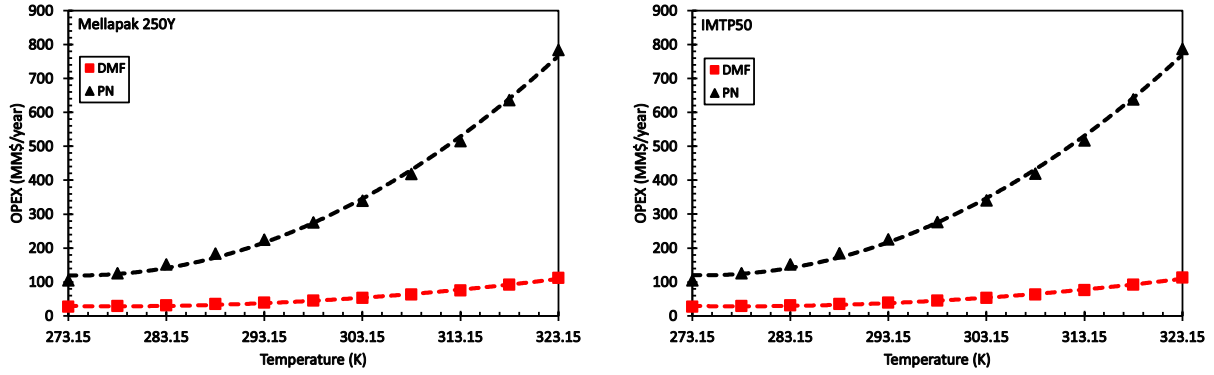
Figure 7.51: OPEX of capture process using Mellapak 250Y and IMTP50 (NHCs)

7.4.9 Levelized Cost

Figure 7.52 shows the LCOC of the NHCs increases with temperature due to the increase of the CAPEX and OPEX. DMF operated at 273.15 K with Mellapak 250Y packing yields the lowest LCOC value at \$8.09/ton CO_2 captured. There is no significant difference between LCOC values using the random and structured packing.
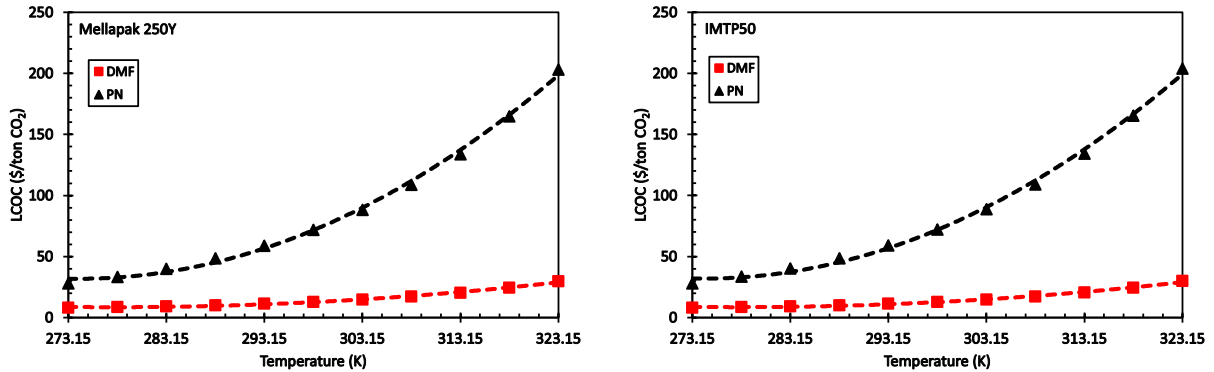
Figure 7.52: LCOC of capture process using Mellapak 250Y and IMTP50 (NHCs)

7.5 Cyclic-Hydrocarbons Used

This category includes the following 5 CycHCs solvents: cis-Decalin, Cyclohexanone, MNPh, NMP, and PC.

7.5.1 Physico-Chemical Properties

Figure 7.53 shows that the density of the CycHCs used ranges from 870 to 1,230 kg/m^3, with PC having the highest and cis-decalin having the lowest density. The vapor pressure of the CycHCs, presented in Figure 7.53, ranges from 1 to more than 2,500 Pa. Cyclohexanone shows the highest vapor pressure, however, it is still lower than those of previously mentioned solvents, which means that the OPEX is not expected to be as strongly affected.
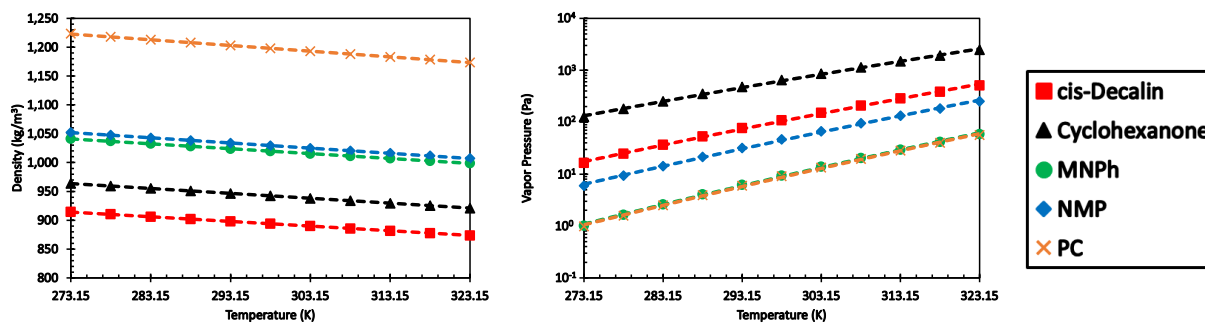
Figure 7.53: Density and vapor pressure of CycHCs

The viscosities of the CycHCs are less than 0.01 Pa.s as shown in Figure 7.54, with NMP having the lowest and MNPh having the highest viscosity on these solvents. The surface tensions of the CycHCs are presented in Figure 7.54 and as can be seen, NMP has the highest surface tension and cis-decalin has the lowest value among these CycHCs.
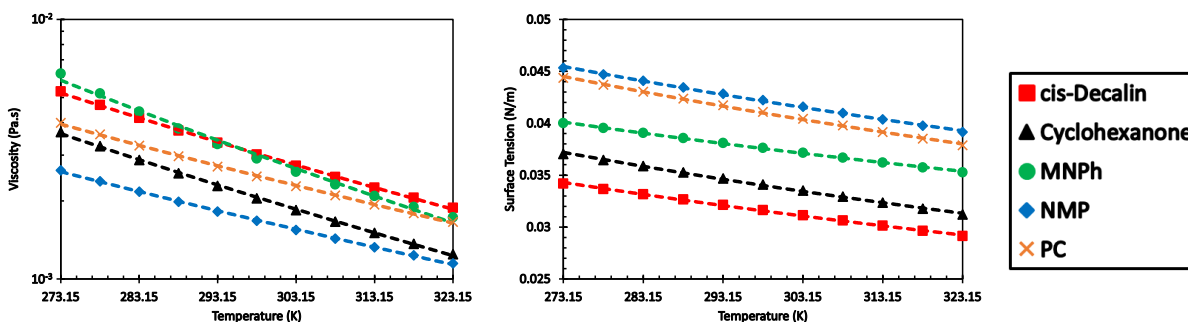
Figure 7.54: Viscosity and surface tension of CycHCs

7.5.2 Solubility of Gases

The solubility of CO_2 in the CycHCs at temperatures 298.15 and 313.15 K are presented in Figure 7.55. The solubility of CO_2 in cyclohexanone is highest while in cis-decalin is the lowest. Also, the solubility of CO_2 decreases in the CycHCs with increasing temperature.
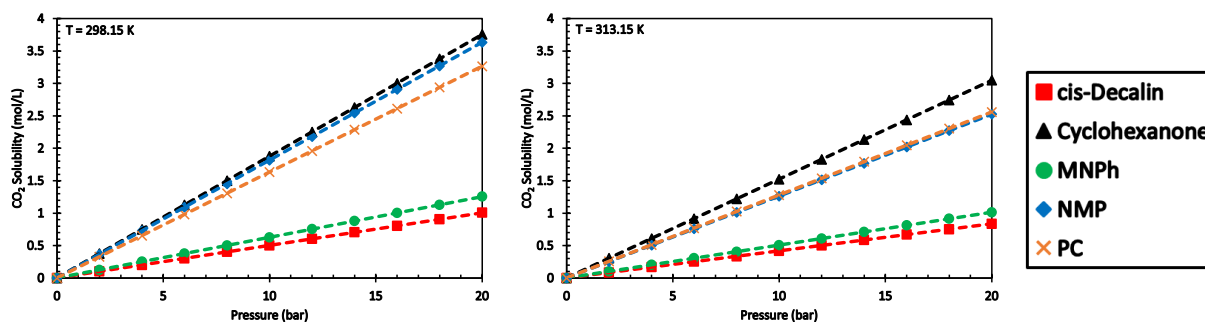
Figure 7.55: Solubility of CO_2 in CycHCs at 298.15 K and 313.15 K

Figure 7.56 shows the solubility of H_2 in the CycHCs increasing with temperature. The H_2 solubility in cis-decalin is the highest at 298.15 K while H_2 solubility in cyclohexanone is the highest at 313.15 K. Also, the H_2 solubilities in MNPh are the lowest at both temperatures.

109
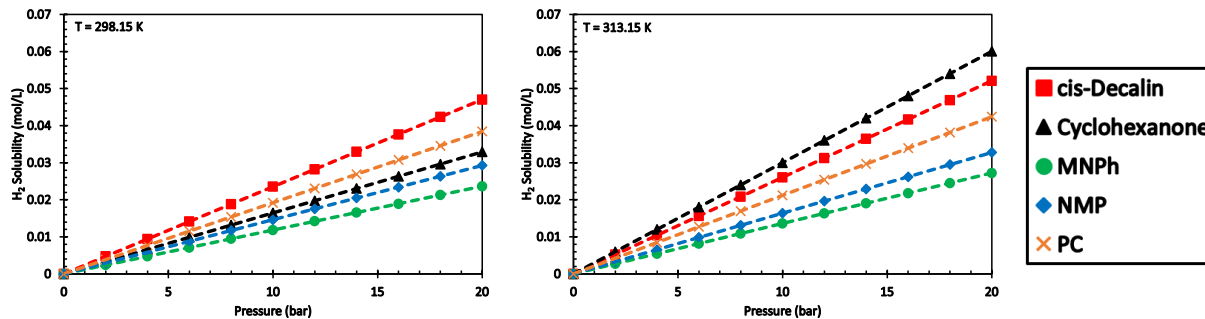
Figure 7.56: Solubility of H_2 in CycHCs at 298.15 K and 313.15 K

7.5.3 Solvent Flow Rate

Figure 7.57 shows the flow rates of CycHCs needed to achieve a 90% CO_2 capture increase with temperature. The required CycHCs flow rate increases due to the decrease of the solubility of CO_2 in the solvents. Since cis-decalin has the lowest CO_2 solubility, it requires the highest solvent flow rate. On the other hand, cyclohexanone needs the lowest flow rate due to its highest CO_2 solubility.
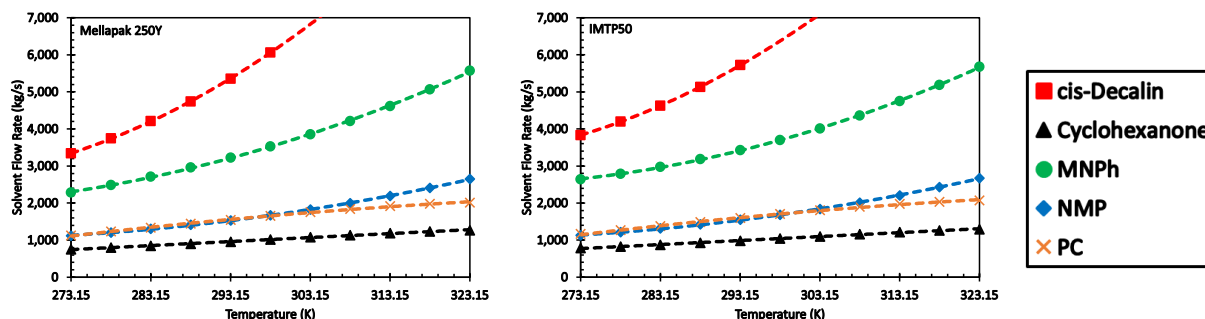
Figure 7.57: Required solvent flow rate using Mellapak 250Y and IMTP50 (CycHCs)

Figure 7.58 shows that cyclohexanone has the most losses among these CycHCs because its vapor pressure is also the highest among them. Also, the percentage loss of solvent increases

110

with increasing temperature. There is also no difference between the solvent loss using the structured and random packing.
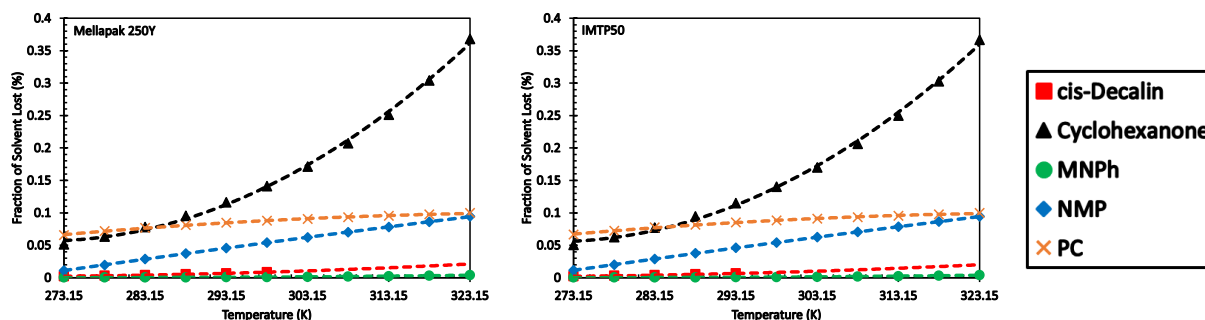
Figure 7.58: Percentage of solvent lost using Mellapak 250Y and IMTP50 (CycHCs)

7.5.4 Absorber

Figures 7.59 and 7.60 show the absorber diameter and height increase with temperature due to the need for high solvent flow rates. The use of cis-decalin solvent requires the largest absorber size due to its high solvent flow rate, whereas cyclohexanone requires a smaller absorber size due to its low solvent flow rate. Using IMTP50 needs a slightly lower diameter than when using Mellapak 250Y because the former can handle higher solvent flow rates without flooding.
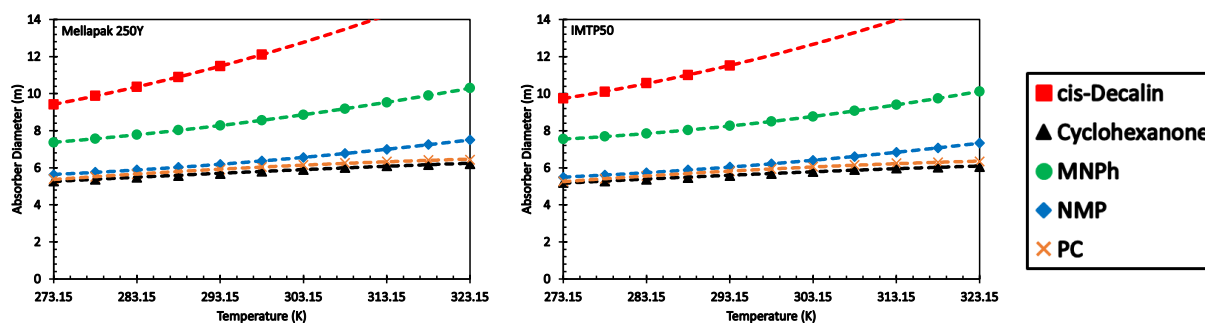
Figure 7.59: Absorber diameter using Mellapak 250Y and IMTP50 (CycHCs)
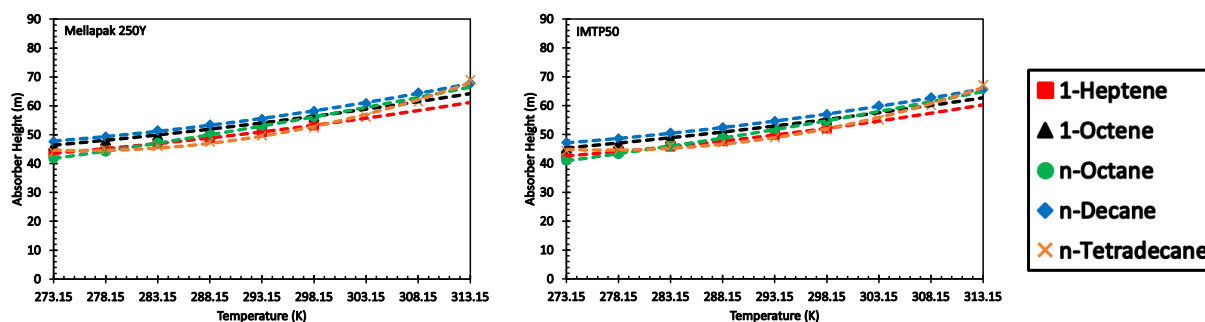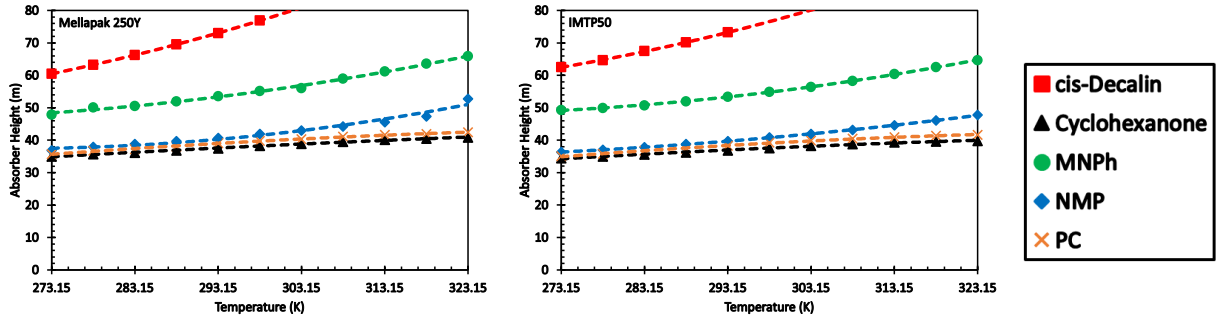
Figure 7.60: Absorber height using Mellapak 250Y and IMTP50 (CycHCs)

7.5.5 HP Flash Drum Pressure

Figure 7.61 shows the pressure of the HP flash drum decreases with temperature, indicating that more H_2 is absorbed at higher temperatures. The cis-decalin shows the lowest flash drum pressures among the CycHCs because it absorbs more fuel gas. Cyclohexanone, NMP, and PC have the highest flash drum pressures, indicating they absorb the least fuel gas.
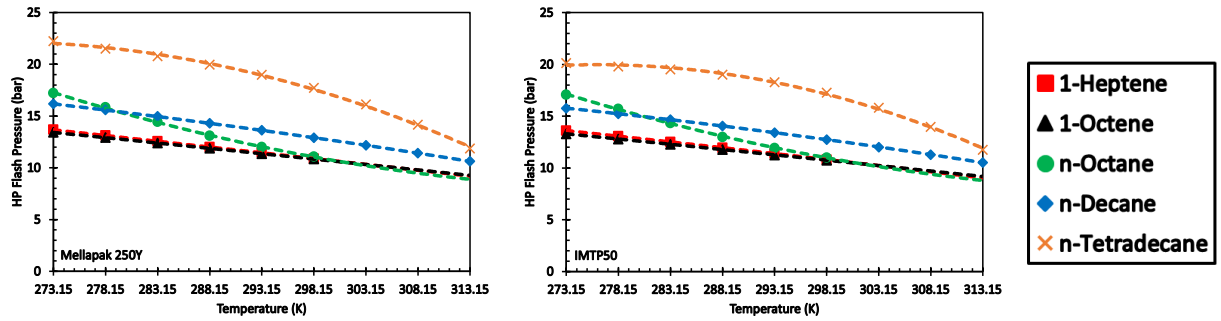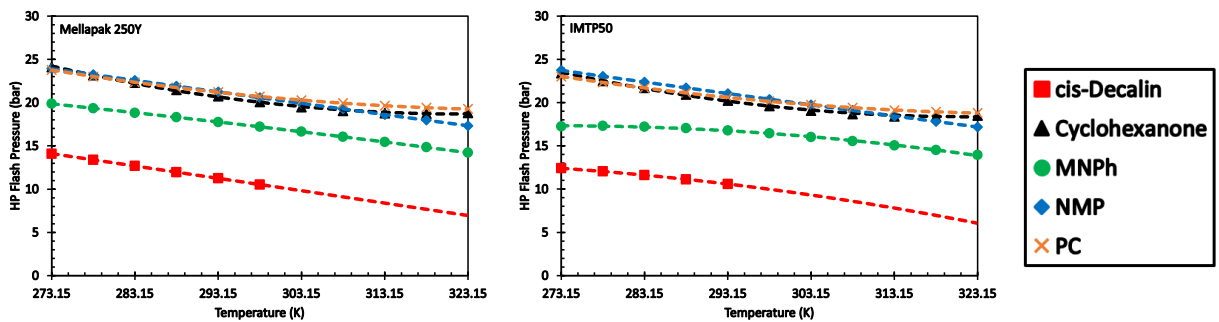

Figure 7.61: Pressure of HP flash drums when using Mellapak 250Y and IMTP50 (CycHCs)

7.5.6 Power

Figure 7.62 shows the power required for the CO_2 capture process using CycHCs increases with increasing temperature. Cyclohexanone needs the lowest power because it needs the lowest flow rates. On the other hand, cis-decalin needs the most power because it requires high solvent flow rates and gas flow rates at the first multi-stage compressors. Also, there is no significant difference between the power requirements when using Mellapak 250Y and IMTP50 packings.
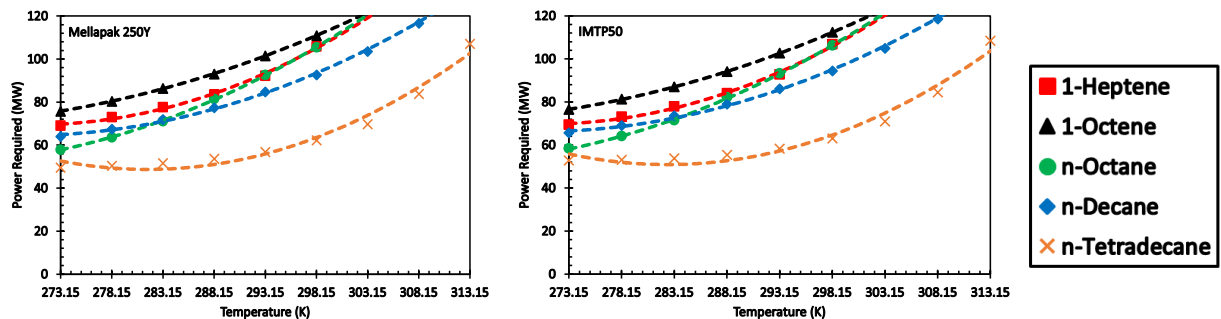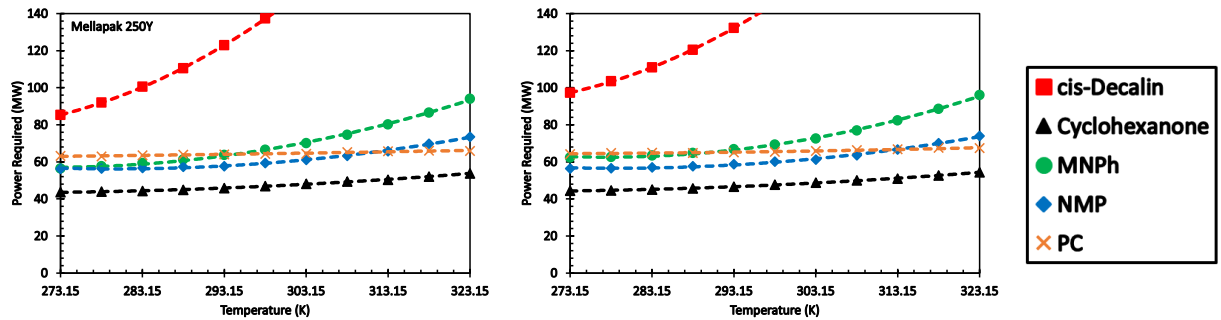

Figure 7.62: Power required to operate plant using Mellapak 250Y and IMTP50 (CycHCs)

7.5.7 Capital Expenditure

The total CAPEX of the CO_2 capture process using CycHCs shown in Figure 7.63 indicates that the CAPEX values increase with temperature. This can be attributed to the need of large equipment. Among the CycHCs used, cyclohexanone shows the lowest CAPEX while cis-decalin shows the highest CAPEX, making it less favorable.
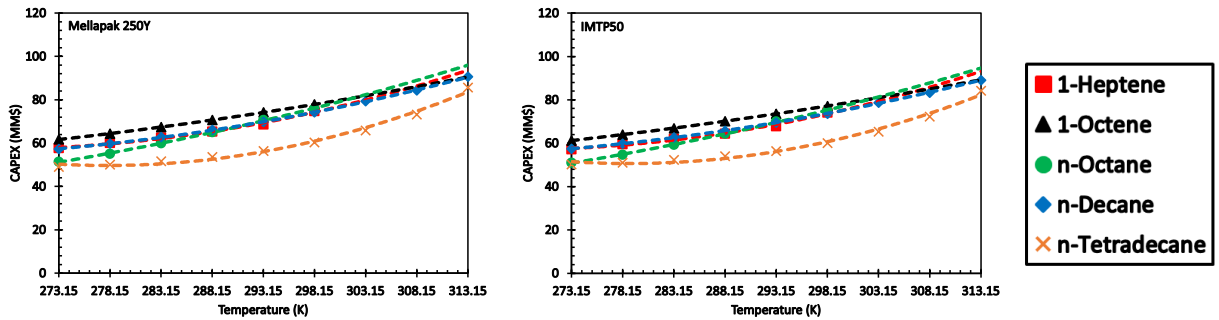
113
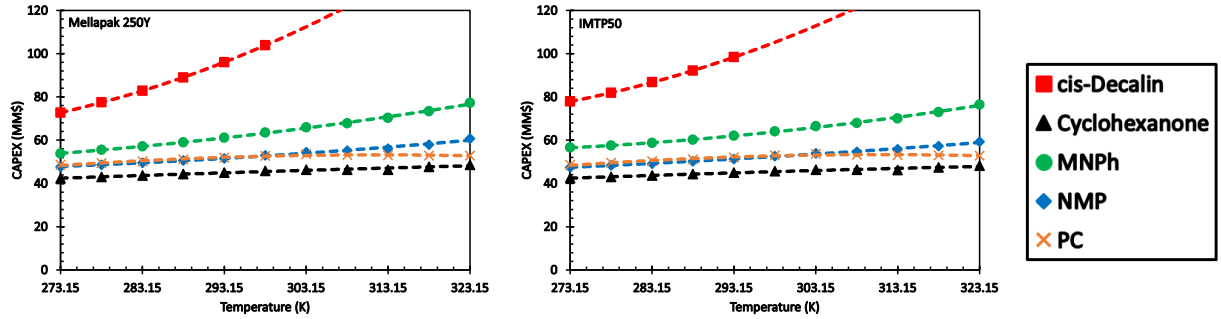
Figure 7.63: CAPEX of capture process using Mellapak 250Y and IMTP50 (CycHCs)

7.5.8 Operating Expenditure

Figure 7.64 shows the total OPEX increases with temperature due to the increase in the power consumption, the increase of the operating and maintenance cost, and solvent losses. MNPh shows the lowest OPEX among the CycHCs, indicating that it is more favorable for the CO_2 capture process. On the other hand, cis-decalin, cyclohexanone, and NMP show the highest OPEX due to the high losses when using cis-decalin and cyclohexanone, and the hydrophilic nature of NMP, which requires further processing to remove the dissolved water.
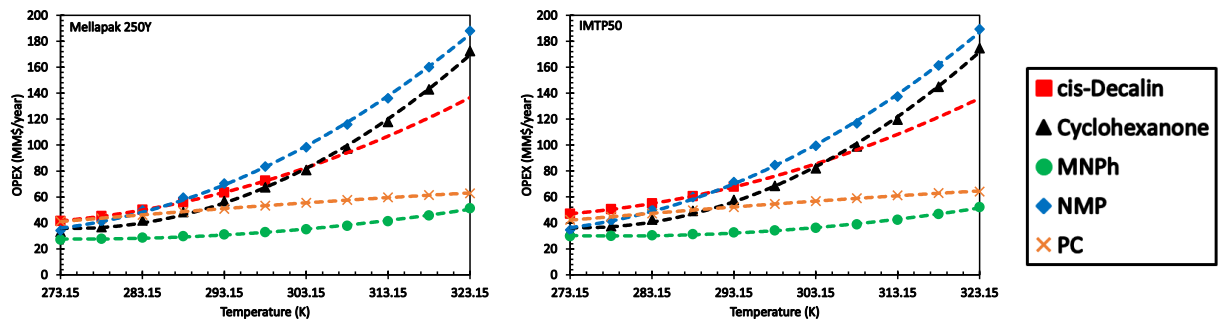
Figure 7.64: OPEX of capture process using Mellapak 250Y and IMTP50 (CycHCs)

7.5.9 Levelized Cost

The LCOC of the CycHCs is presented in Figure 7.65 and as can be seen the LCOC increases with temperature. There is no significant difference between the LCOC values when using the Mellapak 250Y and IMTP50 packings. Also, using MNPh at 273.15 K with Mellapak 250Y packing yields the lowest LCOC value at \$8.56/ton CO_2 captured.
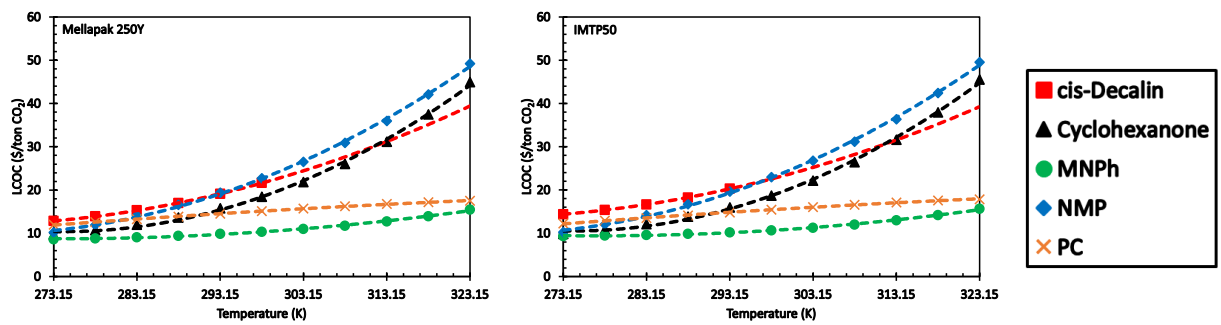
Figure 7.65: LCOC of capture process using Mellapak 250Y and IMTP50 (CycHCs)

7.6 Polymers Used

This category includes the following 3 polymers: PEGDME (which is obtained from Field and Brasington Aspen simulation [38]), PEGPDMS-1, and PEGPDMS-3.

7.6.1 Physico-Chemical Properties

Figure 7.66 shows that the density of the three polymers used ranges from 958 to 1,080 kg/m^3 and PEGDME has the highest, while PEGPDMS-1 has the lowest density. Figure 7.66 also

shows the vapor pressure of the three polymers ranges from 0 to more than 1 Pa, which is found to be very low compared to vapor pressure of the other solvents used. This implies that the losses using these three polymers and accordingly their OPEX would be lower than those of other solvents used.
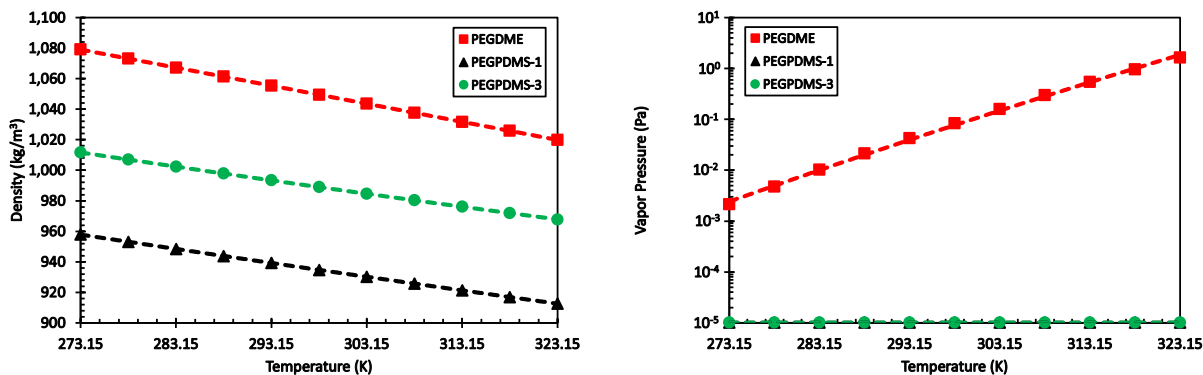
Figure 7.66: Density and vapor pressure of polymers

Figure 7.67 shows that the viscosities of the polymers used are less than 0.1 Pa.s with PEGPDMS-3 having the highest, while PEGPDMS-1 having the lowest viscosity among the three solvents. The surface tension of the polymers is also presented in Figure 7.67 and as can be seen, PEGDME has the highest surface tension, while PEGPDMS-1 and PEGPDMS-3 have lower and similar surface tensions.
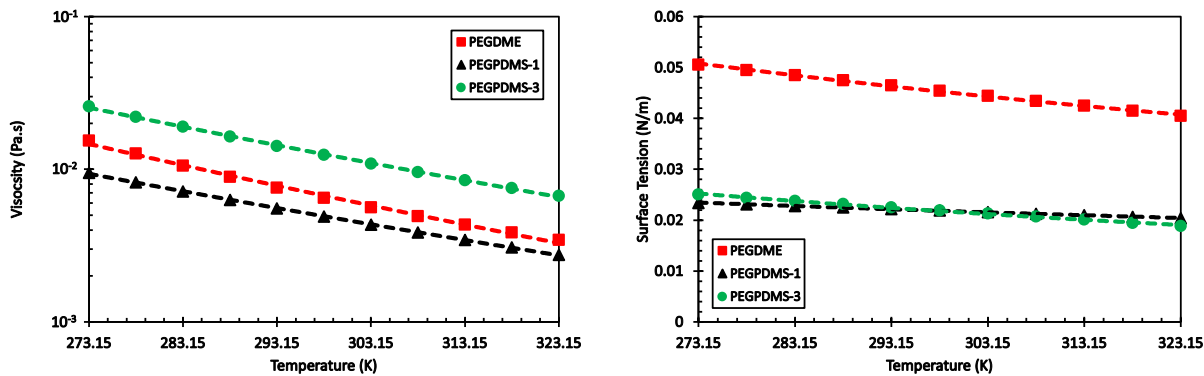
Figure 7.67: Viscosity and surface tension of the polymers

7.6.2 Solubility of Gases

The solubility of CO_2 in the polymers at temperatures 298.15 and 313.15 K are shown in Figure 7.68; and as can be observed the solubility of CO_2 in PEGPDMS-1 is the highest and those in PEGDME and PEGPDMS-3 lower and are similar. In addition, the solubility of CO_2 in the three polymers decreases with increasing temperature.
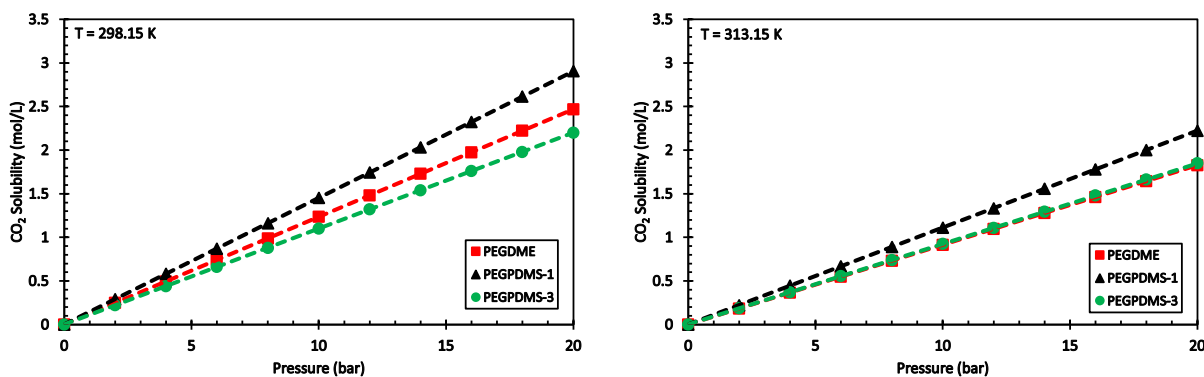
Figure 7.68: Solubility of CO_2 in polymers at 298.15 K and 313.15 K

The solubility of H_2 in the polymers at 298.15 and 313.15 K are shown in Figure 7.69, and as can be seen, the solubility of H_2 PEGPDMS-1 and PEGPDMS-3 increases with temperature.

117

On the other hand, the solubility of H_2 in PEGDME (based on Field and Brasington Aspen simulation [38]) decreases with increasing temperature, which could be questionable.
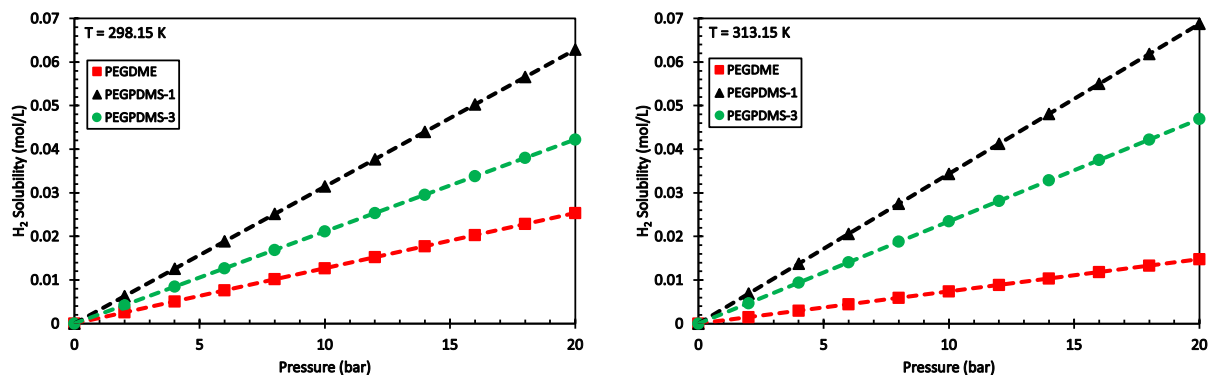
Figure 7.69: Solubility of H_2 in polymers at 298.15 K and 313.15 K

7.6.3 Solvent Flow Rate

The flow rate of the three polymers required to capture 90% of the CO_2 increases with temperature as presented in Figure 7.70, which could be attributed to the decrease of the CO_2 solubility with increasing temperature in the three polymers. Figure 7.70 also shows that PEGPDMS-1 requires the lowest flow rate because it had the highest CO_2 solubility. On the other hand, at low temperatures, PEGDME and PEGPDMS-3 require similar flow rates while at high temperatures, PEGPDMS-3 requires lower flow rates than PEGDME.
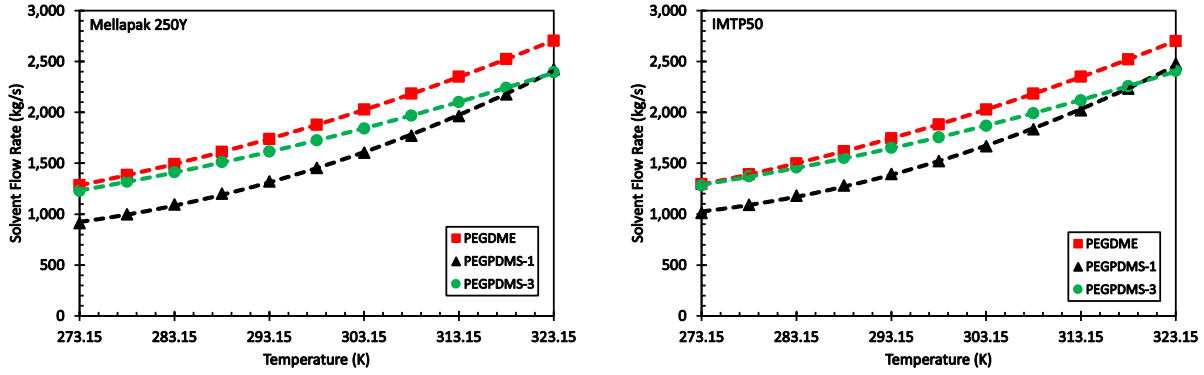
Figure 7.70: Required polymers flow rate using Mellapak 250Y and IMTP50

Figure 7.71 shows the amount of solvent lost is very low for PEGPDMS-1 and PEGPDMS-3 in the as shown in temperature range from 273.15 K to 323.15 K. Figure 7.71 also shows that the losses when using PEGDME are greater than those when using the other two polymers. These are true for the two packings used.
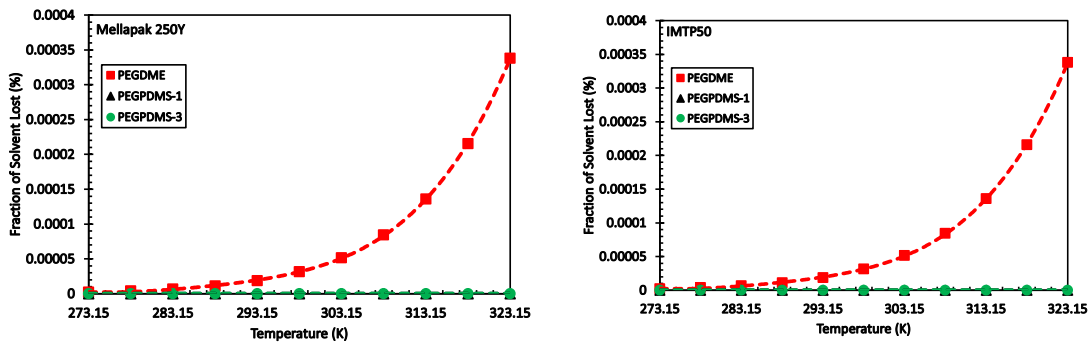
Figure 7.71: Percentage of solvent loss using Mellapak 250Y and IMTP50 (Polymers)

7.6.4 Absorber

Figures 7.72 and 7.73 show that the absorber diameter and height when using the three polymers increase with increasing temperature. This can be attributed to the higher flow rates

needed to achieve 90% CO_2 capture. In addition, using Mellapak 250Y and IMTP50 requires similar absorber sizes for the three polymers used, and no significant effect of the packing type on the absorber size can be observed.
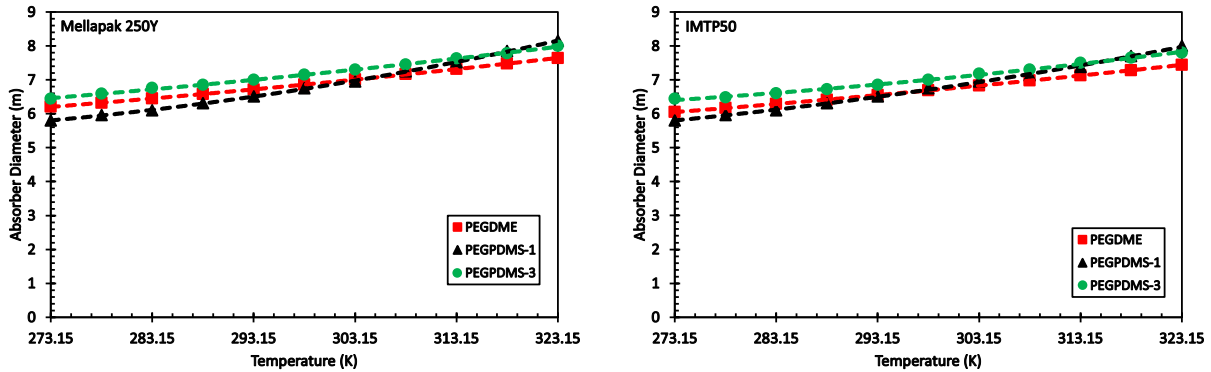
Figure 7.72: Absorber diameter using Mellapak 250Y and IMTP50 (Polymers)
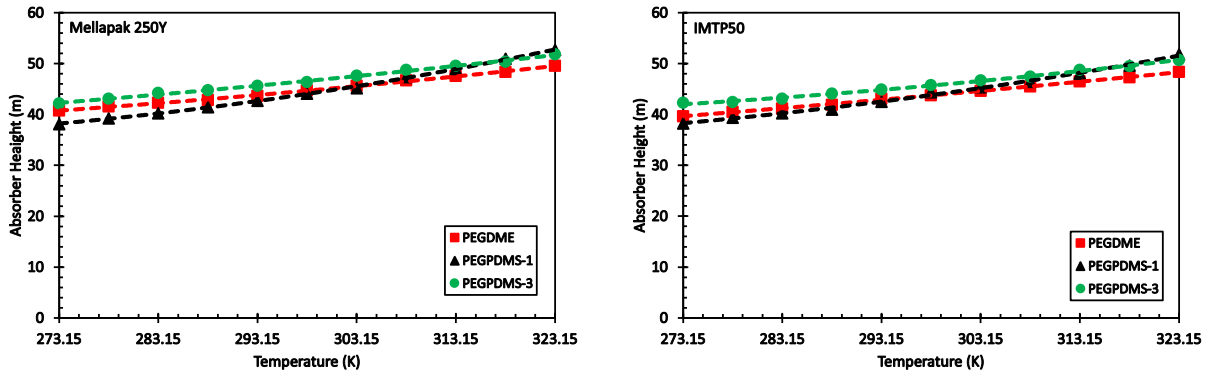
Figure 7.73: Absorber height using Mellapak 250Y and IMTP50 (Polymers)

7.6.5 HP Flash Drum Pressure

The pressure of the HP flash drum presented as a function of temperature is shown in Figure 7.74; and as can be seen for PEGPDMS-1 and PEGPDMS-3 at high process temperatures, lower pressures in the HP flash drum are needed. This is because at high process temperatures fuel gas

is absorbed in the solvent and lower pressures are required to remove it to satisfy the low fuel gas constraint. On the other hand, for PEGDME at high process temperature, higher pressure in the HP flash drum is accepted. This is because at high process temperature, less fuel gas is absorbed in the PEGDME, which is indicated by the decrease of H_2 solubility with temperature in this solvent as depicted in Figure 7.69. Figure 7.74 also shows using IMTP50 requires lower pressures in the HP flash drum than when using Mellapak 250Y, suggesting that more fuel gas is absorbed when using the random packing making the structured packing is more favorable for the capture process.
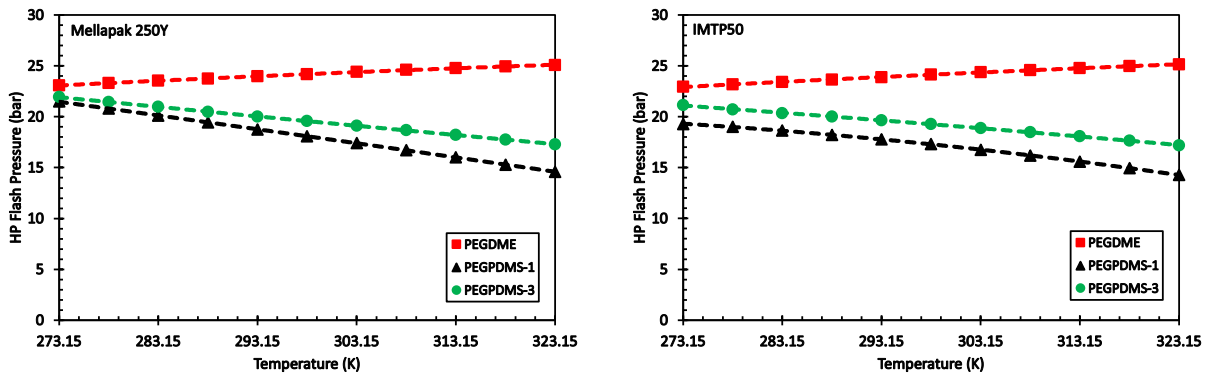
Figure 7.74: Pressure of HP flash drums when using Mellapak 250Y and IMTP50 (Polymers)

7.6.6 Power

Figure 7.75 shows that the power required for the CO_2 capture process when using the three polymers increases with increasing operating temperature. Also, using IMTP50 entails a slightly higher power requirement than when using Mellapak 250Y. In general, Figure 7.75 indicates that at higher temperatures, lower power requirements when using PEGDME than those when using

121

the other two solvents. This behavior can be attributed to the lower amount of fuel gas absorbed and consequently lower gas compression requirements.
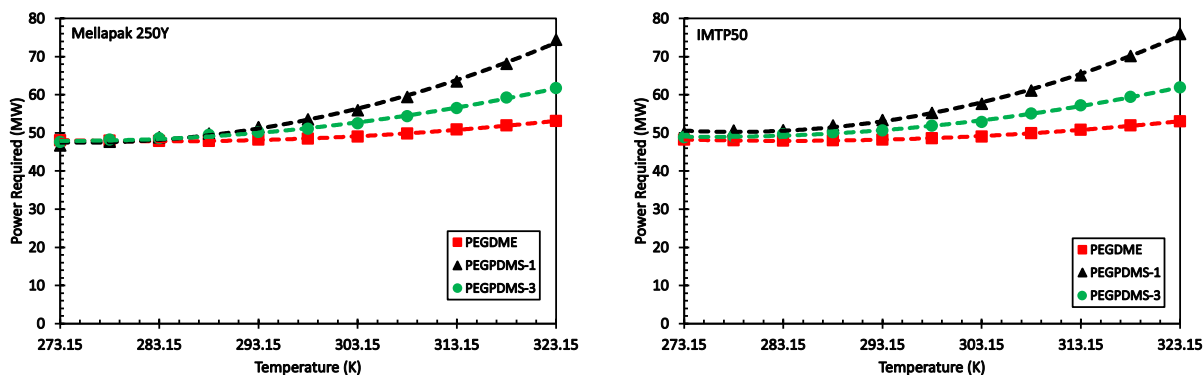
Figure 7.75: Power required to operate plant using Mellapak 250Y and IMTP50 (Polymers)

7.6.7 Capital Expenditure

Figure 7.76 shows the CAPEX of the CO_2 capture process when using the three polymers increases with temperature due to the larger equipment used to handle the high fuel gas and solvent flow rates. From 273.15 to 288.15 K PEGPDMS-1 has the lowest CAPEX among the three polymers used, however, beyond 288.15 K, PEGDME has the lowest CAPEX making it more favorable solvent at high operating temperatures.
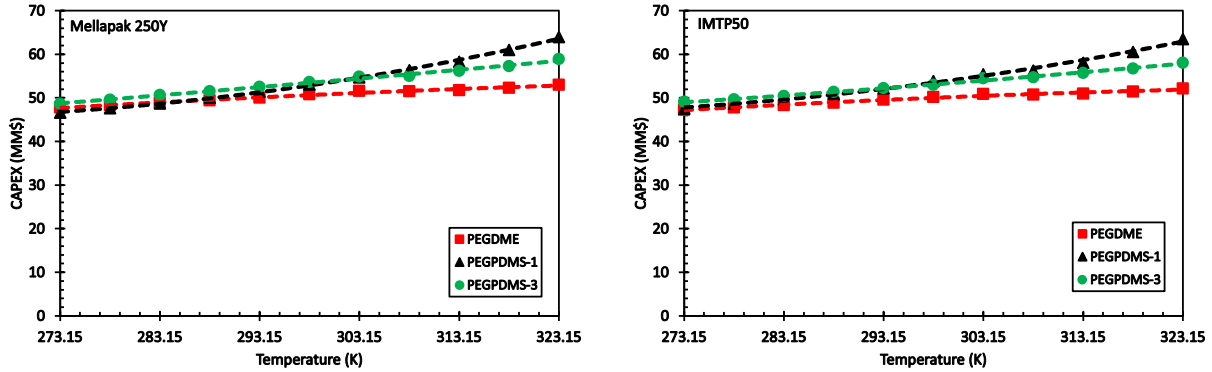
Figure 7.76: CAPEX of capture process using Mellapak 250Y and IMTP50 (Polymers)

7.6.8 Operating Expenditure

Figure 7.77 shows the total OPEX values of the polymers increase with process temperature. This behavior is due to the increase in the power requirement for the CO_2 capture process and the increase of the operating and maintenance cost due to the increased CAPEX. From 273.15 to 283.15 K, PEGPDMS-1 shows the lowest OPEX among the three solvents, while at temperatures greater than 283.15 K, PEGDME shows lower OPEX values. This can be attributed to the decrease of H_2 solubility in PEGDME and its increase in the other two solvents with increasing process temperature. These OPEX values are considered the lowest among those of all the solvents used. Also, there is no significant difference in the OPEX of the three polymers when using either Mellapak 250Y or IMTP50 packing.
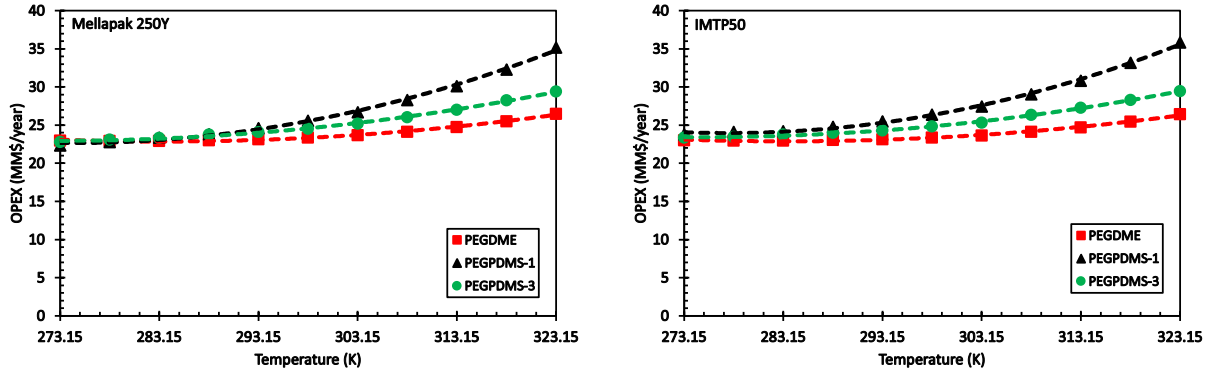
Figure 7.77: OPEX of capture process using Mellapak 250Y and IMTP50 (Polymers)

7.6.9 Levelized Cost

Figure 7.78 shows that the LCOC behavior of the three polymers presented as a function of the process temperature is similar to that of their OPEX shown above in Figure 7.77. As the temperature increases, the LCOC increases with no significant difference between the values when using Mellapak 250Y and IMTP50. In this study, these three polymers were found to be the best performing category due to their high CO_2 solubility combined with their low vapor pressures. The lowest LCOC value ($7.15/ton CO_2 captured) was obtained for PEGDME-1 at 273.15 K when using Mellapak 250Y packing.
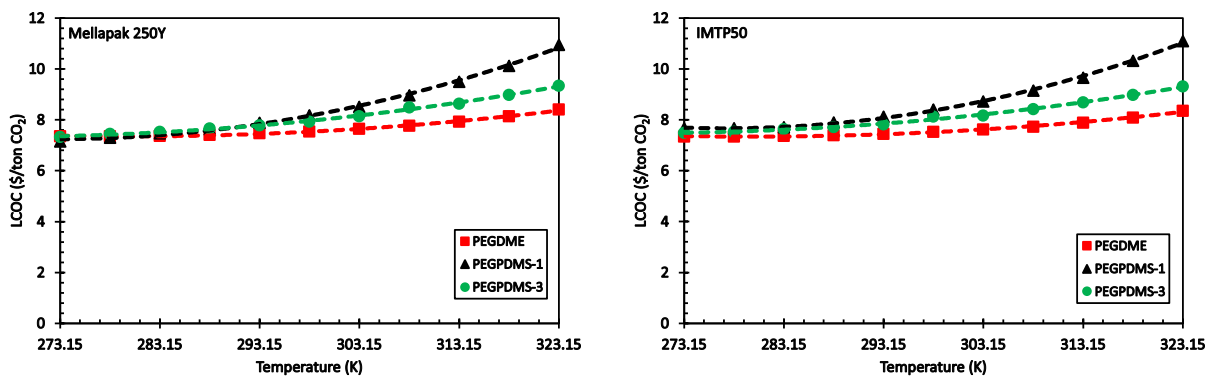
Figure 7.78: LCOC of capture process using Mellapak 250Y and IMTP50 (Polymers)

7.7 Subcooled Solvents Used

This category includes the following 2 solvents: methanol and THF.

7.7.1 Physico-Chemical Properties

Due to the volatility of the methanol and THF, subcooled temperatures were used to reduce the solvent loss. Figure 7.79 shows the density of the two solvents ranges from 807 to 961 kg/m^3 within the temperature range of 223.15 to 273.15 K, with THF having higher density values than methanol. Figure 7.79 also shows the vapor pressure of the two solvents range from 10 to about 10,000 Pa. It should be noted that even at low temperatures, methanol and THF have relatively high vapor pressure, which ultimately leads to high solvent loss and consequently high OPEX.
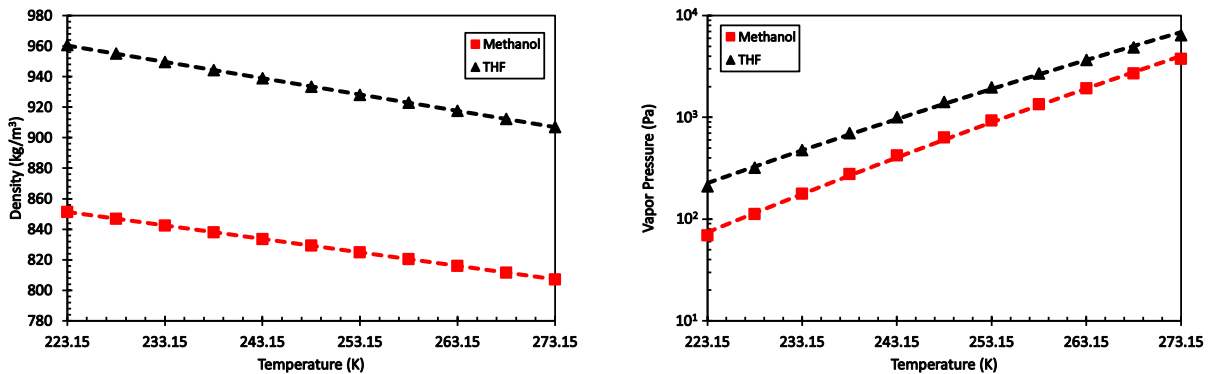
Figure 7.79: Density and vapor pressure of subcooled solvents

The viscosity of the two solvents, shown in Figure 7.80 are very low compared to the other solvents used in this study. This is considered an advantage because they will require smaller absorbers and lower pumping costs. The surface tension of the two solvents is also presented in

Figure 7.80 and indicates that THF exhibits higher surface tensions than methanol at the same temperature.
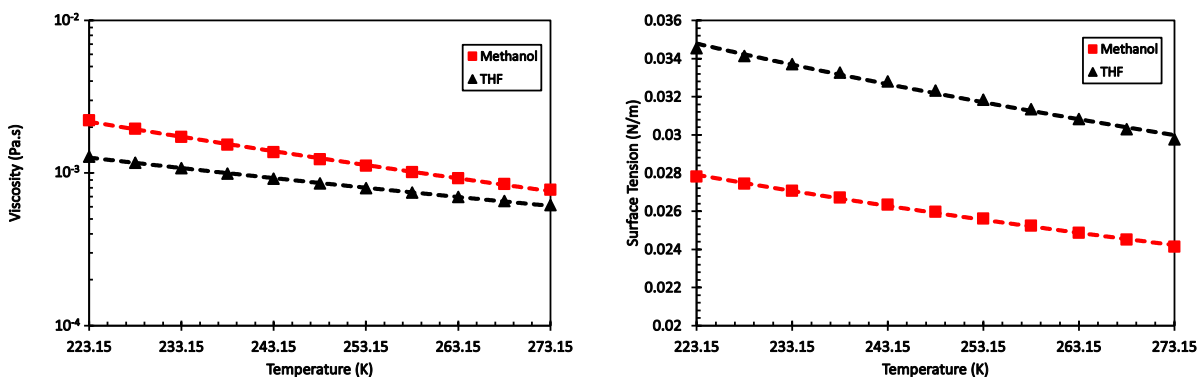
Figure 7.80: Viscosity and surface tension of subcooled solvents

7.7.2 Solubility of Gases

The solubility of CO_2 in the subcooled solvents at temperatures 233.15 and 248.15 K are shown at Figure 7.81 and as can be observed, the solubility values of CO_2 in THF is greater than those in methanol. These two solvents showed very high solubilities compared to other solvents due to the very low temperatures used in the CO_2 capture process. Figure 7.81 shows the CO_2 solubilities in both solvents decrease with increasing temperature.
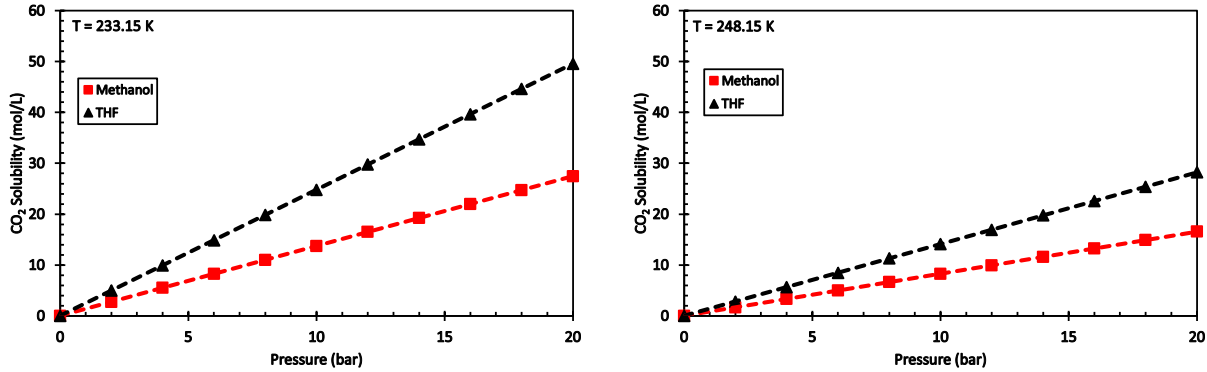
Figure 7.81: Solubility of CO₂ in subcooled solvents at 233.15 K and 248.15 K

The solubility of H_2 in the two solvents at 233.15 and 248.15 K are shown in Figure 7.82 and as can be observed the solubility values of H_2 in the two solvents decrease with increasing temperature because. The H_2 solubility in methanol is significantly higher than that in THF and other solvents used in this study due to the low process temperature.
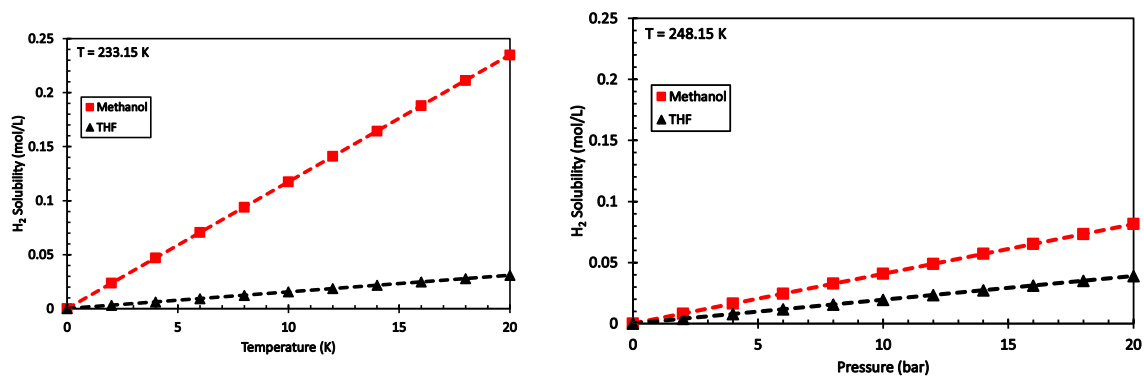
Figure 7.82: Solubility of H₂ in the subcooled Solvents at 233.15 K and 248.15 K

7.7.3 Solvent Flow Rate

Figure 7.83 shows that the flow rate of the two solvents required for 90 mol% CO_2 capture increases with the process temperature because CO_2 solubility in the two solvents decrease with

increasing temperatures. From temperatures 223.15 to 243.15 K, methanol requires a lower flow rate than THF and after 243.15 K THF requires a lower flow rate. This is due to the CO_2 solubility in methanol being higher than that of THF at lower temperatures and becomes lower at higher temperatures. In this study, the flow rates of methanol and THF are the lowest among those of all solvents used.
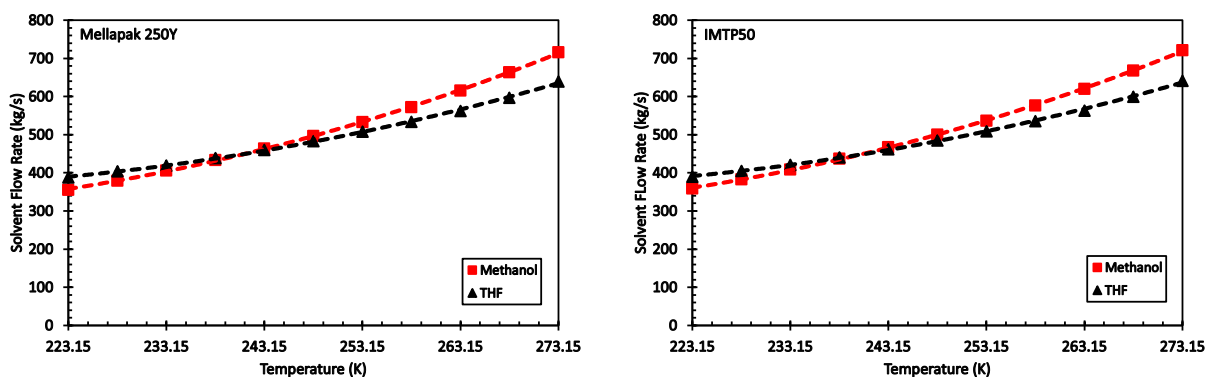
Figure 7.83: Required solvent flow rate using Mellapak 250Y and IMTP50 (Subcooled)

However, due to the high vapor pressures of the two solvents, the amount of solvent lost increases with temperature and is significant as shown in Figure 7.84. In addition, there is no difference between the amount of solvent lost using the structured and random packings.
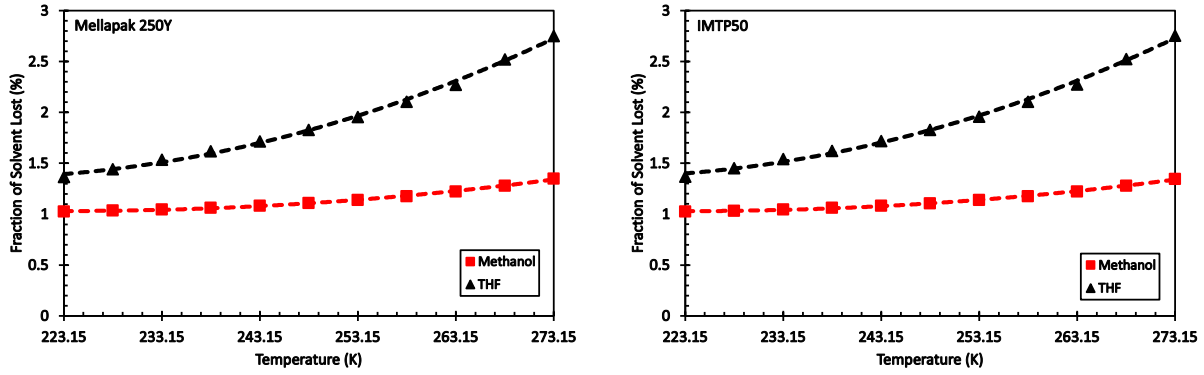
Figure 7.84: Percentage of solvent lost using Mellapak 250Y and IMTP50 (Subcooled)

7.7.4 Absorber

The absorber diameter and height are shown in Figures 7.85 and 7.86 for methanol and THF; and as can be seen the absorber diameter and height increase with increasing process temperature. Also, the figures indicate that using IMTP50 packing requires a smaller absorber due to its ability to handle higher flow rates without flooding. In this study, the absorber sizes for methanol and THF are the lowest among those of all solvents used due to smallest required flow rates.
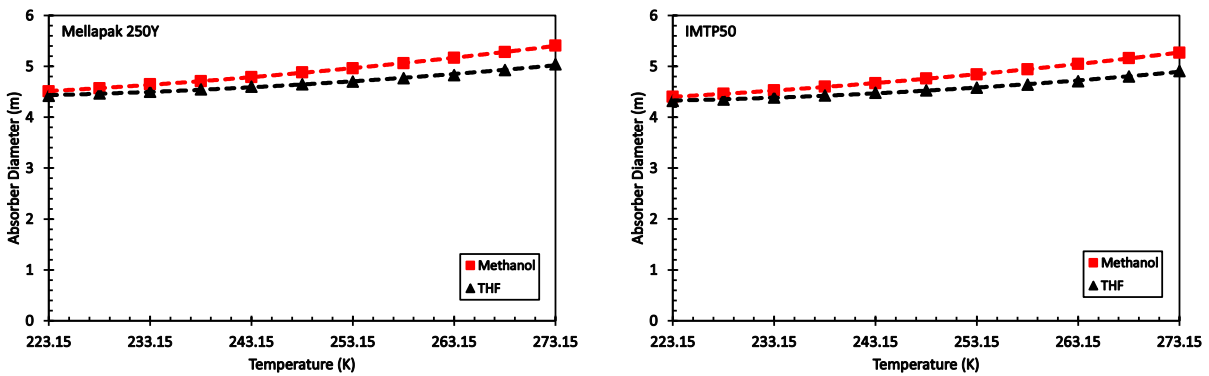
Figure 7.85: Absorber diameter using Mellapak 250Y and IMTP50 (Subcooled)
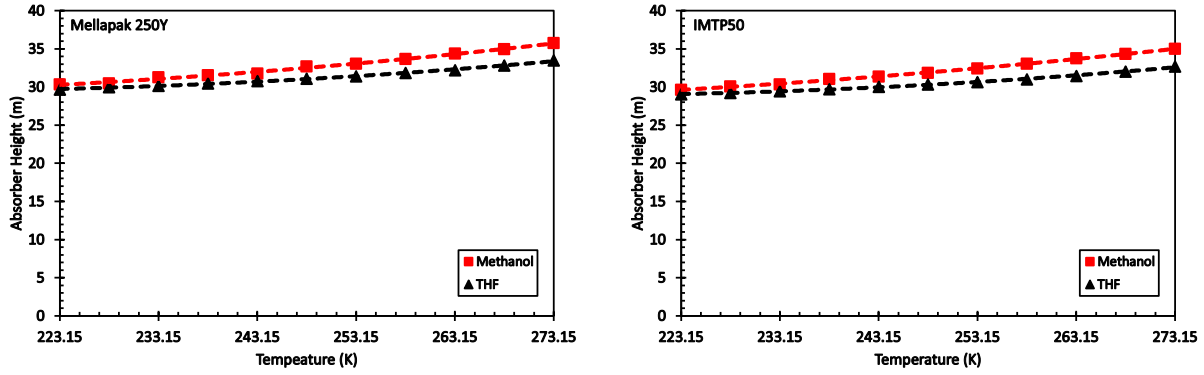
Figure 7.86: Absorber height using Mellapak 250Y and IMTP50 (Subcooled)

7.7.5 HP Flash Drum Pressure

The pressure of the HP flash drum presented as a function of temperature is shown in Figure 7.87, and as can be seen for methanol and THF at high process temperatures, lower pressures in the HP flash drum are needed. This is because at high process temperatures fuel gas is absorbed in the solvent and lower pressures are required to remove it to satisfy the low fuel gas constraint. In addition, there is no significant difference between the flash drum pressures when using methanol and THF. The pressure of the HP flash drum is similar when using Mellapak 250Y and IMTP50, indicating the amount of fuel gas absorbed is identical for these two packings.
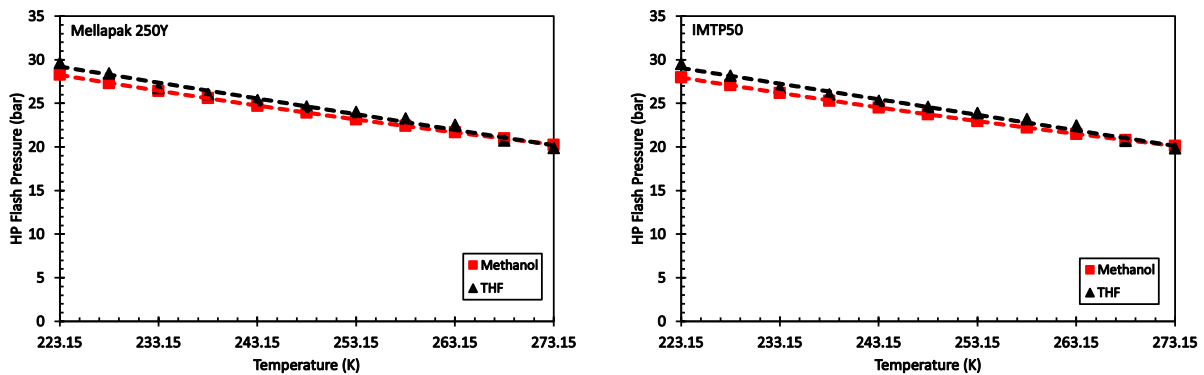
Figure 7.87: Pressure of HP flash drums when using Mellapak 250Y and IMTP50 (Subcooled)

7.7.6 Power

Figure 7.88 shows that the power required to operate the CO_2 capture plant decreases with increasing temperature from 223.15 to 253.15 K, then above 253.15 K, the power starts to increase. The decrease at temperatures up to 253.15 K is due to the higher cooling requirement at the lower temperatures. Above 253.15 K, the multi-stage compressors consume more power than the cooling requirement. Figure 7.88 also indicates that using THF needed lower power than when using methanol and there is no obvious effect of the packing type on the power requirements.
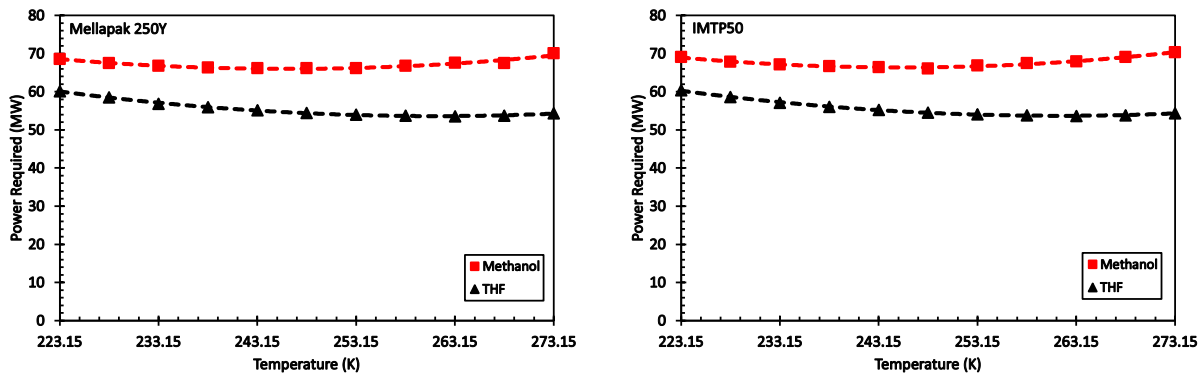
Figure 7.88: Power required to operate plant using Mellapak 250Y and IMTP50 (Subcooled)

7.7.7 Capital Expenditure

Figure 7.89 shows the total CAPEX values increase with temperature for methanol and THF. This is due to the need for large equipment to achieve a 90 mol% CO_2 capture. Mellapak 250Y shows larger CAPEX values than Mellapak 250Y because of its larger absorbers needed.

131
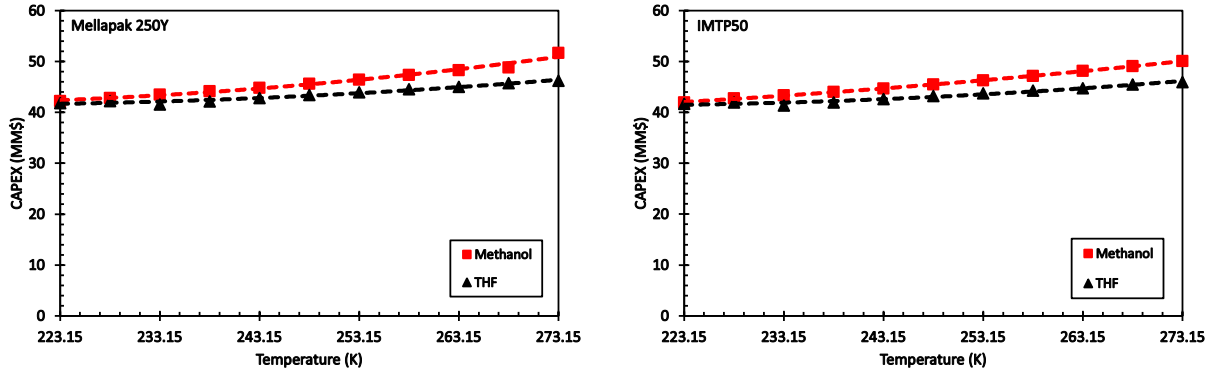
Figure 7.89: CAPEX of capture process using Mellapak 250Y and IMTP50 (Subcooled)

7.7.8 Operating Expenditure

Figure 7.90 shows the total OPEX values increase with process temperature due to the change in the power consumption, increase of the operating and maintenance cost, which increases with CAPEX, and the amount of solvent lost, which requires solvent makeup. IMTP50 shows slightly higher OPEX requirement than Mellapak 250Y due to the need for a larger solvent flow rate.
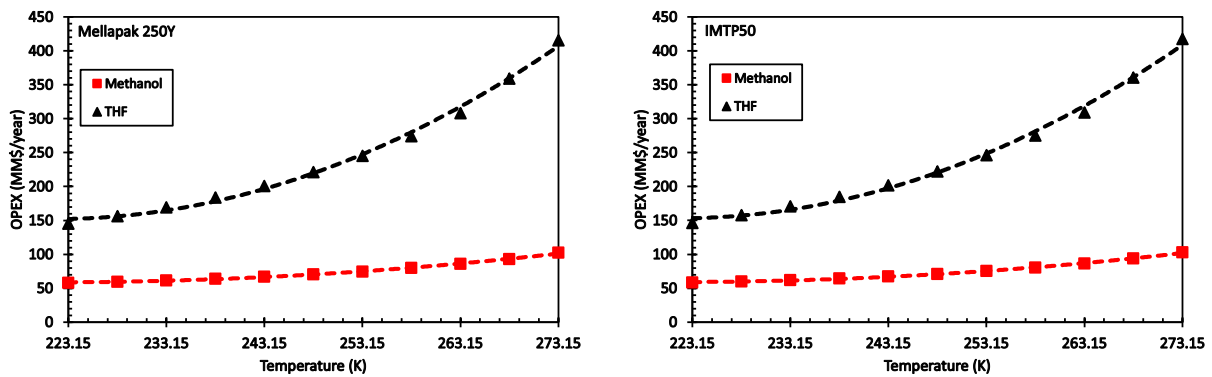
Figure 7.90: OPEX of the CO_2 capture process using Mellapak 250Y and IMTP50 (Subcooled)

7.7.9 Levelized Cost

Figure 7.91 shows the LCOC values for methanol and THF increase with temperature. The figure also indicates that IMTP50 exhibit slightly higher values than Mellapak 250Y due to its higher OPEX. It should be noted that the LCOC has a similar trend to the OPEX, implying that the effect of OPEX on LCOC is more significant than that of CAPEX. Using methanol at 223.15 K with Mellapak 250Y gives LCOC value of \$15.95/ton of CO_2 captured.
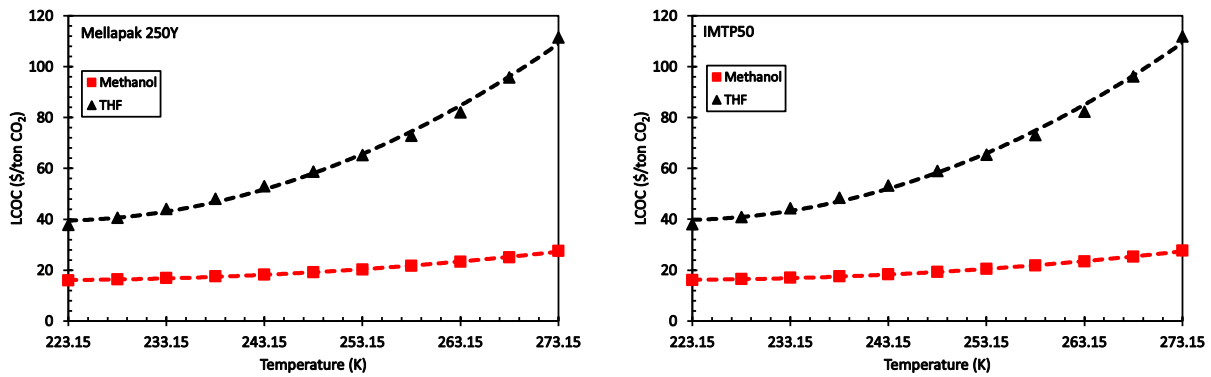
Figure 7.91: LCOC of capture process using Mellapak 250Y and IMTP50 (Subcooled)

7.8 Comparison Among All Solvents Used

Table 7.1 lists the solvents from each category used with the most favorable economics for the CO_2 capture process according to Aspen Plus simulations. For all categories, the lowest operating temperature tested and Mellapak 250Y were the optimal conditions for the pre-combustion CO_2 capture since at the lowest temperature the solubility of CO_2 was the highest and Mellapak 250Y provided a larger specific surface area leading to better mass transfer.

Table 7.1: Most favorable solvents for pre-combustion CO$_2$ capture

Category	Solvent	Temperature (K)	Packing
ILs	[emim][Tf$_2$N]	273.15	Mellapak 250Y
HCs	n-Tetradecane	273.15	Mellapak 250Y
OHCs	DES	273.15	Mellapak 250Y
NHCs	DMF	273.15	Mellapak 250Y
CycHCs	MNPh	273.15	Mellapak 250Y
Polymers	PEGPDMS-1	273.15	Mellapak 250Y
Subcooled	Methanol	223.15	Mellapak 250Y

Figure 7.92 compares the CAPEX, OPEX, and LCOC of the seven selected solvents at their optimal conditions. In this figure, the lowest CAPEX is for DMF followed by methanol due to the need for small absorbers and low solvent costs, while the highest values are for MNPh and [emim][Tf$_2$N] due to the need for large absorbers and high cost of the ILs. The lowest OPEX values are for DES and PEGPDMS-1 with only $40,000 difference between them, while the highest values are for methanol due to the high cooling requirements and high solvent losses. Figure 7.92 also shows that the lowest LCOC values are for DES and PEGPDMS-1, while the highest values are for methanol. It should be noted that the LCOC values behave similarly to those of OPEX.
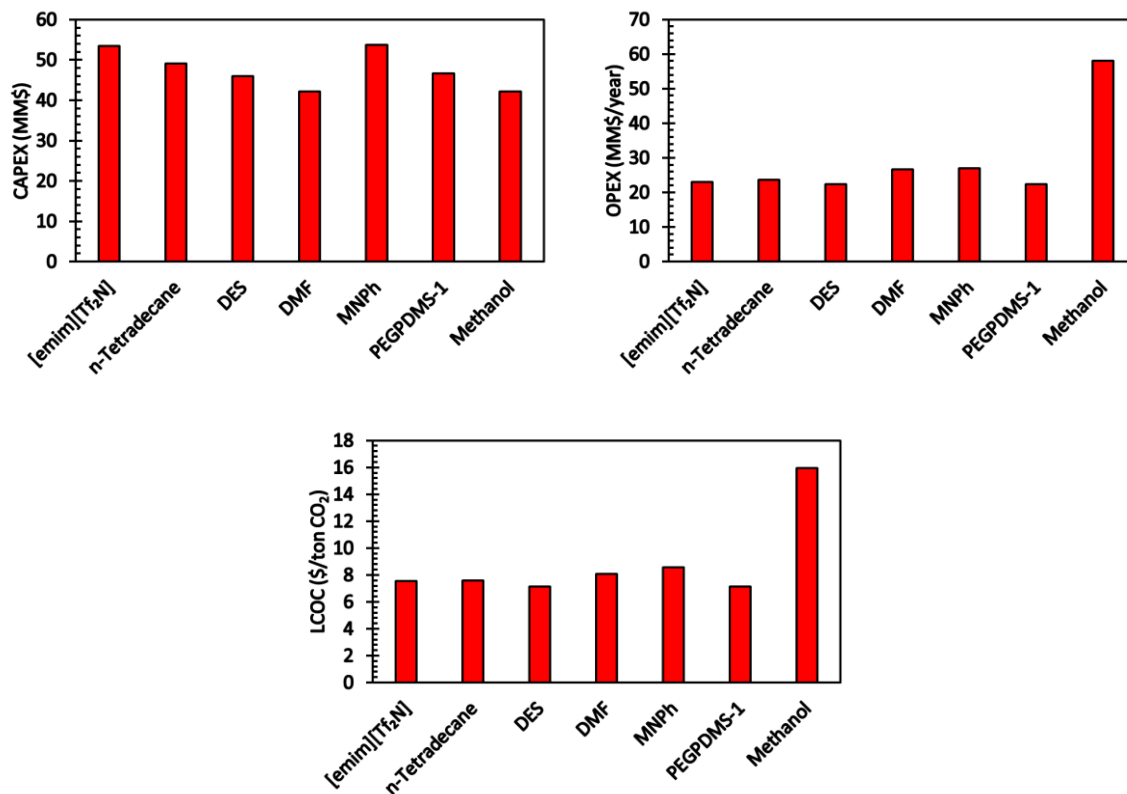
Figure 7.92: CAPEX, OPEX, and LCOC of the best performing solvents for pre-combustion CO₂ capture

7.9 Effect of Plant Scale

Recently, there has been a renewed focus on the development of small-scale modular gasifiers, which can take advantage of local solid feedstocks, and modular-scale synthesis reactors, which can generate local-used fuels, chemicals, and fertilizers [495]. The simulations of the capture process using five potential solvents ([bmim][Tf$_2$N], [emim][Tf$_2$N], DES, PEGPDMS-1, and PEGPDMS-3) at 54 to 543 MW and at temperatures 283.15, 293.15, and 313.15 K. The flow rate of the fuel gas at each plant capacity are shown in Table 7.2.

Table 7.2: Fuel gas flow rate at each plant capacity

Plant power capacity (MW)	Fuel gas flow rate (kmol/h)	CO_2 to be captured (kmol/h)
543	28,182	10,344
443	22,982	8,435
343	17,782	6,527
216	11,219	4,118
136	7,079	2,598
86	4,467	1,640
54	2,818	1,034

7.9.1 Solvent Flow Rate

Figure 7.93 shows that the required solvent flow rate increases with the power plant capacity for the five solvents at the three temperatures. This is expected due to the increase in gas flow rate and the amount of CO_2 to be captured. In addition, the required solvent flow rates increase with temperature because the CO_2 solubilities in the solvents decrease with temperature as noted in previous sections.
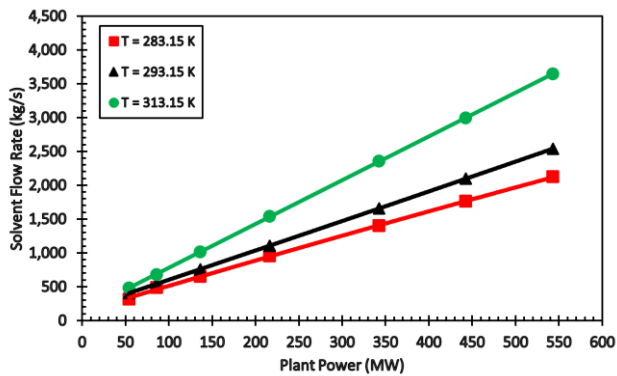
(a)
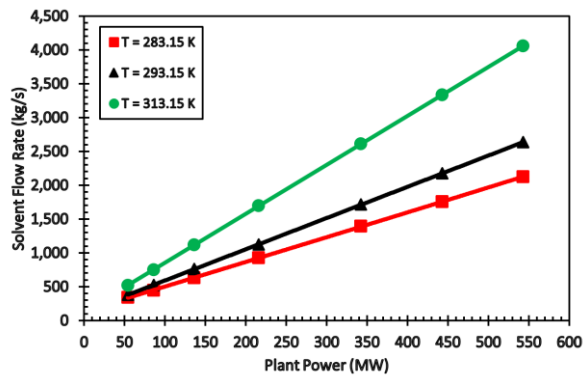
(b)
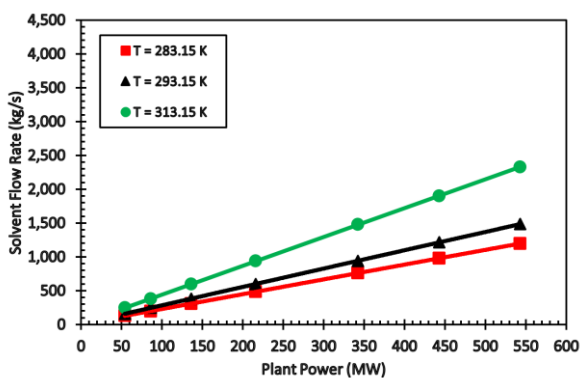
(c)
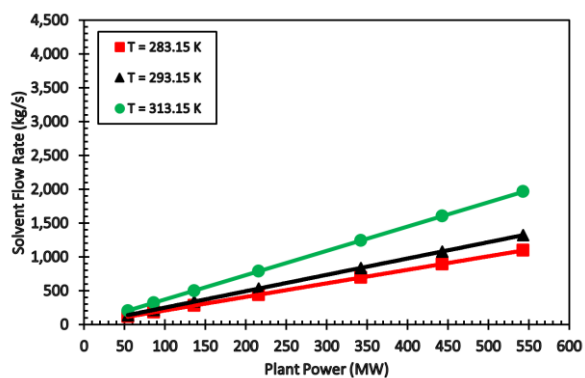
(d)
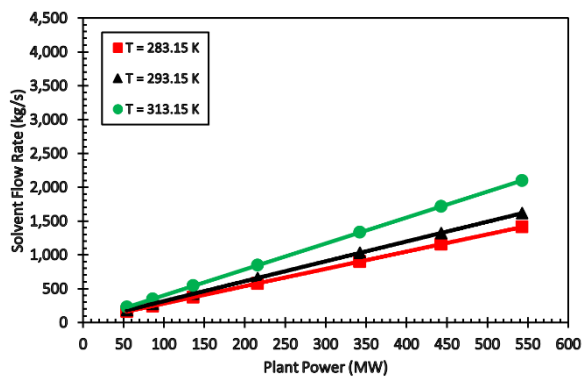
(e)

Figure 7.93: Solvent flow rate of (a) [bmim][Tf$_2$N], (b) [emim][Tf$_2$N], (c) DES, (d) PEGPDMS-1, and (e)

PEGPDMS-3

137

7.9.2 Absorber

Figure 7.94 shows that the required absorber internal diameter increases with the power plant capacity for all solvents used, which is expected due to the increase of the fuel gas and required solvent flow rates with increasing the power plant capacity. Also, the absorber internal diameter increases with temperature, which can be attributed to higher solvent flow rate required due to the requirement to satisfy the no flooding constraint imposed on the CO_2 capture process.

The height of the absorbers also increased as the plant capacity increased as indicated by Figure 7.95 due to the requirement of maintaining the absorber height to diameter ratio of greater than or equal to 6. This will lead to solvents that need larger absorber diameters to have taller absorbers which will also lead to a higher CAPEX.
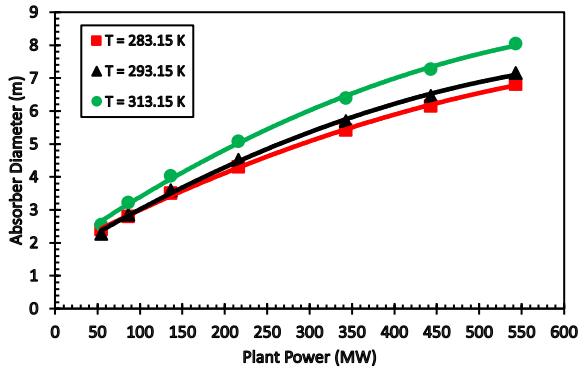
(a)
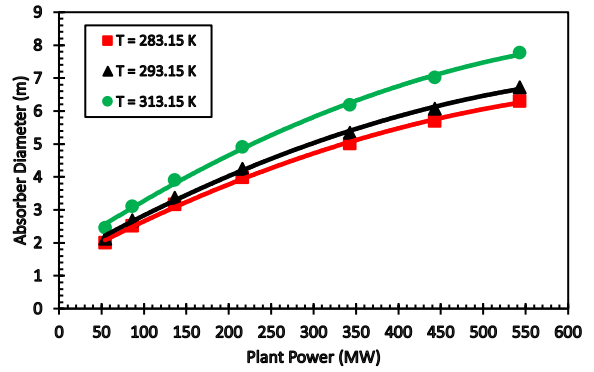
(b)
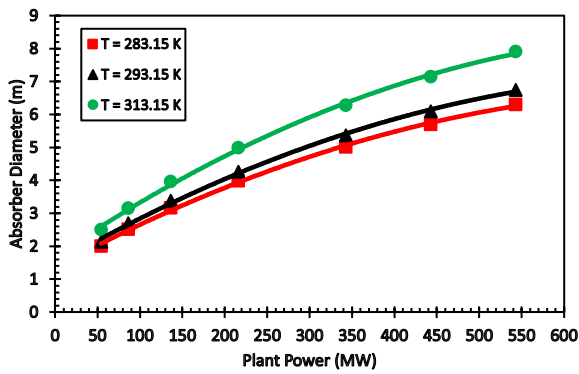
(c)
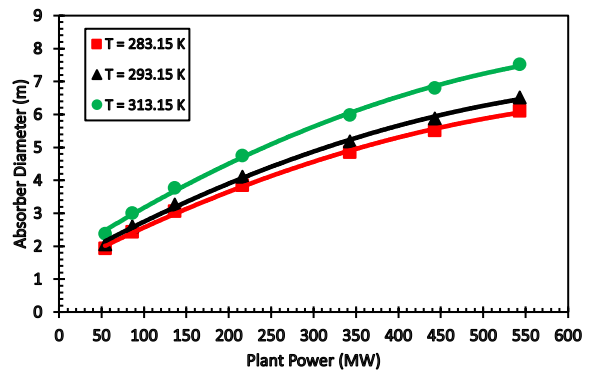
(d)
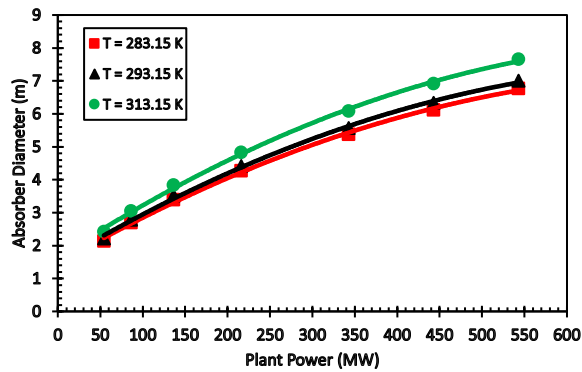
(e)

Figure 7.94: Absorber diameter using (a) [bmim][Tf$_2$N], (b) [emim][Tf$_2$N], (c) DES, (d) PEGPDMS-1, and (e)

PEGPDMS-3

139
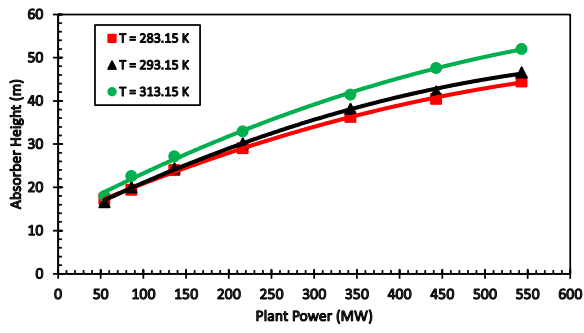
(a)
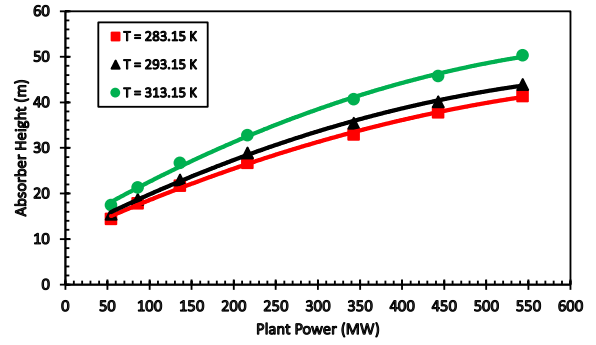
(b)
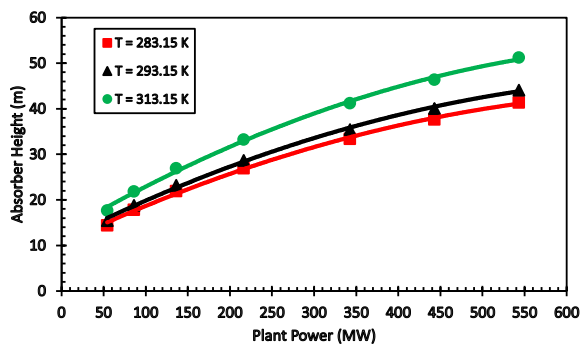
(c)
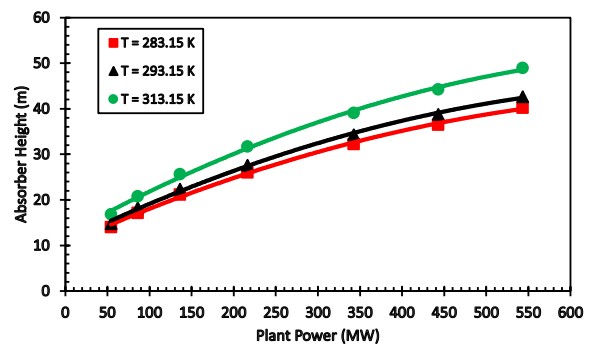
(d)
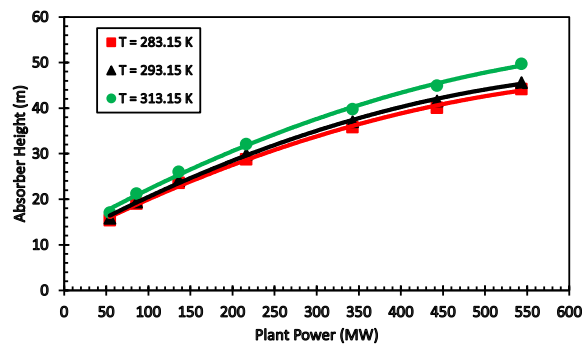
(e)

Figure 7.95: Absorber height using (a) [bmim][Tf$_2$N], (b) [emim][Tf$_2$N], (c) DES, (d) PEGPDMS-1, and (e) PEGPDMS-3

7.9.3 Economics

Figure 7.96 shows the total CAPEX for the five solvents as a function of power plant capacity, and as can be observed, the total CAPEX increases with power plant capacity, due to the use of larger equipment at higher power plant capacity. Figure 7.97 indicates that the total OPEX also increases with power plant capacity for the five solvents. This can be related to the cost of operating and maintaining larger equipment and handling high solvent and gas flow rates.

Figure 7.98 shows the LCOC decreases with increasing the power plant capacity for the five solvents used, which is due primarily to the increase of the tonnage of CO_2 captured. The Aspen Plus simulations show that as the power plant capacity increases, the amount of CO_2 captured increases more than the corresponding increase in the CAPEX and OPEX, leading to lower LCOC at larger scale power plants.
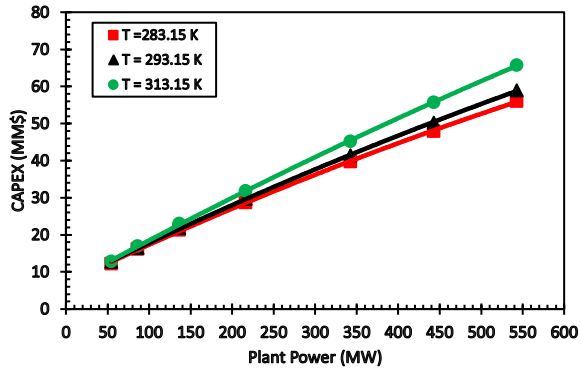
(a)
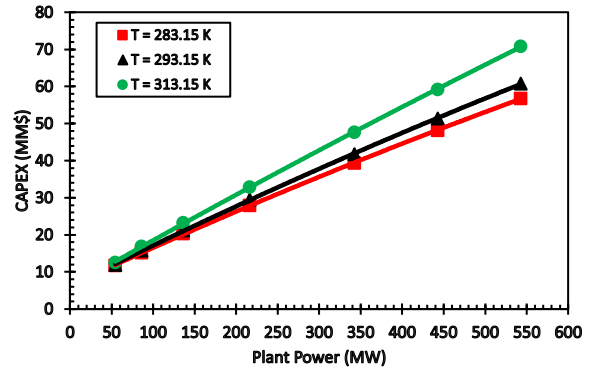
(b)
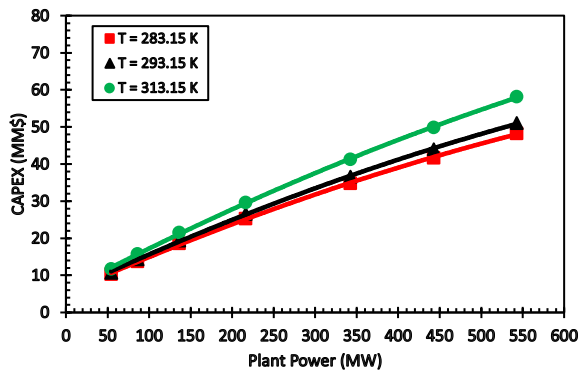
(c)
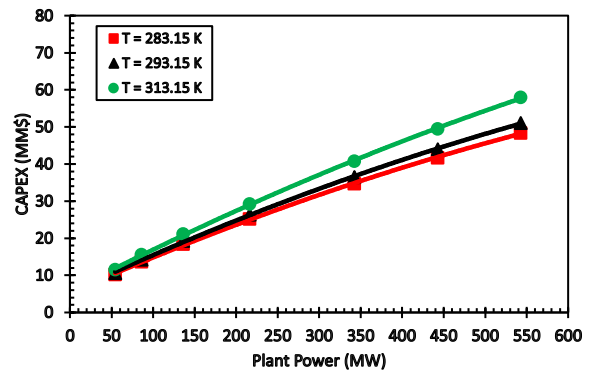
(d)
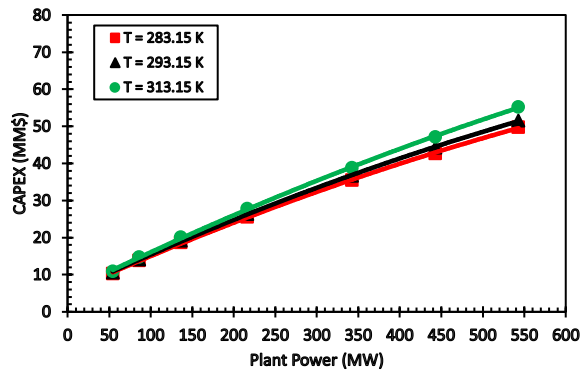
(e)

Figure 7.96: CAPEX using (a) [bmim][Tf$_2$N], (b) [emim][Tf$_2$N], (c) DES, (d) PEGPDMS-1, and (e) PEGPDMS-3
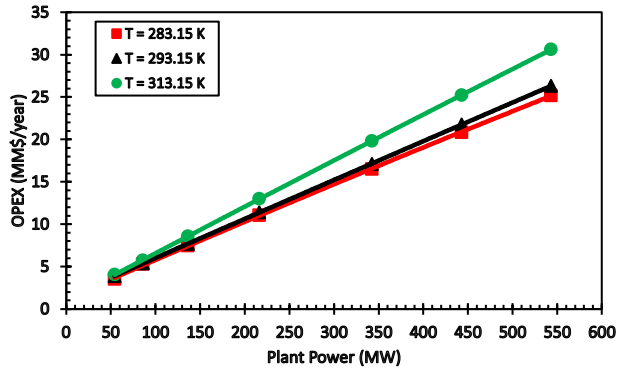
(a)
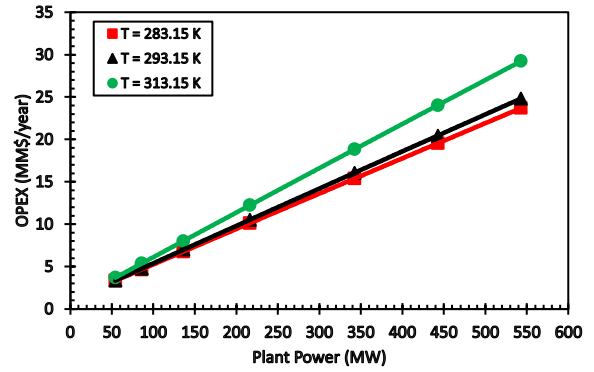
(b)
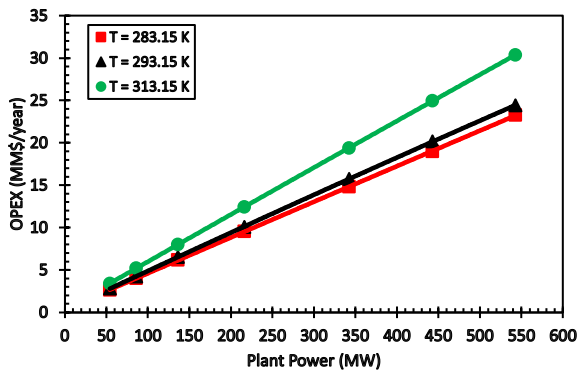
(c)
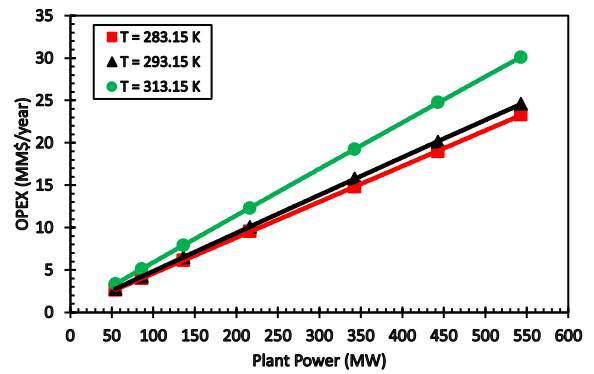
(d)
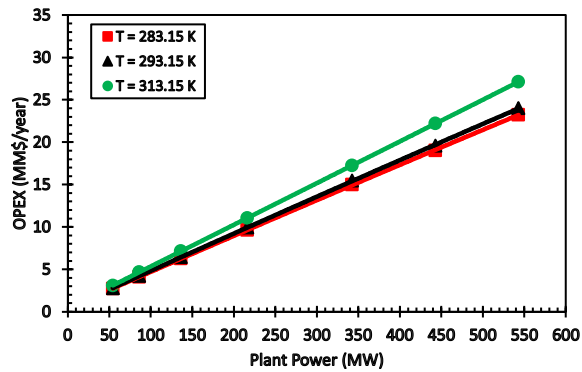
(e)

Figure 7.97: OPEX using (a) [bmim][Tf$_2$N], (b) [emim][Tf$_2$N], (c) DES, (d) PEGPDMS-1, and (e) PEGPDMS-3
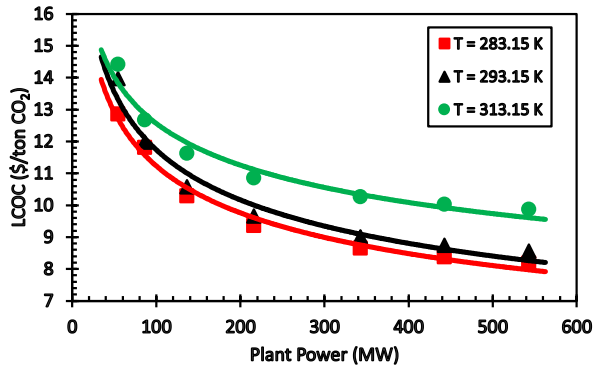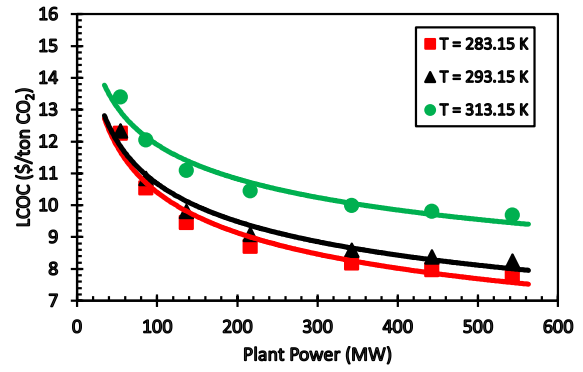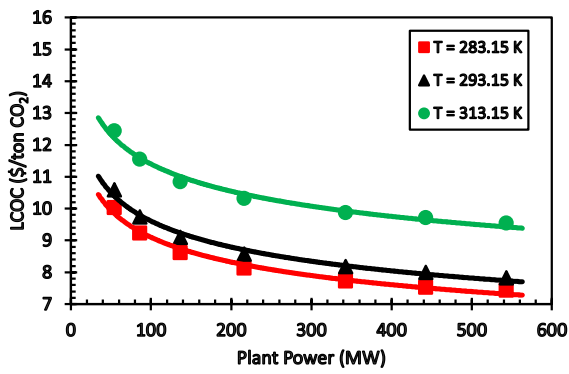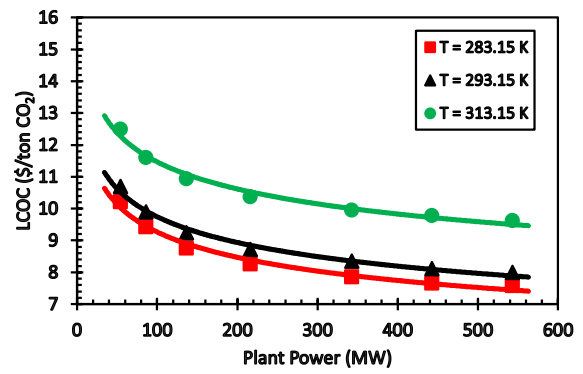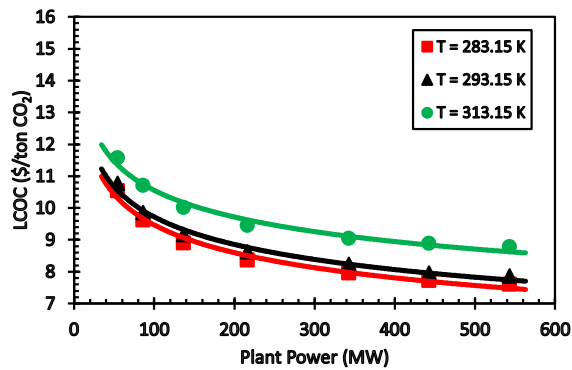
Figure 7.98: LCOC using (a) [bmim][Tf$_2$N], (b) [emim][Tf$_2$N], (c) DES, (d) PEGPDMS-1, and (e) PEGPDMS-3

8.0 Artificial Neural Network

An artificial neural network (ANN) is a machine learning (ML) tool used to emulate the human brain; and like biological neurons, an ANN has the ability to learn from an input and provide an output. An ANN consists of layers and nodes to perform complex transfer functions and provide an output, replicating biological neurons. In engineering applications, ANNs are mainly used for predictions and pattern recognition [496]. The ANN could have as many layers and nodes as possible to provide an accurate output. The layers include multiple nodes, consisting of weights and biases. There are many transfer functions that a node can perform as given in Table 8.1, where using non-linear transfer functions gives better results than linear transfer functions [497].

Table 8.1: Transfer functions [498, 499]

Name	Transfer function
Linear	$f(x_i) = x_i$
Sigmoid	$f(x_i) = \dfrac{1}{1 + e^{-x_i}}$
Hyperbolic tangent	$f(x_i) = \tanh(x_i)$
Gaussian	$f(x_i) = e^{x_i^2}$
Step	$f(x_i) = \begin{cases} 0, x_i \leq a \\ 1, x_i > a \end{cases}$

In general, the input and output data for the ANN are normalized using Equation (8.1).

$$I_{norm} = 2 \left(\frac{I_{input/output} - I_{min}}{I_{max} - I_{min}} \right) - 1 \tag{8.1}$$

where I_{norm} is the normalized parameter, $I_{input/output}$ is the input or output value, I_{min} and I_{max} are the minimum and maximum values of the input or output data, respectively.

After finishing the calculations, the last hidden layer converts them to final results and sends them to the output layer. Equation (8.2) shows the form of a node output [500].

$$x_{ij} = f\left(\sum_{j=1}^{N} w_j x_{i-1j} + b\right) \tag{8.2}$$

where x_{ij} is the output of the node, f is the transfer function, w_i is the weight of the node, x_{i-1j} is the input to the node, b is the bias, and N is the number of nodes in the previous layer. The subscript i represents the layer number and j represents the node number.

It should be noted that Equations (8.1) and (8.2) are dependent on the minimum and maximum values of the input and output data. It is also important to mention that the ANN should only be used for interpolations within the validity range from the minimum to the maximum values used for its development. This means that the ANN will completely fail to make any reliable predictions below or above the validity range.

8.1 Training of the ANN

Among the training methods of an ANN are back-propagation, Levenberg-Marquardt, and Bayesian Regularization.

8.1.1 Back-Propagation

Back-propagation is one of the most common methods used for training a feed-forward ANN. This method was developed in the 1970's [501] and was made popular in 1986 by Rumelhart et al. [502]. In this method, the hidden layer weights are determined based on the gradient descent

146

and more details can be found in Funahashi [503] and Hornik *et al* [504]. In 2001, Fillion [501] used this method to develop an ANN to predict the mass transfer and hydrodynamic parameters in a gas-inducing agitated reactor. His experimental mass transfer data were predicted with a regression coefficient greater than 0.99 and an average deviation of 8.1%. Also, his experimental Sauter mean bubble diameters were predicted with a regression coefficient of 0.98 and a deviation of 4%. In 2003, Lemoine *et al.* [505] used the same method to develop an ANN to predict the mass transfer coefficients in a lab-scale gas-inducing reactor. They built two ANN configurations (10-10-1 and 10-15-1) which performed significantly better than their empirical correlations and those found in literature in predicting their data. The R^2 values for the two ANNs were 0.905 and 0.886, respectively. In 2005, Behkish *et al.* [506] used the back-propagation method to create an ANN to predict the holdup of small and large gas bubbles in a bubble column and a slurry bubble column reactor. They used the sigmoid activation function and two hidden layers with 9 and 7 nodes, respectively. Their ANN predicted the experimental holdup of small gas bubbles with an AARE of 16%, a standard deviation of 19%, and an R^2 of 0.90. It also predicted the experimental holdup of large gas bubbles with an AARE of 10%, a standard deviation of 14% and an R^2 of 0.93.

8.1.2 Levenburg-Marquardt

The Levenburg-Marquardt method considers the use of a loss or error function such as the sum squared error as expressed by Equation (8.3). The Jacobian matrix is calculated using Equation (8.4), and the gradient vector is calculated using Equation (8.5). The Hessian (H_f) of E can then be calculated using Equation (8.6). Minimizing these parameters by altering the weights in the ANN leads to the desired solution, and more details about this training method can be found elsewhere [507, 508].

$$E = \sum_{i=1}^{N} [y_i - ANN(inputs_i)]^2 \qquad (8.3)$$

$$J_{i,j} = \frac{\partial [y_i - ANN(inputs_i)]^2}{\partial w_j} \qquad (8.4)$$

$$\nabla E = 2J^T \cdot E \qquad (8.5)$$

$$H_f E = 2J^T \cdot J \qquad (8.6)$$

This method has recently been used to model the disease control cases, including the current COVID-19 pandemic [509].

8.1.3 Bayesian Regularization

The Bayesian Regularization is considered better than the other two training methods because of its validation process [510]. This method has some advantages, such as (1) Overtrain difficulty because it provides a stopping criterion without the need for a set of validation data; (2) Overfit difficulty due to its ability to train with the effective number of weights and bias; and (3) As long as the lowest number of nodes is provided, this method will provide the best solution.

The error equation when using this method includes a damping factor, which is expressed by Equation (8.7).

$$E = \beta E_D + \alpha E_w \qquad (8.7)$$

E_D and E_W are calculated as follows:

$$E_D = \sum_{i=1}^{N} [y_i - ANN(inputs_i)]^2 \qquad (8.8)$$

$$E_w = \sum_{i=1}^{N_w} w_i^2 \tag{8.9}$$

where N_w is the number of weights, α and β are the hyperparameters calculated using Equations (8.10) and (8.11), respectively.

$$\alpha = \frac{\gamma}{2E_w} \tag{8.10}$$

$$\beta = \frac{(N-\gamma)}{2E_D} \tag{8.11}$$

Details for calculating γ can be found elsewhere [497, 511]. Initial values of α and β are used and E is then minimized by adjusting w_j. After E is minimized, the minimum number of parameters (γ) can be determined and new values for α and β are calculated.

8.2 Architecture of the ANN used in this study

The selection of a solvent for the CO_2 capture process is a mandatory step in the development of the ANN. Since the input of the ANN is mainly based on the solvent type, computational and thermochemical simulations are required to screen the solvents for pre-combustion applications. Once the solvent is selected, its price is defined, and its physico-chemical properties are obtained and correlated as a function of temperature. These solvent properties along with operating variables, power plant capacity expressing the fuel gas flow rate, and packing properties, are then used to develop the ANN.

Figure 8.1 shows the ANN developed in this study includes one input layer (10 nodes), two hidden layers (10 nodes each), and one output layer (3 nodes). The output layer includes the predicted CAPEX, OPEX, and LCOC of the CO_2 capture process. The red circles are the nodes of

the input layer, the black circles are the nodes of hidden layers, and the green circles are the nodes of the output layer. There are ten inputs, including: operating temperature; solvent properties (density, viscosity, vapor pressure, CO_2 Henry's Law constant and H_2 Henry's Law constant); solvent price; solvent hydrophobicity; plant power capacity; and absorber packing specific surface area. The data from the input layer pass through the hidden layers, then the CAPEX, OPEX, and LCOC are calculated and come out through the output layer. In this study, the sigmoid transfer function was used for the hidden layers, while the linear transfer function was used for the output layer.
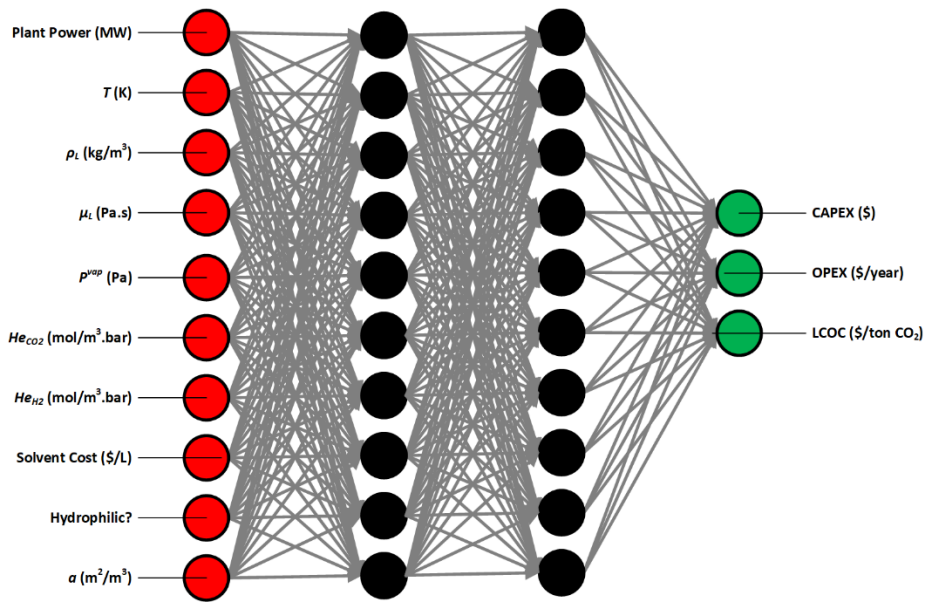
Figure 8.1: Architecture of the develpoped ANN

Table 8.2 shows the values of the minimum and maximum input data used for the development of the ANN. Again, the predictions of this ANN are only valid within these ranges.

Table 8.2: Minimum and maximum values of the input and output data

Parameter	Minimum	Maximum
Power plant capacity (MW)	54.3	543
Temperature (K)	223.15	323.15
Density (kg/m^3)	691.77	1,581.53
Viscosity (Pa.s)	3.19×10^{-4}	1.37
Vapor pressure (Pa)	1.01325×10^{-5}	18,899.26
CO_2 Henry's law constant (mol/m^3.bar)	37.49	3,790.67
H_2 Henry's law constant (mol/m^3.bar)	0.07897	37.5115
Solvent cost ($/L)	0.18	41.50
Hydrophilicity (binary)	0	1
Specific surface area of packing (m^2/m^3)	102	256
CAPEX ($)	10,171,495	216,736,909
OPEX ($/year)	2,622,825	1,370,783,510
LCOC ($/ton CO_2)	7.14	355.15

8.3 ANN Predictions

A total of 801 cases of Aspen Plus calculated data tabulated in Appendix B were used to develop the ANN in MATLAB® R2020a. For training this ANN, 320 cases (40% of the data) randomly selected were used, and for testing it, 481 cases (60% of the data) were used. As mentioned above, the Bayesian Regularization training method was employed because it was expected to provide more accurate results with a lower computational cost. Tables 8.3 and 8.4 give the values of the weights (w_i) and biases (b) of the hidden layers and the output layer of the ANN used, respectively.

Table 8.3: Parameters of the hidden layers

Parameter	$N_{1,1}$	$N_{1,2}$	$N_{1,3}$	$N_{1,4}$	$N_{1,5}$	$N_{1,6}$	$N_{1,7}$	$N_{1,8}$	$N_{1,9}$	$N_{1,10}$
b	1.3979	5.8985	14.2125	3.6186	-3.1425	-7.0696	-5.4967	4.4852	-12.1557	2.5044
w_1	-1.0853	-1.0971	-0.9474	0.9354	-0.8773	2.9543	-0.5054	0.6863	1.2714	-0.8898
w_2	3.5967	-2.6501	-0.3705	0.5187	1.6555	-0.5704	-1.8544	-0.5874	0.1677	-0.4846
w_3	2.9506	-8.4239	0.8361	-1.3487	-2.0063	-7.9695	-6.3544	1.2163	-0.8549	5.4082
w_4	-0.6475	-7.3156	0.4099	-0.5542	-0.6583	0.2106	-5.4709	0.1598	-0.4048	1.9033
w_5	2.7894	-3.0449	-0.7569	9.9450	-2.5229	-2.1981	-1.8898	-0.1043	-0.4157	-0.7650
w_6	1.9658	5.5094	17.2534	-0.7362	-1.4666	-4.9282	-3.0716	0.3303	-0.1366	1.5709
w_7	0.0902	6.9620	-5.1597	-4.0294	-1.4631	4.4577	1.7948	3.8541	-8.0712	-10.4048
w_8	1.3255	-2.8392	0.3940	-1.1682	1.5838	7.3950	-0.4154	-0.5976	-1.5666	1.8999
w_9	0.8507	-0.4300	-0.5586	0.5348	1.8732	-3.1484	0.5194	1.0114	-1.8617	0.0877
w_{10}	-0.0223	-0.1583	0.0135	-0.0010	0.0174	-0.0074	-0.0877	-0.0013	-0.0012	0.0292

Parameter	$N_{2,1}$	$N_{2,2}$	$N_{2,3}$	$N_{2,4}$	$N_{2,5}$	$N_{2,6}$	$N_{2,7}$	$N_{2,8}$	$N_{2,9}$	$N_{2,10}$
b	-6.7295	-6.6353	3.7494	4.2713	2.3253	-2.9488	5.6376	-5.4734	8.2421	2.1218
w_1	1.7058	-0.4979	0.6481	-1.3305	-1.1018	0.1655	-1.9222	0.1827	-0.2559	-2.5348
w_2	-0.0194	2.2712	-3.2189	-5.4336	6.2551	2.8506	-0.2395	7.5293	1.8326	-9.7184
w_3	-1.3231	-2.5645	-9.3739	-1.0795	2.2210	4.7470	1.3627	9.2075	12.8435	-2.7198
w_4	-5.6679	12.2821	-3.5966	-4.9490	-4.8169	1.8052	4.7043	1.9600	-1.3041	1.1995
w_5	0.9666	-6.0123	0.8685	0.2330	-0.7559	-0.9199	-0.6816	-1.5313	0.2619	5.4681
w_6	-0.8471	5.2916	1.7989	-2.1601	-2.5259	-2.0838	0.3945	-2.8614	-3.6613	3.1200
w_7	8.4890	-0.8241	-2.7508	4.0604	1.8835	-3.1789	-8.1598	1.0689	3.3459	-0.1430
w_8	1.9005	-7.6580	0.9570	0.3441	-1.4289	-5.0483	-1.6115	2.1616	-4.0240	-2.0301
w_9	2.1655	-11.2098	3.4068	0.8197	-0.1979	-2.9295	-1.7917	-2.7036	-6.3429	0.0797
w_{10}	1.9821	5.7471	4.6769	2.8400	-2.2917	-0.3720	-1.0831	-6.3219	-11.0442	2.3464

Table 8.4: Parameters of the output layer

Parameter	$N_{3,1}$	$N_{3,2}$	$N_{3,3}$		Parameter	$N_{3,1}$	$N_{3,2}$	$N_{3,3}$
b	-5.7138	2.2804	2.0730					
w_1	0.5130	-4.2665	-4.1351		w_6	-1.5195	-0.1076	0.0920
w_2	0.4255	4.9638	5.0199		w_7	0.7403	-4.2725	-4.1503
w_3	10.7818	0.2429	0.4730		w_8	8.2738	0.1908	0.3590
w_4	-0.3023	1.4343	1.3853		w_9	-9.4807	-0.7270	-0.9230
w_5	6.0286	0.1545	0.2736		w_{10}	3.6175	0.0732	0.1462

Figure 8.2 shows the CAPEX, OPEX, and LCOC values calculated using Aspen Plus and those predicted using the ANN for the 35 solvents used are in very good agreement. To quantify this accuracy, the coefficient of determination (R^2) and the absolute average relative error (AARE) for the cases used for training and testing the ANN were calculated and listed in Table 8.5. As can be observed R^2 for the cases used to train the ANN are 0.9996, 0.9998, and 0.9998 for CAPEX, OPEX, and LCOC, respectively; and R^2 for the cases used for testing the ANN are 0.9934, 0.9992, and 0.9991 for CAPEX, OPEX, and LCOC, respectively. In addition, AARE values for the cases used for training and testing the ANN are 1.664, 5.697, and 3.547% for CAPEX, OPEX, and LCOC, respectively. These data confirm that the ANN is capable of predicting the CAPEX, OPEX, and LCOC of the CO_2 capture process in pre-combustion applications.

Table 8.5: Coefficient of determination and AARE for the ANN output parameters

Output	R^2 in Training	R^2 in Testing	AARE (%)
CAPEX	0.9996	0.9934	1.664
OPEX	0.9998	0.9992	5.697
LCOC	0.9998	0.9991	3.547
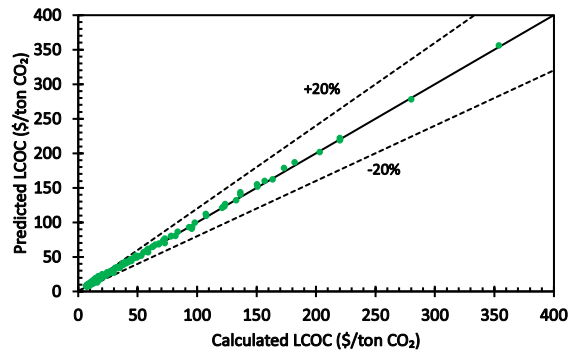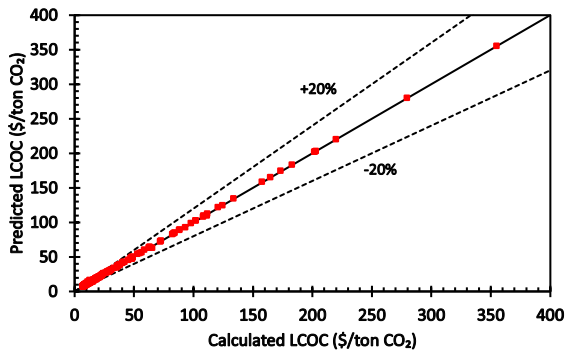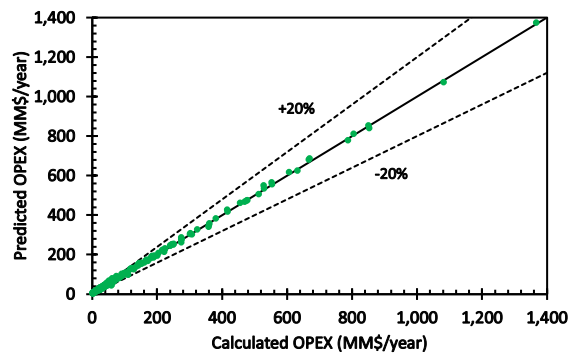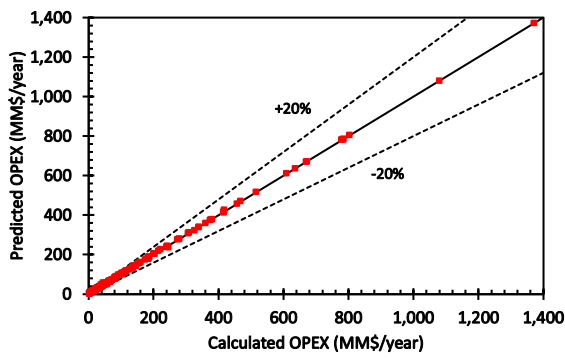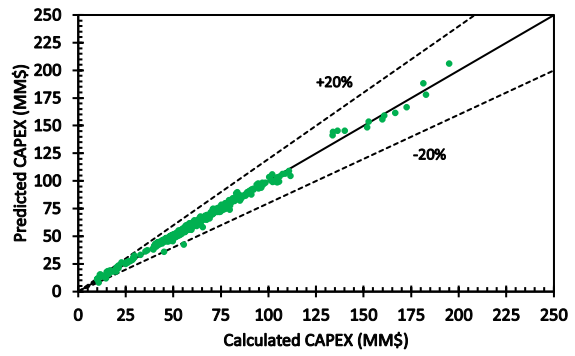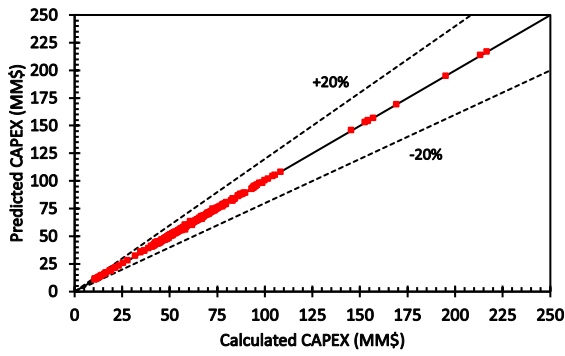
Training

Testing

Figure 8.2: Calculated and predicted CAPEX, OPEX, and LCOC of the CO$_2$ capture process

8.4 Using the ANN to Predict the Performance of Some Solvents Used

The ANN developed was used to predict the CAPEX, OPEX, and LCOC for three different solvents used in this study, namely [emim][Tf$_2$N], DES, and PEGDPMS-1. These data were predicted for temperatures 273.15 – 323.15 K, power plant capacities 54.3 – 543 MW, fuel gas flow rates 2,818 – 28,182 kmol/h, and a pressure of 51.4 bar. As can be seen in Figures 8.3, 8.4, and 8.5 the predicted data for the three solvents using the ANN are in a good agreement (± 20%) with the calculated values using Aspen Plus.
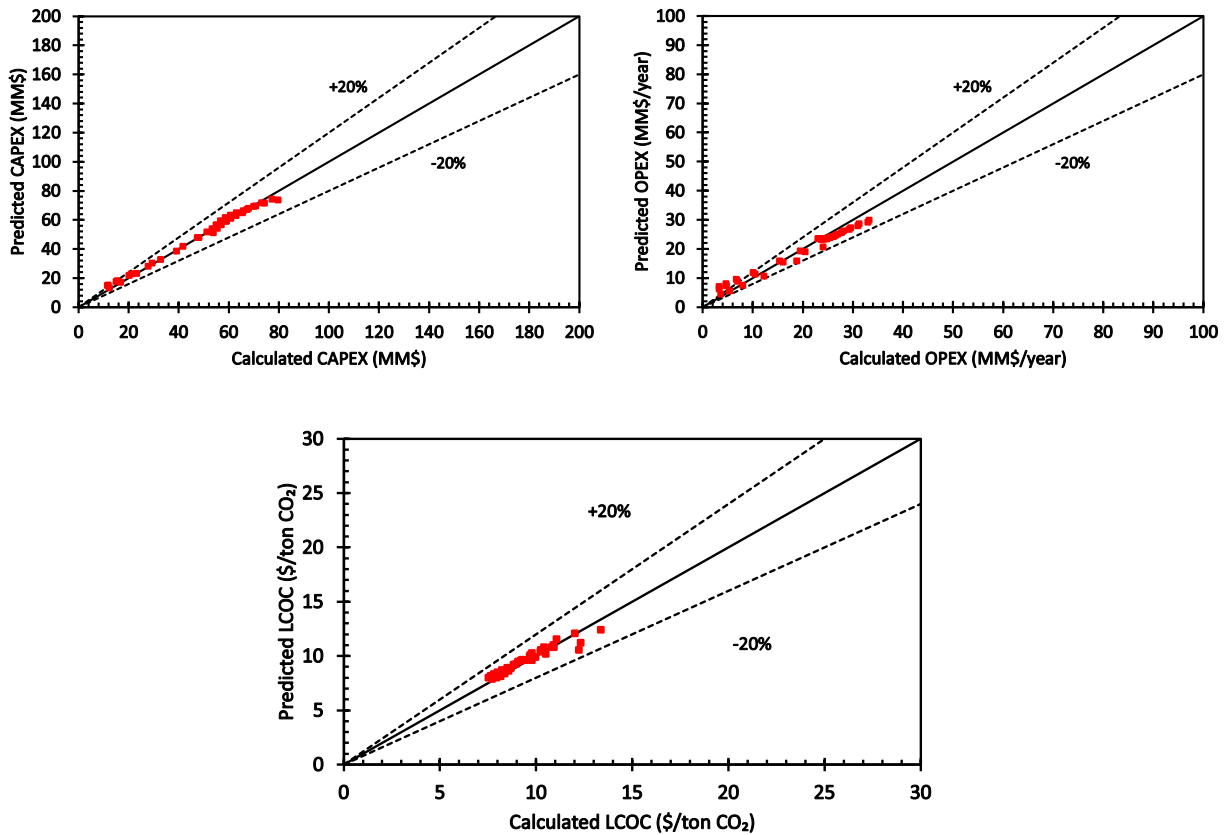
Figure 8.3: Comaprison between ANN predictions and Aspen Plus calculations for [emim][Tf$_2$N]
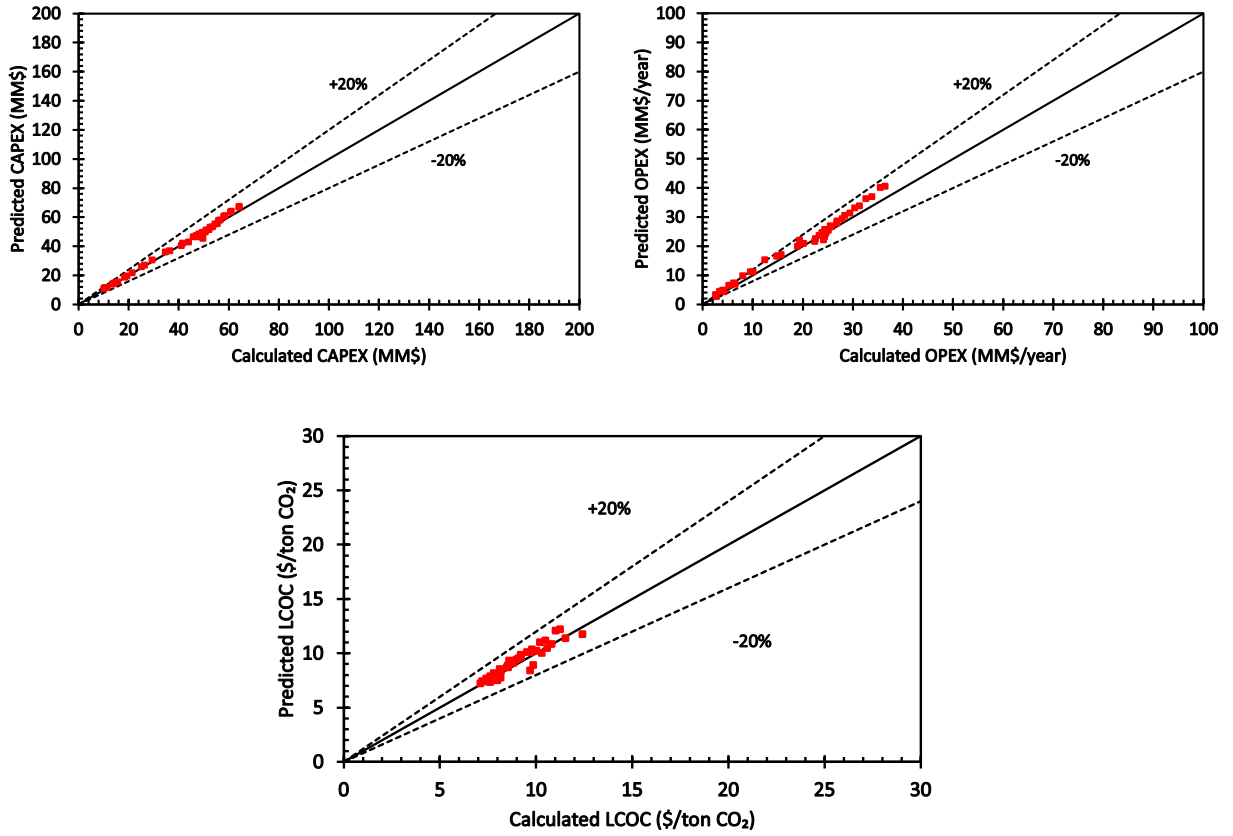
Figure 8.4: Comaprison between ANN predictions and Aspen Plus calculations for DES
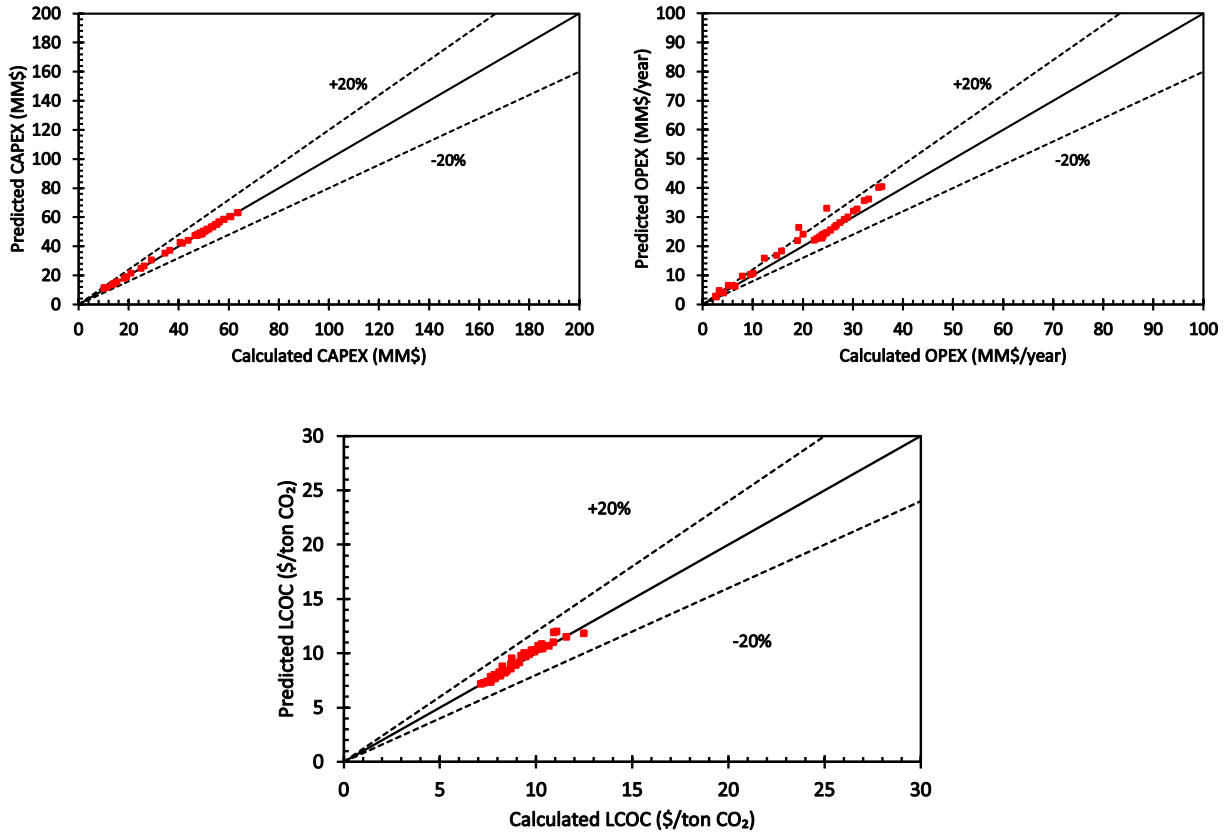
Figure 8.5: Comaprison between ANN predictions and Aspen Plus calculations for PEGPDMS-1

8.5 Using the ANN to Predict the Performances of PEGPDMS-1 and PEGDPMS-3

The ANN was used to predict the CAPEX, OPEX, and LCOC of PEGPDMS-1 and PEGDPMS-3 at a temperature of 298.15 K, power plant capacity of 543 MW, fuel gas flow rate of 28,182 kmol/h, and a pressure of 51.4 bar. The properties of the two solvents are given in Table 8.6. It should be mentioned that 298.15 K is the inlet solvent temperature at the top of the packing.

Table 8.6: Properties of PEGPDMS-1 and PEGDPMS-3 at 298.15 K

Solvent	Density (kg/m^3)	Viscosity (Pa.s)	Vapor pressure (Pa)	He_{CO2} (mol/m^3.bar)	He_{H2} (mol/m^3.bar)
PEGPDMS-1	934.69	0.00489	1.013×10^{-5}	145.26	3.14
PEGPDMS-3	988.94	0.01242	1.013×10^{-5}	109.95	2.11

Table 8.7 shows the calculated CAPEX, OPEX, and LCOC data using Aspen Plus and those predicted using the ANN along with the deviation for Aspen Plus calculations. As can be seen in this table, the CAPEX, OPEX, and LCOC values calculated using Aspen Plus and those predicted using the ANN for the PEGPDMS-1 and PEGPDMS-3 as single solvents are in a good agreement as the deviations from Aspen Plus calculations are -0.003 to 0.085%, -0.422 to 1.543%, and -3.255 to 0.293% for the CAPEX, OPEX, and LCOC, respectively.

Table 8.7: Comaprison between the calculated and prediced TEA data at 298.15 K

Solvent	Criterion	Units	Aspen Plus	ANN	Deviation from Aspen Plus
PEGPDMS-1	CAPEX	MM$	53.100	53.145	0.085%
	OPEX	MM$/year	25.564	25.456	-0.422%
	LCOC	$/ton CO_2	8.18	7.91	-3.255%
PEGPDMS-3	CAPEX	MM$	53.618	53.616	-0.003%
	OPEX	MM$/year	24.492	24.870	1.543%
	LCOC	$/ton CO_2	7.92	7.95	0.293%

9.0 Concluding Remarks

Aspen Plus v.8.8 was used to perform TEA of the CO_2 capture process in pre-combustion applications. The CAPEX, OPEX, and the LCOC were calculated to assess the feasibility of the process. 35 physical solvents, classified into 7 different categories, were used for CO_2 capture from an actual shifted fuel at 51.4 bar in a 543 MW power plant. The process included a countercurrent packed-bed absorber with Mellapak 250Y or IMTP50, followed by three pressure-swing flash drums for solvent regeneration. For the hydrophilic solvents used (NMP, PC, methanol, and THF) a tray distillation column was added to the process for water removal. Multi-stage compressors with intercooling were also used to prepare the CO_2 for sequestration by boosting its pressure to 152.7 bar. The process constraints were (1) 90% CO_2 capture efficiency, (2) no flooding in the absorber, (3) absorber height to diameter ratio is $\geq$ 6, (4) the CO_2 gas stream destined for sequestration should contain $\leq$ 0.5 mol% of fuel gas (H_2, CH_4, and CO), and (5) < 600 ppm of water.

The PC-SAFT EOS was used to model the solvent density and VLE of the gas-liquid systems used. Other solvent physico-chemical properties (viscosity, surface tension, and vapor pressure) were acquired from experimental data, literature, and Aspen Plus. The CAPEX, OPEX, and LCOC values of the CO_2 capture process calculated using Aspen Plus were carried out at temperatures from 223.15 to 273.15 K for the subcooled solvents (methanol and THF) and from 273.15 to 323.15 K for all other solvents. In addition, an artificial neural network (ANN) was developed using the CAPEX, OPEX, and LCOC of the CO_2 capture process calculated with Aspen Plus. The input to the ANN included plant power capacity, operating temperature, solvent properties, and packing specific surface area. 320 randomly selected cases were used for training

the ANN and 481 cases were used for testing it. The results discussed in this study led to following conclusions:

1. In general, operating at low temperatures and using the structured packing (Mellapak 250Y) with large specific surface area, increased CO_2 solubility and improved mass transfer, which lowered LCOC values.

2. High density solvents circumvented flooding and enabled using small-size absorbers, which lowered LCOC; high viscosity solvents increased pumping costs and large-size absorbers were needed to avoid flooding, which increased LCOC; and high vapor pressure solvents exhibited significant loss and required continuous solvent makeup, which increased LCOC.

3. The solvent with the lowest LCOC among the seven categories used obtained with Mellapak 250Y packing and the rationale for its behavior are summarized in Table 9.1.

Table 9.1: Solvents with the lowest LCOC

Category (Temperature)	Solvent LCOC	Rationale
Ionic liquids (273.15 K)	[emim][Tf$_2$N] $7.55/ton CO_2 captured	Solvent's high density, low viscosity, and high CO_2 solubility. ILs with negligible vapor pressure have high viscosity and would be suitable for warm/hot temperature CO_2 capture.
Hydrocarbons (273.15 K)	n-tetradecane 7.58/ton CO_2 captured	Solvent has the lowest vapor pressure in this category, leading to low solvent losses and consequently low OPEX.
Oxygenated-hydrocarbons (273.15 K)	DES $7.14/ton CO_2 captured	Solvent's high density, low vapor pressure, high CO_2 solubility, and low H_2 solubility leading to a small absorber size, low solvent loss, and minimal fuel gas loss.
Nitrogenized-hydrocarbons (273.15 K)	DMF 8.09/ton CO_2 captured	Solvent's high density and low vapor pressure leading to a small absorber size and minimal solvent losses, thereby reducing the CAPEX and OPEX.
Cyclic-hydrocarbons (273.15 K)	MNPh $8.56/ton CO_2 captured	Solvent's low vapor pressure, limiting the amount of solvent loss and its hydrophobicity, which was an advantage over other low volatility solvents in this category (NMP and PC).
Polymers (273.15 K)	PEGPDMS-1 $7.15/ton CO_2 captured	Solvent has the lowest viscosity and highest CO_2 solubility in this category, which led to using a small absorber and low flow rates, which lowered the CAPEX and OPEX.
Subcooled (223.15 K)	Methanol $15.95/ton CO_2 captured	Solvent's hydrophilicity and additional cooling requirements increased the OPEX compared to all other solvents used. However, this solvent is inexpensive compared to THF.

4. Decreasing the plant power capacity decreased the CAPEX and OPEX, however, the LCOC increased due to the small tonnage of CO_2 captured.

5. The ANN was capable of predicting the calculated CAPEX, OPEX, and LCOC using Aspen Plus with a coefficient of determination (R^2) of 0.9961, 0.9994, 0.9995, respectively and an AARE of 1.664, 5.697, and 3.547%, respectively.

Appendix A PC-SAFT EOS

The compressibility factor in the PC-SAFT EOS is computed using Equation (A.1).

$$Z = PV/nRT \tag{A.1}$$

Z is defined as:

$$Z = Z^{ideal} + Z^{hc} + Z^{disp} + Z^{assoc} \tag{A.2}$$

where Z^{ideal} is the ideal gas compressibility factor, which equals 1. Z^{hc}, Z^{disp}, and Z^{assoc} are the hard chain structure, dispersion, and association gas compressibility factors, respectively. Z^{hc} can be calculated using Equation (A.3).

$$Z^{hc} = \bar{m}Z^{hs} - \sum_i x_i(m_i - 1)(\rho_N)\frac{\partial \ln g_{ii}^{hs}}{\partial \rho_N} \tag{A.3}$$

$$\bar{m} = \sum_i x_i m_i \tag{A.4}$$

where x_i is the mole fraction of the ith component, m_i is the number of segments, and ρ_N is the total number density of the molecules.

Z^{hs} and g_{ii}^{hs} are the compressibility factor and radial pair of the hard sphere variables, which can be calculated using Equations (A.5)and (A.6)from Boublik [512] and Mansouri *et al.* [513].

$$Z^{hs} = \frac{\xi_3}{1 - \xi_3} + \frac{3\xi_1\xi_2}{\xi_0(1 - \xi_3)^2} + \frac{3\xi_2^3 - \xi_3\xi_2^3}{\xi_0(1 - \xi_3)^3} \tag{A.5}$$

$$g_{ij}^{hs} = \frac{1}{(1 - \xi_3)} + \left(\frac{d_i d_j}{d_i + d_j}\right)\frac{3\xi_2}{(1 - \xi_3)} + \left(\frac{d_i d_j}{d_i + d_j}\right)^2 \frac{2\xi_2^2}{(1 - \xi_3)^3} \tag{A.6}$$

where:

$$\xi_n = \frac{\pi}{6}(\rho_N) \sum_i x_i m_i d_i^n \tag{A.7}$$

$$d_i(T) = \sigma_i \left[1 - 0.12 \exp\left(\frac{-3\epsilon_i}{k_B T}\right) \right] \tag{A.8}$$

where d_i is the effective collision diameter, σ_i is the segment diameter, ϵ_i is the segment energy, and k_B is the Boltzmann constant.

Z^{disp} can be calculated using the following equation:

$$
\begin{aligned}
Z^{disp} = &-2\pi\rho_N \frac{\partial(\eta I_1)}{\partial \eta} \sum_i \sum_j x_i x_j m_i m_j \left(\frac{\epsilon_{ij}}{k_B T}\right) \sigma_{ij}^3 \\
&- \pi\rho_N \bar{m} \left[C_1 \frac{\partial(\eta I_2)}{\partial \eta} + \left(\frac{\partial C_1}{\partial \eta}\right) \eta I_2 \right] \sum_i \sum_j x_i x_j m_i m_j \left(\frac{\epsilon_{ij}}{k_B T}\right)^2 \sigma_{ij}^3
\end{aligned}
\tag{A.9}
$$

where:

$$\frac{\partial(\eta I_1)}{\partial \eta} = \sum_{j=0}^{6} a_j(\bar{m})(j+1)\eta^j \tag{A.10}$$

$$\frac{\partial(\eta I_2)}{\partial \eta} = \sum_{j=0}^{6} b_j(\bar{m})(j+1)\eta^j \tag{A.11}$$

$$C_1 = \left(1 + Z^{hc} + \rho_N \frac{\partial Z^{hc}}{\partial \rho_N} \right)^{-1} \tag{A.12}$$

$$\sigma_{ij} = 0.5(\sigma_i + \sigma_j) \tag{A.13}$$

$$\epsilon_{ij} = (1 - k_{ij})\sqrt{\epsilon_i \epsilon_j} \tag{A.14}$$

$$a_i(\bar{m}) = a_{0i} + \left(\frac{\bar{m}-1}{\bar{m}}\right) a_{1i} + \left(\frac{\bar{m}-1}{\bar{m}}\right)\left(\frac{\bar{m}-2}{\bar{m}}\right) a_{2i} \tag{A.15}$$

$$b_i(\bar{m}) = b_{0i} + \left(\frac{\bar{m}-1}{\bar{m}}\right) b_{1i} + \left(\frac{\bar{m}-1}{\bar{m}}\right)\left(\frac{\bar{m}-2}{\bar{m}}\right) b_{2i} \tag{A.16}$$

The constants in Equations (A.15) and(A.16), provided by Gross and Sadowski [112], are shown in Table A.1. The binary interaction parameter (k_{ij}) is calculated in Aspen Plus as:

$$k_{ij} = a_{ij} + \frac{b_{ij}}{T_{norm}} + c_{ij} \ln T_{norm} + d_{ij} T_{norm} + e_{ij} T_{norm}^2 \tag{A.17}$$

$$T_{norm} = \frac{T}{298.15} \tag{A.18}$$

Table A.1: Universal model constants for Equations (A.15) and (A.16) [112]

i	a_{0i}	a_{1i}	a_{2i}	b_{0i}	b_{1i}	b_{2i}
0	0.910563	-0.3084	-0.09061	0.724095	-0.57555	0.097688
1	0.636128	0.186053	0.452784	2.238279	0.69951	-0.25576
2	2.686135	-2.503	0.59627	-4.00258	3.892567	-9.15586
3	-26.5474	21.41979	-1.72418	-21.0036	-17.2155	20.64208
4	97.75921	-65.2559	-4.13021	26.85564	192.6723	-38.8044
5	-159.592	83.31868	13.77663	206.5513	-161.826	93.62677
6	91.29777	-33.7469	-8.67285	-355.602	-165.208	-29.6669

The parameters m, σ, and ε can be obtained either from regressing experimental data or from the literature [112, 114, 115]. For organic compounds, group contribution methods can be used to determine these parameters [514, 515].

The contribution of the fluid's association can be calculated by Chapman *et al.* [516]:

$$Z^{assoc} = \sum_i x_i \frac{\mu_i^{assoc}}{RT} - \frac{a^{assoc}}{RT} \tag{A.19}$$

$$\frac{\mu_i^{assoc}}{RT} = \sum_{A_i} \left[\ln x^{A_i} - \frac{x^{A_i}}{2} \right] + 0.5 M_i + \sum_j \rho_j \sum_{A_j} \left[\left(\frac{\partial x^{A_j}}{\partial \rho_i} \right)_{T, \rho_k \neq i} \left[\frac{1}{x^{A_j}} - \frac{1}{2} \right] \right] \tag{A.20}$$

$$\frac{a^{assoc}}{RT} = \sum_i x_i \left(\sum_{A_i} \left[\ln x^{A_i} - \frac{x^{A_i}}{2} \right] + 0.5 M_i \right) \tag{A.21}$$

$$x^{A_i} = \left[1 + N_{AV} \sum_j \sum_{B_j} \rho_j x^{B_j} \Delta_{ij}^{AB} \right]^{-1} \tag{A.22}$$

$$\Delta_{ij}^{AB} = d_{ij}^3 g_{ij}^{hs} \kappa_{ij}^{AB} \left[\exp\left(\frac{\epsilon_{ij}^{AB}}{k_B T} \right) - 1 \right] \tag{A.23}$$

$$d_{ij} = 0.5\left(d_i + d_j \right) \tag{A.24}$$

$$\epsilon_{ij}^{AB} = 0.5\left(\epsilon_i^{AB} + \epsilon_j^{AB} \right) \tag{A.25}$$

$$\kappa_{ij}^{AB} = \left(\kappa_i^{AB} \kappa_j^{AB} \right)^{0.5} \left[\frac{\sqrt{\sigma_i \sigma_j}}{0.5\left(\sigma_i + \sigma_j \right)} \right]^3 \tag{A.26}$$

where A_i and B_i denote the association site of the ith molecule, M_i is the total number of association sites, N_{AV} is Avogadro's number, κ^{AB} is the volume of interaction between sites A and B, and ϵ^{AB} is the association energy of interaction between sites A and B. All these parameters can be obtained either from the literature or from regressing experimental data [113].

Appendix B Data

Table B.1: IL cases

Solvent	Plant Power (MW)	T (K)	ρ_L (kg/m³)	μ_L (Pa.s)	P^{vap} (Pa)	He_{CO2} (mol/m³.bar)	He_{H2} (mol/m³.bar)	Solvent cost ($/L)	Hydro-philicity	a (m⁻¹)	Calculated			ANN prediction		
											CAPEX ($)	OPEX ($/year)	LCOC ($/ton CO₂)	CAPEX ($)	OPEX ($/year)	LCOC ($/ton CO₂)
[aPy][Tf₂N]	543	273.15	1,539.08	0.05888	1.013×10⁻⁵	155.986	0.182	40.00	0	256	57,797,343	23,446,613	7.80	59,069,537	25,487,659	8.16
[aPy][Tf₂N]	543	278.15	1,533.27	0.05075	1.013×10⁻⁵	140.550	0.237	40.00	0	256	59,320,064	23,702,730	7.92	60,133,962	25,312,438	8.20
[aPy][Tf₂N]	543	283.15	1,527.58	0.04375	1.013×10⁻⁵	127.152	0.300	40.00	0	256	61,147,689	24,064,163	8.07	61,473,732	25,320,086	8.29
[aPy][Tf₂N]	543	288.15	1,522.01	0.03771	1.013×10⁻⁵	115.473	0.373	40.00	0	256	63,191,383	24,507,141	8.25	63,152,931	25,558,409	8.46
[aPy][Tf₂N]	543	293.15	1,516.54	0.03251	1.013×10⁻⁵	105.247	0.456	40.00	0	256	65,184,509	25,069,259	8.45	65,201,235	26,036,286	8.69
[aPy][Tf₂N]	543	298.15	1,511.17	0.02802	1.013×10⁻⁵	96.257	0.552	40.00	0	256	67,913,180	25,789,512	8.72	67,618,363	26,717,539	8.98
[aPy][Tf₂N]	543	303.15	1,505.90	0.02415	1.013×10⁻⁵	88.325	0.660	40.00	0	256	70,719,977	26,713,347	9.05	70,390,826	27,535,708	9.32
[aPy][Tf₂N]	543	308.15	1,500.72	0.02082	1.013×10⁻⁵	81.300	0.783	40.00	0	256	73,288,179	27,996,850	9.46	73,517,260	28,425,083	9.68
[aPy][Tf₂N]	543	313.15	1,495.63	0.01795	1.013×10⁻⁵	75.056	0.920	40.00	0	256	76,707,536	29,651,128	9.99	77,024,426	29,354,162	10.05
[aPy][Tf₂N]	543	318.15	1,490.62	0.01547	1.013×10⁻⁵	69.488	1.073	40.00	0	256	81,108,256	31,772,445	10.66	80,977,549	30,346,336	10.45
[aPy][Tf₂N]	543	323.15	1,485.70	0.01334	1.013×10⁻⁵	64.508	1.244	40.00	0	256	87,059,061	34,586,590	11.57	85,484,200	31,485,290	10.91
[aPy][Tf₂N]	543	273.15	1,539.08	0.05888	1.013×10⁻⁵	155.986	0.182	40.00	0	102	58,534,851	24,342,529	8.05	58,638,064	25,795,447	8.22
[aPy][Tf₂N]	543	278.15	1,533.27	0.05075	1.013×10⁻⁵	140.550	0.237	40.00	0	102	60,073,345	24,561,514	8.16	59,863,677	25,694,972	8.29
[aPy][Tf₂N]	543	283.15	1,527.58	0.04375	1.013×10⁻⁵	127.152	0.300	40.00	0	102	61,750,843	24,838,416	8.28	61,380,017	25,788,748	8.41
[aPy][Tf₂N]	543	288.15	1,522.01	0.03771	1.013×10⁻⁵	115.473	0.373	40.00	0	102	63,329,641	25,240,827	8.44	63,243,641	26,120,516	8.60
[aPy][Tf₂N]	543	293.15	1,516.54	0.03251	1.013×10⁻⁵	105.247	0.456	40.00	0	102	65,570,125	25,695,966	8.62	65,476,214	26,691,672	8.86

166

Table B.1 continued.

Solvent	Plant Power (MW)	T (K)	ρ_L (kg/m³)	μ_L (Pa.s)	P^{vap} (Pa)	He_{CO2} (mol/m³.bar)	He_{H2} (mol/m³.bar)	Solvent cost ($/L)	Hydro-philicity	a (m⁻¹)	Calculated CAPEX ($)	Calculated OPEX ($/year)	Calculated LCOC ($/ton CO₂)	ANN prediction CAPEX ($)	ANN prediction OPEX ($/year)	ANN prediction LCOC ($/ton CO₂)
[aPy][Tf₂N]	543	298.15	1,511.17	0.02802	1.013×10^{-5}	96.257	0.552	40.00	0	102	67,813,988	26,336,371	8.86	68,071,712	27,457,964	9.18
[aPy][Tf₂N]	543	303.15	1,505.90	0.02415	1.013×10^{-5}	88.325	0.660	40.00	0	102	70,362,323	27,165,911	9.15	71,014,624	28,347,891	9.54
[aPy][Tf₂N]	543	308.15	1,500.72	0.02082	1.013×10^{-5}	81.300	0.783	40.00	0	102	72,243,685	28,374,715	9.52	74,305,195	29,295,985	9.92
[aPy][Tf₂N]	543	313.15	1,495.63	0.01795	1.013×10^{-5}	75.056	0.920	40.00	0	102	75,399,171	29,962,424	10.02	77,974,411	30,275,874	10.31
[aPy][Tf₂N]	543	318.15	1,490.62	0.01547	1.013×10^{-5}	69.488	1.073	40.00	0	102	79,509,722	32,016,612	10.67	82,093,469	31,318,976	10.73
[aPy][Tf₂N]	543	323.15	1,485.70	0.01334	1.013×10^{-5}	64.508	1.244	40.00	0	102	85,155,461	34,729,773	11.54	86,777,428	32,517,915	11.20
[bmim][BF₄]	543	273.15	1,227.77	0.42161	1.013×10^{-5}	144.745	0.777	18.11	0	256	59,385,870	25,138,456	8.28	57,009,405	27,494,431	8.64
[bmim][BF₄]	543	278.15	1,223.42	0.30683	1.013×10^{-5}	129.823	0.819	18.11	0	256	60,755,698	25,211,330	8.34	60,492,333	26,426,416	8.39
[bmim][BF₄]	543	283.15	1,219.17	0.22717	1.013×10^{-5}	116.906	0.859	18.11	0	256	62,390,995	25,737,399	8.54	58,931,974	24,493,835	7.76
[bmim][BF₄]	543	288.15	1,215.02	0.17093	1.013×10^{-5}	105.675	0.896	18.11	0	256	64,528,363	26,041,036	8.68	60,630,029	24,371,354	7.74
[bmim][BF₄]	543	293.15	1,210.96	0.13059	1.013×10^{-5}	95.870	0.931	18.11	0	256	66,344,499	26,502,415	8.85	64,724,538	26,154,510	8.30
[bmim][BF₄]	543	298.15	1,206.98	0.10122	1.013×10^{-5}	87.275	0.963	18.11	0	256	67,990,245	27,019,727	9.04	67,928,290	28,271,183	8.91
[bmim][BF₄]	543	303.15	1,203.08	0.07953	1.013×10^{-5}	79.714	0.993	18.11	0	256	69,879,092	27,611,857	9.25	69,893,512	29,753,559	9.34
[bmim][BF₄]	543	308.15	1,199.25	0.06329	1.013×10^{-5}	73.036	1.021	18.11	0	256	71,050,786	28,356,535	9.47	70,987,990	30,390,884	9.54
[bmim][BF₄]	543	313.15	1,195.49	0.05099	1.013×10^{-5}	67.119	1.047	18.11	0	256	72,320,742	29,282,878	9.75	72,097,417	30,460,285	9.64
[bmim][BF₄]	543	318.15	1,191.80	0.04155	1.013×10^{-5}	61.858	1.071	18.11	0	256	74,555,614	30,297,510	10.08	74,376,222	30,401,471	9.78
[bmim][BF₄]	543	323.15	1,188.18	0.03423	1.013×10^{-5}	57.166	1.093	18.11	0	256	76,890,621	31,471,504	10.45	77,857,707	30,461,296	10.04
[bmim][BF₄]	543	273.15	1,227.77	0.42161	1.013×10^{-5}	144.745	0.777	18.11	0	102	59,825,463	25,713,943	8.44	60,588,993	27,843,542	8.84
[bmim][BF₄]	543	278.15	1,223.42	0.30683	1.013×10^{-5}	129.823	0.819	18.11	0	102	64,164,007	27,439,189	9.01	60,194,905	25,450,169	8.14
[bmim][BF₄]	543	283.15	1,219.17	0.22717	1.013×10^{-5}	116.906	0.859	18.11	0	102	65,709,534	27,652,922	9.12	57,723,548	22,715,213	7.34
[bmim][BF₄]	543	288.15	1,215.02	0.17093	1.013×10^{-5}	105.675	0.896	18.11	0	102	67,629,722	28,394,739	9.37	64,786,460	24,086,416	7.91
[bmim][BF₄]	543	293.15	1,210.96	0.13059	1.013×10^{-5}	95.870	0.931	18.11	0	102	69,915,941	28,883,954	9.57	69,877,544	27,755,758	8.98
[bmim][BF₄]	543	298.15	1,206.98	0.10122	1.013×10^{-5}	87.275	0.963	18.11	0	102	71,606,316	29,438,405	9.76	71,698,813	31,333,547	9.90
[bmim][BF₄]	543	303.15	1,203.08	0.07953	1.013×10^{-5}	79.714	0.993	18.11	0	102	73,412,120	29,922,870	9.94	72,036,477	33,647,333	10.47

Table B.1 continued.

Solvent	Plant Power (MW)	T (K)	ρ_L (kg/m³)	μ_L (Pa.s)	P^{vap} (Pa)	He_{CO2} (mol/m³.bar)	He_{H2} (mol/m³.bar)	Solvent cost ($/L)	Hydro-philicity	a (m⁻¹)	Calculated CAPEX ($)	Calculated OPEX ($/year)	Calculated LCOC ($/ton CO₂)	ANN prediction CAPEX ($)	ANN prediction OPEX ($/year)	ANN prediction LCOC ($/ton CO₂)
[bmim][BF₄]	543	308.15	1,199.25	0.06329	1.013×10⁻⁵	73.036	1.021	18.11	0	102	73,999,672	30,537,329	10.12	71,878,337	34,524,459	10.68
[bmim][BF₄]	543	313.15	1,195.49	0.05099	1.013×10⁻⁵	67.119	1.047	18.11	0	102	75,147,404	31,258,724	10.34	71,997,846	34,320,960	10.65
[bmim][BF₄]	543	318.15	1,191.80	0.04155	1.013×10⁻⁵	61.858	1.071	18.11	0	102	76,462,725	32,102,937	10.59	73,724,879	33,640,265	10.59
[bmim][BF₄]	543	323.15	1,188.18	0.03423	1.013×10⁻⁵	57.166	1.093	18.11	0	102	78,088,459	33,077,854	10.89	78,326,976	33,045,897	10.70
[bmim][MeSO₄]	543	273.15	1,225.86	0.99956	1.013×10⁻⁵	92.609	0.561	18.14	0	256	95,239,802	36,930,192	12.43	95,173,748	35,717,011	12.11
[bmim][MeSO₄]	543	278.15	1,222.31	0.70268	1.013×10⁻⁵	83.194	0.589	18.14	0	256	94,408,680	35,726,264	12.10	94,617,894	36,950,715	12.46
[bmim][MeSO₄]	543	283.15	1,218.81	0.50374	1.013×10⁻⁵	75.056	0.617	18.14	0	256	93,357,868	35,133,648	11.91	93,346,347	37,856,690	12.63
[bmim][MeSO₄]	543	288.15	1,215.35	0.36784	1.013×10⁻⁵	67.990	0.644	18.14	0	256	93,178,205	34,797,763	11.82	92,619,272	37,416,801	12.42
[bmim][MeSO₄]	543	293.15	1,211.95	0.27331	1.013×10⁻⁵	61.826	0.670	18.14	0	256	94,284,143	34,492,613	11.78	94,552,671	36,342,363	12.11
[bmim][MeSO₄]	543	298.15	1,208.59	0.20643	1.013×10⁻⁵	56.425	0.695	18.14	0	256	94,727,728	34,804,271	11.88	97,238,083	35,658,420	11.93
[bmim][MeSO₄]	543	303.15	1,205.28	0.15835	1.013×10⁻⁵	51.673	0.720	18.14	0	256	97,059,310	35,021,324	12.01	98,071,964	35,532,016	11.87
[bmim][MeSO₄]	543	308.15	1,202.01	0.12325	1.013×10⁻⁵	47.477	0.745	18.14	0	256	97,142,375	35,898,231	12.23	97,999,169	35,974,356	11.97
[bmim][MeSO₄]	543	313.15	1,198.78	0.09727	1.013×10⁻⁵	43.756	0.769	18.14	0	256	98,849,623	37,014,941	12.57	98,148,834	36,850,347	12.24
[bmim][MeSO₄]	543	318.15	1,195.59	0.07777	1.013×10⁻⁵	40.447	0.792	18.14	0	256	102,321,234	38,300,925	13.01	98,577,662	37,985,513	12.62
[bmim][MeSO₄]	543	323.15	1,192.44	0.06296	1.013×10⁻⁵	37.492	0.815	18.14	0	256	105,771,598	39,920,934	13.53	99,028,763	39,336,161	13.10
[bmim][MeSO₄]	543	273.15	1,225.86	0.99956	1.013×10⁻⁵	92.609	0.561	18.14	0	102	93,938,840	37,428,473	12.51	96,399,461	36,199,523	12.27
[bmim][MeSO₄]	543	278.15	1,222.31	0.70268	1.013×10⁻⁵	83.194	0.589	18.14	0	102	95,935,871	37,421,699	12.57	96,549,542	37,649,762	12.69
[bmim][MeSO₄]	543	283.15	1,218.81	0.50374	1.013×10⁻⁵	75.056	0.617	18.14	0	102	97,446,869	37,552,176	12.66	96,269,034	38,554,126	12.89
[bmim][MeSO₄]	543	288.15	1,215.35	0.36784	1.013×10⁻⁵	67.990	0.644	18.14	0	102	98,513,979	37,912,985	12.78	98,018,091	37,915,460	12.70
[bmim][MeSO₄]	543	293.15	1,211.95	0.27331	1.013×10⁻⁵	61.826	0.670	18.14	0	102	100,572,629	38,052,152	12.89	103,290,428	36,809,246	12.47
[bmim][MeSO₄]	543	298.15	1,208.59	0.20643	1.013×10⁻⁵	56.425	0.695	18.14	0	102	102,278,401	38,386,968	13.03	105,621,244	35,921,020	12.22
[bmim][MeSO₄]	543	303.15	1,205.28	0.15835	1.013×10⁻⁵	51.673	0.720	18.14	0	102	104,118,126	38,845,868	13.20	104,031,752	35,680,907	12.05
[bmim][MeSO₄]	543	308.15	1,202.01	0.12325	1.013×10⁻⁵	47.477	0.745	18.14	0	102	104,623,304	39,612,723	13.41	102,790,388	36,408,253	12.18
[bmim][MeSO₄]	543	313.15	1,198.78	0.09727	1.013×10⁻⁵	43.756	0.769	18.14	0	102	105,961,806	40,612,162	13.71	103,515,288	37,787,510	12.60

Table B.1 continued.

Solvent	Plant Power (MW)	T (K)	ρ_L (kg/m^3)	μ_L (Pa.s)	P^{gap} (Pa)	He_{CO2} (mol/m^3.bar)	He_{H2} (mol/m^3.bar)	Solvent cost ($/L)	Hydro-philicity	a (m^{-1})	Calculated			ANN prediction		
											CAPEX ($)	OPEX ($/year)	LCOC ($/ton CO$_2$)	CAPEX ($)	OPEX ($/year)	LCOC ($/ton CO$_2$)
[bmim][MeSO$_4$]	543	318.15	1,195.59	0.07777	1.013×10^{-5}	40.447	0.792	18.14	0	102	107,592,230	41,853,459	14.07	105,798,572	39,420,058	13.17
[bmim][MeSO$_4$]	543	323.15	1,192.44	0.06296	1.013×10^{-5}	37.492	0.815	18.14	0	102	110,895,415	43,208,642	14.52	108,473,926	41,063,506	13.80
[bmim][PF$_6$]	543	273.15	1,388.74	1.37450	1.013×10^{-5}	158.544	0.933	14.65	0	256	69,277,067	30,557,529	9.97	65,697,468	28,371,079	9.16
[bmim][PF$_6$]	543	278.15	1,383.99	0.96583	1.013×10^{-5}	141.606	0.960	14.65	0	256	69,636,542	30,008,605	9.84	68,254,648	28,856,708	9.43
[bmim][PF$_6$]	543	283.15	1,379.34	0.69086	1.013×10^{-5}	127.020	0.987	14.65	0	256	70,423,379	30,009,054	9.88	70,155,947	29,256,586	9.66
[bmim][PF$_6$]	543	288.15	1,374.77	0.50253	1.013×10^{-5}	114.400	1.014	14.65	0	256	71,018,875	29,787,557	9.83	71,348,382	29,595,537	9.84
[bmim][PF$_6$]	543	293.15	1,370.30	0.37138	1.013×10^{-5}	103.431	1.041	14.65	0	256	71,824,830	29,827,710	9.87	72,154,409	29,923,754	10.00
[bmim][PF$_6$]	543	298.15	1,365.90	0.27859	1.013×10^{-5}	93.857	1.068	14.65	0	256	72,911,654	29,995,113	9.95	73,028,217	30,276,053	10.17
[bmim][PF$_6$]	543	303.15	1,361.59	0.21196	1.013×10^{-5}	85.465	1.095	14.65	0	256	74,194,884	30,297,633	10.06	74,054,094	30,656,319	10.35
[bmim][PF$_6$]	543	308.15	1,357.35	0.16344	1.013×10^{-5}	78.082	1.122	14.65	0	256	74,727,118	30,910,346	10.24	75,053,021	31,087,858	10.56
[bmim][PF$_6$]	543	313.15	1,353.18	0.12763	1.013×10^{-5}	71.562	1.150	14.65	0	256	75,743,254	31,805,525	10.49	75,984,618	31,660,110	10.81
[bmim][PF$_6$]	543	318.15	1,349.09	0.10087	1.013×10^{-5}	65.784	1.178	14.65	0	256	77,640,701	32,865,243	10.82	77,172,807	32,534,124	11.15
[bmim][PF$_6$]	543	323.15	1,345.05	0.08063	1.013×10^{-5}	60.646	1.207	14.65	0	256	79,731,937	34,117,714	11.21	79,249,062	33,906,909	11.65
[bmim][PF$_6$]	543	273.15	1,388.74	1.37450	1.013×10^{-5}	158.544	0.933	14.65	0	102	65,755,431	29,063,202	9.47	65,613,663	28,409,182	9.16
[bmim][PF$_6$]	543	278.15	1,383.99	0.96583	1.013×10^{-5}	141.606	0.960	14.65	0	102	67,633,185	29,780,169	9.72	68,055,278	28,914,298	9.44
[bmim][PF$_6$]	543	283.15	1,379.34	0.69086	1.013×10^{-5}	127.020	0.987	14.65	0	102	69,894,622	30,434,112	9.96	69,985,512	29,361,985	9.68
[bmim][PF$_6$]	543	288.15	1,374.77	0.50253	1.013×10^{-5}	114.400	1.014	14.65	0	102	71,897,976	31,019,756	10.17	71,399,499	29,782,108	9.89
[bmim][PF$_6$]	543	293.15	1,370.30	0.37138	1.013×10^{-5}	103.431	1.041	14.65	0	102	73,519,874	31,670,700	10.39	72,667,521	30,221,069	10.09
[bmim][PF$_6$]	543	298.15	1,365.90	0.27859	1.013×10^{-5}	93.857	1.068	14.65	0	102	75,850,954	32,041,159	10.56	74,235,322	30,695,372	10.31
[bmim][PF$_6$]	543	303.15	1,361.59	0.21196	1.013×10^{-5}	85.465	1.095	14.65	0	102	77,323,572	32,730,854	10.78	76,050,845	31,182,671	10.55
[bmim][PF$_6$]	543	308.15	1,357.35	0.16344	1.013×10^{-5}	78.082	1.122	14.65	0	102	77,906,918	33,545,409	11.00	77,737,007	31,687,652	10.80
[bmim][PF$_6$]	543	313.15	1,353.18	0.12763	1.013×10^{-5}	71.562	1.150	14.65	0	102	78,864,290	34,493,034	11.27	79,094,313	32,296,260	11.07
[bmim][PF$_6$]	543	318.15	1,349.09	0.10087	1.013×10^{-5}	65.784	1.178	14.65	0	102	80,666,008	35,521,524	11.59	80,394,222	33,183,100	11.42
[bmim][PF$_6$]	543	323.15	1,345.05	0.08063	1.013×10^{-5}	60.646	1.207	14.65	0	102	82,522,272	36,738,615	11.96	82,342,988	34,573,521	11.93

Table B.1 continued.

Solvent	Plant Power (MW)	T (K)	ρ_L (kg/m³)	μ_L (Pa.s)	P^{vap} (Pa)	He_{CO2} (mol/m³.bar)	He_{H2} (mol/m³.bar)	Solvent cost ($/L)	Hydro-philicity	a (m⁻¹)	Calculated CAPEX ($)	Calculated OPEX ($/year)	Calculated LCOC ($/ton CO₂)	ANN prediction CAPEX ($)	ANN prediction OPEX ($/year)	ANN prediction LCOC ($/ton CO₂)
[bmim][Tf₂N]	543	273.15	1,462.11	0.18866	1.013×10⁻⁵	173.450	1.277	14.37	0	256	53,549,102	24,617,330	7.95	54,264,510	27,841,919	8.45
[bmim][Tf₂N]	543	278.15	1,456.64	0.14035	1.013×10⁻⁵	156.328	1.324	14.37	0	256	54,799,194	24,836,033	8.05	54,556,889	27,905,217	8.52
[bmim][Tf₂N]	543	283.15	1,451.28	0.10641	1.013×10⁻⁵	141.464	1.370	14.37	0	256	56,067,963	25,180,744	8.18	55,840,746	28,036,027	8.65
[bmim][Tf₂N]	543	288.15	1,446.02	0.08213	1.013×10⁻⁵	128.502	1.415	14.37	0	256	57,454,586	25,678,446	8.35	57,760,428	28,216,305	8.82
[bmim][Tf₂N]	543	293.15	1,440.87	0.06445	1.013×10⁻⁵	117.149	1.459	14.37	0	256	58,962,447	26,309,434	8.56	59,895,046	28,430,034	9.01
[bmim][Tf₂N]	543	298.15	1,435.82	0.05139	1.013×10⁻⁵	107.166	1.502	14.37	0	256	60,820,841	27,075,423	8.81	61,827,853	28,669,107	9.21
[bmim][Tf₂N]	543	303.15	1,430.85	0.04158	1.013×10⁻⁵	98.354	1.544	14.37	0	256	62,554,578	28,009,985	9.10	63,309,401	28,957,809	9.40
[bmim][Tf₂N]	543	308.15	1,425.98	0.03412	1.013×10⁻⁵	90.546	1.586	14.37	0	256	63,897,685	29,206,686	9.45	64,399,115	29,374,602	9.63
[bmim][Tf₂N]	543	313.15	1,421.19	0.02837	1.013×10⁻⁵	83.604	1.627	14.37	0	256	65,720,438	30,621,484	9.86	65,487,012	30,051,294	9.92
[bmim][Tf₂N]	543	318.15	1,416.47	0.02389	1.013×10⁻⁵	77.411	1.667	14.37	0	256	68,055,775	32,236,245	10.35	67,174,114	31,142,530	10.33
[bmim][Tf₂N]	543	323.15	1,411.84	0.02036	1.013×10⁻⁵	71.869	1.706	14.37	0	256	70,764,190	34,079,236	10.90	70,055,376	32,773,912	10.92
[bmim][Tf₂N]	543	273.15	1,462.11	0.18866	1.013×10⁻⁵	173.450	1.277	14.37	0	102	54,253,114	25,453,953	8.19	54,233,635	28,055,229	8.51
[bmim][Tf₂N]	543	278.15	1,456.64	0.14035	1.013×10⁻⁵	156.328	1.324	14.37	0	102	55,486,293	25,844,115	8.33	54,547,779	28,161,284	8.59
[bmim][Tf₂N]	543	283.15	1,451.28	0.10641	1.013×10⁻⁵	141.464	1.370	14.37	0	102	56,954,234	26,236,092	8.47	55,734,955	28,297,216	8.72
[bmim][Tf₂N]	543	288.15	1,446.02	0.08213	1.013×10⁻⁵	128.502	1.415	14.37	0	102	58,333,066	26,744,103	8.65	57,530,974	28,464,525	8.88
[bmim][Tf₂N]	543	293.15	1,440.87	0.06445	1.013×10⁻⁵	117.149	1.459	14.37	0	102	59,678,773	27,366,713	8.85	59,614,051	28,669,428	9.07
[bmim][Tf₂N]	543	298.15	1,435.82	0.05139	1.013×10⁻⁵	107.166	1.502	14.37	0	102	61,272,336	28,068,087	9.08	61,586,816	28,914,916	9.26
[bmim][Tf₂N]	543	303.15	1,430.85	0.04158	1.013×10⁻⁵	98.354	1.544	14.37	0	102	62,949,025	28,911,548	9.34	63,149,354	29,226,953	9.47
[bmim][Tf₂N]	543	308.15	1,425.98	0.03412	1.013×10⁻⁵	90.546	1.586	14.37	0	102	63,579,206	29,751,725	9.57	64,314,509	29,686,412	9.71
[bmim][Tf₂N]	543	313.15	1,421.19	0.02837	1.013×10⁻⁵	83.604	1.627	14.37	0	102	65,591,775	31,335,540	10.04	65,484,674	30,434,462	10.02
[bmim][Tf₂N]	543	318.15	1,416.47	0.02389	1.013×10⁻⁵	77.411	1.667	14.37	0	102	67,321,397	32,895,255	10.49	67,326,619	31,638,775	10.47
[bmim][Tf₂N]	543	323.15	1,411.84	0.02036	1.013×10⁻⁵	71.869	1.706	14.37	0	102	70,284,472	34,629,861	11.02	70,505,307	33,432,904	11.11
[bmim][Tf₂N]	443	283.15	1,451.28	0.10641	1.013×10⁻⁵	141.464	1.370	14.37	0	256	47,951,444	20,854,546	8.37	45,023,658	23,422,334	7.86
[bmim][Tf₂N]	443	293.15	1,440.87	0.06445	1.013×10⁻⁵	117.149	1.459	14.37	0	256	50,247,133	21,764,306	8.74	47,844,406	22,695,098	7.97

Table B.1 continued.

Solvent	Plant Power (MW)	T (K)	ρ_L (kg/m³)	μ_L (Pa.s)	P^{vap} (Pa)	He_{CO2} (mol/m³.bar)	He_{H2} (mol/m³.bar)	Solvent cost ($/L)	Hydro-philicity	a (m⁻¹)	Calculated CAPEX ($)	Calculated OPEX ($/year)	Calculated LCOC ($/ton CO₂)	ANN prediction CAPEX ($)	ANN prediction OPEX ($/year)	ANN prediction LCOC ($/ton CO₂)
[bmim][Tf₂N]	443	313.15	1,421.19	0.02837	1.013×10⁻⁵	83.604	1.627	14.37	0	256	55,723,355	25,206,464	10.02	42,120,604	20,088,302	7.55
[bmim][Tf₂N]	343	283.15	1,451.28	0.10641	1.013×10⁻⁵	141.464	1.370	14.37	0	256	39,706,919	16,491,988	8.65	37,653,005	20,575,013	8.23
[bmim][Tf₂N]	343	293.15	1,440.87	0.06445	1.013×10⁻⁵	117.149	1.459	14.37	0	256	41,497,050	17,136,463	9.00	41,371,806	19,693,559	8.49
[bmim][Tf₂N]	343	313.15	1,421.19	0.02837	1.013×10⁻⁵	83.604	1.627	14.37	0	256	45,257,260	19,824,157	10.26	35,547,835	17,253,155	8.26
[bmim][Tf₂N]	216	283.15	1,451.28	0.10641	1.013×10⁻⁵	141.464	1.370	14.37	0	256	28,693,362	11,048,377	9.36	28,255,021	15,714,324	9.63
[bmim][Tf₂N]	216	293.15	1,440.87	0.06445	1.013×10⁻⁵	117.149	1.459	14.37	0	256	29,701,366	11,384,592	9.65	32,203,713	14,715,774	10.16
[bmim][Tf₂N]	216	313.15	1,421.19	0.02837	1.013×10⁻⁵	83.604	1.627	14.37	0	256	31,886,275	12,994,017	10.85	31,930,381	14,453,637	10.79
[bmim][Tf₂N]	136	283.15	1,451.28	0.10641	1.013×10⁻⁵	141.464	1.370	14.37	0	256	21,289,724	7,474,264	10.28	20,680,578	10,837,951	10.93
[bmim][Tf₂N]	136	293.15	1,440.87	0.06445	1.013×10⁻⁵	117.149	1.459	14.37	0	256	21,826,168	7,702,261	10.58	23,304,975	9,657,085	11.61
[bmim][Tf₂N]	136	313.15	1,421.19	0.02837	1.013×10⁻⁵	83.604	1.627	14.37	0	256	23,034,461	8,586,515	11.62	25,914,298	11,205,024	12.72
[bmim][Tf₂N]	86	283.15	1,451.28	0.10641	1.013×10⁻⁵	141.464	1.370	14.37	0	256	16,192,041	5,316,273	11.81	15,404,705	6,725,389	11.90
[bmim][Tf₂N]	86	293.15	1,440.87	0.06445	1.013×10⁻⁵	117.149	1.459	14.37	0	256	16,446,895	5,390,809	11.98	16,695,763	5,380,492	12.62
[bmim][Tf₂N]	86	313.15	1,421.19	0.02837	1.013×10⁻⁵	83.604	1.627	14.37	0	256	16,978,064	5,751,700	12.66	18,734,462	8,003,439	13.86
[bmim][Tf₂N]	54	283.15	1,451.28	0.10641	1.013×10⁻⁵	141.464	1.370	14.37	0	256	12,222,536	3,505,285	12.85	12,177,009	3,637,472	12.54
[bmim][Tf₂N]	54	293.15	1,440.87	0.06445	1.013×10⁻⁵	117.149	1.459	14.37	0	256	12,694,244	3,885,173	13.96	12,587,946	2,176,480	13.27
[bmim][Tf₂N]	54	313.15	1,421.19	0.02837	1.013×10⁻⁵	83.604	1.627	14.37	0	256	12,807,319	4,046,625	14.41	12,732,989	5,413,356	14.50
[bmPyr][Tf₂N]	543	273.15	1,424.37	0.30652	1.013×10⁻⁵	148.798	1.342	32.17	0	256	67,054,340	27,146,564	9.04	66,823,896	28,055,008	8.91
[bmPyr][Tf₂N]	543	278.15	1,418.93	0.22383	1.013×10⁻⁵	131.945	1.381	32.17	0	256	69,304,415	27,632,680	9.23	69,640,432	28,360,272	9.11
[bmPyr][Tf₂N]	543	283.15	1,413.61	0.16668	1.013×10⁻⁵	117.641	1.418	32.17	0	256	71,857,761	28,342,347	9.50	72,482,179	28,887,163	9.36
[bmPyr][Tf₂N]	543	288.15	1,408.40	0.12644	1.013×10⁻⁵	105.431	1.454	32.17	0	256	74,803,583	29,222,337	9.82	75,473,024	29,635,771	9.68
[bmPyr][Tf₂N]	543	293.15	1,403.29	0.09759	1.013×10⁻⁵	94.953	1.490	32.17	0	256	77,975,819	30,338,132	10.20	78,677,282	30,622,854	10.08
[bmPyr][Tf₂N]	543	298.15	1,398.28	0.07656	1.013×10⁻⁵	85.913	1.524	32.17	0	256	81,832,931	31,692,343	10.67	82,160,123	31,876,987	10.56
[bmPyr][Tf₂N]	543	303.15	1,393.36	0.06100	1.013×10⁻⁵	78.078	1.558	32.17	0	256	86,114,536	33,317,453	11.22	86,002,614	33,417,052	11.12
[bmPyr][Tf₂N]	543	308.15	1,388.53	0.04931	1.013×10⁻⁵	71.254	1.591	32.17	0	256	89,982,647	35,377,229	11.87	90,281,268	35,222,225	11.77

Table B.1 continued.

Solvent	Plant Power (MW)	T (K)	ρ_L (kg/m³)	μ_L (Pa.s)	P^{vap} (Pa)	He_{CO2} (mol/m³.bar)	He_{H2} (mol/m³.bar)	Solvent cost ($/L)	Hydro-philicity	a (m⁻¹)	Calculated			ANN prediction		
											CAPEX ($)	OPEX ($/year)	LCOC ($/ton CO₂)	CAPEX ($)	OPEX ($/year)	LCOC ($/ton CO₂)
[bmPyr][Tf₂N]	543	313.15	1,383.78	0.04042	1.013×10⁻⁵	65.286	1.624	32.17	0	256	95,190,676	37,862,083	12.66	95,046,083	37,212,312	12.49
[bmPyr][Tf₂N]	543	318.15	1,379.11	0.03356	1.013×10⁻⁵	60.045	1.655	32.17	0	256	101,501,730	40,729,063	13.59	100,314,084	39,254,031	13.23
[bmPyr][Tf₂N]	543	323.15	1,374.52	0.02821	1.013×10⁻⁵	55.423	1.686	32.17	0	256	108,986,135	44,131,437	14.69	106,083,575	41,198,175	13.97
[bmPyr][Tf₂N]	543	273.15	1,424.37	0.30652	1.013×10⁻⁵	148.798	1.342	32.17	0	102	67,086,438	27,958,341	9.24	66,998,459	28,364,476	8.99
[bmPyr][Tf₂N]	543	278.15	1,418.93	0.22383	1.013×10⁻⁵	131.945	1.381	32.17	0	102	70,107,295	28,794,853	9.55	69,914,178	28,771,281	9.21
[bmPyr][Tf₂N]	543	283.15	1,413.61	0.16668	1.013×10⁻⁵	117.641	1.418	32.17	0	102	73,034,929	29,696,455	9.87	72,852,845	29,425,192	9.50
[bmPyr][Tf₂N]	543	288.15	1,408.40	0.12644	1.013×10⁻⁵	105.431	1.454	32.17	0	102	76,182,235	30,745,538	10.24	75,945,802	30,330,937	9.86
[bmPyr][Tf₂N]	543	293.15	1,403.29	0.09759	1.013×10⁻⁵	94.953	1.490	32.17	0	102	79,654,721	31,968,954	10.67	79,264,369	31,510,319	10.31
[bmPyr][Tf₂N]	543	298.15	1,398.28	0.07656	1.013×10⁻⁵	85.913	1.524	32.17	0	102	83,287,449	33,369,551	11.14	82,882,513	32,994,677	10.85
[bmPyr][Tf₂N]	543	303.15	1,393.36	0.06100	1.013×10⁻⁵	78.078	1.558	32.17	0	102	87,533,966	34,948,711	11.67	86,890,100	34,799,293	11.49
[bmPyr][Tf₂N]	543	308.15	1,388.53	0.04931	1.013×10⁻⁵	71.254	1.591	32.17	0	102	91,079,399	36,958,512	12.30	91,369,672	36,890,545	12.21
[bmPyr][Tf₂N]	543	313.15	1,383.78	0.04042	1.013×10⁻⁵	65.286	1.624	32.17	0	102	95,908,963	39,352,911	13.06	96,373,884	39,168,172	13.01
[bmPyr][Tf₂N]	543	318.15	1,379.11	0.03356	1.013×10⁻⁵	60.045	1.655	32.17	0	102	101,847,369	42,150,101	13.95	101,920,658	41,478,426	13.83
[bmPyr][Tf₂N]	543	323.15	1,374.52	0.02821	1.013×10⁻⁵	55.423	1.686	32.17	0	102	108,438,275	45,412,734	14.99	108,009,321	43,659,340	14.64
[emim][BF₄]	543	273.15	1,308.90	0.11773	1.013×10⁻⁵	92.685	2.183	17.34	0	256	133,980,032	34,896,223	13.21	140,809,816	40,002,919	14.65
[emim][BF₄]	543	278.15	1,303.63	0.09167	1.013×10⁻⁵	89.966	2.281	17.34	0	256	134,065,890	35,078,436	13.25	144,158,997	39,803,476	14.76
[emim][BF₄]	543	283.15	1,298.53	0.07246	1.013×10⁻⁵	86.965	2.372	17.34	0	256	136,489,026	35,396,766	13.41	144,978,064	39,564,147	14.75
[emim][BF₄]	543	288.15	1,293.59	0.05809	1.013×10⁻⁵	83.750	2.456	17.34	0	256	140,316,103	36,041,621	13.70	145,175,448	39,421,963	14.71
[emim][BF₄]	543	293.15	1,288.80	0.04720	1.013×10⁻⁵	80.379	2.533	17.34	0	256	145,484,558	37,020,795	14.12	145,701,817	39,438,728	14.72
[emim][BF₄]	543	298.15	1,284.13	0.03884	1.013×10⁻⁵	76.903	2.604	17.34	0	256	152,112,334	38,386,272	14.68	148,223,252	39,839,437	14.90
[emim][BF₄]	543	303.15	1,279.59	0.03234	1.013×10⁻⁵	73.369	2.670	17.34	0	256	160,089,756	40,186,437	15.40	155,400,983	41,046,176	15.45
[emim][BF₄]	543	308.15	1,275.16	0.02723	1.013×10⁻⁵	69.813	2.730	17.34	0	256	169,159,863	42,559,943	16.30	169,136,392	43,433,465	16.55
[emim][BF₄]	543	313.15	1,270.83	0.02317	1.013×10⁻⁵	66.270	2.784	17.34	0	256	181,552,803	45,510,888	17.44	187,819,619	46,915,860	18.12
[emim][BF₄]	543	318.15	1,266.60	0.01991	1.013×10⁻⁵	62.766	2.834	17.34	0	256	195,240,566	49,096,027	18.80	205,831,686	50,823,766	19.79

Table B.1 continued.

Solvent	Plant Power (MW)	T (K)	ρ_L (kg/m^3)	μ_L (Pa.s)	P^{gap} (Pa)	He_{CO2} (mol/m^3.bar)	He_{H2} (mol/m^3.bar)	Solvent cost ($/L)	Hydro-philicity	a (m^{-1})	Calculated			ANN prediction		
											CAPEX ($)	OPEX ($/year)	LCOC ($/ton CO$_2$)	CAPEX ($)	OPEX ($/year)	LCOC ($/ton CO$_2$)
[emim][BF$_4$]	543	323.15	1,262.46	0.01728	1.013×10^{-5}	59.324	2.879	17.34	0	256	216,736,910	53,447,176	20.61	216,612,635	54,317,931	21.12
[emim][BF$_4$]	543	273.15	1,308.90	0.11773	1.013×10^{-5}	92.685	2.183	17.34	0	102	154,310,991	40,372,061	15.25	153,959,200	40,142,664	15.32
[emim][BF$_4$]	543	278.15	1,303.63	0.09167	1.013×10^{-5}	89.966	2.281	17.34	0	102	152,778,178	40,712,380	15.29	152,999,612	39,518,048	15.17
[emim][BF$_4$]	543	283.15	1,298.53	0.07246	1.013×10^{-5}	86.965	2.372	17.34	0	102	152,961,210	40,407,414	15.22	153,157,670	39,451,169	15.17
[emim][BF$_4$]	543	288.15	1,293.59	0.05809	1.013×10^{-5}	83.750	2.456	17.34	0	102	154,308,402	40,406,091	15.26	154,665,990	39,718,690	15.27
[emim][BF$_4$]	543	293.15	1,288.80	0.04720	1.013×10^{-5}	80.379	2.533	17.34	0	102	157,099,721	40,787,247	15.45	156,719,621	40,132,664	15.42
[emim][BF$_4$]	543	298.15	1,284.13	0.03884	1.013×10^{-5}	76.903	2.604	17.34	0	102	161,079,306	41,639,630	15.80	158,687,543	40,626,315	15.59
[emim][BF$_4$]	543	303.15	1,279.59	0.03234	1.013×10^{-5}	73.369	2.670	17.34	0	102	166,792,565	42,909,170	16.31	161,106,863	41,334,246	15.84
[emim][BF$_4$]	543	308.15	1,275.16	0.02723	1.013×10^{-5}	69.813	2.730	17.34	0	102	172,772,304	44,851,633	16.99	166,354,504	42,678,057	16.36
[emim][BF$_4$]	543	313.15	1,270.83	0.02317	1.013×10^{-5}	66.270	2.784	17.34	0	102	182,995,129	47,346,497	17.95	177,526,357	45,221,427	17.41
[emim][BF$_4$]	543	318.15	1,266.60	0.01991	1.013×10^{-5}	62.766	2.834	17.34	0	102	195,120,896	50,570,664	19.17	194,943,412	49,160,165	19.05
[emim][BF$_4$]	543	323.15	1,262.46	0.01728	1.013×10^{-5}	59.324	2.879	17.34	0	102	213,410,050	54,585,824	20.78	213,615,457	53,906,829	20.96
[emim][Tf$_2$N]	543	273.15	1,548.40	0.08335	1.013×10^{-5}	185.117	1.144	30.38	0	256	53,433,751	23,009,283	7.55	53,673,447	23,407,461	7.96
[emim][Tf$_2$N]	543	278.15	1,542.17	0.06841	1.013×10^{-5}	164.419	1.191	30.38	0	256	55,136,612	23,289,160	7.67	56,555,447	23,362,218	8.12
[emim][Tf$_2$N]	543	283.15	1,536.08	0.05664	1.013×10^{-5}	146.550	1.237	30.38	0	256	56,790,710	23,699,701	7.83	59,166,860	23,340,605	8.29
[emim][Tf$_2$N]	543	288.15	1,530.14	0.04728	1.013×10^{-5}	131.061	1.281	30.38	0	256	58,698,254	24,195,084	8.02	61,361,058	23,381,179	8.46
[emim][Tf$_2$N]	543	293.15	1,524.32	0.03978	1.013×10^{-5}	117.583	1.325	30.38	0	256	60,788,068	24,823,301	8.25	63,141,241	23,551,917	8.64
[emim][Tf$_2$N]	543	298.15	1,518.62	0.03371	1.013×10^{-5}	105.813	1.367	30.38	0	256	63,187,485	25,611,598	8.52	64,654,263	23,930,806	8.87
[emim][Tf$_2$N]	543	303.15	1,513.04	0.02877	1.013×10^{-5}	95.498	1.409	30.38	0	256	65,941,836	26,558,271	8.85	66,116,150	24,571,372	9.16
[emim][Tf$_2$N]	543	308.15	1,507.57	0.02472	1.013×10^{-5}	86.428	1.450	30.38	0	256	67,959,211	27,760,232	9.22	67,707,263	25,472,125	9.51
[emim][Tf$_2$N]	543	313.15	1,502.21	0.02137	1.013×10^{-5}	78.426	1.490	30.38	0	256	70,830,363	29,232,701	9.69	69,503,819	26,571,484	9.91
[emim][Tf$_2$N]	543	318.15	1,496.94	0.01858	1.013×10^{-5}	71.345	1.529	30.38	0	256	74,481,598	30,993,413	10.25	71,476,161	27,771,107	10.34
[emim][Tf$_2$N]	543	323.15	1,491.77	0.01625	1.013×10^{-5}	65.062	1.567	30.38	0	256	79,861,526	33,046,569	10.94	73,535,981	28,970,866	10.76
[emim][Tf$_2$N]	543	273.15	1,548.40	0.08335	1.013×10^{-5}	185.117	1.144	30.38	0	102	53,950,988	23,649,712	7.72	51,132,849	23,190,346	7.81

Table B.1 continued.

Solvent	Plant Power (MW)	T (K)	ρ_L (kg/m³)	μ_L (Pa.s)	P^{vap} (Pa)	He_{CO2} (mol/m³.bar)	He_{H2} (mol/m³.bar)	Solvent cost ($/L)	Hydro-philicity	a (m⁻¹)	Calculated			ANN prediction		
											CAPEX ($)	OPEX ($/year)	LCOC ($/ton CO₂)	CAPEX ($)	OPEX ($/year)	LCOC ($/ton CO₂)
[emim][Tf₂N]	543	278.15	1,542.17	0.06841	1.013×10⁻⁵	164.419	1.191	30.38	0	102	55,503,614	23,958,433	7.85	53,965,619	23,174,136	7.98
[emim][Tf₂N]	543	283.15	1,536.08	0.05664	1.013×10⁻⁵	146.550	1.237	30.38	0	102	57,207,025	24,343,455	8.01	56,628,658	23,207,744	8.16
[emim][Tf₂N]	543	288.15	1,530.14	0.04728	1.013×10⁻⁵	131.061	1.281	30.38	0	102	59,085,620	24,815,499	8.19	58,982,950	23,332,759	8.36
[emim][Tf₂N]	543	293.15	1,524.32	0.03978	1.013×10⁻⁵	117.583	1.325	30.38	0	102	60,943,635	25,426,207	8.40	61,036,975	23,616,882	8.58
[emim][Tf₂N]	543	298.15	1,518.62	0.03371	1.013×10⁻⁵	105.813	1.367	30.38	0	102	63,085,065	26,149,150	8.66	62,932,699	24,131,888	8.86
[emim][Tf₂N]	543	303.15	1,513.04	0.02877	1.013×10⁻⁵	95.498	1.409	30.38	0	102	65,625,936	27,025,161	8.96	64,863,296	24,918,492	9.20
[emim][Tf₂N]	543	308.15	1,507.57	0.02472	1.013×10⁻⁵	86.428	1.450	30.38	0	102	67,324,282	28,180,485	9.30	66,968,873	25,958,933	9.60
[emim][Tf₂N]	543	313.15	1,502.21	0.02137	1.013×10⁻⁵	78.426	1.490	30.38	0	102	70,049,384	29,575,819	9.75	69,278,949	27,177,565	10.04
[emim][Tf₂N]	543	318.15	1,496.94	0.01858	1.013×10⁻⁵	71.345	1.529	30.38	0	102	73,293,689	31,256,762	10.27	71,724,627	28,468,662	10.51
[emim][Tf₂N]	543	323.15	1,491.77	0.01625	1.013×10⁻⁵	65.062	1.567	30.38	0	102	77,450,284	33,285,182	10.92	74,194,482	29,732,211	10.96
[emim][Tf₂N]	443	283.15	1,536.08	0.05664	1.013×10⁻⁵	146.550	1.237	30.38	0	256	48,170,313	19,536,643	7.97	47,675,116	19,165,827	7.94
[emim][Tf₂N]	443	293.15	1,524.32	0.03978	1.013×10⁻⁵	117.583	1.325	30.38	0	256	51,370,868	20,455,161	8.38	51,635,441	18,938,562	8.33
[emim][Tf₂N]	443	313.15	1,502.21	0.02137	1.013×10⁻⁵	78.426	1.490	30.38	0	256	59,220,686	24,046,660	9.81	59,055,808	20,472,661	9.56
[emim][Tf₂N]	343	283.15	1,536.08	0.05664	1.013×10⁻⁵	146.550	1.237	30.38	0	256	39,308,799	15,391,414	8.19	38,297,947	15,664,467	8.08
[emim][Tf₂N]	343	293.15	1,524.32	0.03978	1.013×10⁻⁵	117.583	1.325	30.38	0	256	41,797,801	16,066,835	8.59	41,764,450	15,283,603	8.56
[emim][Tf₂N]	343	313.15	1,502.21	0.02137	1.013×10⁻⁵	78.426	1.490	30.38	0	256	47,660,425	18,828,478	9.99	47,849,683	15,766,880	9.84
[emim][Tf₂N]	216	283.15	1,536.08	0.05664	1.013×10⁻⁵	146.550	1.237	30.38	0	256	27,956,733	10,109,438	8.70	27,930,539	11,721,414	8.82
[emim][Tf₂N]	216	293.15	1,524.32	0.03978	1.013×10⁻⁵	117.583	1.325	30.38	0	256	29,501,331	10,503,993	9.08	30,184,388	11,239,649	9.43
[emim][Tf₂N]	216	313.15	1,502.21	0.02137	1.013×10⁻⁵	78.426	1.490	30.38	0	256	32,877,379	12,225,498	10.45	32,725,727	10,542,848	10.74
[emim][Tf₂N]	136	283.15	1,536.08	0.05664	1.013×10⁻⁵	146.550	1.237	30.38	0	256	20,357,138	6,770,468	9.45	21,542,095	9,346,950	9.57
[emim][Tf₂N]	136	293.15	1,524.32	0.03978	1.013×10⁻⁵	117.583	1.325	30.38	0	256	21,257,736	7,007,046	9.81	22,814,062	8,749,955	10.21
[emim][Tf₂N]	136	313.15	1,502.21	0.02137	1.013×10⁻⁵	78.426	1.490	30.38	0	256	23,285,274	8,018,004	11.09	23,058,986	7,399,054	11.50
[emim][Tf₂N]	86	283.15	1,536.08	0.05664	1.013×10⁻⁵	146.550	1.237	30.38	0	256	15,188,017	4,646,101	10.54	17,434,833	7,857,932	10.13
[emim][Tf₂N]	86	293.15	1,524.32	0.03978	1.013×10⁻⁵	117.583	1.325	30.38	0	256	15,729,767	4,765,839	10.84	18,067,240	7,167,318	10.78

Table B.1 continued.

Solvent	Plant Power (MW)	T (K)	ρ_L (kg/m³)	μ_L (Pa.s)	P^{vap} (Pa)	He_{CO2} (mol/m³.bar)	He_{H2} (mol/m³.bar)	Solvent cost ($/L)	Hydro-philicity	a (m⁻¹)	Calculated			ANN prediction		
											CAPEX ($)	OPEX ($/year)	LCOC ($/ton CO₂)	CAPEX ($)	OPEX ($/year)	LCOC ($/ton CO₂)
[emim][Tf₂N]	86	313.15	1,502.21	0.02137	1.013×10^{-5}	78.426	1.490	30.38	0	256	16,858,099	5,375,014	12.04	17,027,187	5,465,762	12.03
[emim][Tf₂N]	54	283.15	1,536.08	0.05664	1.013×10^{-5}	146.550	1.237	30.38	0	256	11,673,457	3,340,504	12.26	14,800,374	6,917,845	10.51
[emim][Tf₂N]	54	293.15	1,524.32	0.03978	1.013×10^{-5}	117.583	1.325	30.38	0	256	11,928,580	3,338,223	12.34	15,038,445	6,164,848	11.15
[emim][Tf₂N]	54	313.15	1,502.21	0.02137	1.013×10^{-5}	78.426	1.490	30.38	0	256	12,524,322	3,680,355	13.39	13,278,143	4,272,962	12.37
[hmim][(C₂F₅)₃PF₃]	543	273.15	1,581.53	0.39415	1.013×10^{-5}	146.812	1.932	34.16	0	256	60,161,327	25,347,422	8.36	57,453,581	25,787,852	8.33
[hmim][(C₂F₅)₃PF₃]	543	278.15	1,574.94	0.28121	1.013×10^{-5}	133.861	2.029	34.16	0	256	62,064,883	25,944,386	8.57	61,659,027	26,118,306	8.62
[hmim][(C₂F₅)₃PF₃]	543	283.15	1,568.50	0.20464	1.013×10^{-5}	122.449	2.131	34.16	0	256	64,487,863	26,644,904	8.83	65,087,281	26,644,372	8.93
[hmim][(C₂F₅)₃PF₃]	543	288.15	1,562.23	0.15172	1.013×10^{-5}	112.358	2.236	34.16	0	256	66,875,865	27,591,361	9.14	68,112,754	27,511,838	9.30
[hmim][(C₂F₅)₃PF₃]	543	293.15	1,556.09	0.11447	1.013×10^{-5}	103.406	2.347	34.16	0	256	69,782,317	28,802,665	9.54	71,173,064	28,840,778	9.77
[hmim][(C₂F₅)₃PF₃]	543	298.15	1,550.09	0.08781	1.013×10^{-5}	95.438	2.461	34.16	0	256	73,321,692	30,372,717	10.06	74,603,654	30,674,988	10.37
[hmim][(C₂F₅)₃PF₃]	543	303.15	1,544.22	0.06842	1.013×10^{-5}	88.323	2.582	34.16	0	256	77,671,527	32,335,527	10.69	78,551,831	32,964,741	11.09
[hmim][(C₂F₅)₃PF₃]	543	308.15	1,538.47	0.05410	1.013×10^{-5}	81.953	2.707	34.16	0	256	81,950,303	34,932,400	11.48	82,989,951	35,593,502	11.91
[hmim][(C₂F₅)₃PF₃]	543	313.15	1,532.83	0.04338	1.013×10^{-5}	76.231	2.838	34.16	0	256	87,674,499	38,162,591	12.49	87,801,766	38,432,280	12.78
[hmim][(C₂F₅)₃PF₃]	543	318.15	1,527.31	0.03524	1.013×10^{-5}	71.079	2.976	34.16	0	256	94,979,708	42,262,824	13.76	92,878,450	41,390,430	13.68
[hmim][(C₂F₅)₃PF₃]	543	323.15	1,521.88	0.02899	1.013×10^{-5}	66.426	3.120	34.16	0	256	104,696,424	47,413,694	15.37	98,181,722	44,443,547	14.60
[hmim][(C₂F₅)₃PF₃]	543	273.15	1,581.53	0.39415	1.013×10^{-5}	146.812	1.932	34.16	0	102	59,598,149	25,600,578	8.40	55,369,330	25,650,944	8.22
[hmim][(C₂F₅)₃PF₃]	543	278.15	1,574.94	0.28121	1.013×10^{-5}	133.861	2.029	34.16	0	102	62,197,468	26,406,609	8.69	59,403,365	26,021,379	8.52
[hmim][(C₂F₅)₃PF₃]	543	283.15	1,568.50	0.20464	1.013×10^{-5}	122.449	2.131	34.16	0	102	64,746,011	27,359,258	9.01	62,840,944	26,633,826	8.85
[hmim][(C₂F₅)₃PF₃]	543	288.15	1,562.23	0.15172	1.013×10^{-5}	112.358	2.236	34.16	0	102	67,309,255	28,491,722	9.38	66,061,362	27,632,859	9.26
[hmim][(C₂F₅)₃PF₃]	543	293.15	1,556.09	0.11447	1.013×10^{-5}	103.406	2.347	34.16	0	102	70,271,023	29,816,643	9.81	69,481,288	29,126,849	9.78
[hmim][(C₂F₅)₃PF₃]	543	298.15	1,550.09	0.08781	1.013×10^{-5}	95.438	2.461	34.16	0	102	73,791,430	31,399,340	10.33	73,386,655	31,139,394	10.44
[hmim][(C₂F₅)₃PF₃]	543	303.15	1,544.22	0.06842	1.013×10^{-5}	88.323	2.582	34.16	0	102	77,879,131	33,390,947	10.96	77,859,594	33,599,250	11.22
[hmim][(C₂F₅)₃PF₃]	543	308.15	1,538.47	0.05410	1.013×10^{-5}	81.953	2.707	34.16	0	102	81,964,903	35,891,542	11.73	82,811,762	36,374,978	12.09
[hmim][(C₂F₅)₃PF₃]	543	313.15	1,532.83	0.04338	1.013×10^{-5}	76.231	2.838	34.16	0	102	87,269,811	39,083,202	12.70	88,086,581	39,333,326	13.00

Table B.1 continued.

Solvent	Plant Power (MW)	T (K)	ρ_L (kg/m³)	μ_L (Pa.s)	P^{vap} (Pa)	He_{CO2} (mol/m³.bar)	He_{H2} (mol/m³.bar)	Solvent cost ($/L)	Hydro-philicity	a (m⁻¹)	Calculated			ANN prediction		
											CAPEX ($)	OPEX ($/year)	LCOC ($/ton CO₂)	CAPEX ($)	OPEX ($/year)	LCOC ($/ton CO₂)
[hmim][(C₂F₅)₃PF₃]	543	318.15	1,527.31	0.03524	1.013×10⁻⁵	71.079	2.976	34.16	0	102	94,191,651	43,118,596	13.94	93,560,441	42,389,133	13.94
[hmim][(C₂F₅)₃PF₃]	543	323.15	1,521.88	0.02899	1.013×10⁻⁵	66.426	3.120	34.16	0	102	103,141,942	48,145,780	15.50	99,202,283	45,529,820	14.90
[hmim][Tf₂N]	543	273.15	1,391.79	0.29536	1.013×10⁻⁵	157.966	1.401	41.50	0	256	70,997,002	27,303,929	9.20	74,193,871	30,458,228	9.80
[hmim][Tf₂N]	543	278.15	1,387.26	0.21335	1.013×10⁻⁵	141.931	1.452	41.50	0	256	73,772,736	27,724,926	9.39	75,501,278	29,390,540	9.59
[hmim][Tf₂N]	543	283.15	1,382.81	0.15735	1.013×10⁻⁵	128.050	1.501	41.50	0	256	76,116,362	28,275,916	9.61	77,059,926	29,119,874	9.60
[hmim][Tf₂N]	543	288.15	1,378.44	0.11833	1.013×10⁻⁵	115.977	1.549	41.50	0	256	78,563,113	28,958,206	9.87	79,101,350	29,404,793	9.77
[hmim][Tf₂N]	543	293.15	1,374.14	0.09065	1.013×10⁻⁵	105.432	1.595	41.50	0	256	81,467,164	29,829,091	10.19	81,669,008	30,095,904	10.07
[hmim][Tf₂N]	543	298.15	1,369.91	0.07065	1.013×10⁻⁵	96.182	1.639	41.50	0	256	84,361,018	30,891,918	10.55	84,706,495	31,085,275	10.46
[hmim][Tf₂N]	543	303.15	1,365.75	0.05597	1.013×10⁻⁵	88.036	1.682	41.50	0	256	88,504,531	32,129,759	11.00	88,127,168	32,263,365	10.93
[hmim][Tf₂N]	543	308.15	1,361.65	0.04503	1.013×10⁻⁵	80.836	1.724	41.50	0	256	92,499,153	33,678,438	11.52	91,849,891	33,496,153	11.42
[hmim][Tf₂N]	543	313.15	1,357.62	0.03675	1.013×10⁻⁵	74.449	1.765	41.50	0	256	95,731,696	35,545,605	12.09	95,813,031	34,635,193	11.90
[hmim][Tf₂N]	543	318.15	1,353.64	0.03041	1.013×10⁻⁵	68.763	1.804	41.50	0	256	101,567,415	37,708,671	12.83	99,979,963	35,553,912	12.33
[hmim][Tf₂N]	543	323.15	1,349.73	0.02550	1.013×10⁻⁵	63.687	1.842	41.50	0	256	111,694,521	40,389,908	13.84	104,339,186	36,185,781	12.70
[hmim][Tf₂N]	543	273.15	1,391.79	0.29536	1.013×10⁻⁵	157.966	1.401	41.50	0	102	71,021,540	27,977,405	9.38	74,172,633	31,040,641	9.94
[hmim][Tf₂N]	543	278.15	1,387.26	0.21335	1.013×10⁻⁵	141.931	1.452	41.50	0	102	74,600,902	28,760,718	9.69	75,316,125	30,067,390	9.75
[hmim][Tf₂N]	543	283.15	1,382.81	0.15735	1.013×10⁻⁵	128.050	1.501	41.50	0	102	76,823,831	29,417,329	9.93	76,750,923	29,990,268	9.79
[hmim][Tf₂N]	543	288.15	1,378.44	0.11833	1.013×10⁻⁵	115.977	1.549	41.50	0	102	79,578,303	30,343,091	10.25	78,746,952	30,557,882	10.03
[hmim][Tf₂N]	543	293.15	1,374.14	0.09065	1.013×10⁻⁵	105.432	1.595	41.50	0	102	82,533,315	31,203,534	10.57	81,349,579	31,602,560	10.42
[hmim][Tf₂N]	543	298.15	1,369.91	0.07065	1.013×10⁻⁵	96.182	1.639	41.50	0	102	85,553,236	32,197,440	10.92	84,487,314	32,988,985	10.92
[hmim][Tf₂N]	543	303.15	1,365.75	0.05597	1.013×10⁻⁵	88.036	1.682	41.50	0	102	89,102,556	33,327,945	11.32	88,055,829	34,571,132	11.49
[hmim][Tf₂N]	543	308.15	1,361.65	0.04503	1.013×10⁻⁵	80.836	1.724	41.50	0	102	91,499,734	34,816,565	11.77	91,960,404	36,174,671	12.08
[hmim][Tf₂N]	543	313.15	1,357.62	0.03675	1.013×10⁻⁵	74.449	1.765	41.50	0	102	95,913,543	36,551,812	12.35	96,131,274	37,617,639	12.64
[hmim][Tf₂N]	543	318.15	1,353.64	0.03041	1.013×10⁻⁵	68.763	1.804	41.50	0	102	100,077,536	38,600,169	13.01	100,528,054	38,756,295	13.13
[hmim][Tf₂N]	543	323.15	1,349.73	0.02550	1.013×10⁻⁵	63.687	1.842	41.50	0	102	105,301,357	41,006,064	13.78	105,138,192	39,525,816	13.54

176

Table B.1 continued.

Solvent	Plant Power (MW)	T (K)	ρ_L (kg/m³)	μ_L (Pa.s)	P^{vap} (Pa)	He_{CO2} (mol/m³.bar)	He_{H2} (mol/m³.bar)	Solvent cost ($/L)	Hydro-philicity	a (m⁻¹)	Calculated			ANN prediction		
											CAPEX ($)	OPEX ($/year)	LCOC ($/ton CO₂)	CAPEX ($)	OPEX ($/year)	LCOC ($/ton CO₂)
[omim][Tf₂N]	543	273.15	1,348.02	0.36581	1.013×10⁻⁵	147.036	1.461	26.44	0	256	65,880,320	27,411,486	9.06	66,368,036	27,964,335	8.92
[omim][Tf₂N]	543	278.15	1,342.62	0.26870	1.013×10⁻⁵	135.268	1.512	26.44	0	256	66,845,538	27,616,679	9.15	67,005,604	28,085,211	8.96
[omim][Tf₂N]	543	283.15	1,337.31	0.20076	1.013×10⁻⁵	124.968	1.562	26.44	0	256	68,112,456	27,951,945	9.27	67,963,616	28,414,924	9.06
[omim][Tf₂N]	543	288.15	1,332.09	0.15242	1.013×10⁻⁵	115.913	1.610	26.44	0	256	69,607,818	28,413,537	9.44	69,185,826	28,919,526	9.22
[omim][Tf₂N]	543	293.15	1,326.96	0.11748	1.013×10⁻⁵	107.919	1.657	26.44	0	256	71,261,843	28,979,984	9.64	70,483,839	29,570,171	9.44
[omim][Tf₂N]	543	298.15	1,321.92	0.09185	1.013×10⁻⁵	100.834	1.703	26.44	0	256	73,018,908	29,750,395	9.89	71,802,777	30,380,530	9.72
[omim][Tf₂N]	543	303.15	1,316.95	0.07278	1.013×10⁻⁵	94.532	1.747	26.44	0	256	75,054,356	30,594,479	10.17	73,305,887	31,415,731	10.07
[omim][Tf₂N]	543	308.15	1,312.05	0.05841	1.013×10⁻⁵	88.906	1.791	26.44	0	256	76,255,555	31,680,953	10.48	75,337,612	32,769,915	10.54
[omim][Tf₂N]	543	313.15	1,307.23	0.04744	1.013×10⁻⁵	83.867	1.833	26.44	0	256	78,266,084	32,922,500	10.86	78,315,903	34,522,211	11.14
[omim][Tf₂N]	543	318.15	1,302.47	0.03897	1.013×10⁻⁵	79.341	1.874	26.44	0	256	80,585,302	34,271,362	11.27	82,604,446	36,688,484	11.90
[omim][Tf₂N]	543	323.15	1,297.77	0.03237	1.013×10⁻⁵	75.263	1.913	26.44	0	256	83,147,616	35,755,362	11.73	88,428,173	39,193,562	12.80
[omim][Tf₂N]	543	273.15	1,348.02	0.36581	1.013×10⁻⁵	147.036	1.461	26.44	0	102	66,961,430	28,866,730	9.47	67,017,080	28,315,530	9.02
[omim][Tf₂N]	543	278.15	1,342.62	0.26870	1.013×10⁻⁵	135.268	1.512	26.44	0	102	68,867,363	29,014,189	9.56	68,297,999	28,608,179	9.12
[omim][Tf₂N]	543	283.15	1,337.31	0.20076	1.013×10⁻⁵	124.968	1.562	26.44	0	102	70,380,322	29,852,224	9.83	70,077,971	29,160,933	9.29
[omim][Tf₂N]	543	288.15	1,332.09	0.15242	1.013×10⁻⁵	115.913	1.610	26.44	0	102	71,925,162	30,481,049	10.04	72,072,505	29,916,699	9.54
[omim][Tf₂N]	543	293.15	1,326.96	0.11748	1.013×10⁻⁵	107.919	1.657	26.44	0	102	73,630,742	31,108,199	10.25	73,875,423	30,813,519	9.83
[omim][Tf₂N]	543	298.15	1,321.92	0.09185	1.013×10⁻⁵	100.834	1.703	26.44	0	102	75,482,965	31,798,377	10.48	75,316,851	31,843,970	10.17
[omim][Tf₂N]	543	303.15	1,316.95	0.07278	1.013×10⁻⁵	94.532	1.747	26.44	0	102	77,140,648	32,625,849	10.75	76,561,481	33,073,822	10.57
[omim][Tf₂N]	543	308.15	1,312.05	0.05841	1.013×10⁻⁵	88.906	1.791	26.44	0	102	78,315,775	33,552,438	11.02	78,056,401	34,616,021	11.06
[omim][Tf₂N]	543	313.15	1,307.23	0.04744	1.013×10⁻⁵	83.867	1.833	26.44	0	102	79,878,599	34,614,476	11.34	80,385,364	36,573,538	11.70
[omim][Tf₂N]	543	318.15	1,302.47	0.03897	1.013×10⁻⁵	79.341	1.874	26.44	0	102	81,482,312	35,865,140	11.71	84,081,272	38,975,021	12.50
[omim][Tf₂N]	543	323.15	1,297.77	0.03237	1.013×10⁻⁵	75.263	1.913	26.44	0	102	83,780,447	37,165,153	12.10	89,489,921	41,738,691	13.45

Table B.2: HC cases

Solvent	Plant Power (MW)	T (K)	ρ_L (kg/m³)	μ_L (Pa.s)	P^{vap} (Pa)	He_{CO2} (mol/m³.bar)	He_{H2} (mol/m³.bar)	Solvent cost ($/L)	Hydro-philicity	a (m⁻¹)	Calculated			ANN prediction		
											CAPEX ($)	OPEX ($/year)	LCOC ($/ton CO₂)	CAPEX ($)	OPEX ($/year)	LCOC ($/ton CO₂)
1-Heptene	543	273.15	713.07	0.00048	1,949.477	283.605	3.290	1.39	0	256	57,691,231	416,692,850	107.63	56,786,967	426,299,835	111.42
1-Heptene	543	278.15	708.81	0.00045	2,614.587	241.835	3.472	1.39	0	256	59,953,580	528,430,588	136.64	59,344,469	548,440,167	143.01
1-Heptene	543	283.15	704.55	0.00043	3,463.090	208.351	3.651	1.39	0	256	62,557,203	670,501,014	173.45	61,939,739	684,608,506	178.09
1-Heptene	543	288.15	700.30	0.00040	4,533.320	181.242	3.827	1.39	0	256	65,281,896	851,078,623	220.32	64,793,673	852,851,395	221.33
1-Heptene	543	293.15	696.04	0.00038	5,868.884	159.089	3.999	1.39	0	256	68,561,969	1,079,838,191	279.65	68,541,104	1,079,804,297	279.65
1-Heptene	543	298.15	691.77	0.00036	7,518.916	140.830	4.168	1.39	0	256	74,755,521	1,367,354,551	354.15	74,002,026	1,374,183,953	355.36
1-Heptene	543	273.15	713.07	0.00048	1,949.477	283.605	3.290	1.39	0	102	57,195,254	418,163,458	107.99	56,997,562	415,528,140	108.66
1-Heptene	543	278.15	708.81	0.00045	2,614.587	241.835	3.472	1.39	0	102	59,499,407	529,846,626	136.74	59,509,981	534,167,044	139.36
1-Heptene	543	283.15	704.55	0.00043	3,463.090	208.351	3.651	1.39	0	102	62,032,341	672,245,039	173.52	62,068,395	669,315,387	174.17
1-Heptene	543	288.15	700.30	0.00040	4,533.320	181.242	3.827	1.39	0	102	64,437,947	853,298,405	220.40	64,916,530	839,428,743	217.89
1-Heptene	543	293.15	696.04	0.00038	5,868.884	159.089	3.999	1.39	0	102	67,848,293	1,082,961,923	280.30	68,694,748	1,071,074,063	277.41
1-Heptene	543	298.15	691.77	0.00036	7,518.916	140.830	4.168	1.39	0	102	74,106,147	1,370,783,510	355.15	74,198,629	1,372,177,002	354.84
1-Octene	543	273.15	729.99	0.00065	504.289	174.443	5.083	2.13	0	256	61,662,531	216,082,067	56.44	61,773,542	218,280,940	56.31
1-Octene	543	278.15	725.87	0.00061	703.177	158.708	5.100	2.13	0	256	64,407,587	278,189,703	72.26	64,326,955	278,745,237	71.79
1-Octene	543	283.15	721.76	0.00057	966.676	144.987	5.116	2.13	0	256	67,370,268	360,260,523	93.30	67,388,709	358,755,924	92.48
1-Octene	543	288.15	717.66	0.00054	1,311.263	132.966	5.132	2.13	0	256	70,669,229	467,532,621	120.87	70,866,371	470,306,548	121.47
1-Octene	543	293.15	713.56	0.00051	1,756.374	122.385	5.148	2.13	0	256	74,220,796	606,673,716	156.98	74,481,498	616,743,593	159.51
1-Octene	543	298.15	709.48	0.00048	2,324.730	113.030	5.164	2.13	0	256	77,835,899	784,402,984	202.47	77,752,797	782,064,698	202.39
1-Octene	543	273.15	729.99	0.00065	504.289	174.443	5.083	2.13	0	102	61,231,796	217,270,265	56.73	61,470,170	221,357,934	57.03
1-Octene	543	278.15	725.87	0.00061	703.177	158.708	5.100	2.13	0	102	63,969,414	279,738,090	72.66	63,865,415	279,879,264	72.02
1-Octene	543	283.15	721.76	0.00057	966.676	144.987	5.116	2.13	0	102	66,934,740	362,035,564	93.70	66,749,216	357,346,090	92.06
1-Octene	543	288.15	717.66	0.00054	1,311.263	132.966	5.132	2.13	0	102	70,165,226	469,908,956	121.46	70,047,047	466,346,972	120.40
1-Octene	543	293.15	713.56	0.00051	1,756.374	122.385	5.148	2.13	0	102	73,606,044	609,604,443	157.80	73,508,820	611,185,424	158.04
1-Octene	543	298.15	709.48	0.00048	2,324.730	113.030	5.164	2.13	0	102	77,131,074	787,550,763	203.40	76,683,889	776,793,619	200.99

Table B.2 continued.

Solvent	Plant Power (MW)	T (K)	ρ_L (kg/m³)	μ_L (Pa.s)	P^{vap} (Pa)	He_{CO2} (mol/m³.bar)	He_{H2} (mol/m³.bar)	Solvent cost ($/L)	Hydro-philicity	a (m⁻¹)	Calculated			ANN prediction		
											CAPEX ($)	OPEX ($/year)	LCOC ($/ton CO₂)	CAPEX ($)	OPEX ($/year)	LCOC ($/ton CO₂)
n-Octane	543	273.15	719.16	0.00071	384.942	187.771	0.448	0.70	0	256	51,395,032	67,350,692	18.66	51,578,109	63,876,718	17.91
n-Octane	543	278.15	715.06	0.00066	541.426	170.161	0.997	0.70	0	256	55,080,350	84,852,609	23.21	55,274,020	80,331,289	22.12
n-Octane	543	283.15	710.95	0.00062	750.698	154.883	1.692	0.70	0	256	59,823,221	109,076,185	29.48	59,536,631	106,472,842	28.74
n-Octane	543	288.15	706.82	0.00058	1,026.909	141.563	2.516	0.70	0	256	65,009,657	142,700,418	38.20	64,953,631	142,906,024	37.94
n-Octane	543	293.15	702.69	0.00054	1,386.956	129.899	3.394	0.70	0	256	70,693,285	185,055,411	49.01	71,125,384	186,872,823	49.13
n-Octane	543	298.15	698.54	0.00051	1,850.850	119.639	4.220	0.70	0	256	75,901,849	241,119,003	63.34	75,944,986	245,319,428	64.24
n-Octane	543	273.15	719.16	0.00071	384.942	187.771	0.448	0.70	0	102	50,993,741	67,661,752	18.72	50,792,171	69,055,593	19.19
n-Octane	543	278.15	715.06	0.00066	541.426	170.161	0.997	0.70	0	102	54,636,473	85,252,722	23.29	54,315,385	84,845,903	23.22
n-Octane	543	283.15	710.95	0.00062	750.698	154.883	1.692	0.70	0	102	59,262,241	109,573,377	29.59	58,526,372	109,668,712	29.49
n-Octane	543	288.15	706.82	0.00058	1,026.909	141.563	2.516	0.70	0	102	64,335,748	143,336,280	38.34	64,004,042	144,052,090	38.17
n-Octane	543	293.15	702.69	0.00054	1,386.956	129.899	3.394	0.70	0	102	69,986,835	185,841,701	49.19	70,137,668	185,626,103	48.75
n-Octane	543	298.15	698.54	0.00051	1,850.850	119.639	4.220	0.70	0	102	75,016,099	242,038,666	63.55	74,831,066	242,947,900	63.57
n-Decane	543	273.15	745.76	0.00127	26.551	111.400	2.131	0.73	0	256	57,251,697	34,166,130	10.47	59,472,909	36,060,724	10.94
n-Decane	543	278.15	741.83	0.00116	40.421	103.855	2.259	0.73	0	256	59,819,927	37,545,187	11.40	60,587,082	37,007,637	11.19
n-Decane	543	283.15	737.93	0.00107	60.435	96.953	2.387	0.73	0	256	62,737,867	42,147,137	12.65	62,660,040	39,999,780	11.98
n-Decane	543	288.15	734.05	0.00099	88.838	90.629	2.516	0.73	0	256	66,027,940	48,241,092	14.30	65,725,948	45,724,969	13.48
n-Decane	543	293.15	730.19	0.00091	128.513	84.827	2.644	0.73	0	256	69,672,674	56,729,641	16.55	69,652,281	54,785,603	15.83
n-Decane	543	298.15	726.35	0.00085	183.113	79.494	2.773	0.73	0	256	74,161,424	67,560,478	19.42	74,190,992	67,573,583	19.13
n-Decane	543	303.15	722.52	0.00079	257.205	74.585	2.902	0.73	0	256	79,256,609	82,558,841	23.35	79,064,793	84,069,938	23.35
n-Decane	543	308.15	718.70	0.00073	356.421	70.060	3.031	0.73	0	256	84,337,981	102,464,696	28.51	84,041,336	103,600,558	28.33
n-Decane	543	313.15	714.89	0.00068	487.622	65.884	3.160	0.73	0	256	90,543,433	128,847,998	35.36	88,964,401	124,677,627	33.70
n-Decane	543	273.15	745.76	0.00127	26.551	111.400	2.131	0.73	0	102	57,437,144	34,906,349	10.66	59,201,543	39,963,451	11.90
n-Decane	543	278.15	741.83	0.00116	40.421	103.855	2.259	0.73	0	102	59,818,636	38,288,418	11.59	60,069,482	40,738,393	12.10
n-Decane	543	283.15	737.93	0.00107	60.435	96.953	2.387	0.73	0	102	62,659,485	42,885,193	12.84	61,922,410	43,574,307	12.84

Table B.2 continued.

Solvent	Plant Power (MW)	T (K)	ρ_L (kg/m³)	μ_L (Pa.s)	P^{vap} (Pa)	He_{CO2} (mol/m³.bar)	He_{H2} (mol/m³.bar)	Solvent cost ($/L)	Hydro-philicity	a (m⁻¹)	Calculated			ANN prediction		
											CAPEX ($)	OPEX ($/year)	LCOC ($/ton CO₂)	CAPEX ($)	OPEX ($/year)	LCOC ($/ton CO₂)
n-Decane	543	288.15	734.05	0.00099	88.838	90.629	2.516	0.73	0	102	65,749,105	49,056,906	14.49	64,844,536	49,190,269	14.30
n-Decane	543	293.15	730.19	0.00091	128.513	84.827	2.644	0.73	0	102	69,450,567	57,421,740	16.72	68,745,562	58,198,372	16.63
n-Decane	543	298.15	726.35	0.00085	183.113	79.494	2.773	0.73	0	102	73,626,088	68,488,299	19.64	73,398,315	70,967,635	19.92
n-Decane	543	303.15	722.52	0.00079	257.205	74.585	2.902	0.73	0	102	78,730,047	83,375,957	23.54	78,517,752	87,419,009	24.14
n-Decane	543	308.15	718.70	0.00073	356.421	70.060	3.031	0.73	0	102	83,309,973	103,544,507	28.76	83,836,246	106,790,541	29.09
n-Decane	543	313.15	714.89	0.00068	487.622	65.884	3.160	0.73	0	102	89,114,591	129,967,509	35.58	89,142,617	127,508,603	34.37
n-Tetradecane	543	273.15	780.39	0.00367	0.116	110.962	0.376	0.76	0	256	49,045,710	23,710,306	7.58	50,365,325	27,433,854	8.40
n-Tetradecane	543	278.15	776.30	0.00325	0.214	103.708	0.476	0.76	0	256	50,080,602	24,092,608	7.71	50,510,738	25,082,394	7.83
n-Tetradecane	543	283.15	772.24	0.00289	0.383	96.989	0.589	0.76	0	256	51,597,418	24,723,155	7.92	51,447,425	23,683,039	7.52
n-Tetradecane	543	288.15	768.21	0.00259	0.670	90.537	0.712	0.76	0	256	53,617,641	25,738,863	8.24	53,372,875	23,665,074	7.59
n-Tetradecane	543	293.15	764.20	0.00232	1.144	84.185	0.846	0.76	0	256	56,392,345	27,303,447	8.72	56,420,516	25,383,373	8.15
n-Tetradecane	543	298.15	760.22	0.00209	1.909	77.843	0.990	0.76	0	256	60,243,007	29,976,870	9.52	60,724,778	29,095,365	9.25
n-Tetradecane	543	303.15	756.26	0.00188	3.120	71.481	1.143	0.76	0	256	65,756,800	33,717,837	10.64	66,497,523	34,930,995	10.94
n-Tetradecane	543	308.15	752.31	0.00171	4.998	65.113	1.304	0.76	0	256	73,129,817	40,541,686	12.60	74,005,987	42,847,093	13.22
n-Tetradecane	543	313.15	748.38	0.00155	7.857	58.782	1.471	0.76	0	256	85,582,696	51,926,629	15.87	83,361,448	52,577,128	16.02
n-Tetradecane	543	273.15	780.39	0.00367	0.116	110.962	0.376	0.76	0	102	49,958,330	25,116,079	8.08	50,628,502	31,422,782	9.41
n-Tetradecane	543	278.15	776.30	0.00325	0.214	103.708	0.476	0.76	0	102	50,643,248	25,282,768	8.15	50,601,790	29,053,629	8.83
n-Tetradecane	543	283.15	772.24	0.00289	0.383	96.989	0.589	0.76	0	102	52,047,999	25,674,893	8.30	51,350,515	27,574,221	8.49
n-Tetradecane	543	288.15	768.21	0.00259	0.670	90.537	0.712	0.76	0	102	53,667,320	26,498,808	8.56	53,115,428	27,427,454	8.53
n-Tetradecane	543	293.15	764.20	0.00232	1.144	84.185	0.846	0.76	0	102	56,090,267	27,951,149	9.02	56,076,138	28,974,487	9.04
n-Tetradecane	543	298.15	760.22	0.00209	1.909	77.843	0.990	0.76	0	102	59,644,946	30,298,973	9.73	60,396,918	32,468,214	10.09
n-Tetradecane	543	303.15	756.26	0.00188	3.120	71.481	1.143	0.76	0	102	64,849,319	34,189,621	10.89	66,279,694	38,021,992	11.71
n-Tetradecane	543	308.15	752.31	0.00171	4.998	65.113	1.304	0.76	0	102	71,824,826	40,775,609	12.79	73,925,537	45,568,113	13.90
n-Tetradecane	543	313.15	748.38	0.00155	7.857	58.782	1.471	0.76	0	102	83,672,010	52,367,761	16.12	83,330,458	54,819,781	16.58

Table B.3: OHC cases

Solvent	Plant Power (MW)	T (K)	ρ_L (kg/m³)	μ_L (Pa.s)	P^{vap} (Pa)	He_{CO2} (mol/m³.bar)	He_{H2} (mol/m³.bar)	Solvent cost ($/L)	Hydro-philicity	a (m⁻¹)	Calculated CAPEX ($)	Calculated OPEX ($/year)	Calculated LCOC ($/ton CO₂)	ANN prediction CAPEX ($)	ANN prediction OPEX ($/year)	ANN prediction LCOC ($/ton CO₂)
1-Hexanol	543	273.15	832.56	0.01049	11.131	128.522	2.137	0.82	0	256	58,837,578	31,021,112	9.88	59,559,462	29,876,218	9.15
1-Hexanol	543	278.15	828.96	0.00877	18.182	116.280	2.217	0.82	0	256	61,448,186	33,094,993	10.49	61,729,969	31,322,290	9.60
1-Hexanol	543	283.15	825.38	0.00738	29.107	105.683	2.295	0.82	0	256	64,309,923	35,946,566	11.31	64,078,916	33,563,473	10.25
1-Hexanol	543	288.15	821.81	0.00625	45.712	96.468	2.373	0.82	0	256	67,054,776	39,590,993	12.33	66,688,068	36,938,249	11.21
1-Hexanol	543	293.15	818.25	0.00532	70.501	88.419	2.450	0.82	0	256	70,659,612	44,499,901	13.69	69,710,279	41,826,645	12.56
1-Hexanol	543	298.15	814.69	0.00455	106.878	81.361	2.526	0.82	0	256	74,647,274	50,968,615	15.45	73,301,718	48,652,283	14.42
1-Hexanol	543	303.15	811.13	0.00392	159.397	75.147	2.602	0.82	0	256	79,265,903	59,730,923	17.81	77,486,344	57,875,922	16.90
1-Hexanol	543	308.15	807.58	0.00339	234.058	69.657	2.677	0.82	0	256	83,139,847	71,671,156	20.95	82,005,189	69,958,379	20.10
1-Hexanol	543	313.15	804.01	0.00294	338.647	64.790	2.752	0.82	0	256	88,158,459	87,697,601	25.14	86,235,890	85,249,692	24.09
1-Hexanol	543	273.15	832.56	0.01049	11.131	128.522	2.137	0.82	0	102	58,624,690	31,566,954	9.86	60,277,883	32,360,325	9.80
1-Hexanol	543	278.15	828.96	0.00877	18.182	116.280	2.217	0.82	0	102	61,109,979	33,586,475	10.46	62,583,136	34,012,659	10.30
1-Hexanol	543	283.15	825.38	0.00738	29.107	105.683	2.295	0.82	0	102	63,691,388	36,158,247	11.18	65,042,304	36,412,756	11.00
1-Hexanol	543	288.15	821.81	0.00625	45.712	96.468	2.373	0.82	0	102	66,656,940	39,738,728	12.18	67,719,011	39,889,677	11.98
1-Hexanol	543	293.15	818.25	0.00532	70.501	88.419	2.450	0.82	0	102	69,950,940	44,614,367	13.51	70,752,810	44,815,274	13.35
1-Hexanol	543	298.15	814.69	0.00455	106.878	81.361	2.526	0.82	0	102	73,832,017	50,980,385	15.24	74,291,499	51,606,635	15.20
1-Hexanol	543	303.15	811.13	0.00392	159.397	75.147	2.602	0.82	0	102	78,202,127	59,664,599	17.56	78,351,634	60,719,447	17.64
1-Hexanol	543	308.15	807.58	0.00339	234.058	69.657	2.677	0.82	0	102	81,851,310	71,500,916	20.66	82,664,116	72,609,361	20.79
1-Hexanol	543	313.15	804.01	0.00294	338.647	64.790	2.752	0.82	0	102	85,949,677	87,034,782	24.20	86,596,606	87,617,590	24.69
1-Nonanal	543	273.15	847.37	0.00189	5.418	232.353	3.626	6.62	0	256	51,603,541	33,052,254	10.00	51,787,075	33,973,147	10.36
1-Nonanal	543	278.15	842.96	0.00177	8.754	206.144	3.653	6.62	0	256	52,987,818	37,164,892	11.08	53,156,672	37,160,707	11.23
1-Nonanal	543	283.15	838.59	0.00166	13.854	183.852	3.679	6.62	0	256	54,680,505	43,029,023	12.61	54,880,271	42,189,349	12.60
1-Nonanal	543	288.15	834.25	0.00157	21.504	164.784	3.703	6.62	0	256	56,503,046	51,377,099	14.76	56,852,578	49,892,901	14.65
1-Nonanal	543	293.15	829.94	0.00148	32.768	148.388	3.727	6.62	0	256	58,564,086	63,166,286	17.79	58,929,105	61,293,284	17.64
1-Nonanal	543	298.15	825.65	0.00139	49.074	134.218	3.751	6.62	0	256	60,913,234	79,699,285	22.02	61,035,726	77,707,472	21.92

Table B.3 continued.

Solvent	Plant Power (MW)	T (K)	ρ_L (kg/m³)	μ_L (Pa.s)	P^{vap} (Pa)	He_{CO2} (mol/m³.bar)	He_{H2} (mol/m³.bar)	Solvent cost ($/L)	Hydro-philicity	a (m⁻¹)	Calculated			ANN prediction		
											CAPEX ($)	OPEX ($/year)	LCOC ($/ton CO₂)	CAPEX ($)	OPEX ($/year)	LCOC ($/ton CO₂)
1-Nonanal	543	303.15	821.38	0.00132	72.298	121.913	3.774	6.62	0	256	63,550,078	102,772,942	27.89	63,266,005	100,901,169	27.92
1-Nonanal	543	308.15	817.14	0.00125	104.873	111.180	3.796	6.62	0	256	65,812,784	135,103,994	36.07	65,843,999	133,295,381	36.28
1-Nonanal	543	313.15	812.90	0.00119	149.908	101.778	3.819	6.62	0	256	68,859,871	179,688,492	47.36	68,920,170	178,242,025	47.85
1-Nonanal	543	318.15	808.68	0.00113	211.320	93.507	3.841	6.62	0	256	72,499,605	240,710,948	62.80	72,326,309	240,369,321	63.81
1-Nonanal	543	323.15	804.46	0.00107	293.985	86.204	3.864	6.62	0	256	76,783,999	324,650,450	83.99	75,467,463	325,880,798	85.74
1-Nonanal	543	273.15	847.37	0.00189	5.418	232.353	3.626	6.62	0	102	51,258,450	33,252,961	10.04	51,541,716	37,764,401	11.31
1-Nonanal	543	278.15	842.96	0.00177	8.754	206.144	3.653	6.62	0	102	52,739,742	37,411,808	11.13	52,721,848	41,087,564	12.21
1-Nonanal	543	283.15	838.59	0.00166	13.854	183.852	3.679	6.62	0	102	54,366,675	43,371,891	12.68	54,212,509	46,123,653	13.57
1-Nonanal	543	288.15	834.25	0.00157	21.504	164.784	3.703	6.62	0	102	56,137,409	51,799,262	14.86	55,950,155	53,713,686	15.58
1-Nonanal	543	293.15	829.94	0.00148	32.768	148.388	3.727	6.62	0	102	58,206,402	63,693,262	17.91	57,858,919	64,886,958	18.51
1-Nonanal	543	298.15	825.65	0.00139	49.074	134.218	3.751	6.62	0	102	60,500,448	80,378,583	22.17	59,937,192	80,956,824	22.70
1-Nonanal	543	303.15	821.38	0.00132	72.298	121.913	3.774	6.62	0	102	63,010,907	103,565,597	28.07	62,316,366	103,659,304	28.58
1-Nonanal	543	308.15	817.14	0.00125	104.873	111.180	3.796	6.62	0	102	65,271,273	136,115,383	36.31	65,193,208	135,342,693	36.77
1-Nonanal	543	313.15	812.90	0.00119	149.908	101.778	3.819	6.62	0	102	68,167,790	180,986,188	47.66	68,626,689	179,225,060	48.08
1-Nonanal	543	318.15	808.68	0.00113	211.320	93.507	3.841	6.62	0	102	71,744,784	242,543,277	63.23	72,326,010	239,718,405	63.64
1-Nonanal	543	323.15	804.46	0.00107	293.985	86.204	3.864	6.62	0	102	75,839,786	326,678,452	84.45	75,587,027	322,706,067	84.92
1-Octanol	543	273.15	839.03	0.01746	0.670	112.286	2.037	0.82	0	256	64,755,842	33,085,450	10.45	64,288,650	34,278,757	10.43
1-Octanol	543	278.15	835.34	0.01455	1.199	101.862	2.117	0.82	0	256	67,587,227	35,019,808	11.03	67,187,988	35,839,078	10.93
1-Octanol	543	283.15	831.68	0.01220	2.093	92.807	2.196	0.82	0	256	71,278,041	37,322,580	11.73	70,252,983	37,820,574	11.56
1-Octanol	543	288.15	828.04	0.01029	3.571	84.908	2.274	0.82	0	256	75,175,920	40,437,517	12.64	73,571,174	40,363,454	12.34
1-Octanol	543	293.15	824.41	0.00873	5.963	77.989	2.351	0.82	0	256	80,056,765	44,090,144	13.72	77,344,102	43,577,446	13.31
1-Octanol	543	298.15	820.81	0.00745	9.756	71.906	2.427	0.82	0	256	85,310,125	48,483,162	14.99	81,837,489	47,530,253	14.50
1-Octanol	543	303.15	817.21	0.00639	15.654	66.539	2.503	0.82	0	256	91,258,407	54,182,218	16.62	87,257,628	52,238,766	15.91
1-Octanol	543	308.15	813.62	0.00551	24.657	61.789	2.578	0.82	0	256	96,418,670	61,554,398	18.65	93,598,207	57,667,065	17.53

Table B.3 continued.

Solvent	Plant Power (MW)	T (K)	ρ_L (kg/m³)	μ_L (Pa.s)	P^{vap} (Pa)	He_{CO2} (mol/m³.bar)	He_{H2} (mol/m³.bar)	Solvent cost ($/L)	Hydro-philicity	a (m⁻¹)	Calculated			ANN prediction		
											CAPEX ($)	OPEX ($/year)	LCOC ($/ton CO₂)	CAPEX ($)	OPEX ($/year)	LCOC ($/ton CO₂)
1-Octanol	543	273.15	839.03	0.01746	0.670	112.286	2.037	0.82	0	102	65,279,044	34,565,413	10.84	65,417,368	36,906,596	11.12
1-Octanol	543	278.15	835.34	0.01455	1.199	101.862	2.117	0.82	0	102	68,096,293	36,384,792	11.39	68,541,637	38,701,153	11.70
1-Octanol	543	283.15	831.68	0.01220	2.093	92.807	2.196	0.82	0	102	71,307,324	38,571,382	12.04	71,808,132	40,859,576	12.37
1-Octanol	543	288.15	828.04	0.01029	3.571	84.908	2.274	0.82	0	102	75,122,973	41,336,068	12.86	75,283,077	43,505,059	13.19
1-Octanol	543	293.15	824.41	0.00873	5.963	77.989	2.351	0.82	0	102	79,723,245	44,858,112	13.90	79,153,757	46,731,513	14.17
1-Octanol	543	298.15	820.81	0.00745	9.756	71.906	2.427	0.82	0	102	84,073,287	49,153,889	15.12	83,679,426	50,593,879	15.34
1-Octanol	543	303.15	817.21	0.00639	15.654	66.539	2.503	0.82	0	102	89,822,051	54,678,784	16.70	89,062,824	55,101,047	16.69
1-Octanol	543	308.15	813.62	0.00551	24.657	61.789	2.578	0.82	0	102	94,535,263	61,084,531	17.95	95,289,978	60,215,211	18.23
DES	543	273.15	981.14	0.00958	0.000	237.707	1.821	0.96	0	256	46,032,225	22,371,503	7.14	46,464,793	21,423,002	7.15
DES	543	278.15	976.66	0.00835	0.000	208.496	1.902	0.96	0	256	47,063,018	22,588,443	7.23	47,229,117	22,514,959	7.40
DES	543	283.15	972.25	0.00731	0.000	183.879	1.982	0.96	0	256	48,248,477	23,271,619	7.44	48,237,646	23,536,175	7.62
DES	543	288.15	967.88	0.00643	0.000	163.013	2.060	0.96	0	256	49,536,476	23,877,331	7.63	49,508,936	24,541,727	7.85
DES	543	293.15	963.55	0.00568	0.001	145.228	2.138	0.96	0	256	51,065,243	24,423,119	7.82	51,063,737	25,617,983	8.10
DES	543	298.15	959.26	0.00504	0.001	129.990	2.215	0.96	0	256	52,737,666	25,481,511	8.14	52,919,418	26,875,541	8.42
DES	543	303.15	955.01	0.00449	0.002	116.869	2.291	0.96	0	256	54,646,480	26,893,564	8.56	55,082,963	28,438,918	8.83
DES	543	308.15	950.80	0.00401	0.005	105.518	2.366	0.96	0	256	56,027,870	28,390,474	8.98	57,546,906	30,434,002	9.37
DES	543	313.15	946.61	0.00360	0.009	95.656	2.440	0.96	0	256	58,154,254	30,368,382	9.55	60,294,133	32,973,989	10.07
DES	543	318.15	942.45	0.00324	0.018	87.049	2.513	0.96	0	256	60,873,234	32,658,597	10.21	63,317,315	36,143,708	10.95
DES	543	323.15	938.30	0.00293	0.033	79.510	2.585	0.96	0	256	64,258,423	35,496,063	11.04	66,654,572	39,980,892	12.02
DES	543	273.15	981.14	0.00958	0.000	237.707	1.821	0.96	0	102	47,781,346	24,120,043	7.64	46,499,636	22,012,955	7.29
DES	543	278.15	976.66	0.00835	0.000	208.496	1.902	0.96	0	102	48,620,256	24,413,259	7.74	47,289,839	23,200,531	7.56
DES	543	283.15	972.25	0.00731	0.000	183.879	1.982	0.96	0	102	49,655,288	24,612,316	7.82	48,332,707	24,305,690	7.80
DES	543	288.15	967.88	0.00643	0.000	163.013	2.060	0.96	0	102	50,803,575	25,125,902	7.99	49,648,801	25,377,842	8.05
DES	543	293.15	963.55	0.00568	0.001	145.228	2.138	0.96	0	102	52,188,152	25,764,187	8.20	51,260,484	26,499,148	8.32

183

Table B.3 continued.

Solvent	Plant Power (MW)	T (K)	ρ_L (kg/m³)	μ_L (Pa.s)	P^{vap} (Pa)	He_{CO2} (mol/m³.bar)	He_{H2} (mol/m³.bar)	Solvent cost ($/L)	Hydro-philicity	a (m⁻¹)	Calculated			ANN prediction		
											CAPEX ($)	OPEX ($/year)	LCOC ($/ton CO₂)	CAPEX ($)	OPEX ($/year)	LCOC ($/ton CO₂)
DES	543	298.15	959.26	0.00504	0.001	129.990	2.215	0.96	0	102	53,680,350	26,765,950	8.50	53,185,552	27,777,282	8.64
DES	543	303.15	955.01	0.00449	0.002	116.869	2.291	0.96	0	102	55,529,284	27,925,919	8.85	55,429,534	29,334,427	9.06
DES	543	308.15	950.80	0.00401	0.005	105.518	2.366	0.96	0	102	56,629,890	29,394,185	9.25	57,981,572	31,293,566	9.60
DES	543	313.15	946.61	0.00360	0.009	95.656	2.440	0.96	0	102	58,584,820	31,354,837	9.81	60,820,275	33,762,915	10.28
DES	543	318.15	942.45	0.00324	0.018	87.049	2.513	0.96	0	102	61,209,999	33,779,399	10.50	63,935,319	36,818,486	11.14
DES	543	323.15	938.30	0.00293	0.033	79.510	2.585	0.96	0	102	64,432,152	36,438,910	11.28	67,365,317	40,483,329	12.17
DES	443	283.15	972.25	0.00731	0.000	183.879	1.982	0.96	0	256	41,666,950	18,965,920	7.53	41,901,937	19,831,649	7.32
DES	443	293.15	963.55	0.00568	0.001	145.228	2.138	0.96	0	256	44,024,824	20,193,387	8.00	42,940,954	20,758,333	7.45
DES	443	313.15	946.61	0.00360	0.009	95.656	2.440	0.96	0	256	49,831,734	24,976,213	9.71	45,281,324	25,343,507	8.37
DES	343	283.15	972.25	0.00731	0.000	183.879	1.982	0.96	0	256	34,752,435	14,829,300	7.73	35,825,763	16,420,206	7.60
DES	343	293.15	963.55	0.00568	0.001	145.228	2.138	0.96	0	256	36,640,164	15,728,455	8.18	36,851,588	16,904,691	7.69
DES	343	313.15	946.61	0.00360	0.009	95.656	2.440	0.96	0	256	41,233,489	19,374,679	9.87	40,447,519	21,921,895	8.84
DES	216	283.15	972.25	0.00731	0.000	183.879	1.982	0.96	0	256	25,277,028	9,553,512	8.13	25,922,635	11,070,407	8.49
DES	216	293.15	963.55	0.00568	0.001	145.228	2.138	0.96	0	256	26,574,891	10,098,657	8.58	26,959,527	11,012,670	8.64
DES	216	313.15	946.61	0.00360	0.009	95.656	2.440	0.96	0	256	29,625,915	12,445,473	10.31	30,495,637	15,184,602	9.97
DES	136	283.15	972.25	0.00731	0.000	183.879	1.982	0.96	0	256	18,560,595	6,166,700	8.61	18,623,867	7,149,050	9.27
DES	136	293.15	963.55	0.00568	0.001	145.228	2.138	0.96	0	256	19,450,156	6,534,551	9.10	19,483,799	6,771,462	9.48
DES	136	313.15	946.61	0.00360	0.009	95.656	2.440	0.96	0	256	21,517,724	8,002,041	10.84	21,583,834	9,739,444	10.79
DES	86	283.15	972.25	0.00731	0.000	183.879	1.982	0.96	0	256	13,749,571	4,013,069	9.23	13,938,301	4,669,879	9.82
DES	86	293.15	963.55	0.00568	0.001	145.228	2.138	0.96	0	256	14,382,166	4,251,342	9.74	14,622,956	4,152,406	10.06
DES	86	313.15	946.61	0.00360	0.009	95.656	2.440	0.96	0	256	15,801,441	5,203,352	11.55	15,481,045	6,365,443	11.33
DES	54	283.15	972.25	0.00731	0.000	183.879	1.982	0.96	0	256	10,282,270	2,637,647	10.03	11,044,908	3,164,559	10.17
DES	54	293.15	963.55	0.00568	0.001	145.228	2.138	0.96	0	256	10,740,914	2,798,615	10.59	11,597,965	2,594,404	10.44
DES	54	313.15	946.61	0.00360	0.009	95.656	2.440	0.96	0	256	11,720,066	3,405,734	12.44	11,602,249	4,393,496	11.69

Table B.3 continued.

Solvent	Plant Power (MW)	T (K)	ρ_L (kg/m³)	μ_L (Pa.s)	P^{vap} (Pa)	He_{CO2} (mol/m³.bar)	He_{H2} (mol/m³.bar)	Solvent cost ($/L)	Hydro-philicity	a (m⁻¹)	Calculated			ANN prediction		
											CAPEX ($)	OPEX ($/year)	LCOC ($/ton CO₂)	CAPEX ($)	OPEX ($/year)	LCOC ($/ton CO₂)
NBAc	543	273.15	899.97	0.00099	290.859	452.882	3.279	0.88	0	256	43,382,455	55,766,845	15.47	43,646,095	48,450,730	13.93
NBAc	543	278.15	894.89	0.00091	417.713	404.205	3.412	0.88	0	256	43,940,418	66,923,781	18.32	43,789,139	62,785,852	17.48
NBAc	543	283.15	889.84	0.00084	590.475	362.464	3.545	0.88	0	256	44,547,591	81,271,752	21.98	44,104,556	81,307,257	22.07
NBAc	543	288.15	884.82	0.00078	822.346	326.476	3.677	0.88	0	256	45,179,657	99,695,475	26.71	44,638,258	102,907,075	27.45
NBAc	543	293.15	879.82	0.00072	1129.310	295.285	3.808	0.88	0	256	45,732,362	123,273,086	32.75	45,437,190	125,966,407	33.26
NBAc	543	298.15	874.83	0.00067	1530.468	268.117	3.937	0.88	0	256	46,329,444	153,449,703	40.44	46,522,761	152,294,493	40.01
NBAc	543	303.15	869.86	0.00062	2048.384	244.341	4.066	0.88	0	256	46,367,013	191,645,378	50.15	47,876,247	188,743,820	49.44
NBAc	543	308.15	864.89	0.00058	2709.418	223.437	4.193	0.88	0	256	48,990,581	240,842,045	62.76	49,450,234	239,921,874	62.64
NBAc	543	313.15	859.93	0.00055	3544.045	204.979	4.319	0.88	0	256	51,528,160	302,214,077	78.19	51,208,232	303,609,181	79.00
NBAc	543	318.15	854.96	0.00051	4587.157	188.612	4.444	0.88	0	256	53,833,817	379,822,095	97.99	53,223,325	378,723,073	98.25
NBAc	543	323.15	850.00	0.00048	5878.340	174.038	4.568	0.88	0	256	56,403,075	476,641,200	122.72	55,751,521	472,888,859	122.42
NBAc	543	273.15	899.97	0.00099	290.859	452.882	3.279	0.88	0	102	43,134,513	55,990,920	15.52	43,654,606	49,828,121	14.26
NBAc	543	278.15	894.89	0.00091	417.713	404.205	3.412	0.88	0	102	43,714,593	67,142,358	18.36	43,808,286	64,553,066	17.91
NBAc	543	283.15	889.84	0.00084	590.475	362.464	3.545	0.88	0	102	44,301,487	81,539,651	22.04	44,139,004	83,487,021	22.60
NBAc	543	288.15	884.82	0.00078	822.346	326.476	3.677	0.88	0	102	44,987,147	99,890,313	26.71	44,694,149	105,498,610	28.09
NBAc	543	293.15	879.82	0.00072	1129.310	295.285	3.808	0.88	0	102	45,614,424	123,529,256	32.74	45,521,540	128,997,405	34.01
NBAc	543	298.15	874.83	0.00067	1530.468	268.117	3.937	0.88	0	102	46,158,475	153,769,170	40.41	46,641,043	155,861,750	40.89
NBAc	543	303.15	869.86	0.00062	2048.384	244.341	4.066	0.88	0	102	46,290,316	192,078,764	50.12	48,028,368	192,854,539	50.46
NBAc	543	308.15	864.89	0.00058	2709.418	223.437	4.193	0.88	0	102	48,859,584	241,359,194	62.66	49,627,165	244,225,754	63.70
NBAc	543	313.15	859.93	0.00055	3544.045	204.979	4.319	0.88	0	102	51,131,789	303,531,809	78.50	51,390,985	307,462,600	79.94
NBAc	543	318.15	854.96	0.00051	4587.157	188.612	4.444	0.88	0	102	53,441,094	381,423,190	98.38	53,377,238	381,541,452	98.90
NBAc	543	323.15	850.00	0.00048	5878.340	174.038	4.568	0.88	0	102	55,953,393	478,536,511	123.19	55,803,484	474,403,573	122.71
NPAc	543	273.15	908.64	0.00078	909.410	1,142.829	3.117	0.88	0	256	40,724,664	110,832,813	29.70	40,982,012	97,338,484	26.61
NPAc	543	278.15	902.75	0.00072	1281.950	994.553	3.261	0.88	0	256	40,833,340	135,825,926	36.36	40,427,816	135,706,664	36.52

Table B.3 continued.

Solvent	Plant Power (MW)	T (K)	ρ_L (kg/m³)	μ_L (Pa.s)	P^{vap} (Pa)	He_{CO2} (mol/m³.bar)	He_{H2} (mol/m³.bar)	Solvent cost ($/L)	Hydro-philicity	a (m⁻¹)	Calculated			ANN prediction		
											CAPEX ($)	OPEX ($/year)	LCOC ($/ton CO₂)	CAPEX ($)	OPEX ($/year)	LCOC ($/ton CO₂)
NPAc	543	283.15	896.93	0.00067	1777.539	869.642	3.402	0.88	0	256	40,776,955	166,638,156	44.74	40,504,274	167,782,968	45.18
NPAc	543	288.15	891.17	0.00062	2427.206	763.793	3.542	0.88	0	256	40,406,176	204,260,401	55.06	41,144,364	202,149,478	54.79
NPAc	543	293.15	885.47	0.00058	3267.303	673.594	3.679	0.88	0	256	41,542,153	250,771,586	68.15	41,987,205	248,904,681	67.75
NPAc	543	298.15	879.81	0.00055	4339.938	596.321	3.814	0.88	0	256	42,766,349	307,132,612	83.52	42,762,652	306,139,477	83.48
NPAc	543	303.15	874.19	0.00051	5693.353	529.785	3.948	0.88	0	256	43,875,447	374,887,956	101.92	43,522,417	374,680,421	102.30
NPAc	543	308.15	868.59	0.00048	7382.273	472.217	4.079	0.88	0	256	44,994,955	455,977,026	124.04	44,552,619	460,402,070	125.83
NPAc	543	313.15	863.02	0.00046	9468.198	422.181	4.208	0.88	0	256	46,166,224	552,706,628	150.59	46,067,898	564,085,620	154.31
NPAc	543	318.15	857.46	0.00043	12019.650	378.500	4.335	0.88	0	256	47,382,486	667,594,866	182.32	47,594,000	680,278,151	186.09
NPAc	543	323.15	851.91	0.00041	15112.360	340.210	4.460	0.88	0	256	48,745,669	803,668,246	220.17	48,710,151	804,500,028	219.90
NPAc	543	273.15	908.64	0.00078	909.410	1,142.829	3.117	0.88	0	102	40,539,480	111,775,351	29.94	40,958,424	97,508,570	26.64
NPAc	543	278.15	902.75	0.00072	1281.950	994.553	3.261	0.88	0	102	40,719,251	136,805,378	36.62	40,408,776	137,097,180	36.86
NPAc	543	283.15	896.93	0.00067	1777.539	869.642	3.402	0.88	0	102	40,533,835	167,739,545	45.03	40,501,315	170,860,636	45.94
NPAc	543	288.15	891.17	0.00062	2427.206	763.793	3.542	0.88	0	102	40,200,831	205,436,992	55.37	41,171,686	206,710,435	55.91
NPAc	543	293.15	885.47	0.00058	3267.303	673.594	3.679	0.88	0	102	41,243,583	252,015,858	68.49	42,043,406	253,893,168	68.97
NPAc	543	298.15	879.81	0.00055	4339.938	596.321	3.814	0.88	0	102	42,464,108	308,457,985	83.87	42,826,837	309,930,694	84.37
NPAc	543	303.15	874.19	0.00051	5693.353	529.785	3.948	0.88	0	102	43,576,713	376,342,061	102.30	43,558,847	375,320,687	102.33
NPAc	543	308.15	868.59	0.00048	7382.273	472.217	4.079	0.88	0	102	44,688,952	457,574,940	124.48	44,509,293	455,800,475	124.42
NPAc	543	313.15	863.02	0.00046	9468.198	422.181	4.208	0.88	0	102	45,839,534	554,468,053	151.06	45,880,844	553,812,700	151.25
NPAc	543	318.15	857.46	0.00043	12019.650	378.500	4.335	0.88	0	102	47,101,197	669,563,944	182.85	47,245,800	670,635,592	182.83
NPAc	543	323.15	851.91	0.00041	15112.360	340.210	4.460	0.88	0	102	48,416,832	805,897,738	220.80	48,546,892	810,015,227	219.96
TBP	543	273.15	993.70	0.00603	0.006	209.820	2.064	1.96	0	256	49,493,317	24,726,824	7.85	47,426,451	21,393,162	7.10
TBP	543	278.15	989.20	0.00531	0.011	189.025	2.152	1.96	0	256	50,479,916	25,074,215	7.97	48,232,371	22,406,870	7.33
TBP	543	283.15	984.75	0.00470	0.022	171.037	2.238	1.96	0	256	51,578,851	25,751,327	8.17	49,233,796	23,358,482	7.55
TBP	543	288.15	980.35	0.00418	0.041	155.404	2.323	1.96	0	256	53,033,106	26,394,377	8.38	50,442,664	24,291,036	7.78

Table B.3 continued.

Solvent	Plant Power (MW)	T (K)	ρ_L (kg/m^3)	μ_L (Pa.s)	P^{vap} (Pa)	He_{CO2} (mol/m^3.bar)	He_{H2} (mol/m^3.bar)	Solvent cost ($/L)	Hydro-philicity	a (m^{-1})	Calculated			ANN prediction		
											CAPEX ($)	OPEX ($/year)	LCOC ($/ton CO$_2$)	CAPEX ($)	OPEX ($/year)	LCOC ($/ton CO$_2$)
TBP	543	293.15	975.99	0.00373	0.074	141.756	2.408	1.96	0	256	54,593,669	27,382,845	8.68	51,870,057	25,274,699	8.02
TBP	543	298.15	971.68	0.00334	0.131	129.792	2.491	1.96	0	256	56,384,594	28,558,154	9.04	53,522,716	26,400,237	8.31
TBP	543	303.15	967.40	0.00300	0.228	119.261	2.573	1.96	0	256	58,388,298	30,151,237	9.50	55,399,114	27,769,807	8.67
TBP	543	308.15	963.15	0.00271	0.388	109.956	2.653	1.96	0	256	59,907,888	32,030,735	10.02	57,487,039	29,485,723	9.14
TBP	543	313.15	958.94	0.00245	0.645	101.705	2.733	1.96	0	256	61,956,488	34,412,496	10.69	59,765,850	31,637,395	9.72
TBP	543	318.15	954.76	0.00222	1.053	94.364	2.812	1.96	0	256	64,573,190	36,975,315	11.42	62,217,617	34,286,098	10.45
TBP	543	323.15	950.60	0.00203	1.685	87.810	2.889	1.96	0	256	67,692,462	40,337,465	12.36	64,850,438	37,446,087	11.32
TBP	543	273.15	993.70	0.00603	0.006	209.820	2.064	1.96	0	102	49,903,609	25,776,498	8.25	47,487,603	21,953,971	7.23
TBP	543	278.15	989.20	0.00531	0.011	189.025	2.152	1.96	0	102	50,853,390	26,278,318	8.41	48,320,481	23,041,465	7.48
TBP	543	283.15	984.75	0.00470	0.022	171.037	2.238	1.96	0	102	51,952,441	26,719,194	8.56	49,355,175	24,055,415	7.72
TBP	543	288.15	980.35	0.00418	0.041	155.404	2.323	1.96	0	102	53,144,081	27,494,192	8.79	50,603,941	25,033,103	7.95
TBP	543	293.15	975.99	0.00373	0.074	141.756	2.408	1.96	0	102	54,717,038	28,464,182	9.09	52,077,216	26,039,310	8.20
TBP	543	298.15	971.68	0.00334	0.131	129.792	2.491	1.96	0	102	56,419,965	29,593,490	9.44	53,779,632	27,159,670	8.49
TBP	543	303.15	967.40	0.00300	0.228	119.261	2.573	1.96	0	102	58,370,395	30,976,567	9.85	55,705,831	28,491,031	8.85
TBP	543	308.15	963.15	0.00271	0.388	109.956	2.653	1.96	0	102	59,632,295	32,838,530	10.37	57,838,395	30,129,467	9.30
TBP	543	313.15	958.94	0.00245	0.645	101.705	2.733	1.96	0	102	61,643,469	35,231,524	11.04	60,151,310	32,156,195	9.86
TBP	543	318.15	954.76	0.00222	1.053	94.364	2.812	1.96	0	102	64,121,478	37,762,990	11.76	62,623,143	34,621,063	10.55
TBP	543	323.15	950.60	0.00203	1.685	87.810	2.889	1.96	0	102	67,020,157	41,115,658	12.70	65,262,448	37,522,068	11.36

Table B.4: NHC cases

Solvent	Plant Power (MW)	T (K)	ρ_L (kg/m³)	μ_L (Pa.s)	P^{vap} (Pa)	He_{CO2} (mol/m³.bar)	He_{H2} (mol/m³.bar)	Solvent cost ($/L)	Hydro-philicity	a (m⁻¹)	Calculated			ANN prediction		
											CAPEX ($)	OPEX ($/year)	LCOC ($/ton CO₂)	CAPEX ($)	OPEX ($/year)	LCOC ($/ton CO₂)
DMF	543	273.15	967.69	0.00116	93.750	353.993	1.483	0.76	0	256	42,107,462	26,676,145	8.09	44,149,133	25,204,491	8.28
DMF	543	278.15	962.83	0.00108	137.970	315.426	1.552	0.76	0	256	42,477,747	28,516,920	8.56	44,105,724	28,481,224	9.10
DMF	543	283.15	958.04	0.00101	199.660	282.347	1.621	0.76	0	256	42,851,367	31,042,479	9.21	44,155,052	32,761,291	10.15
DMF	543	288.15	953.32	0.00094	284.417	253.840	1.690	0.76	0	256	43,209,254	34,422,333	10.07	44,290,215	38,432,023	11.55
DMF	543	293.15	948.65	0.00088	399.209	229.159	1.759	0.76	0	256	43,611,627	38,935,539	11.22	44,503,885	45,806,602	13.35
DMF	543	298.15	944.03	0.00083	552.599	207.698	1.828	0.76	0	256	44,072,210	44,845,326	12.72	44,790,671	54,912,129	15.57
DMF	543	303.15	939.46	0.00078	754.987	188.957	1.897	0.76	0	256	44,493,302	52,514,671	14.66	45,147,365	65,271,093	18.11
DMF	543	308.15	934.93	0.00074	1,018.860	172.526	1.967	0.76	0	256	44,510,488	62,381,175	17.13	45,569,204	75,969,351	20.73
DMF	543	313.15	930.44	0.00069	1,359.050	158.063	2.037	0.76	0	256	44,811,938	74,971,820	20.31	46,043,843	86,311,975	23.28
DMF	543	318.15	925.98	0.00066	1,792.999	145.286	2.108	0.76	0	256	45,683,938	91,347,789	24.45	46,553,607	96,689,874	25.85
DMF	543	323.15	921.55	0.00062	2,341.025	133.957	2.179	0.76	0	256	47,659,564	112,042,190	29.72	47,115,411	108,570,014	28.84
DMF	543	273.15	967.69	0.00116	93.750	353.993	1.483	0.76	0	102	41,853,708	26,730,754	8.09	44,136,034	25,789,623	8.42
DMF	543	278.15	962.83	0.00108	137.970	315.426	1.552	0.76	0	102	42,219,616	28,598,235	8.58	44,096,275	29,185,085	9.26
DMF	543	283.15	958.04	0.00101	199.660	282.347	1.621	0.76	0	102	42,573,491	31,152,585	9.23	44,148,537	33,582,849	10.35
DMF	543	288.15	953.32	0.00094	284.417	253.840	1.690	0.76	0	102	42,941,072	34,562,976	10.10	44,284,298	39,370,504	11.77
DMF	543	293.15	948.65	0.00088	399.209	229.159	1.759	0.76	0	102	43,362,319	39,070,369	11.24	44,494,037	46,873,256	13.60
DMF	543	298.15	944.03	0.00083	552.599	207.698	1.828	0.76	0	102	43,773,862	45,000,569	12.75	44,769,942	56,154,266	15.87
DMF	543	303.15	939.46	0.00078	754.987	188.957	1.897	0.76	0	102	44,177,444	52,705,600	14.69	45,106,860	66,810,237	18.47
DMF	543	308.15	934.93	0.00074	1,018.860	172.526	1.967	0.76	0	102	44,148,384	62,633,967	17.18	45,499,594	78,039,391	21.22
DMF	543	313.15	930.44	0.00069	1,359.050	158.063	2.037	0.76	0	102	44,430,974	75,333,222	20.38	45,937,812	89,261,087	23.98
DMF	543	318.15	925.98	0.00066	1,792.999	145.286	2.108	0.76	0	102	45,254,535	91,654,226	24.51	46,408,150	100,920,382	26.88
DMF	543	323.15	921.55	0.00062	2,341.025	133.957	2.179	0.76	0	102	47,241,202	112,611,578	29.84	46,932,095	114,456,428	30.28
PN	543	273.15	800.68	0.00056	1,445.571	384.991	1.797	0.78	0	256	46,044,051	104,557,009	27.98	45,925,796	104,282,572	28.24
PN	543	278.15	795.80	0.00052	1,948.970	343.136	1.885	0.78	0	256	46,735,775	125,493,016	33.35	46,467,242	124,921,820	33.74

Table B.4 continued.

Solvent	Plant Power (MW)	T (K)	ρ_L (kg/m³)	μ_L (Pa.s)	P^{sup} (Pa)	He_{CO2} (mol/m³.bar)	He_{H2} (mol/m³.bar)	Solvent cost ($/L)	Hydro-philicity	a (m⁻¹)	Calculated CAPEX ($)	Calculated OPEX ($/year)	Calculated LCOC ($/ton CO₂)	ANN prediction CAPEX ($)	ANN prediction OPEX ($/year)	ANN prediction LCOC ($/ton CO₂)
PN	543	283.15	790.88	0.00049	2,600.035	307.326	1.973	0.78	0	256	47,464,838	151,604,205	40.06	47,204,873	153,132,942	41.15
PN	543	288.15	785.92	0.00046	3,434.003	276.522	2.063	0.78	0	256	48,172,044	184,107,844	48.44	48,125,801	187,058,554	49.95
PN	543	293.15	780.92	0.00044	4,492.529	249.890	2.152	0.78	0	256	48,648,400	224,586,914	58.87	49,221,803	226,965,453	60.21
PN	543	298.15	775.87	0.00041	5,824.450	226.754	2.243	0.78	0	256	50,256,222	275,510,172	71.95	50,582,091	276,390,955	72.85
PN	543	303.15	770.77	0.00039	7,486.603	206.561	2.335	0.78	0	256	52,742,365	339,211,839	88.34	52,397,782	339,668,790	89.01
PN	543	308.15	765.61	0.00037	9,544.612	188.860	2.427	0.78	0	256	55,162,200	418,074,848	108.65	54,838,261	419,473,246	109.42
PN	543	313.15	760.38	0.00035	12,073.720	173.278	2.520	0.78	0	256	57,716,130	515,546,030	133.75	57,771,110	516,347,368	134.23
PN	543	318.15	755.08	0.00034	15,159.620	159.504	2.615	0.78	0	256	60,448,650	635,958,931	164.84	60,386,148	635,615,539	164.71
PN	543	323.15	749.71	0.00032	18,899.260	147.283	2.710	0.78	0	256	63,437,762	784,453,632	203.25	63,821,662	785,080,167	202.92
PN	543	273.15	800.68	0.00056	1,445.571	384.991	1.797	0.78	0	102	45,725,334	104,939,486	28.07	46,055,124	107,415,831	29.03
PN	543	278.15	795.80	0.00052	1,948.970	343.136	1.885	0.78	0	102	46,435,839	125,917,904	33.45	46,635,776	128,666,441	34.69
PN	543	283.15	790.88	0.00049	2,600.035	307.326	1.973	0.78	0	102	47,183,692	152,065,715	40.17	47,419,202	157,168,581	42.18
PN	543	288.15	785.92	0.00046	3,434.003	276.522	2.063	0.78	0	102	47,830,528	184,749,519	48.60	48,391,872	190,753,162	50.89
PN	543	293.15	780.92	0.00044	4,492.529	249.890	2.152	0.78	0	102	48,307,675	225,405,732	59.07	49,542,409	229,534,634	60.86
PN	543	298.15	775.87	0.00041	5,824.450	226.754	2.243	0.78	0	102	49,877,491	276,022,223	72.07	50,946,482	276,903,470	72.96
PN	543	303.15	770.77	0.00039	7,486.603	206.561	2.335	0.78	0	102	52,357,476	338,922,291	88.25	52,763,505	336,934,125	88.27
PN	543	308.15	765.61	0.00037	9,544.612	188.860	2.427	0.78	0	102	54,778,511	416,784,076	108.32	55,108,290	412,290,853	107.52
PN	543	313.15	760.38	0.00035	12,073.720	173.278	2.520	0.78	0	102	57,270,332	513,231,979	133.17	57,767,293	505,094,898	131.22
PN	543	318.15	755.08	0.00034	15,159.620	159.504	2.615	0.78	0	102	60,036,050	632,280,512	163.92	59,863,212	624,713,371	161.68
PN	543	323.15	749.71	0.00032	18,899.260	147.283	2.710	0.78	0	102	62,969,342	779,205,521	201.89	62,602,302	781,245,206	201.54

Table B.5: CycHC cases

Solvent	Plant Power (MW)	T (K)	ρ_L (kg/m³)	μ_L (Pa.s)	P^{vap} (Pa)	He_{CO2} (mol/m³.bar)	He_{H2} (mol/m³.bar)	Solvent cost ($/L)	Hydro-philicity	a (m⁻¹)	Calculated CAPEX ($)	Calculated OPEX ($/year)	Calculated LCOC ($/ton CO₂)	ANN prediction CAPEX ($)	ANN prediction OPEX ($/year)	ANN prediction LCOC ($/ton CO₂)
cis-Decalin	543	273.15	914.48	0.00528	16.337	73.102	1.914	0.45	0	256	72,719,820	41,496,599	12.83	74,624,938	45,559,469	13.62
cis-Decalin	543	278.15	910.25	0.00468	24.638	67.369	2.003	0.45	0	256	77,505,605	45,200,617	13.91	79,312,997	49,108,656	14.67
cis-Decalin	543	283.15	906.06	0.00417	36.532	62.316	2.091	0.45	0	256	82,903,994	50,075,610	15.31	84,239,108	53,142,782	15.85
cis-Decalin	543	288.15	901.91	0.00373	53.308	57.846	2.179	0.45	0	256	89,038,043	55,924,764	16.98	89,287,994	57,857,418	17.21
cis-Decalin	543	293.15	897.79	0.00335	76.618	53.876	2.266	0.45	0	256	96,012,737	63,390,544	19.09	94,367,845	63,478,392	18.81
cis-Decalin	543	298.15	893.69	0.00302	108.556	50.337	2.351	0.45	0	256	103,928,754	72,512,922	21.64	99,443,015	70,258,958	20.70
cis-Decalin	543	273.15	914.48	0.00528	16.337	73.102	1.914	0.45	0	102	77,892,479	47,075,793	14.40	76,550,470	47,653,371	14.21
cis-Decalin	543	278.15	910.25	0.00468	24.638	67.369	2.003	0.45	0	102	81,865,506	50,547,402	15.40	81,654,635	51,507,509	15.35
cis-Decalin	543	283.15	906.06	0.00417	36.532	62.316	2.091	0.45	0	102	86,791,368	54,948,011	16.66	87,021,289	55,851,704	16.62
cis-Decalin	543	288.15	901.91	0.00373	53.308	57.846	2.179	0.45	0	102	92,157,762	60,607,206	18.26	92,512,907	60,870,140	18.08
cis-Decalin	543	293.15	897.79	0.00335	76.618	53.876	2.266	0.45	0	102	98,391,766	67,814,496	20.28	98,010,830	66,773,644	19.76
Cyclohexanone	543	273.15	963.89	0.00368	126.292	308.971	0.079	0.94	0	256	42,362,586	33,063,589	9.70	43,173,659	33,441,028	10.54
Cyclohexanone	543	278.15	959.50	0.00325	179.894	274.833	0.213	0.94	0	256	43,002,016	36,934,472	10.70	43,128,288	35,961,006	11.16
Cyclohexanone	543	283.15	955.14	0.00288	252.590	246.742	0.424	0.94	0	256	43,644,591	41,935,392	11.97	43,278,991	38,927,245	11.87
Cyclohexanone	543	288.15	950.80	0.00256	349.880	223.457	0.737	0.94	0	256	44,344,268	48,415,538	13.63	43,660,752	43,102,652	12.84
Cyclohexanone	543	293.15	946.49	0.00228	478.462	204.030	1.152	0.94	0	256	45,047,038	56,788,765	15.76	44,268,285	49,749,184	14.39
Cyclohexanone	543	298.15	942.20	0.00205	646.394	187.728	1.646	0.94	0	256	45,798,118	67,465,732	18.46	45,047,599	60,486,878	16.93
Cyclohexanone	543	303.15	937.93	0.00184	863.276	173.980	2.166	0.94	0	256	46,368,588	80,901,525	21.86	45,910,474	76,758,580	20.84
Cyclohexanone	543	308.15	933.68	0.00166	1,140.420	162.335	2.642	0.94	0	256	46,374,027	97,558,644	26.04	46,767,526	98,856,065	26.24
Cyclohexanone	543	313.15	929.45	0.00151	1,491.027	152.437	3.001	0.94	0	256	46,394,268	117,884,638	31.15	47,557,717	124,916,107	32.70
Cyclohexanone	543	318.15	925.23	0.00137	1,930.372	143.999	3.190	0.94	0	256	47,672,266	142,901,258	37.49	48,231,886	150,148,182	39.07
Cyclohexanone	543	323.15	921.02	0.00125	2,475.967	136.791	3.185	0.94	0	256	48,562,806	172,427,478	44.95	48,680,824	166,974,765	43.41
Cyclohexanone	543	273.15	963.89	0.00368	126.292	308.971	0.079	0.94	0	102	42,422,033	33,636,481	9.85	43,162,103	34,158,726	10.71
Cyclohexanone	543	278.15	959.50	0.00325	179.894	274.833	0.213	0.94	0	102	42,992,984	37,541,194	10.85	43,118,174	36,798,431	11.36

Table B.5 continued.

Solvent	Plant Power (MW)	T (K)	ρ_L (kg/m³)	μ_L (Pa.s)	P^{vap} (Pa)	He_{CO2} (mol/m³.bar)	He_{H2} (mol/m³.bar)	Solvent cost ($/L)	Hydro-philicity	a (m⁻¹)	Calculated CAPEX ($)	Calculated OPEX ($/year)	Calculated LCOC ($/ton CO₂)	ANN prediction CAPEX ($)	ANN prediction OPEX ($/year)	ANN prediction LCOC ($/ton CO₂)
Cyclohexanone	543	283.15	955.14	0.00288	252.590	246.742	0.424	0.94	0	102	43,629,220	42,600,671	12.14	43,269,324	39,874,853	12.09
Cyclohexanone	543	288.15	950.80	0.00256	349.880	223.457	0.737	0.94	0	102	44,314,619	49,199,339	13.82	43,650,864	44,159,592	13.09
Cyclohexanone	543	293.15	946.49	0.00228	478.462	204.030	1.152	0.94	0	102	45,026,184	57,722,363	15.99	44,258,398	50,939,653	14.67
Cyclohexanone	543	298.15	942.20	0.00205	646.394	187.728	1.646	0.94	0	102	45,718,234	68,544,554	18.73	45,038,822	61,890,110	17.26
Cyclohexanone	543	303.15	937.93	0.00184	863.276	173.980	2.166	0.94	0	102	46,306,046	82,159,132	22.17	45,903,453	78,562,842	21.27
Cyclohexanone	543	308.15	933.68	0.00166	1,140.420	162.335	2.642	0.94	0	102	46,302,727	99,080,494	26.42	46,759,191	101,425,330	26.86
Cyclohexanone	543	313.15	929.45	0.00151	1,491.027	152.437	3.001	0.94	0	102	46,259,046	119,684,059	31.60	47,537,038	128,776,427	33.65
Cyclohexanone	543	318.15	925.23	0.00137	1,930.372	143.999	3.190	0.94	0	102	47,418,609	144,937,783	37.99	48,177,552	155,768,952	40.45
Cyclohexanone	543	323.15	921.02	0.00125	2,475.967	136.791	3.185	0.94	0	102	48,227,075	174,772,689	45.52	48,562,683	174,522,842	45.27
MNPh	543	273.15	1,041.49	0.00618	1.013	95.766	0.883	1.02	0	256	53,786,215	27,018,411	8.56	54,777,602	27,041,788	8.59
MNPh	543	278.15	1,037.04	0.00518	1.641	87.334	0.943	1.02	0	256	55,527,004	27,709,901	8.79	56,170,835	28,664,944	9.02
MNPh	543	283.15	1,032.63	0.00441	2.607	79.965	1.003	1.02	0	256	57,101,288	28,602,909	9.07	57,721,162	30,191,641	9.44
MNPh	543	288.15	1,028.27	0.00380	4.066	73.498	1.063	1.02	0	256	59,041,429	29,717,113	9.42	59,423,328	31,664,687	9.85
MNPh	543	293.15	1,023.96	0.00331	6.229	67.797	1.122	1.02	0	256	61,192,470	31,093,696	9.83	61,270,958	33,158,158	10.26
MNPh	543	298.15	1,019.68	0.00291	9.387	62.752	1.182	1.02	0	256	63,529,658	32,831,692	10.34	63,259,861	34,775,115	10.72
MNPh	543	303.15	1,015.45	0.00259	13.924	58.272	1.241	1.02	0	256	65,939,080	34,987,716	10.97	65,394,106	36,642,831	11.25
MNPh	543	308.15	1,011.25	0.00231	20.349	54.278	1.301	1.02	0	256	67,836,970	37,809,890	11.74	67,694,498	38,905,463	11.88
MNPh	543	313.15	1,007.08	0.00209	29.321	50.706	1.360	1.02	0	256	70,262,064	41,372,285	12.71	70,210,982	41,714,188	12.66
MNPh	543	318.15	1,002.95	0.00189	41.684	47.501	1.419	1.02	0	256	73,424,316	45,802,439	13.93	73,037,769	45,212,416	13.63
MNPh	543	323.15	998.85	0.00173	58.507	44.617	1.477	1.02	0	256	77,205,817	51,291,430	15.43	76,335,980	49,515,062	14.82
MNPh	543	273.15	1,041.49	0.00618	1.013	95.766	0.883	1.02	0	102	56,581,814	29,721,977	9.33	55,037,456	27,391,408	8.68
MNPh	543	278.15	1,037.04	0.00518	1.641	87.334	0.943	1.02	0	102	57,506,289	29,956,965	9.42	56,490,579	29,036,259	9.12
MNPh	543	283.15	1,032.63	0.00441	2.607	79.965	1.003	1.02	0	102	58,677,798	30,499,705	9.60	58,105,663	30,571,130	9.54
MNPh	543	288.15	1,028.27	0.00380	4.066	73.498	1.063	1.02	0	102	60,210,161	31,345,809	9.86	59,874,727	32,032,183	9.94

Table B.5 continued.

Solvent	Plant Power (MW)	T (K)	ρ_L (kg/m³)	μ_L (Pa.s)	P^{vap} (Pa)	He_{CO2} (mol/m³.bar)	He_{H2} (mol/m³.bar)	Solvent cost ($/L)	Hydro-philicity	a (m⁻¹)	Calculated CAPEX ($)	OPEX ($/year)	LCOC ($/ton CO₂)	ANN prediction CAPEX ($)	OPEX ($/year)	LCOC ($/ton CO₂)
MNPh	543	293.15	1,023.96	0.00331	6.229	67.797	1.122	1.02	0	102	62,051,392	32,515,461	10.22	61,786,966	33,485,739	10.36
MNPh	543	298.15	1,019.68	0.00291	9.387	62.752	1.182	1.02	0	102	64,129,916	34,099,223	10.68	63,831,908	35,026,035	10.80
MNPh	543	303.15	1,015.45	0.00259	13.924	58.272	1.241	1.02	0	102	66,476,191	36,121,150	11.27	66,005,584	36,770,250	11.29
MNPh	543	308.15	1,011.25	0.00231	20.349	54.278	1.301	1.02	0	102	67,894,608	38,871,351	12.00	68,319,670	38,851,321	11.88
MNPh	543	313.15	1,007.08	0.00209	29.321	50.706	1.360	1.02	0	102	70,099,947	42,385,081	12.96	70,814,883	41,408,051	12.60
MNPh	543	318.15	1,002.95	0.00189	41.684	47.501	1.419	1.02	0	102	73,002,598	46,743,252	14.15	73,577,489	44,571,164	13.49
MNPh	543	323.15	998.85	0.00173	58.507	44.617	1.477	1.02	0	102	76,520,861	52,212,120	15.64	76,762,715	48,443,510	14.57
NMP	543	273.15	1,052.25	0.00262	5.976	358.203	1.203	2.00	1	256	47,727,165	34,138,749	10.16	48,150,582	35,685,786	10.84
NMP	543	278.15	1,047.59	0.00238	9.326	310.900	1.252	2.00	1	256	48,644,222	41,073,312	11.93	49,065,633	40,869,837	12.06
NMP	543	283.15	1,042.98	0.00217	14.291	270.534	1.303	2.00	1	256	49,561,198	49,688,948	14.12	50,032,108	48,236,792	13.81
NMP	543	288.15	1,038.41	0.00198	21.526	236.097	1.355	2.00	1	256	50,576,695	59,394,277	16.59	51,018,563	57,816,655	16.12
NMP	543	293.15	1,033.87	0.00182	31.901	206.716	1.408	2.00	1	256	51,603,656	70,407,496	19.39	51,994,151	69,559,506	18.98
NMP	543	298.15	1,029.37	0.00167	46.554	181.641	1.463	2.00	1	256	53,039,327	83,553,221	22.74	52,944,119	83,410,236	22.41
NMP	543	303.15	1,024.89	0.00154	66.955	160.228	1.520	2.00	1	256	54,454,062	98,440,126	26.52	53,883,721	99,375,658	26.41
NMP	543	308.15	1,020.44	0.00143	94.977	141.928	1.578	2.00	1	256	55,121,347	115,771,688	30.89	54,879,542	117,558,729	31.02
NMP	543	313.15	1,016.02	0.00132	132.978	126.275	1.639	2.00	1	256	56,080,966	135,984,231	36.00	56,089,877	138,151,794	36.31
NMP	543	318.15	1,011.61	0.00123	183.888	112.873	1.701	2.00	1	256	57,910,400	160,044,333	42.10	57,833,267	161,404,343	42.36
NMP	543	323.15	1,007.22	0.00115	251.312	101.388	1.765	2.00	1	256	60,713,849	187,949,496	49.19	60,687,772	187,593,918	49.27
NMP	543	273.15	1,052.25	0.00262	5.976	358.203	1.203	2.00	1	102	47,462,934	34,508,355	10.24	48,023,016	36,064,158	10.93
NMP	543	278.15	1,047.59	0.00238	9.326	310.900	1.252	2.00	1	102	48,292,885	41,664,264	12.06	48,942,062	41,188,516	12.13
NMP	543	283.15	1,042.98	0.00217	14.291	270.534	1.303	2.00	1	102	49,200,744	50,104,332	14.21	49,909,526	48,491,934	13.87
NMP	543	288.15	1,038.41	0.00198	21.526	236.097	1.355	2.00	1	102	50,240,331	59,973,862	16.72	50,893,274	57,982,865	16.15
NMP	543	293.15	1,033.87	0.00182	31.901	206.716	1.408	2.00	1	102	51,337,822	71,485,986	19.65	51,864,042	69,587,861	18.98
NMP	543	298.15	1,029.37	0.00167	46.554	181.641	1.463	2.00	1	102	52,627,345	84,465,020	22.95	52,812,134	83,228,181	22.36

Table B.5 continued.

Solvent	Plant Power (MW)	T (K)	ρ_L (kg/m³)	μ_L (Pa.s)	P^{vap} (Pa)	He_{CO2} (mol/m³.bar)	He_{H2} (mol/m³.bar)	Solvent cost ($/L)	Hydro-philicity	a (m⁻¹)	Calculated			ANN prediction		
											CAPEX ($)	OPEX ($/year)	LCOC ($/ton CO₂)	CAPEX ($)	OPEX ($/year)	LCOC ($/ton CO₂)
NMP	543	303.15	1,024.89	0.00154	66.955	160.228	1.520	2.00	1	102	54,002,983	99,372,182	26.74	53,763,388	98,885,345	26.29
NMP	543	308.15	1,020.44	0.00143	94.977	141.928	1.578	2.00	1	102	54,654,089	116,833,247	31.14	54,804,223	116,631,131	30.80
NMP	543	313.15	1,016.02	0.00132	132.978	126.275	1.639	2.00	1	102	55,740,376	137,396,700	36.34	56,127,119	136,616,072	35.95
NMP	543	318.15	1,011.61	0.00123	183.888	112.873	1.701	2.00	1	102	57,313,146	161,375,363	42.41	58,103,736	159,035,383	41.81
NMP	543	323.15	1,007.22	0.00115	251.312	101.388	1.765	2.00	1	102	59,246,700	189,442,950	49.52	61,384,455	184,106,058	48.46
PC	543	273.15	1,223.42	0.00399	0.980	273.923	1.571	0.60	1	256	48,553,681	41,321,939	11.98	48,735,303	41,178,117	11.91
PC	543	278.15	1,218.22	0.00361	1.586	243.826	1.644	0.60	1	256	49,422,274	43,528,663	12.56	49,780,783	42,757,824	12.20
PC	543	283.15	1,213.08	0.00327	2.516	218.508	1.715	0.60	1	256	50,235,201	46,098,890	13.23	50,815,699	45,367,266	12.74
PC	543	288.15	1,208.00	0.00297	3.920	197.074	1.785	0.60	1	256	51,103,525	48,511,813	13.86	51,780,226	48,666,662	13.47
PC	543	293.15	1,202.96	0.00271	6.002	178.819	1.854	0.60	1	256	51,983,049	50,927,523	14.50	52,601,469	52,283,466	14.30
PC	543	298.15	1,197.97	0.00248	9.041	163.185	1.923	0.60	1	256	52,800,144	53,308,415	15.12	53,194,541	55,833,121	15.11
PC	543	303.15	1,193.03	0.00228	13.407	149.728	1.989	0.60	1	256	53,495,916	55,440,126	15.68	53,476,276	58,946,045	15.84
PC	543	308.15	1,188.12	0.00210	19.590	138.088	2.055	0.60	1	256	53,185,246	57,788,235	16.26	53,402,340	61,315,127	16.40
PC	543	313.15	1,183.25	0.00193	28.227	127.975	2.120	0.60	1	256	52,980,920	59,791,481	16.75	53,037,193	62,773,397	16.76
PC	543	318.15	1,178.41	0.00179	40.136	119.153	2.184	0.60	1	256	52,910,283	61,508,657	17.18	52,658,893	63,431,532	16.96
PC	543	323.15	1,173.60	0.00166	56.354	111.427	2.247	0.60	1	256	52,866,973	62,706,336	17.48	52,889,914	63,856,179	17.15
PC	543	273.15	1,223.42	0.00399	0.980	273.923	1.571	0.60	1	102	48,632,844	42,307,419	12.23	48,097,405	42,532,661	12.24
PC	543	278.15	1,218.22	0.00361	1.586	243.826	1.644	0.60	1	102	49,479,802	44,873,002	12.90	49,077,866	44,199,167	12.55
PC	543	283.15	1,213.08	0.00327	2.516	218.508	1.715	0.60	1	102	50,399,958	47,295,008	13.54	50,037,951	46,911,942	13.13
PC	543	288.15	1,208.00	0.00297	3.920	197.074	1.785	0.60	1	102	51,175,660	49,601,887	14.14	50,922,327	50,328,307	13.90
PC	543	293.15	1,202.96	0.00271	6.002	178.819	1.854	0.60	1	102	52,109,655	52,094,604	14.80	51,669,003	54,060,788	14.76
PC	543	298.15	1,197.97	0.00248	9.041	163.185	1.923	0.60	1	102	52,961,849	54,541,377	15.44	52,215,790	57,691,462	15.61
PC	543	303.15	1,193.03	0.00228	13.407	149.728	1.989	0.60	1	102	53,703,555	56,923,663	16.06	52,521,688	60,794,918	16.35
PC	543	308.15	1,188.12	0.00210	19.590	138.088	2.055	0.60	1	102	53,307,017	59,147,998	16.60	52,612,649	62,990,194	16.89

Table B.5 continued.

Solvent	Plant Power (MW)	T (K)	ρ_L (kg/m³)	μ_L (Pa.s)	P^{vap} (Pa)	He_{CO2} (mol/m³.bar)	He_{H2} (mol/m³.bar)	Solvent cost ($/L)	Hydro-philicity	a (m⁻¹)	Calculated			ANN prediction		
											CAPEX ($)	OPEX ($/year)	LCOC ($/ton CO₂)	CAPEX ($)	OPEX ($/year)	LCOC ($/ton CO₂)
PC	543	313.15	1,183.25	0.00193	28.227	127.975	2.120	0.60	1	102	53,095,382	61,190,835	17.11	52,657,325	64,044,923	17.17
PC	543	318.15	1,178.41	0.00179	40.136	119.153	2.184	0.60	1	102	53,021,122	63,076,313	17.58	53,068,514	64,065,652	17.25
PC	543	323.15	1,173.60	0.00166	56.354	111.427	2.247	0.60	1	102	52,913,560	64,233,819	17.87	54,613,205	63,759,364	17.32

Table B.6: Polymer cases

Solvent	Plant Power (MW)	T (K)	ρ_L (kg/m³)	μ_L (Pa.s)	P^{vap} (Pa)	He_{CO2} (mol/m³.bar)	He_{H2} (mol/m³.bar)	Solvent cost ($/L)	Hydro-philicity	a (m⁻¹)	Calculated			ANN prediction		
											CAPEX ($)	OPEX ($/year)	LCOC ($/ton CO₂)	CAPEX ($)	OPEX ($/year)	LCOC ($/ton CO₂)
PEGDME	543	273.15	1,079.08	0.01539	0.002	231.197	4.225	4.00	0	256	47,786,621	22,972,521	7.35	47,423,965	23,997,792	7.78
PEGDME	543	278.15	1,073.14	0.01269	0.005	200.962	3.186	4.00	0	256	48,293,314	22,924,989	7.35	48,428,972	22,024,823	7.33
PEGDME	543	283.15	1,067.21	0.01057	0.010	176.035	2.459	4.00	0	256	48,859,746	22,912,996	7.37	49,281,404	21,272,826	7.18
PEGDME	543	288.15	1,061.30	0.00891	0.021	155.323	1.938	4.00	0	256	49,411,958	22,979,973	7.41	49,932,779	21,463,938	7.26
PEGDME	543	293.15	1,055.39	0.00758	0.043	137.983	1.555	4.00	0	256	50,034,843	23,142,688	7.47	50,418,526	22,214,568	7.48
PEGDME	543	298.15	1,049.49	0.00651	0.084	123.368	1.267	4.00	0	256	50,806,790	23,349,831	7.54	50,781,033	23,231,573	7.76
PEGDME	543	303.15	1,043.58	0.00564	0.160	110.971	1.047	4.00	0	256	51,576,777	23,644,849	7.64	51,054,498	24,346,108	8.06
PEGDME	543	308.15	1,037.66	0.00493	0.298	100.391	0.875	4.00	0	256	51,536,316	24,118,235	7.76	51,263,494	25,471,077	8.36
PEGDME	543	313.15	1,031.74	0.00434	0.540	91.314	0.739	4.00	0	256	51,767,793	24,727,034	7.92	51,417,831	26,540,484	8.65
PEGDME	543	318.15	1,025.80	0.00385	0.955	83.485	0.629	4.00	0	256	52,267,887	25,503,100	8.13	51,498,893	27,452,569	8.89
PEGDME	543	323.15	1,019.83	0.00344	1.632	76.701	0.538	4.00	0	256	53,018,264	26,482,285	8.40	51,440,205	28,022,523	9.05
PEGDME	543	273.15	1,079.08	0.01539	0.002	231.197	4.225	4.00	0	102	47,274,219	23,002,977	7.34	47,412,776	24,376,827	7.86
PEGDME	543	278.15	1,073.14	0.01269	0.005	200.962	3.186	4.00	0	102	47,794,904	22,949,799	7.34	48,383,728	22,292,904	7.37
PEGDME	543	283.15	1,067.21	0.01057	0.010	176.035	2.459	4.00	0	102	48,307,557	22,947,501	7.36	49,200,731	21,375,447	7.18
PEGDME	543	288.15	1,061.30	0.00891	0.021	155.323	1.938	4.00	0	102	48,847,556	23,024,902	7.40	49,813,137	21,349,741	7.21
PEGDME	543	293.15	1,055.39	0.00758	0.043	137.983	1.555	4.00	0	102	49,547,251	23,140,526	7.45	50,251,275	21,840,973	7.37
PEGDME	543	298.15	1,049.49	0.00651	0.084	123.368	1.267	4.00	0	102	50,176,450	23,371,541	7.53	50,551,014	22,563,337	7.57
PEGDME	543	303.15	1,043.58	0.00564	0.160	110.971	1.047	4.00	0	102	50,876,269	23,640,712	7.62	50,739,442	23,354,188	7.79
PEGDME	543	308.15	1,037.66	0.00493	0.298	100.391	0.875	4.00	0	102	50,731,987	24,105,104	7.73	50,834,338	24,135,033	8.00
PEGDME	543	313.15	1,031.74	0.00434	0.540	91.314	0.739	4.00	0	102	50,950,028	24,684,699	7.88	50,840,105	24,854,166	8.19
PEGDME	543	318.15	1,025.80	0.00385	0.955	83.485	0.629	4.00	0	102	51,403,120	25,449,765	8.09	50,735,263	25,431,664	8.34
PEGDME	543	323.15	1,019.83	0.00344	1.632	76.701	0.538	4.00	0	102	52,106,075	26,406,616	8.35	50,454,023	25,711,597	8.42
PEGPDMS-1	543	273.15	957.82	0.00946	1.013×10^{-5}	245.531	2.610	4.00	0	256	46,607,755	22,337,904	7.15	47,143,858	21,904,546	7.12
PEGPDMS-1	543	278.15	953.09	0.00821	1.013×10^{-5}	219.105	2.721	4.00	0	256	47,654,340	22,785,331	7.30	47,985,927	22,492,998	7.23

Table B.6 continued.

Solvent	Plant Power (MW)	T (K)	ρ_L (kg/m³)	μ_L (Pa.s)	P^{vap} (Pa)	He_{CO2} (mol/m³.bar)	He_{H2} (mol/m³.bar)	Solvent cost ($/L)	Hydro-philicity	a (m⁻¹)	Calculated			ANN prediction		
											CAPEX ($)	OPEX ($/year)	LCOC ($/ton CO₂)	CAPEX ($)	OPEX ($/year)	LCOC ($/ton CO₂)
PEGPDMS-1	543	283.15	948.42	0.00717	1.013×10^{-5}	196.440	2.829	4.00	0	256	48,691,741	23,332,907	7.47	49,008,421	23,038,455	7.33
PEGPDMS-1	543	288.15	943.79	0.00628	1.013×10^{-5}	176.903	2.936	4.00	0	256	50,014,445	23,814,303	7.63	50,216,156	23,631,494	7.45
PEGPDMS-1	543	293.15	939.22	0.00554	1.013×10^{-5}	159.982	3.040	4.00	0	256	51,436,659	24,609,170	7.88	51,603,510	24,391,326	7.64
PEGPDMS-1	543	298.15	934.69	0.00489	1.013×10^{-5}	145.260	3.143	4.00	0	256	53,099,519	25,563,980	8.18	53,144,519	25,456,090	7.91
PEGPDMS-1	543	303.15	930.19	0.00434	1.013×10^{-5}	132.396	3.243	4.00	0	256	54,699,180	26,691,379	8.51	54,790,539	26,971,859	8.31
PEGPDMS-1	543	308.15	925.73	0.00386	1.013×10^{-5}	121.110	3.341	4.00	0	256	56,316,725	28,278,720	8.96	56,490,789	29,080,819	8.88
PEGPDMS-1	543	313.15	921.31	0.00344	1.013×10^{-5}	111.171	3.436	4.00	0	256	58,277,452	30,121,872	9.49	58,250,174	31,907,726	9.65
PEGPDMS-1	543	318.15	916.91	0.00307	1.013×10^{-5}	102.384	3.530	4.00	0	256	60,994,333	32,279,463	10.12	60,220,944	35,541,232	10.64
PEGPDMS-1	543	323.15	912.53	0.00275	1.013×10^{-5}	94.590	3.622	4.00	0	256	63,927,920	35,161,595	10.94	62,787,169	40,001,098	11.87
PEGPDMS-1	543	273.15	957.82	0.00946	1.013×10^{-5}	245.531	2.610	4.00	0	102	47,550,983	23,808,774	7.67	47,197,995	22,627,899	7.29
PEGPDMS-1	543	278.15	953.09	0.00821	1.013×10^{-5}	219.105	2.721	4.00	0	102	48,734,473	24,110,213	7.67	48,057,283	23,308,552	7.42
PEGPDMS-1	543	283.15	948.42	0.00717	1.013×10^{-5}	196.440	2.829	4.00	0	102	49,667,052	24,184,768	7.72	49,098,251	23,928,734	7.54
PEGPDMS-1	543	288.15	943.79	0.00628	1.013×10^{-5}	176.903	2.936	4.00	0	102	50,822,490	24,766,118	7.90	50,323,617	24,573,363	7.68
PEGPDMS-1	543	293.15	939.22	0.00554	1.013×10^{-5}	159.982	3.040	4.00	0	102	52,195,153	25,476,815	8.12	51,724,080	25,357,297	7.87
PEGPDMS-1	543	298.15	934.69	0.00489	1.013×10^{-5}	145.260	3.143	4.00	0	102	53,853,784	26,362,811	8.40	53,268,913	26,415,319	8.15
PEGPDMS-1	543	303.15	930.19	0.00434	1.013×10^{-5}	132.396	3.243	4.00	0	102	55,362,918	27,442,266	8.72	54,906,197	27,890,300	8.54
PEGPDMS-1	543	308.15	925.73	0.00386	1.013×10^{-5}	121.110	3.341	4.00	0	102	56,285,335	29,020,832	9.15	56,588,843	29,920,055	9.09
PEGPDMS-1	543	313.15	921.31	0.00344	1.013×10^{-5}	111.171	3.436	4.00	0	102	58,052,994	30,823,014	9.66	58,339,431	32,621,793	9.83
PEGPDMS-1	543	318.15	916.91	0.00307	1.013×10^{-5}	102.384	3.530	4.00	0	102	60,547,441	33,146,198	10.32	60,344,962	36,070,189	10.78
PEGPDMS-1	543	323.15	912.53	0.00275	1.013×10^{-5}	94.590	3.622	4.00	0	102	63,504,911	35,809,993	11.09	63,032,139	40,259,515	11.96
PEGPDMS-1	443	283.15	948.42	0.00717	1.013×10^{-5}	196.440	2.829	4.00	0	256	41,682,612	18,961,689	7.66	42,008,716	21,823,106	7.81
PEGPDMS-1	443	293.15	939.22	0.00554	1.013×10^{-5}	159.982	3.040	4.00	0	256	43,979,903	20,108,542	8.11	43,812,767	23,969,636	8.21
PEGPDMS-1	443	313.15	921.31	0.00344	1.013×10^{-5}	111.171	3.436	4.00	0	256	49,497,140	24,766,008	9.79	48,395,759	32,845,488	10.20
PEGPDMS-1	343	283.15	948.42	0.00717	1.013×10^{-5}	196.440	2.829	4.00	0	256	34,686,327	14,831,748	7.86	35,052,754	16,733,987	7.95

Table B.6 continued.

Solvent	Plant Power (MW)	T (K)	ρ_L (kg/m^3)	μ_L (Pa.s)	P^{vap} (Pa)	He_{CO2} (mol/m^3.bar)	He_{H2} (mol/m^3.bar)	Solvent cost ($/L)	Hydro-philicity	a (m^{-1})	Calculated CAPEX ($)	OPEX ($/year)	LCOC ($/ton CO$_2$)	ANN prediction CAPEX ($)	OPEX ($/year)	LCOC ($/ton CO$_2$)
PEGPDMS-1	343	293.15	939.22	0.00554	1.013×10^{-5}	159.982	3.040	4.00	0	256	36,531,525	15,790,188	8.35	36,919,270	18,156,443	8.25
PEGPDMS-1	343	313.15	921.31	0.00344	1.013×10^{-5}	111.171	3.436	4.00	0	256	40,794,624	19,225,621	9.95	42,660,243	26,296,439	10.11
PEGPDMS-1	216	283.15	948.42	0.00717	1.013×10^{-5}	196.440	2.829	4.00	0	256	25,146,175	9,534,469	8.26	24,667,018	10,126,697	8.73
PEGPDMS-1	216	293.15	939.22	0.00554	1.013×10^{-5}	159.982	3.040	4.00	0	256	26,386,338	10,069,993	8.71	26,220,555	10,508,173	8.96
PEGPDMS-1	216	313.15	921.31	0.00344	1.013×10^{-5}	111.171	3.436	4.00	0	256	29,208,310	12,305,814	10.38	30,528,611	15,677,478	10.41
PEGPDMS-1	136	283.15	948.42	0.00717	1.013×10^{-5}	196.440	2.829	4.00	0	256	18,427,483	6,149,332	8.76	17,732,597	6,209,239	9.47
PEGPDMS-1	136	293.15	939.22	0.00554	1.013×10^{-5}	159.982	3.040	4.00	0	256	19,279,423	6,507,606	9.24	18,907,469	6,156,446	9.72
PEGPDMS-1	136	313.15	921.31	0.00344	1.013×10^{-5}	111.171	3.436	4.00	0	256	21,165,453	7,927,801	10.93	21,271,828	9,581,098	10.97
PEGPDMS-1	86	283.15	948.42	0.00717	1.013×10^{-5}	196.440	2.829	4.00	0	256	13,627,263	4,012,011	9.42	13,466,463	3,945,647	9.99
PEGPDMS-1	86	293.15	939.22	0.00554	1.013×10^{-5}	159.982	3.040	4.00	0	256	14,231,784	4,225,700	9.90	14,354,966	3,734,780	10.26
PEGPDMS-1	86	313.15	921.31	0.00344	1.013×10^{-5}	111.171	3.436	4.00	0	256	15,517,266	5,122,478	11.60	15,304,033	6,326,543	11.44
PEGPDMS-1	54	283.15	948.42	0.00717	1.013×10^{-5}	196.440	2.829	4.00	0	256	10,171,495	2,622,825	10.21	10,870,136	2,621,415	10.33
PEGPDMS-1	54	293.15	939.22	0.00554	1.013×10^{-5}	159.982	3.040	4.00	0	256	10,593,681	2,756,588	10.70	11,562,457	2,356,887	10.63
PEGPDMS-1	54	313.15	921.31	0.00344	1.013×10^{-5}	111.171	3.436	4.00	0	256	11,487,937	3,344,287	12.50	11,589,010	4,547,658	11.77
PEGPDMS-3	543	273.15	1,011.67	0.02579	1.013×10^{-5}	153.865	1.692	4.00	0	256	48,662,287	22,775,608	7.33	49,548,218	21,986,566	7.25
PEGPDMS-3	543	278.15	1,006.97	0.02205	1.013×10^{-5}	143.131	1.778	4.00	0	256	49,605,768	23,091,888	7.44	50,217,847	22,621,285	7.40
PEGPDMS-3	543	283.15	1,002.35	0.01896	1.013×10^{-5}	133.502	1.863	4.00	0	256	50,687,400	23,287,324	7.52	50,969,954	23,168,885	7.53
PEGPDMS-3	543	288.15	997.81	0.01638	1.013×10^{-5}	124.838	1.947	4.00	0	256	51,488,139	23,732,217	7.66	51,795,083	23,677,825	7.65
PEGPDMS-3	543	293.15	993.34	0.01423	1.013×10^{-5}	117.021	2.029	4.00	0	256	52,560,411	24,075,010	7.78	52,681,755	24,217,280	7.78
PEGPDMS-3	543	298.15	988.94	0.01242	1.013×10^{-5}	109.949	2.110	4.00	0	256	53,617,562	24,492,308	7.92	53,616,090	24,870,150	7.95
PEGPDMS-3	543	303.15	984.61	0.01089	1.013×10^{-5}	103.533	2.190	4.00	0	256	54,838,882	25,184,993	8.14	54,580,835	25,723,535	8.17
PEGPDMS-3	543	308.15	980.32	0.00958	1.013×10^{-5}	97.699	2.269	4.00	0	256	54,976,038	26,012,141	8.49	55,553,923	26,857,058	8.46
PEGPDMS-3	543	313.15	976.10	0.00847	1.013×10^{-5}	92.381	2.346	4.00	0	256	56,171,805	26,991,382	8.64	56,507,800	28,328,880	8.84
PEGPDMS-3	543	318.15	971.92	0.00752	1.013×10^{-5}	87.522	2.421	4.00	0	256	57,238,090	28,235,923	8.98	57,412,751	30,158,939	9.31

Table B.6 continued.

Solvent	Plant Power (MW)	T (K)	ρ_L (kg/m³)	μ_L (Pa.s)	P^{vap} (Pa)	He_{CO2} (mol/m³.bar)	He_{H2} (mol/m³.bar)	Solvent cost ($/L)	Hydro-philicity	a (m⁻¹)	Calculated CAPEX ($)	Calculated OPEX ($/year)	Calculated LCOC ($/ton CO₂)	ANN prediction CAPEX ($)	ANN prediction OPEX ($/year)	ANN prediction LCOC ($/ton CO₂)
PEGPDMS-3	543	323.15	967.79	0.00669	1.013×10^{-5}	83.073	2.496	4.00	0	256	58,880,336	29,404,599	9.33	58,249,850	32,308,726	9.87
PEGPDMS-3	543	273.15	1,011.67	0.02579	1.013×10^{-5}	153.865	1.692	4.00	0	102	49,117,951	23,345,646	7.49	49,652,853	22,454,430	7.36
PEGPDMS-3	543	278.15	1,006.97	0.02205	1.013×10^{-5}	143.131	1.778	4.00	0	102	49,614,120	23,434,475	7.53	50,344,951	23,128,398	7.52
PEGPDMS-3	543	283.15	1,002.35	0.01896	1.013×10^{-5}	133.502	1.863	4.00	0	102	50,420,226	23,757,920	7.63	51,118,306	23,698,586	7.65
PEGPDMS-3	543	288.15	997.81	0.01638	1.013×10^{-5}	124.838	1.947	4.00	0	102	51,322,145	23,971,467	7.72	51,960,363	24,206,537	7.78
PEGPDMS-3	543	293.15	993.34	0.01423	1.013×10^{-5}	117.021	2.029	4.00	0	102	52,245,860	24,270,473	7.82	52,855,090	24,714,266	7.90
PEGPDMS-3	543	298.15	988.94	0.01242	1.013×10^{-5}	109.949	2.110	4.00	0	102	52,969,327	24,823,124	8.12	53,782,695	25,297,213	8.05
PEGPDMS-3	543	303.15	984.61	0.01089	1.013×10^{-5}	103.533	2.190	4.00	0	102	54,471,637	25,314,227	8.16	54,719,198	26,034,469	8.24
PEGPDMS-3	543	308.15	980.32	0.00958	1.013×10^{-5}	97.699	2.269	4.00	0	102	54,724,993	26,317,260	8.42	55,636,145	26,996,747	8.49
PEGPDMS-3	543	313.15	976.10	0.00847	1.013×10^{-5}	92.381	2.346	4.00	0	102	55,713,355	27,268,954	8.69	56,501,653	28,231,923	8.81
PEGPDMS-3	543	318.15	971.92	0.00752	1.013×10^{-5}	87.522	2.421	4.00	0	102	56,717,077	28,289,819	8.98	57,285,758	29,747,685	9.20
PEGPDMS-3	543	323.15	967.79	0.00669	1.013×10^{-5}	83.073	2.496	4.00	0	102	58,012,224	29,444,399	9.31	57,975,192	31,490,497	9.66
PEGPDMS-3	443	283.15	1,002.35	0.01896	1.013×10^{-5}	133.502	1.863	4.00	0	256	42,726,531	19,024,481	7.72	42,636,605	18,505,098	6.97
PEGPDMS-3	443	293.15	993.34	0.01423	1.013×10^{-5}	117.021	2.029	4.00	0	256	44,305,265	19,581,824	7.96	43,189,595	18,605,882	6.97
PEGPDMS-3	443	313.15	976.10	0.00847	1.013×10^{-5}	92.381	2.346	4.00	0	256	47,158,448	22,190,682	8.89	44,932,669	21,485,922	7.64
PEGPDMS-3	343	283.15	1,002.35	0.01896	1.013×10^{-5}	133.502	1.863	4.00	0	256	35,456,601	14,971,571	7.96	35,832,235	14,765,955	7.25
PEGPDMS-3	343	293.15	993.34	0.01423	1.013×10^{-5}	117.021	2.029	4.00	0	256	36,699,757	15,481,732	8.23	36,458,588	14,400,038	7.24
PEGPDMS-3	343	313.15	976.10	0.00847	1.013×10^{-5}	92.381	2.346	4.00	0	256	38,856,375	17,233,850	9.05	39,023,358	17,044,782	8.08
PEGPDMS-3	216	283.15	1,002.35	0.01896	1.013×10^{-5}	133.502	1.863	4.00	0	256	25,568,612	9,639,457	8.37	25,428,513	9,546,486	8.28
PEGPDMS-3	216	293.15	993.34	0.01423	1.013×10^{-5}	117.021	2.029	4.00	0	256	26,398,116	9,940,358	8.63	25,958,300	8,755,151	8.36
PEGPDMS-3	216	313.15	976.10	0.00847	1.013×10^{-5}	92.381	2.346	4.00	0	256	27,769,210	11,055,775	9.46	27,260,197	10,182,607	9.34
PEGPDMS-3	136	283.15	1,002.35	0.01896	1.013×10^{-5}	133.502	1.863	4.00	0	256	18,681,358	6,258,302	8.91	18,061,039	5,950,694	9.17
PEGPDMS-3	136	293.15	993.34	0.01423	1.013×10^{-5}	117.021	2.029	4.00	0	256	19,221,584	6,437,886	9.16	18,344,339	5,036,346	9.34
PEGPDMS-3	136	313.15	976.10	0.00847	1.013×10^{-5}	92.381	2.346	4.00	0	256	20,112,192	7,161,753	10.01	17,823,167	5,647,202	10.37

Table B.6 continued.

Solvent	Plant Power (MW)	T (K)	ρ_L (kg/m^3)	μ_L (Pa.s)	P^{vap} (Pa)	He_{CO2} (mol/m^3.bar)	He_{H2} (mol/m^3.bar)	Solvent cost ($/L)	Hydro-philicity	a (m^{-1})	Calculated			ANN prediction		
											CAPEX ($)	OPEX ($/year)	LCOC ($/ton CO$_2$)	CAPEX ($)	OPEX ($/year)	LCOC ($/ton CO$_2$)
PEGPDMS-3	86	283.15	1,002.35	0.01896	1.013×10^{-5}	133.502	1.863	4.00	0	256	13,805,414	4,111,654	9.62	13,412,561	3,733,730	9.78
PEGPDMS-3	86	293.15	993.34	0.01423	1.013×10^{-5}	117.021	2.029	4.00	0	256	14,162,442	4,212,544	9.86	13,482,035	2,828,004	10.00
PEGPDMS-3	86	313.15	976.10	0.00847	1.013×10^{-5}	92.381	2.346	4.00	0	256	14,739,617	4,670,116	10.71	11,635,528	3,080,128	11.06
PEGPDMS-3	54	283.15	1,002.35	0.01896	1.013×10^{-5}	133.502	1.863	4.00	0	256	10,329,721	2,729,244	10.54	10,559,854	2,402,563	10.17
PEGPDMS-3	54	293.15	993.34	0.01423	1.013×10^{-5}	117.021	2.029	4.00	0	256	10,575,504	2,791,470	10.78	10,473,451	1,538,955	10.43
PEGPDMS-3	54	313.15	976.10	0.00847	1.013×10^{-5}	92.381	2.346	4.00	0	256	10,914,874	3,060,672	11.58	7,770,220	1,642,418	11.50

Table B.7: Subcooled cases

Solvent	Plant Power (MW)	T (K)	ρ_L (kg/m³)	μ_L (Pa.s)	P^{vap} (Pa)	He_{CO2} (mol/m³.bar)	He_{H2} (mol/m³.bar)	Solvent cost ($/L)	Hydro-philicity	a (m⁻¹)	Calculated CAPEX ($)	Calculated OPEX ($/year)	Calculated LCOC ($/ton CO₂)	ANN prediction CAPEX ($)	ANN prediction OPEX ($/year)	ANN prediction LCOC ($/ton CO₂)
Methanol	543	223.15	851.36	0.00222	68.755	2,010.72	37.511	0.18	1	256	42,192,765	58,021,856	15.95	41,960,184	57,431,394	15.94
Methanol	543	228.15	846.87	0.00195	111.704	1,653.93	19.933	0.18	1	256	42,842,716	59,607,474	16.37	42,503,651	43,303,229	12.45
Methanol	543	233.15	842.42	0.00172	177.456	1,373.49	11.740	0.18	1	256	43,519,686	61,612,335	16.90	43,648,114	61,948,713	17.16
Methanol	543	238.15	837.99	0.00153	276.067	1,150.77	7.585	0.18	1	256	44,127,570	64,040,233	17.53	44,369,702	62,872,062	17.49
Methanol	543	243.15	833.57	0.00137	421.132	972.20	5.337	0.18	1	256	44,834,709	66,952,234	18.28	45,308,733	67,867,037	18.92
Methanol	543	248.15	829.17	0.00123	630.720	827.73	4.075	0.18	1	256	45,653,954	70,486,877	19.20	46,060,249	73,094,271	20.49
Methanol	543	253.15	824.76	0.00111	928.453	709.87	3.376	0.18	1	256	46,440,551	74,582,185	20.29	46,711,451	75,971,680	21.49
Methanol	543	258.15	820.36	0.00101	1,344.744	612.96	3.037	0.18	1	256	47,348,315	79,711,980	21.65	47,349,242	79,459,927	22.62
Methanol	543	263.15	815.95	0.00092	1,918.186	532.69	2.964	0.18	1	256	48,292,873	85,873,215	23.26	48,110,014	85,505,940	24.30
Methanol	543	268.15	811.53	0.00085	2,697.105	465.74	3.123	0.18	1	256	48,805,452	92,736,721	25.03	49,174,277	94,073,935	26.44
Methanol	543	273.15	807.10	0.00078	3,741.242	409.55	3.525	0.18	1	256	51,701,493	102,339,920	27.58	50,733,160	102,330,894	28.24
Methanol	543	223.15	851.36	0.00222	68.755	2,010.72	37.511	0.18	1	102	41,970,630	58,455,112	16.05	41,959,115	57,655,720	16.00
Methanol	543	228.15	846.87	0.00195	111.704	1,653.93	19.933	0.18	1	102	42,726,014	59,967,871	16.46	42,473,025	44,181,938	12.67
Methanol	543	233.15	842.42	0.00172	177.456	1,373.49	11.740	0.18	1	102	44,021,283	64,423,483	17.62	43,656,586	64,750,380	17.86
Methanol	543	238.15	837.99	0.00153	276.067	1,150.77	7.585	0.18	1	102	44,687,644	67,346,208	18.37	44,365,446	66,559,666	18.41
Methanol	543	243.15	833.57	0.00137	421.132	972.20	5.337	0.18	1	102	45,457,580	70,706,030	19.25	45,290,881	70,067,954	19.47
Methanol	543	248.15	829.17	0.00123	630.720	827.73	4.075	0.18	1	102	46,271,599	75,188,730	20.44	46,042,118	74,230,300	20.77
Methanol	543	253.15	824.76	0.00111	928.453	709.87	3.376	0.18	1	102	47,185,530	80,349,747	21.81	46,701,830	76,383,832	21.60
Methanol	543	258.15	820.36	0.00101	1,344.744	612.96	3.037	0.18	1	102	47,185,530	80,349,747	21.81	47,356,024	79,199,139	22.55
Methanol	543	263.15	815.95	0.00092	1,918.186	532.69	2.964	0.18	1	102	48,121,379	86,357,431	23.38	48,142,536	84,483,136	24.03
Methanol	543	268.15	811.53	0.00085	2,697.105	465.74	3.123	0.18	1	102	49,076,406	93,842,221	25.32	49,245,861	92,108,192	25.93
Methanol	543	273.15	807.10	0.00078	3,741.242	409.55	3.525	0.18	1	102	50,082,337	102,827,700	27.65	50,861,590	99,176,854	27.42
THF	543	223.15	960.67	0.00128	209.671	3,790.67	1.272	0.62	1	256	41,836,137	145,425,024	37.86	42,063,001	144,284,039	38.56
THF	543	228.15	955.16	0.00117	319.838	3,048.27	1.406	0.62	1	256	42,208,752	156,502,975	40.64	41,647,225	156,971,820	41.65

Table B.7 continued.

Solvent	Plant Power (MW)	T (K)	ρ_L (kg/m³)	μ_L (Pa.s)	P^{sup} (Pa)	He_{CO2} (mol/m³.bar)	He_{H2} (mol/m³.bar)	Solvent cost ($/L)	Hydro-philicity	a (m⁻¹)	Calculated			ANN prediction		
											CAPEX ($)	OPEX ($/year)	LCOC ($/ton CO₂)	CAPEX ($)	OPEX ($/year)	LCOC ($/ton CO₂)
THF	543	233.15	949.68	0.00108	477.689	2,478.02	1.540	0.62	1	256	41,585,998	169,287,118	44.08	42,053,271	172,238,084	45.55
THF	543	238.15	944.25	0.00099	699.528	2,034.91	1.675	0.62	1	256	42,183,989	183,675,617	48.13	42,602,114	187,136,751	49.46
THF	543	243.15	938.86	0.00092	1,005.722	1,686.83	1.810	0.62	1	256	42,809,717	200,820,070	53.05	43,193,022	204,545,823	54.15
THF	543	248.15	933.50	0.00085	1,421.301	1,410.62	1.945	0.62	1	256	43,418,663	221,178,696	58.74	43,761,209	226,635,363	60.12
THF	543	253.15	928.17	0.00080	1,976.559	1,189.35	2.080	0.62	1	256	43,946,663	245,481,500	65.21	44,250,766	251,507,350	66.83
THF	543	258.15	922.87	0.00074	2,707.641	1,010.52	2.216	0.62	1	256	44,528,263	274,091,642	72.87	44,645,875	275,467,177	73.25
THF	543	263.15	917.58	0.00070	3,657.112	864.78	2.351	0.62	1	256	45,002,009	308,124,028	82.03	44,973,886	300,658,376	79.92
THF	543	268.15	912.32	0.00065	4,874.476	745.06	2.487	0.62	1	256	45,735,736	358,908,120	95.81	45,309,112	339,018,465	89.94
THF	543	273.15	907.06	0.00062	6,416.662	645.99	2.622	0.62	1	256	46,205,632	415,820,465	111.43	45,831,887	413,621,235	109.26
THF	543	223.15	960.67	0.00128	209.671	3,790.67	1.272	0.62	1	102	41,668,765	146,429,992	38.10	41,691,381	142,389,243	38.04
THF	543	228.15	955.16	0.00117	319.838	3,048.27	1.406	0.62	1	102	41,987,889	157,659,895	40.93	41,529,744	158,273,328	41.98
THF	543	233.15	949.68	0.00108	477.689	2,478.02	1.540	0.62	1	102	41,935,459	184,767,584	48.42	41,990,424	177,203,655	46.82
THF	543	238.15	944.25	0.00099	699.528	2,034.91	1.675	0.62	1	102	42,594,453	201,817,697	53.32	42,565,650	194,126,890	51.25
THF	543	243.15	938.86	0.00092	1,005.722	1,686.83	1.810	0.62	1	102	43,195,200	222,184,253	59.00	43,173,561	212,740,934	56.24
THF	543	248.15	933.50	0.00085	1,421.301	1,410.62	1.945	0.62	1	102	43,737,001	246,414,113	65.45	43,754,466	235,618,625	62.42
THF	543	253.15	928.17	0.00080	1,976.559	1,189.35	2.080	0.62	1	102	44,277,289	275,168,875	73.14	44,253,167	260,895,384	69.23
THF	543	258.15	922.87	0.00074	2,707.641	1,010.52	2.216	0.62	1	102	44,277,289	275,168,875	73.14	44,654,455	284,952,657	75.68
THF	543	263.15	917.58	0.00070	3,657.112	864.78	2.351	0.62	1	102	44,762,651	309,267,058	82.32	44,989,471	310,262,491	82.38
THF	543	268.15	912.32	0.00065	4,874.476	745.06	2.487	0.62	1	102	45,478,589	360,522,933	96.24	45,338,967	349,256,375	92.56
THF	543	273.15	907.06	0.00062	6,416.662	645.99	2.622	0.62	1	102	45,978,567	417,346,206	111.84	45,890,921	425,625,056	112.32

Bibliography

[1]   BP, "Statistical Review of World Energy," 2020.

[2]   EPA. "Overview of Greenhouse Gases." https://www.epa.gov/ghgemissions/overview-greenhouse-gases#main-content (Accessed 31-May-2021).

[3]   EPA. "Sources of Greenhouse Gas Emissions." https://www.epa.gov/ghgemissions/sources-greenhouse-gas-emissions#electricity (Accessed 31-May-2021).

[4]   M. Kanniche, R. Gros-Bonnivard, P. Jaud, J. Valle-Marcos, J. M. Amann, and C. Bouallou, "Pre-Combustion, Post-Combustion and Oxy-Combustion in Thermal Power Plant For CO_2 Capture," *Applied Thermal Engineering,* vol. 30, pp. 53-62, 2010, doi: 10.1016/j.applthermaleng.2009.05.005.

[5]   K. Gerdes, R. Stevens, T. Fout, J. Fisher, G. Hackett, and W. Shelton, "Current and Future Power Generation Technologies: Pathways to Reducing the Cost of Carbon Capture for Coal-Fueled Power Plants," *Energy Procedia,* vol. 63, pp. 7541-7557, 2014, doi: 10.1016/j.egypro.2014.11.790.

[6]   J. Ratafia-Brown, L. M. Manfredo, J. W. Hoffmann, M. Ramezan, and G. J. Stiegel, "An Environmental Assessment of IGCC Power Systems," *19th Annual Pittsburgh Coal Conference,* 2002.

[7]   J. Vidaurri, R. Larsen, J. Martin, M. Looker, S. Gebhard, and G. Srinivas. Multicontaminant Warm Gas Cleanup.

[8]   R. Beavis, J. Forsyth, E. Roberts, B. Song, G. Combes, J. Abbott, N. Macleod, E. Vass, M. Davies, and I. Barton, "A Step-Change Sour Shift Process for Improving the Efficiency of IGCC with CCS," *Energy Procedia,* vol. 37, pp. 2256-2264, 2013, doi: 10.1016/j.egypro.2013.06.106.

[9]   M. Maroto-Valer, *Developments and Innovation in Carbon Dioxide (CO_2) Capture and Storage Technology: Carbon Dioxide (CO_2) Capture, Transport and Industrial Applications*. CRC Press, 2010.

[10]   T. Wang and G. J. Stiegel, *Integrated Gasification Combined Cycle (IGCC) Technologies*. Elsevier Science, 2016.

[11]   H.-B. Xie, Y. Zhou, Y. Zhang, and J. K. Johnson, "Reaction Mechanism of Monoethanolamine with CO_2 in Aqueous Solution from Molecular Modeling," *The Journal of Physical Chemistry A,* vol. 114, pp. 11844-11852, 2010, doi: 10.1021/jp107516k.

[12]   G. T. Rochelle, "Amine Scrubbing for CO_2 Capture," *Science,* vol. 325, pp. 1652-1655, 2009, doi: 10.1126/science.1181637.

[13]   Y. Peng, B. Zhao, and L. Li, "Advance in Post-Combustion CO_2 Capture with Alkaline Solution: A Brief Review," *Energy Procedia,* vol. 14, pp. 1515-1522, 2012, doi: 10.1016/j.egypro.2011.12.1126.

[14]   R. Wang, "Modelling of CO_2 Absorption from Gas Mixtures Using Chemical Absorbents in Adiabatic Packed-Beds," Chemical and Petroleum Engineering Department, University of Pittsburgh, 2019.

[15]   R. Wang, H. E. Ashkanani, B. Li, and B. I. Morsi, "Modelling of CO_2 Absorption from Gas Mixtures Using Chemical Absorbents in Adiabatic Packed-Beds," *Proceedings of the 36th Annual International Pittsburgh Coal Conference, September 3-6,* 2019.

[16]   K. P. Resnik, J. T. Yeh, and H. W. Pennline, "Aqua Ammonia Process for Simultaneous Removal of CO_2, SO_2, and NO_x," *International Journal of Environmental Technology and Management,* vol. 4, pp. 89-104, 2004.

[17]   V. Darde, K. Thomsen, W. J. M. van Well, and E. H. Stenby, "Chilled Ammonia Process for CO_2 Capture," *Energy Procedia,* vol. 1, pp. 1035-1042, 2009, doi: 10.1016/j.egypro.2009.01.137.

[18]   W. M. Budzianowski, "Mitigating NH_3 Vaporization from an Aqueous Ammonia Process for CO_2 Capture," *International Journal of Chemical Reactor Engineering,* vol. 9, 2012, doi: 10.1515/1542-6580.2711.

[19]   F. Kozak, A. Petig, E. Morris, R. Rhudy, and D. Thimsen, "Chilled Ammonia Process for CO_2 Capture," *Energy Procedia,* vol. 1, pp. 1419-1426, 2009, doi: 10.1016/j.egypro.2009.01.137.

[20]   H. E. Benson, J. H. Field, and R. M. Jimeson, "CO$_2$ Absorption: Employing Hot Potassium Carbonate Solutions," *Chem. Eng. Prog.;(United States),* vol. 50, 1954.

[21]   F. Yi, H. K. Zou, G. W. Chu, L. Shao, and J. F. Chen, "Modeling and Experimental Studies on Absorption of CO$_2$ by Benfield Solution in Rotating Packed Bed," *Chemical Engineering Journal,* vol. 145, pp. 377-384, 2009, doi: 10.1016/j.cej.2008.08.004.

[22]   K. A. Mumford, K. H. Smith, C. J. Anderson, S. Shen, W. Tao, Y. A. Suryaputradinata, A. Qader, B. Hooper, R. A. Innocenzi, S. E. Kentish, and G. W. Stevens, "Post-Combustion Capture Of CO$_2$: Results From the Solvent Absorption Capture Plant at Hazelwood Power Station Using Potassium Carbonate Solvent," *Energy and Fuels,* vol. 26, pp. 138-146, 2012, doi: 10.1021/ef201192n.

[23]   M. Ahmadi, V. G. Gomes, and K. Ngian, "Advanced Modelling in Performance Optimization for Reactive Separation in Industrial CO$_2$ Removal," *Separation and Purification Technology,* vol. 63, pp. 107-115, 2008, doi: 10.1016/j.seppur.2008.04.016.

[24]   D. W. Savage, G. Astarita, and S. Joshi, "Chemical Absorption and Desorption of Carbon Dioxide from Hot Carbonate Solutions," *Chemical Engineering Science,* vol. 35, pp. 1513-1522, 1980.

[25]   A. H. G. Cents, D. W. F. Brilman, and G. F. Versteeg, "CO$_2$ Absorption in Carbonate/Bicarbonate Solutions: The Danckwerts-Criterion Revisited," *Chemical Engineering Science,* vol. 60, pp. 5830-5835, 2005, doi: 10.1016/j.ces.2005.05.020.

[26]   H.-J. Song, L. Joonho, D. C. Span, J.-W. Park, S. Lee, T. P. Filburn, and K. Park, "Simplified Estimation of Regeneration Energy of 30 Wt % Sodium Glycinate Solution for Carbon Dioxide Absorption," *Industrial and Engineering Chemistry Research,* vol. 47, pp. 9925-9930, 2008, doi: 10.1021/ie8007117.

[27]   H. J. Song, S. Lee, S. Maken, J. J. Park, and J. W. Park, "Solubilities of Carbon Dioxide in Aqueous Solutions of Sodium Glycinate," *Fluid Phase Equilibria,* vol. 246, pp. 1-5, 2006, doi: 10.1016/j.fluid.2006.05.012.

[28]   V. Salazar, Y. Sánchez-Vicente, C. Pando, J. A. R. Renuncio, and A. Cabañas, "Enthalpies of Absorption of Carbon Dioxide in Aqueous Sodium Glycinate Solutions at Temperatures of (313.15 and 323.15) K," *Journal of Chemical and Engineering Data,* vol. 55, pp. 1215-1218, 2010, doi: 10.1021/je9005954.

[29] S. W. Park, Y. S. Son, D. W. Park, and K. J. Oh, "Absorption of Carbon Dioxide into Aqueous Solution of Sodium Glycinate," *Separation Science and Technology,* vol. 43, pp. 3003-3019, 2008, doi: 10.1080/01496390802219620.

[30] S. Mazinani, A. Samsami, A. Jahanmiri, and A. Sardarian, "Solubility (At Low Partial Pressures), Density, Viscosity, and Corrosion Rate of Carbon Dioxide in Blend Solutions of Monoethanolamine (MEA) and Sodium Glycinate (SG)," *Journal of Chemical and Engineering Data,* vol. 56, pp. 3163-3168, 2011, doi: 10.1021/je2002418.

[31] S. Lee, H. J. Song, S. Maken, S. K. Yoo, J. W. Park, S. Kim, J. G. Shim, and K. R. Jang, "Simulation of CO_2 Removal with Aqueous Sodium Glycinate Solutions in a Pilot Plant," *Korean Journal of Chemical Engineering,* vol. 25, pp. 1-6, 2008, doi: 10.1007/s11814-008-0001-x.

[32] S. Lee, H. J. Song, S. Maken, H. C. Shin, H. C. Song, and J. W. Park, "Physical Solubility and Diffusivity of N_2O and CO_2 in Aqueous Sodium Glycinate Solutions," *Journal of Chemical and Engineering Data,* vol. 51, pp. 504-509, 2006, doi: 10.1021/je0503913.

[33] S. Lee, H. J. Song, S. Maken, and J. W. Park, "Kinetics of CO_2 Absorption in Aqueous Sodium Glycinate Solutions," *Industrial and Engineering Chemistry Research,* vol. 46, pp. 1578-1583, 2007, doi: 10.1021/ie061270e.

[34] F. Harris, K. A. Kurnia, M. I. A. Mutalib, and M. Thanapalan, "Solutions Before and After CO_2 Absorption," *Journal of Chemical and Engineering Data,* vol. 54, no. 1, pp. 144-147, 2009.

[35] P. Tontiwachwuthikul, A. Meisen, and C. J. Lim, "CO_2 Absorption by NaOH, Monoethanolamine and 2-Amino-2-Methyl-1-Propanol Solutions in a Packed Column," *Chemical Engineering Science,* vol. 47, no. 2, pp. 381-390, 1992.

[36] N. Korens, D. R. Simbeck, D. J. Wilhelm, J. R. Longanbach, and G. J. Stiegal, "Process Screening Analysis of Alternative Gas Treating and Sulfur Removal for Gasification: Revised Final Report," 2002.

[37] D. Gielen, "The Energy Policy Consequences of Future CO_2 Capture and Sequestration Technologies," *Proceedings of the 2nd Annual Conference on Carbon,* pp. 1-11, 2003.

[38] R. P. Field and R. Brasington, "Baseline Flowsheet Model for IGCC with Carbon Capture," *Industrial and Engineering Chemistry Research,* vol. 50, pp. 11306-11312, 2011, doi: 10.1021/ie200288u.

[39]   Z. Kapetaki, P. Brandani, S. Brandani, and H. Ahn, "Process Simulation of a Dual-Stage Selexol Process for 95% Carbon Capture Efficiency at an Integrated Gasification Combined Cycle Power Plant," *International Journal of Greenhouse Gas Control,* vol. 39, pp. 17-26, 2015, doi: 10.1016/j.ijggc.2015.04.015.

[40]   B. P. Spigarelli and S. K. Kawatra, "Opportunities and Challenges in Carbon Dioxide Capture," *Journal of CO_2 Utilization,* vol. 1, pp. 69-87, 2013.

[41]   H. Yamada, "Amine-Based Capture of CO_2 for Utilization and Storage," *Polymer Journal,* vol. 53, pp. 93-102, 2021, doi: 10.1038/s41428-020-00400-y.

[42]   Y. J. Heintz, "Carbon Dioxide Capture from Fuel Gas Streams under Elevated Pressures and Temperatures Using Novel Physical Solvents," Chemical and Petroleum Engineering Department, University of Pittsburgh, 2011.

[43]   S. P. Peletiri, N. Rahmanian, and I. M. Mujtaba, "CO_2 Pipeline Design: A Review," *Energies,* vol. 11, 2018, doi: 10.3390/en11092184.

[44]   J. M. Coulson, J. F. Richardson, J. R. Blackhurst, and J. H. Harker, *Chemical Engineering*. Paragamon Press Inc., 1977.

[45]   W. G. Whitman, "The Two Film Theory of Gas Absorption," *International Journal of Heat and Mass Transfer,* vol. 5, pp. 429-433, 1962, doi: https://doi.org/10.1016/0017-9310(62)90032-7.

[46]   J. R. Welty, C. E. Wicks, R. E. Wilson, and G. Rorrer, *Fundamentals Of Momentum, Heat And Mass Transfer*, 5th ed. John Wiley and Sons, Inc., 2007.

[47]   M.-Y. Chang, "Mass Transfer Characteristics of Gases in Aqueous and Organic Liquids at Elevated Pressures and Temperatures in Agitated Reactors," University of Pittsburgh, 1991.

[48]   H. L. Toor and J. M. Marchello, "Film-Penetration Model for Mass and Heat Transfer," *AIChE Journal,* vol. 4, pp. 97-101, 1958, doi: https://doi.org/10.1002/aic.690040118.

[49]   P. V. Danckwerts, "Significance of Liquid-Film Coefficients in Gas Absorption," *Industrial and Engineering Chemistry,* vol. 43, pp. 1460-1467, 1951, doi: 10.1021/ie50498a055.

[50]   T. W. Chung, T. K. Ghosh, and A. L. Hines, "Comparison Between Random and Structured Packings for Dehumidification of Air by Lithium Chloride Solutions in a Packed Column and their Heat and Mass Transfer Correlations," *Industrial and Engineering Chemistry Research,* vol. 35, pp. 192-198, 1996, doi: 10.1021/ie940652u.

[51]   "Ceramic Raschig Ring Packings." http://www.chemicalpackings.com/product/ceramic-raschig-ring.html (Accessed 06-Sep-2018).

[52]   H. Z. Kister, "Distillation Design," 1992.

[53]   E. E. Ludwig, "Applied Process Design for Chemical and Petroleum Plants Vol. 2," 1997.

[54]   R. H. Perry and D. Green, "Perry's Chemical Engineers' Handbook," 1997.

[55]   R. F. J. Strigle, *Random Packings and Packed Towers*. Houston: Gulf Publishing Company, 1987.

[56]   C. J. Geankoplis, *Transport Processes and Separation Process Principles*, 4th ed. Upper Saddle River, NJ: Prentice Hall, 2011.

[57]   J. S. Eckert, "Design Techniques for Sizing Packed Towers," *Chemical Engineering Progress,* vol. 57, no. 9, 1961.

[58]   M. Leva, "Reconsider Packed-Tower Pressure-Drop Correlations," *Chemical Engineering Progress,* vol. 88, pp. 65-72, 1992.

[59]   J. Stichlmair, J. L. Bravo, and J. R. Fair, "General Model for Prediction of Pressure Drop and Capacity of Countercurrent Gas / Liquid Packed Columns," *Gas Separation Purification,* vol. 3, no. 1, pp. 19-28, 1989.

[60]   H. Z. Kister, "Realistically Predict Capacity and Pressure Drop for Packed Columns," pp. 28-38, 2007.

[61]   R. Tsai, "Mass Transfer Area of Structured Packing," University of Texas at Austin, 2010.

[62]   V. Wolf-zöllner, F. Seibert, and M. Lehner, "Chemical Engineering Research and Design Extended Performance Comparison of Different Pressure Drop , Hold-Up and Flooding

Point Correlations for Packed Columns," *Chemical Engineering Research and Design,* vol. 147, pp. 699-708, 2019, doi: 10.1016/j.cherd.2019.05.028.

[63] S. Piché, F. Larachi, and B. P. A. Grandjean, "Flooding Capacity in Packed Towers: Database, Correlations, and Analysis," *Industrial and Engineering Chemistry Research,* vol. 40, no. 1, pp. 476-487, 2001/01/01 2001, doi: 10.1021/ie000486s.

[64] M. C. Rodwell and M. R. Riazi, "Design Aspects of Separation Units and Processing Equipment," in *Petroleum Refining And Natural Gas Processing*: ASTM International, 2013, pp. 305-353.

[65] R. Billet and M. Schultes, "A Physical Model for the Prediction of Liquid Hold-Up in Two-Phase Countercurrent Columns," *Chemical Engineering and Technology,* vol. 16, pp. 370-375, 1993, doi: 10.1002/ceat.270160603.

[66] T. K. Sherwood and F. A. L. Holloway, "Performance of Packed Towers-Liquid Film Data for Several Packings," *Trans Am. Inst. Chem. Engrs,* vol. 36, pp. 39-70, 1940.

[67] D. W. VanKrevelen and P. J. Hoftijzer, "Kinetics of Simultaneous Absorption and Chemical Reaction," *Chemical Engineering Progress,* vol. 44, pp. 529-536, 1948.

[68] H. L. Shulman, C. F. Ullrich, a. Z. Proulx, and J. Zimmerman, "Gas - and Liquid-phase Mass Transfer Rates," *AIChE Journal,* vol. 1, pp. 253-258, 1955.

[69] E. J. Wilson and C. J. Geankoplis, "Liquid Mass Transfer at Very Low Reynolds Numbers in Packed Beds," *Industrial and Engineering Chemistry Fundamentals,* vol. 5, pp. 9-14, 1966, doi: 10.1021/i160017a002.

[70] K. Onda, H. Takeuchi, and Y. Okumoto, "Mass Transfer Coefficients Between Gas and Liquid Phases in Packed Columns," *Journal of Chemical Engineering of Japan,* vol. 1, pp. 56-62, 1968, doi: 10.1252/jcej.1.56.

[71] D. M. Mohunta, A. S. Vaidyanathan, and G. S. Laddha, "Prediction of Liquid Phase Mass Transfer Coefficients in Columns Packed with Raschig Rings," *Indian Chem. Eng,* vol. 11, pp. 73-79, 1969.

[72] K. Akita and F. Yoshida, "Gas Holdup and Volumetric Mass Transfer Coefficient in Bubble Columns. Effects of Liquid Properties," *Industrial and Engineering Chemistry Process Design and Development,* vol. 12, pp. 76-80, 1973, doi: 10.1021/i260045a015.

[73]   S. Fukushima and K. Kusaka, "Liquid-Phase Volumetric and Mass-Transfer Coefficient , and Boundary of Hydrodynamic Flow Region and Gas-Phase Mass-Transfer Coefficient in Packed Column with Cocurrent Downward Flow," *Journal of Chemical Engineering of Japan,* vol. 11, pp. 241-244, 1978, doi: 10.1252/jcej.11.241.

[74]   R. J. Mangers and A. B. Ponter, "Effect of Viscosity on Liquid Film Resistance to Mass Transfer in a Packed Column," *Industrial and Engineering Chemistry Process Design and Development,* vol. 19, pp. 530-537, 1980.

[75]   R. Echarte, H. Campaña, and E. A. Brignole, "Effective Areas and Liquid Film Mass Transfer Coefficients in Packed Columns," *Industrial and Engineering Chemistry Process Design and Development,* vol. 23, no. 2, pp. 349-354, 1984.

[76]   R. Billet and M. Schultes, "Predicting Mass Transfer in Packed Columns," *Chemical Engineering and Technology,* vol. 16, pp. 1-9, 1993, doi: 10.1002/ceat.270160102.

[77]   S. V. Potnis and T. G. Lenz, "Dimensionless Mass-Transfer Correlations for Packed-Bed Liquid-Desiccant Contactors," *Industrial and Engineering Chemistry Research,* vol. 35, no. 11, pp. 4185-4193, 1996.

[78]   S. Shetty and R. L. Cerro, "Fundamental Liquid Flow Correlations for the Computation of Design Parameters for Ordered Packings," *Industrial and Engineering Chemistry Research,* vol. 36, pp. 771-783, 1997, doi: 10.1021/ie960627j.

[79]   Y. Yuan, M. Han, D. Wang, and Y. Jin, "Liquid Phase Residence Time Distribution for a Two-Phase Countercurrent Flow in a Packed Column with a Novel Internal," *Chemical Engineering and Processing: Process Intensification,* vol. 43, pp. 1469-1474, 2004, doi: 10.1016/j.cep.2004.01.007.

[80]   G. A. Longo and A. Gasparella, "Experimental and Theoretical Analysis of Heat and Mass Transfer in a Packed Column Dehumidifier/Regenerator with Liquid Desiccant," *International Journal of Heat and Mass Transfer,* vol. 48, pp. 5240-5254, 2005, doi: 10.1016/j.ijheatmasstransfer.2005.07.011.

[81]   R. Krupiczka, A. Rotkegel, and Z. Ziobrowski, "Comparative Study of CO_2 Absorption in Packed Column Using Imidazolium Based Ionic Liquids and MEA Solution," *Separation and Purification Technology,* vol. 149, pp. 228-236, 2015, doi: 10.1016/j.seppur.2015.05.026.

[82]   B. E. Kanak, "Analysis of a Gas Absorption System with Soluble Carrier Gas and Volatile Solvent," in *Oak Ridge Gaseous Diffusion Plant*, 1980.

[83]   J. L. Bravo, J. A. Rocha, and J. R. Fair, "Mass Transfer in Gauze Packings," *Hydrocarbon Processing,* pp. 91-95, 1985.

[84]   M. Henriques de Brito, U. Von Stockar, and P. Bomio. Predicting the Liquid Phase Mass Transfer Coefficient k_L for the Sulzer Structured Packing Mellapak.

[85]   R. H. Weiland, K. R. Ahlgren, and M. Evans, "Mass-Transfer Characteristics of Some Structured Packings," *Industrial and Engineering Chemistry Research,* vol. 32, pp. 1411-1418, 1993, doi: 10.1021/ie00019a015.

[86]   J. A. Rocha, J. L. Bravo, and J. R. Fair, "Distillation-Columns Containing Structured Packings - A Comprehensive Model for Their Performance .1. Hydraulic Models," *Industrial and Engineering Chemistry Research,* vol. 32, pp. 641-651, 1993, doi: 10.1021/ie9910773.

[87]   B. Hanley, B. Dunbobbin, and D. Bennett, "A Unified Model for Countercurrent Vapor/Liquid Packed Columns. 2. Equations for the Mass Transfer Coefficients, Mass Transfer Area, the HETP, and the Dynamic Liquid Holdup," *Industrial and Engineering Chemistry Research,* pp. 1222-1230, 1994.

[88]   E. Brunazzi, G. Nardini, A. Paglianti, and L. Petarca, "Interfacial Area of Mellapak Packing: Absorption Of 1,1,1-Trichloroethane By Genosorb 300," *Chemical Engineering and Technology,* vol. 18, pp. 248-255, 1995, doi: 10.1002/ceat.270180405.

[89]   E. Brunazzi and A. Paglianti, "Liquid-Film Mass-Transfer Coefficient in a Column Equipped with Structured Packings," *Industrial and Engineering Chemistry Research,* vol. 36, pp. 3792-3799, 1997, doi: 10.1021/ie970045h.

[90]   J. J. Gualito, F. J. Cerino, J. C. Cardenas, and J. a. Rocha, "Design Method for Distillation Columns Filled with Metallic, Ceramic, or Plastic Structured Packings," *Industrial and Engineering Chemistry Research,* vol. 36, pp. 1747-1757, 1997, doi: 10.1021/ie960625z.

[91]   Z. P. Xu, A. Afacan, and K. T. Chuang, "Predicting Mass Transfer in Packed Columns Containing Structured Packings," *Chemical Engineering Research and Design,* vol. 78, pp. 91-98, 2000, doi: 10.1205/026387600526924.

[92]   L. Raynal, J. P. Ballaguet, and C. Barrere-Tricca, "Determination of Mass Transfer Characteristics of Co-Current Two-Phase Flow within Structured Packing," *Chemical Engineering Science,* vol. 59, pp. 5395-5402, 2004, doi: 10.1016/j.ces.2004.07.030.

[93]   Y. Haroun, D. Legendre, and L. Raynal, "Direct Numerical Simulation of Reactive Absorption in Gas-Liquid Flow on Structured Packing Using Interface Capturing Method," *Chemical Engineering Science,* vol. 65, pp. 351-356, 2010, doi: 10.1016/j.ces.2009.07.018.

[94]   B. Hanley and C.-C. Chen, "New Mass-Transfer Correlations for Packed Towers," *AICHE Journal,* vol. 58, pp. 132-152, 2012, doi: 10.1002/aic.

[95]   A. Padurean, C.-C. Cormos, and P.-S. Agachi, "Pre-Combustion Carbon Dioxide Capture by Gas–Liquid Absorption for Integrated Gasification Combined Cycle Power Plants," *International Journal of Greenhouse Gas Control,* vol. 7, pp. 1-11, 2012, doi: 10.1016/j.ijggc.2011.12.007.

[96]   O. M. Basha, M. J. Keller, D. R. Luebke, K. P. Resnik, and B. I. Morsi, "Development of a Conceptual Process for Selective CO_2 Capture from Fuel Gas Streams using [hmim][Tf$_2$N] Ionic Liquid as a Physical Solvent," *Energy and Fuels,* vol. 27, pp. 3905-3917, 2013, doi: 10.1021/ef400650w.

[97]   O. M. Basha, Y. J. Heintz, M. J. Keller, D. R. Luebke, K. P. Resnik, and B. I. Morsi, "Development of a Conceptual Process for Selective Capture of CO_2 from Fuel Gas Streams using Two TEGO Ionic Liquids as Physical Solvents," *Industrial and Engineering Chemistry Research,* vol. 53, pp. 3184-3195, 2014, doi: 10.1021/ie403375m.

[98]   S. H. Park, S. J. Lee, J. W. Lee, S. N. Chun, and J. B. Lee, "The Quantitative Evaluation of Two-Stage Pre-Combustion CO_2 Capture Processes using the Physical Solvents with Various Design Parameters," *Energy,* vol. 81, pp. 47-55, 2015, doi: 10.1016/j.energy.2014.10.055.

[99]   A. Dave, M. Dave, Y. Huang, S. Rezvani, and N. Hewitt, "Process Design for CO_2 Absorption from Syngas using Physical Solvent DMEPEG," *International Journal of Greenhouse Gas Control,* vol. 49, pp. 436-448, 2016.

[100] N. S. Siefert, S. Agarwal, F. Shi, W. Shi, E. A. Roth, D. Hopkinson, V. A. Kusuma, R. L. Thompson, D. R. Luebke, and H. B. Nulwala, "Hydrophobic Physical Solvents for Pre-Combustion CO_2 Capture: Experiments, Computational Simulations, and Techno-Economic Analysis," *International Journal of Greenhouse Gas Control,* vol. 49, pp. 364-371, 2016, doi: 10.1016/j.ijggc.2016.03.014.

[101] H. Zhai and E. S. Rubin, "Systems Analysis of Physical Absorption of CO_2 in Ionic Liquids for Pre-Combustion Carbon Capture," *Environmental Science and Technology,* vol. 52, pp. 4996-5004, 2018, doi: 10.1021/acs.est.8b00411.

[102] S. Roussanaly, M. Vitvarova, R. Anantharaman, D. Berstad, B. Hagen, J. Jakobsen, V. Novotny, and G. Skaugen, "Techno-Economic Comparison of Three Technologies for Pre-Combustion CO_2 Capture from a Lignite-Fired IGCC," *Frontiers of Chemical Science and Engineering,* vol. 14, pp. 436-452, 2020, doi: 10.1007/s11705-019-1870-8.

[103] D. Simbeck and D. Beecy, "The CCS Paradox: The Much Higher CO_2 Avoidance Costs of Existing Versus New Fossil Fuel Power Plants," *Energy Procedia,* vol. 4, pp. 1917-1924, 2011, doi: 10.1016/j.egypro.2011.02.071.

[104] R. V. Siriwardane, D. C. Cicero, S. Jain, R. P. Gupta, and B. S. Turk, "Durable Zinc Oxide-Based Regenerable Sorbents for Desulfurization of Syngas in a Fixed-Bed Reactor," 2002.

[105] F. Huiling, L. Yanxu, L. Chunhu, G. Hanxian, and X. Kechang, "The Apparent Kinetics of H_2S Removal by Zinc Oxide in the Presence of Hydrogen," *Fuel,* vol. 81, pp. 91-96, 2002, doi: 10.1016/S0016-2361(01)00111-9.

[106] S. Lew, K. Jothimurugesan, and M. Flytzani-stephanopoulos, "High-Temperature H_2S Removal from Fuel Gases by Regenerable Zinc Oxide—Titanium Dioxide Sorbents," *Industrial and Engineering Chemistry Research,* vol. 28, pp. 535-541, 1989, doi: 10.1021/ie00089a006.

[107] I. Rosso, C. Galletti, M. Bizzi, G. Saracco, and V. Specchia, "Zinc Oxide Sorbents for the Removal of Hydrogen Sulfide from Syngas," *Industrial and Engineering Chemistry Research,* vol. 42, pp. 1688-1697, 2003, doi: 10.1021/ie0208467.

[108] T. Fout, A. Zoelle, D. Keairns, M. Turner, M. Woods, N. Kuehn, V. Shah, V. Chou, and L. Pinkerton, "Cost and Performance Baseline for Fossil Energy Plants Volume 1b: Bituminous Coal (IGCC) to Electricity," vol. 1b, p. 265, 2015, doi: DOE/NETL-2010/1397.

[109] Sulzer. "Mellapak 250Y." https://www.sulzer.com/en/shared/products/mellapak-and-mellapakplus (Accessed 22-Nov-2020).

[110] Koch-Glitsch. "Metal Random Packing." https://www.koch-glitsch.com/Products/Packing-and-Internals/?productcategory=Packing-and-Internals&categoryname=Metal-Random-Packing (Accessed 22-Nov-2019).

[111] C. Wang, M. Perry, F. Seibert, and G. Rochelle, "Packing Characterization for Post Combustion CO_2 Capture: Mass Transfer Model Development," *Energy Procedia,* vol. 63, pp. 1727-1744, 2014, doi: 10.1016/j.egypro.2014.11.180.

[112] J. Gross and G. Sadowski, "Perturbed-Chain SAFT: An Equation of State Based on a Perturbation Theory for Chain Molecules," *Industrial and Engineering Chemistry Research,* vol. 40, pp. 1244-1260, 2001, doi: 10.1021/ie0003887.

[113] J. Gross and G. Sadowski, "Application of The Perturbed-Chain SAFT Equation of State to Associating Systems," *Industrial and Engineering Chemistry Research,* vol. 41, pp. 5510-5515, 2002, doi: 10.1021/ie010954d.

[114] M. Aghaie, N. Rezaei, and S. Zendehboudi, "Assessment of Carbon Dioxide Solubility in Ionic Liquid/Toluene/Water Systems by Extended PR And PC-SAFT EOSs: Carbon Capture Implication," *Journal of Molecular Liquids,* vol. 275, pp. 323-337, 2019, doi: 10.1016/j.molliq.2018.11.038.

[115] A. Tihic, "Group Contribution sPC-SAFT Equation of State," Technical University of Denmark, 2008.

[116] W. D. Seider, J. D. Seader, D. R. Lewin, and S. Widagdo, "Product and process design principles 3rd. edition," ed: JOHN WILEY AND SONS. USA, 2009.

[117] T. R. Brown, "Cost Engineering: Equipment Purchase Cost," *Chemical Engineering,* pp. 51-53, 2019.

[118] "Gas-Liquid Separators Sizing Parameter | Campbell Tip of the Month." http://www.jmcampbell.com/tip-of-the-month/2015/09/gas-liquid-separators-sizing-parameter/ (Accessed 10-Sep-2018).

[119] G. Towler and R. Sinnott, *Chemical Engineering Design. Principles, Practice and Economics of Plant and Process Design*. Elsevier, 2008.

[120] M. S. Peters, K. D. Timmerhaus, and R. E. West, *Plant Design and Economics for Chemical Engineers*, 5th ed. New York: McGraw-Hill Book Company, 2004.

[121] "Economic Indicators," *Chemical Engineering,* pp. 48-49, 2020.

[122]   "4.2 Refrigerators." http://physics.weber.edu/thermal/refrigerators.pdf (Accessed 11-Oct-2018).

[123]   J. O. Valderrama and R. E. Rojas, "Critical Properties of Ionic Liquids. Revisited," *Industrial and Engineering Chemistry Research,* vol. 48, pp. 6890-6900, 2009, doi: 10.1021/ie900250g.

[124]   K. M. Klincewicz and R. C. Reid, "Estimation of Critical Properties with Group Contribution Methods," *AIChE Journal,* vol. 30, pp. 137-142, 1984, doi: 10.1002/aic.690300119.

[125]   D. Tomida, A. Kumagai, K. Qiao, and C. Yokoyama, "Viscosity of [bmim][PF_6] and [bmim][BF_4] at High Pressure," *International Journal of Thermophysics,* vol. 27, pp. 39-47, 2006, doi: 10.1007/s10765-006-0020-y.

[126]   J. Kumełan, Á. Pérez-Salado Kamps, D. Tuma, and G. Maurer, "Solubility of Carbon Dioxide in Liquid Mixtures of Water + [bmim][CH_3SO_4]," *Journal of Chemical and Engineering Data,* vol. 56, pp. 4505-4515, 2011, doi: 10.1021/je200477s.

[127]   D. Matkowska and T. Hofman, "Volumetric Properties of the $\{x_1[C_4mim][MeSO_4]$ + (1 - $X_1)MeOH\}$ System at Temperatures from (283.15 to 333.15) K and Pressures from (0.1 to 35) MPa," *Journal of Solution Chemistry,* vol. 42, pp. 979-990, 2013, doi: 10.1007/s10953-013-0016-8.

[128]   S. Singh, M. Aznar, and N. Deenadayalu, "Densities, Speeds of Sound, and Refractive Indices for Binary Mixtures of 1-butyl-3-Methylimidazolium Methyl Sulphate Ionic Liquid with Alcohols at T = (298.15, 303.15, 308.15, and 313.15) K," *Journal of Chemical Thermodynamics,* vol. 57, pp. 238-247, 2013, doi: 10.1016/j.jct.2012.08.030.

[129]   J. Troncoso, C. A. Cerdeiriña, Y. A. Sanmamed, L. Romaní, and L. P. N. Rebelo, "Thermodynamic Properties of Imidazolium-Based Ionic Liquids: Densities, Heat Capacities, and Enthalpies of Fusion of [bmim][PF_6] and [bmim][NTf_2]," *Journal of Chemical and Engineering Data,* vol. 51, pp. 1856-1859, 2006, doi: 10.1021/je060222y.

[130]   K. R. Harris, M. Kanakubo, and L. A. Woolf, "Temperature and Pressure Dependence of the Viscosity of the Ionic Liquids 1-Hexyl-3-Methylimidazolium Hexafluorophosphate and 1-Butyl-3-Methylimidazolium Bis(trifluoromethylsulfonyl)imide," *Journal of Chemical and Engineering Data,* vol. 52, pp. 1080-1085, 2007, doi: 10.1021/je700032n.

[131] R. L. Gardas, H. F. Costa, M. G. Freire, P. J. Carvalho, I. M. Marrucho, I. M. A. Fonseca, A. G. M. Ferreira, and J. A. P. Coutinho, "Densities and Derived Thermodynamic Properties of Imidazolium-, Pyridinium-, Pyrrolidinium-, and Piperidinium-Based Ionic Liquids," *Journal of Chemical and Engineering Data,* vol. 53, pp. 805-811, 2008, doi: 10.1021/je700670k.

[132] J. Kumełan, D. Tuma, Á. L. P. S. Kamps, and G. Maurer, "Solubility of the Single Gases Carbon Dioxide and Hydrogen in the Ionic Liquid [bmpy][Tf_2N]," *Journal of Chemical and Engineering Data,* vol. 55, pp. 165-172, 2010, doi: 10.1021/je900298e.

[133] M. Shamsipur, A. A. M. Beigi, M. Teymouri, S. M. Pourmortazavi, and M. Irandoust, "Physical and Electrochemical Properties of Ionic Liquids 1-Ethyl-3-Methylimidazolium Tetrafluoroborate, 1-Butyl-3-Methylimidazolium Trifluoromethanesulfonate and 1-Butyl-1-Methylpyrrolidinium Bis(trifluoromethylsulfonyl)imide," *Journal of Molecular Liquids,* vol. 157, pp. 43-50, 2010, doi: 10.1016/j.molliq.2010.08.005.

[134] Y. A. Sanmamed, D. González-Salgado, J. Troncoso, L. Romani, A. Baylaucq, and C. Boned, "Experimental Methodology for Precise Determination of Density of RTILs as a Function of Temperature and Pressure using Vibrating Tube Densimeters," *Journal of Chemical Thermodynamics,* vol. 42, pp. 553-563, 2010, doi: 10.1016/j.jct.2009.11.014.

[135] D. Song and J. Chen, "Density and Viscosity Data for Mixtures of Ionic Liquids with a Common Anion," *Journal of Chemical and Engineering Data,* vol. 59, pp. 257-262, 2014, doi: 10.1021/je400332j.

[136] S. M. Reddy, S. M. Nayeem, K. T. S. S. Raju, and B. Hari Babu, "The Study of Solute–Solvent Interactions in 1-Ethyl-3-Methylimidazolium Tetrafluoroborate + 2-Ethoxyethanol from Density, Speed of Sound, and Refractive Index Measurements," *Journal of Thermal Analysis and Calorimetry,* vol. 124, pp. 959-971, 2016, doi: 10.1007/s10973-015-5205-9.

[137] E. Vercher, F. J. Llopis, V. González-Alfaro, P. J. Miguel, V. Orchillés, and A. Martínez-Andreu, "Volumetric Properties, Viscosities and Refractive Indices of Binary Liquid Mixtures of Tetrafluoroborate-Based Ionic Liquids with Methanol at Several Temperatures," *Journal of Chemical Thermodynamics,* vol. 90, pp. 174-184, 2015, doi: 10.1016/j.jct.2015.06.036.

[138] A. Wandschneider, J. K. Lehmann, and A. Heintz, "Surface Tension and Density of Pure Ionic Liquids and some Binary Mixtures with 1-propanol and 1-butanol," *Journal of Chemical and Engineering Data,* vol. 53, pp. 596-599, 2008, doi: 10.1021/je700621d.

[139] J. Jacquemin, P. Husson, A. A. H. Padua, and V. Majer, "Density and Viscosity of Several Pure and Water-Saturated Ionic Liquids," *Green Chemistry,* vol. 8, pp. 172-180, 2006, doi: 10.1039/b513231b.

[140] M. M. Akbar, F. Chemat, A. Arunagiri, and T. Murugesan, "Density and Excess Properties of N-Methyldiethanolamine (MDEA) with 1-Hexyl-3-Methylimidazolium Tris(pentafluoroethyl)Trifluorophosphate [hmim][FAP]," *Journal of Thermal Analysis and Calorimetry,* vol. 123, pp. 785-791, 2016, doi: 10.1007/s10973-015-4957-6.

[141] J. G. Li, Y. F. Hu, S. Ling, and J. Z. Zhang, "Physicochemical Properties of $[C_6mim][PF_6]$ and $[C_6mim][(C_2F_5)_3PF_3]$ Ionic Liquids," *Journal of Chemical and Engineering Data,* vol. 56, pp. 3068-3072, 2011, doi: 10.1021/je200073x.

[142] M. Součková, J. Klomfar, and J. Pátek, "Temperature Dependence of the Surface Tension and 0.1 MPa Density for $1-C_n$-3-Methylimidazolium Tris(pentafluoroethyl)Trifluorophosphate with n = 2, 4, and 6," *Journal of Chemical Thermodynamics,* vol. 48, pp. 267-275, 2012, doi: 10.1016/j.jct.2011.12.033.

[143] J. Kumełan, Á. Pérez-Salado Kamps, D. Tuma, and G. Maurer, "Solubility of CO_2 in the Ionic Liquid $[hmim][Tf_2N]$," *Journal of Chemical Thermodynamics,* vol. 38, pp. 1396-1401, 2006, doi: 10.1016/j.jct.2006.01.013.

[144] J. Łachwa, P. Morgado, J. M. S. S. Esperança, H. J. R. Guedes, J. N. Canongia Lopes, and L. P. N. Rebelo, "Fluid-Phase Behavior of {1-Hexyl-3-Methylimidazolium Bis(Trifluoromethylsulfonyl) Imide, $[C_6Mim][NTf_2]$, + C_2 -C_8 N-Alcohol} Mixtures: Liquid-Liquid Equilibrium and Excess Volumes," *Journal of Chemical and Engineering Data,* vol. 51, pp. 2215-2221, 2006, doi: 10.1021/je060307z.

[145] H. Tokuda, K. Hayamizu, K. Ishii, M. A. B. H. Susan, and M. Watanabe, "Physicochemical Properties and Structures of Room Temperature Ionic Liquids. 2. Variation of Alkyl Chain Length in Imidazolium Cation," *Journal of Physical Chemistry B,* vol. 109, pp. 6103-6110, 2005, doi: 10.1021/jp044626d.

[146] J. A. Widegren and J. W. Magee, "Density, Viscosity, Speed of Sound, and Electrolytic Conductivity for the Ionic Liquid 1-Hexyl-3-Methylimidazolium Bis(Trifluoromethylsulfonyl)Imide and its Mixtures with Water," *Journal of Chemical and Engineering Data,* vol. 52, pp. 2331-2338, 2007, doi: 10.1021/je700329a.

[147] S. Papović, M. Bešter-Rogač, M. Vraneš, and S. Gadžurić, "The Effect of the Alkyl Chain Length on Physicochemical Features of (Ionic Liquids + γ-Butyrolactone) Binary

Mixtures," *Journal of Chemical Thermodynamics,* vol. 99, pp. 1-10, 2016, doi: 10.1016/j.jct.2016.03.034.

[148]   D. Santos, M. Santos, E. Franceschi, C. Dariva, A. Barison, and S. Mattedi, "Experimental Density of Ionic Liquids and Thermodynamic Modeling with Group Contribution Equation of State Based on the Lattice Fluid Theory," *Journal of Chemical and Engineering Data,* vol. 61, pp. 348-353, 2016, doi: 10.1021/acs.jced.5b00592.

[149]   M. Tariq, A. P. Serro, J. L. Mata, B. Saramago, J. M. S. S. Esperança, J. N. C. Lopes, and L. P. N. Rebelo, "High-Temperature Surface Tension and Density Measurements of 1-Alkyl-3-Methylimidazolium Bistriflamide Ionic Liquids," *Fluid Phase Equilibria,* vol. 294, pp. 131-138, 2010, doi: 10.1016/j.fluid.2010.02.020.

[150]   A. Bennett, S. Lamm, H. Orbey, and S. I. Sandler, "Vapor-Liquid Equilibria of Hydrocarbons and Fuel Oxygenates. 2," *Journal of Chemical and Engineering Data,* vol. 38, pp. 263-269, 1993, doi: 10.1021/je00010a021.

[151]   U. Domańska and J. Łachwa, "Excess Molar Volumes of (Hydrocarbon + Ethyl 1,1-Dimethyl Propyl Ether) at T = (298.15 and 308.15) K," *Journal of Chemical Thermodynamics,* vol. 32, pp. 857-875, 2000, doi: 10.1006/jcht.1999.0652.

[152]   B. N. Kireev, "Determination of the Density of Olefins along the Saturation Line," *Nauchn. Tr.⬜ Kursk. Gos. Pedagog. Inst,* vol. 23, pp. 40-45, 1974.

[153]   M. W. Lister, "Heats of Organic Reactions. X. Heats of Bromination of Cyclic Olefins," *Journal of the American Chemical Society,* vol. 63, pp. 143-149, 1941, doi: 10.1021/ja01846a035.

[154]   D. I. Sagdeev, M. G. Fomina, G. K. Mukhamedzyanov, and I. M. Abdulagatov, "Experimental Study and Correlation Models of the Density and Viscosity of 1-Hexene and 1-Heptene at Temperatures from (298 to 473) K and Pressures up to 245 MPa," *Journal of Chemical and Engineering Data,* vol. 59, pp. 1105-1119, 2014, doi: 10.1021/je401015e.

[155]   A. Ahosseini, B. Sensenich, L. R. Weatherley, and A. M. Scurto, "Phase Equilibrium, Volumetric, and Interfacial Properties of the Ionic Liquid, 1-Hexyl-3-Methylimidazolium Bis(trifluoromethylsulfonyl)amide and 1-Octene," *Journal of Chemical and Engineering Data,* vol. 55, pp. 1611-1617, 2010, doi: 10.1021/je900697w.

[156]   A. Jónasson, M. Savoia, O. Persson, and A. Fredenslund, "Isothermal Vapor–Liquid Equilibrium Data for Ether + Glycol, Chloroalkene + Glycol, Epoxy Ether + Alkane,

Epoxy Ether + Alkene, and Epoxy Ether + Chloroalkane Systems," *Journal of Chemical and Engineering Data,* vol. 39, pp. 134-139, 1994, doi: 10.1021/je00013a038.

[157] R. Reich and V. Sanhueza, "Vapor-Liquid Equilibria for α-Pinene and β-Pinene and for these Pinenes with Heptane, Cyclohexane, 1-Octene and Cyclohexene," *Fluid Phase Equilibria,* vol. 77, pp. 313-325, 1992, doi: 10.1016/0378-3812(92)85111-K.

[158] D. I. Sagdeev, M. G. Fomina, G. K. Mukhamedzyanov, and I. M. Abdulagatov, "Experimental Study of the Density and Viscosity of 1-Octene and 1-Decene at High Temperatures and High Pressures.," *High Temperatures--High Pressures,* vol. 42, 2013.

[159] E. C. Bingham and H. J. Fornwalt, "Chemical Constitution and Association," *Journal of Rheology,* vol. 1, no. 4, pp. 372-417, 1930.

[160] J. W. Moore and R. M. Wellek, "Diffusion Coefficients of N-Heptane and N-Decane in N-Alkanes and N-Alcohols at Several Temperatures," *Journal of Chemical and Engineering data,* vol. 19, no. 2, pp. 136-140, 1974.

[161] D. Sagdeev and G. K. Mukhamedzyanov, "Apparatus for Measuring Density of Liquids and High Parameters," *Teplo-Massoobmen Khim Tekhnol,* vol. 5, p. 21, 1977.

[162] R. D. Chirico, A. Nguyen, W. V. Steele, M. M. Strube, and C. Tsonopoulos, "Vapor Pressure of N-Alkanes Revisited. New High-Precision Vapor Pressure Data on N-Decane, N-Eicosane, and N-Octacosane," *Journal of Chemical and Engineering Data,* vol. 34, pp. 149-156, 1989, doi: 10.1021/je00056a002.

[163] D. W. Scott and A. G. Osborn, "Representation of Vapor Pressure Data," *Journal of Physical Chemistry,* vol. 83, pp. 2714-2723, 1979.

[164] E. G. Linder, "Vapor Pressures of Some Hydrocarbons," *Journal of Physical Chemistry,* vol. 35, pp. 531-535, 1931, doi: 10.1021/j150320a010.

[165] E. Morawetz, S. Sunner, and Ö. Wiberg, "Design, Construction, and Testing of a Heat of Vaporization Calorimeter useful in the Vapor Pressure Range 1 to 0.01 mm Hg at 25 degrees C.," *Acta Chemica Scandinavica,* vol. 17, pp. 473-488, 1963, doi: 10.3891/acta.chem.scand.17-0473.

[166] T. E. Thorpe, "On the Relation Between the Molecular Weights of Substances and their Specific Gravities in the Liquid State," *Journal of the Chemical Society,* vol. 37, no. 141, 1880.

[167] H. Landolt and H. Jahn, "The Molecular Refraction of Several Simple Organic Compounds for Rays of Infinitely Great Wave Length," *Z. Phys. Chem., Stoechiom. Verwandschaftsl,* vol. 10, pp. 289-297, 1892.

[168] S. Young, "CIV.—Vapour Pressures, Specific Volumes, and Critical Constants of Normal Octane," *Journal of the Chemical Society, Transactions,* 10.1039/CT9007701145 vol. 77, no. 0, pp. 1145-1151, 1900, doi: 10.1039/CT9007701145.

[169] R. Anonymous, "Properties of Hydrocarbon of High Molecular Wieght," *American Petroleum Institute Research Project, Penn. State Univ.,* vol. 42, 1968.

[170] J. M. P. Regueiro, "Propiedades Termodinamicas de Mezclas Binarias: Carbonato de Dualquilo+ Hidrocarburo," Universidade de Vigo, 1999.

[171] M. Iwahashi, Y. Yamaguchi, Y. Ogura, and M. Suzuki, "Dynamical Structures of Normal Alkanes, Alcohols, and Fatty Acids in the Liquid State as Determined by Viscosity, Self-Diffusion Coefficient, Infrared Spectra, and 13CNMR Spin-Lattice Relaxation Time Measurements," *Bulletin of the Chemical Society of Japan,* vol. 63, no. 8, pp. 2154-2158, 1990.

[172] J. L. Valencia, D. González-Salgado, J. Troncoso, J. Peleteiro, E. Carballo, and L. Romaní, "Thermophysical Characterization of Liquids using Precise Density and Isobaric Heat Capacity Measurements as a Function of Pressure," *Journal of Chemical and Engineering Data,* vol. 54, pp. 904-915, 2009, doi: 10.1021/je8006875.

[173] T. M. Aminabhavi and G. Bindu, "Densities, Viscosities, Refractive Indices, and Speeds of Sound of the Binary Mixtures of Bis (2-methoxyethyl) Ether with Nonane, Decane, Dodecane, Tetradecane, and Hexadecane at 298.15, 308.15, and 318.15 K," *Journal of Chemical and Engineering Data,* vol. 39, no. 3, pp. 529-534, 1994.

[174] I. Mokbel, A. Blondel-Telouk, D. Vellut, and J. Jose, "Vapor-Liquid Equilibria of Two Binary Mixtures: Benzene + N-Tetradecane and Benzene + Squalane," *Fluid Phase Equilibria,* vol. 149, pp. 287-308, 1998, doi: 10.1016/S0378-3812(98)00271-4.

[175] S. C. Bhatia, R. Bhatia, and G. P. Dubey, "Densities, Excess Molar Volumes, Ultrasonic Speeds, and Isentropic Compressibilities of Hexan-1-ol with 1,2-Dichloroethane, 1,2-

Dibromoethane, and 1,1,2,2-Tetrachloroethene at (293.15 and 298.15) K," *International Journal of Thermophysics,* vol. 31, pp. 2119-2146, 2010, doi: 10.1007/s10765-010-0874-x.

[176] M. Čenský, V. Roháč, K. Růžička, M. Fulem, and K. Aim, "Vapor Pressure of Selected Aliphatic Alcohols by Ebulliometry. Part 1," *Fluid Phase Equilibria,* vol. 298, pp. 192-198, 2010, doi: 10.1016/j.fluid.2010.06.019.

[177] M. Chorzewski, M. Dzida, E. Zorębski, and M. Zorębski, "Density, Speed of Sound, Heat Capacity, and Related Properties of 1-Hexanol and 2-Ethyl-1-Butanol as Function of Temperature and Pressure," *Journal of Chemical Thermodynamics,* vol. 58, pp. 389-397, 2013, doi: 10.1016/j.jct.2012.09.027.

[178] K. N. Das, M. Habibullah, I. M. M. Rahman, H. Hasegawa, M. A. Uddin, and K. Saifuddin, "Thermodynamic Properties of the Binary Mixture of Hexan-1-ol with m-Xylene at T =(303.15, 313.15, and 323.15) K," *Journal of Chemical and Engineering Data,* vol. 54, pp. 3300-3302, 2009, doi: 10.1021/je900219w.

[179] M. J. Dávila, R. Alcalde, M. Atilhan, and S. Aparicio, "PρT Measurements and Derived Properties of Liquid 1-Alkanols," *Journal of Chemical Thermodynamics,* vol. 47, pp. 241-259, 2012, doi: 10.1016/j.jct.2011.10.023.

[180] P. Gierycz, A. Kosowski, and R. Swietlik, "Vapor-Liquid Equilibria in Binary Systems Formed by Cyclohexane with Alcohols," *Journal of Chemical and Engineering Data,* vol. 54, pp. 2996-3001, 2009, doi: 10.1021/je900050z.

[181] J. N. Guimbi, H. Kasehgari, I. Mokbel, and J. Jose, "Vapor-Pressures of Primary Alcohols in a Range From 0.3 Pa to 1.15 kPa," *Thermochimica Acta,* vol. 196, pp. 367-377, 1992.

[182] V. D. Lieben and G. Janecek, "Standard Hexyl Alcohol and Standard Heptanoic Acid," *Justus Liebigs Ann. Chem,* vol. 187, pp. 126-152, 1877.

[183] P. T. Ngema, D. Matkowska, P. Naidoo, T. Hofman, and D. Ramjugernath, "Vapor−Liquid Equilibrium Data for Binary Systems of
1-Methyl-4-(1-methylethenyl)-cyclohexene + {Ethanol, Propan-1-ol,
Propan-2-ol, Butan-1-ol, Pentan-1-ol, or Hexan-1-ol} at 40 kPa," *Journal of Chemical and Engineering Data,* vol. 57, pp. 2053-2058, 2012, doi: dx.doi.org/10.1021/je300347z.

[184] K. S. Reddy, A. V. N. Swamy, T. E. V. Prasad, and D. H. L. Prasad, "Vapor-Liquid Equilibria of Binary Mixtures Formed by Hexan-1-ol with Chloroethanes and

Chloroethenes at 95.6 kPa," *Journal of Chemical and Engineering Data,* vol. 55, pp. 2073-2076, 2010, doi: 10.1021/je9000608.

[185]   H. Djojoputro and S. Ismadji, "Density and Viscosity of Several Aldehydes Fragrance Compounds in their Binary Mixtures with Ethanol at 298.15 K, 308.15 K, and 318.15 K," *Journal of Chemical and Engineering Data,* vol. 50, pp. 2003-2007, 2005, doi: 10.1021/je0502344.

[186]   A. H. Uhl, "Non-Heptane Constituents of Digger Pine (Pinussabinana)," *The Journal of the American Pharmaceutical Association (1912),* vol. 24, pp. 380-382, 1935.

[187]   S. P. Verevkin, E. L. Krasnykh, T. V. Vasiltsova, B. Koutek, J. Doubsky, and A. Heintz, "Vapor Pressures and Enthalpies of Vaporization of a Series of the Linear Aliphatic Aldehydes," *Fluid Phase Equilibria,* vol. 206, pp. 331-339, 2003, doi: 10.1016/S0378-3812(03)00035-9.

[188]   S. P. Verevkin, T. V. Vasiltsova, E. Bich, and A. Heintz, "Thermodynamic Properties of Mixtures Containing Ionic Liquids: Activity Coefficients of Aldehydes and Ketones in 1-Methyl-3-Ethyl-Imidazolium Bis(trifluoromethyl-sulfonyl) imide using the Transpiration Method," *Fluid Phase Equilibria,* vol. 218, pp. 165-175, 2004, doi: 10.1016/j.fluid.2003.12.005.

[189]   M. Stoll and A. Rouve, "Secondary Reactions in the Ozonolysis of an Ethylenic Linkage," *Helv. Chim. Acta,* vol. 27, p. 950, 1944.

[190]   C. Coquelet, A. Valtz, D. Richon, and J. C. de la Fuente, "Volumetric Properties of the Boldine + Alcohol Mixtures at Atmospheric Pressure from 283.15 to 333.15 K. A New Method for the Determination of the Density of Pure Boldine," *Fluid Phase Equilibria,* vol. 259, pp. 33-38, 2007, doi: 10.1016/j.fluid.2007.04.030.

[191]   R. R. Dreisbach and S. A. Shrader, "Vapor Pressure–Temperature Data on Some Organic Compounds," *Industrial and Engineering Chemistry,* vol. 41, pp. 2879-2880, 1949, doi: 10.1021/ie50480a054.

[192]   R. Garriga, S. Martínez, P. Pérez, and M. Gracia, "Isothermal Vapour-Liquid Equilibrium at Several Temperatures and Excess Functions at 298.15 K of Butanone with 2-Methyl-1-Propanol or 2-Methyl-2-Propanol," *Fluid Phase Equilibria,* vol. 149, pp. 111-120, 1998, doi: 10.1016/S0378-3812(98)00316-1.

[193] D. Kulikov, S. P. Verevkin, and A. Heintz, "Enthalpies of Vaporization of a Series of Aliphatic Alcohols. Experimental Results and Values Predicted by the ERAS-Model," *Fluid Phase Equilibria,* vol. 192, pp. 187-207, 2001, doi: 10.1016/S0378-3812(01)00633-1.

[194] M. A. Saleh, S. Akhtar, S. Begum, M. S. Ahmed, and S. K. Begum, "Density and Viscosity of 1-Alkanols," *Physics and Chemistry of Liquids,* vol. 42, pp. 615-623, 2004.

[195] C. P. Smyth and W. N. Stoops, "The Dielectric Polarization of Liquids VI. Ethyl Iodide, Ethanol, Normal-Butanol and Normal Octanol," *Journal of the American Chemical Society,* vol. 51, pp. 3312-3329, 1929.

[196] J. L. Trenzado, J. S. Matos, and R. Alcalde, "Volumetric Properties and Viscosities of the Methyl Butanoate + Heptane + 1-Octanol Ternary System and its Binary Constituents in the Temperature Range from 283.15 to 313.15 K," *Fluid Phase Equilibria,* vol. 205, pp. 171-192, 2003, doi: 10.1016/S0378-3812(02)00274-1.

[197] E. Zorębski and A. Przybyła, "Volume Effects for Binary Mixtures of Propane-1,2-diol with Methanol, Propan-1-ol, Hexan-1-ol, Octan-1-ol, or Nonan-1-ol at Temperatures (293.15 to 318.15) K," *Journal of Chemical Thermodynamics,* vol. 59, pp. 127-134, 2013, doi: 10.1016/j.jct.2012.12.003.

[198] H. F. Costa, R. L. Gardas, I. Johnson, I. M. A. Fonseca, and A. G. M. Ferreira, "PVT Property Measurements for Ethyl Propionate, Ethyl Butyrate, and Ethyl Pentanoate Esters from (298 to 393) K and up to 35 MPa," *Journal of Chemical and Engineering Data,* vol. 54, pp. 256-262, 2009, doi: 10.1021/je800251v.

[199] R. Gartenmeister, "Investigation of the Physical Characteristics of Liquid Compounds: VI Boiling Point and Specific Volume of Normal Fatty Acid Esters," *Justus Liebigs Ann. Chem,* vol. 233, pp. 249-315, 1886.

[200] S. A. Karpushina, M. T. Khimenko, and Y. N. Surov, "Density, Refractive Index, and Dielectric Permeability of a Series of Complex Esters as Pure Liquids," *Zh. Fiz. Khim.,* vol. 64, p. 368, 1990.

[201] E. Lladosa, J. B. Montón, M. Cruz Burguet, and R. Muñoz, "Phase Equilibrium for the Esterification Reaction of Acetic Acid + Butan-1-ol at 101.3 kPa," *Journal of Chemical and Engineering Data,* vol. 53, pp. 108-115, 2008, doi: 10.1021/je700411p.

[202] N. I. Malek, A. Singh, R. Surati, and S. P. Ijardar, "Study on Thermo Physical and Excess Molar Properties of Binary Systems of Ionic Liquids. I: [$C_n$mim][PF_6] (n = 6, 8) and Alkyl Acetates," *Journal of Chemical Thermodynamics,* vol. 74, pp. 103-118, 2014, doi: 10.1016/j.jct.2014.01.012.

[203] R. J. McDougal, L. V. Jasperson, and G. M. Wilson, "Vapor-Liquid Equilibrium for Several Compounds Relevant to the Biofuels Industry Modeled with the Wilson Equation," *Journal of Chemical and Engineering Data,* vol. 59, pp. 1069-1085, 2014, doi: 10.1021/je400885z.

[204] J. Timmermans and M. Hennaut-Roland, "Work of the International Bureau of Physico-Chemical Properties Physical Constants of Twenty Organic Compounds," *J. Chim. Phys. Phys.-Chim. Biol,* vol. 56, pp. 984-1023, 1959.

[205] B. F. de Almeida, T. M. Waldrigui, T. d. C. Alves, L. H. de Oliveira, and M. Aznar, "Experimental and Calculated Liquid-Liquid Equilibrium Data for Water+Furfural+Solvents," *Fluid Phase Equilibria,* vol. 334, pp. 97-105, 2012, doi: 10.1016/j.fluid.2012.07.032.

[206] V. Dohnal and K. Řehák, "Thermal and Volumetric Properties of Four Aqueous Aroma Compounds at Infinite Dilution," *Journal of Chemical and Engineering Data,* vol. 57, pp. 1822-1828, 2012, doi: 10.1021/je300280s.

[207] L. Fernández, J. Ortega, E. Pérez, F. Toledo, and J. Canosa, "Multiproperty Correlation of Experimental Data of the Binaries Propyl Ethanoate + Alkanes (Pentane to Decane). New Experimental Information for Vapor-Liquid Equilibrium and Mixing Properties," *Journal of Chemical and Engineering Data,* vol. 58, pp. 686-706, 2013, doi: 10.1021/je3011979.

[208] G. W. A. Kahlbaum, "The Dependence of Boiling Temperature on the Atmospheric Pressure," *Ber. Dtsch. Chem. Ges,* vol. 17, pp. 1245-1262, 1884.

[209] S. Young, "The Vapour-Pressures, Specific Volumes, Heats of Vaporization, and Critical Constants of Thirty Pure Substances," *Sci. Proc. R. Dublin Soc.,* vol. 12, p. 374, 1910.

[210] M. Basu, T. Samanta, and D. Das, "Volumetric and compressibility studies on tri-n-butyl phosphate (TBP)-phase modifier (1-octanol, 1-decanol and isodecanol) interactions from T = (298.15 to 323.15) K," *Journal of Chemical Thermodynamics,* vol. 70, pp. 1-12, 2014, doi: 10.1016/j.jct.2013.10.018.

[211] L. De Lorenzi, M. Fermeglia, and G. Torriano, "Density, Refractive Index, and Kinematic Viscosity of Diesters and Triesters," *Journal of Chemical and Engineering Data,* vol. 42, pp. 919-923, 1997, doi: 10.1021/je970036f.

[212] G. H. Hártel, "Low-Volatility Polar Organic Solvents for Sulfur Dioxide, Hydrogen Sulfide, and Carbonyl Sulfide," *Journal of Chemical and Engineering Data,* vol. 30, pp. 57-61, 1985.

[213] K. Panneerselvam, M. P. Antony, T. G. Srinivasan, and P. R. Vasudeva Rao, "Estimation of Normal Boiling Points of Trialkyl Phosphates using Retention Indices by Gas Chromatography," *Thermochimica Acta,* vol. 511, pp. 107-111, 2010, doi: 10.1016/j.tca.2010.07.032.

[214] W. G. Skene and M. E. Krzymien, "Vapor Pressure of Tri-N-butyl Phosphate," *Journal of Chemical and Engineering Data,* vol. 40, pp. 394-397, 1995.

[215] N. Swain, D. Panda, S. K. Singh, and V. J. Chakravortty, "Viscosity and Density of Tri- N -butyl Phosphate + Benzene + O -Xylene from 30 ° C to 45 ° C," *Journal of Chemical and Engineering Data,* vol. 42, pp. 1235-1237, 1997.

[216] B. B. Breman, A. A. C. M. Beenackers, E. W. J. Rietjens, and R. J. H. Stege, "Gas-Liquid Solubilities of Carbon Monoxide, Carbon Dioxide,Hydrogen, Water, 1-Alcohols (1 ≤ n ≤ 6), and N-Paraffins (2 ≤ n ≤ 6) in Hexadecane, Octacosane, 1-Hexadecanol, Phenanthrene, and Tetraethylene Glycol at Pressures up to 5.5 MPa and Temperatures from 293 to 553 K," *Journal of Chemical and Engineering Data,* vol. 39, pp. 647-666, 1994, doi: 10.1021/je00016a004.

[217] X. Cui, G. Chen, and X. Han, "Experimental Vapor Pressure Data and a Vapor Pressure Equation for N,N-Dimethylformamide," *Journal of Chemical and Engineering Data,* vol. 51, pp. 1860-1861, 2006, doi: 10.1021/je060224i.

[218] S. Gadžurić, A. Tot, N. Zec, S. Papović, and M. Vraneš, "Volumetric Properties of Binary Mixtures of 1-Butyl-1-Methylpyrrolidinium Tris(pentafluoroethyl)trifluorophosphate with N -Methylformamide, N -Ethylformamide, N, N -Dimethylformamide, N, N - Dibutylformamide, and N, N -Dimethylacetamide from (293.15 to 323.15) K," *Journal of Chemical and Engineering Data,* vol. 59, pp. 1225-1231, 2014, doi: 10.1021/je400803f.

[219] H. Kahl, T. Wadewitz, and J. Winkelmann, "Surface Tension of Pure Liquids and Binary Liquid Mixtures," *Journal of Chemical and Engineering Data,* vol. 48, pp. 580-586, 2003, doi: 10.1021/je0201323.

[220] W. M. Melzer, F. Schrodter, and H. Knapp, "Solubilities of Methane, Propane and Carbon Dioxide in Solvent Mixtures Consisting of Water, N,N-DimethylFormamide, and N-Methy-2-Pyrrolidone," *Fluid Phase Equilibria,* vol. 49, pp. 167-186, 1989.

[221] K. Quitzsch, S. D, and G. Geiseler, "Thermodynamics of Binary Liquid Mixtures with Homologous Formamides. 8. Binary systems Normal-Heptane (1)-Dimethylformamide (2) and Normal-heptane (1)-Diethylformamide (2)," *Zeitschrift Fur Physikalische Chemie-Leipzig,* vol. 240, p. 107, 1969.

[222] V. E. Bogoslov, G. I. Mikhalyuk, and A. I. Shamolin, "Vapor-Liquid Equilibrium in Water Dimethyl Acetamide, Water Dimethyl Formamide, Water Normal Methyl Pyrrolidone Systems," *Zhurnal Prikladnoi Khimii,* vol. 45, p. 1154, 1972.

[223] X. J. Yan, S. N. Li, Q. G. Zhai, Y. C. Jiang, and M. C. Hu, "Physicochemical Properties for the Binary Systems of Ionic Liquids $[C_n mim]Cl + N, N$ -Dimethylformamide," *Journal of Chemical and Engineering Data,* vol. 59, pp. 1411-1422, 2014, doi: 10.1021/je4009238.

[224] P. Haimi, P. Uusi-Kyyny, J. P. Pokki, and V. Alopaeus, "Phase Equilibrium Measurements for Systems Containing Propanenitrile with Tert-Butyl Ethyl Ether and C_4-Hydrocarbons," *Fluid Phase Equilibria,* vol. 299, pp. 148-160, 2010, doi: 10.1016/j.fluid.2010.09.023.

[225] G. Milazzo, "The Measurement of Small Vapor Pressure," *Chem.-Ing.-Tech.,* vol. 28, p. 646, 1956.

[226] K. Rajagopal and S. Chenthilnath, "Molecular Interaction Studies and Theoretical Estimation of Ultrasonic Speeds using Scaled Particle Theory in Binary Mixtures of Toluene with Homologous Nitriles at Different Temperatures," *Thermochimica Acta,* vol. 498, pp. 45-53, 2010, doi: 10.1016/j.tca.2009.10.001.

[227] K. Rajagopal and S. Chenthilnath, "Excess Parameter Studies on Binary Liquid Mixtures of 2-Methyl-2-Propanol with Aliphatic Nitriles at Different Temperatures," *Journal of Molecular Liquids,* vol. 160, pp. 72-80, 2011, doi: 10.1016/j.molliq.2011.02.009.

[228] M. Sohda, Y. OIwai, Y. Arai, A. Sakoguchi, R. Ueoka, and Y. Kato, "Vapor Pressures of Cis- and Trans-Decalins," *Netsu Sokutei,* vol. 17, no. 3, pp. 131-133, 1990.

[229] H. Chi, G. Li, Y. Guo, L. Xu, and W. Fang, "Excess Molar Volume along with Viscosity, Flash Point, and Refractive Index for Binary Mixtures of Cis-Decalin or Trans-Decalin with C_9 to C_{11} N-Alkanes," *Journal of Chemical and Engineering Data,* vol. 58, pp. 2224-2232, 2013, doi: 10.1021/je400250u.

225

[230] A. Gupta, S. Gupta, F. R. Groves, and E. McLaughlin, "Measurement of Vapor-Liquid Equilibrium for Binary Systems Containing Polynuclear Aromatic Compounds," *Fluid Phase Equilibria,* vol. 65, pp. 305-326, 1991, doi: 10.1016/0378-3812(91)87032-5.

[231] D. L. Hogenboom, W. Webb, and J. A. Dixon, "Viscosity of Several Liquid Hydrocarbons as a Function of Temperature, Pressure, and Free Volume," *The Journal of Chemical Physics,* vol. 46, pp. 2586-2598, 1967, doi: 10.1063/1.1841088.

[232] N. G. Tsierkezos, I. E. Molinou, and G. A. Polizos, "Relative Permittivities, Speeds of Sound, Viscosities, and Densities of Cyclohexanone + Cis-Decalin and Cyclohexanone + Trans-Decalin Mixtures at 283.15, 293.15, and 303.15 K," *Journal of Chemical and Engineering Data,* vol. 47, pp. 1492-1495, 2002, doi: 10.1021/je020084m.

[233] C. K. Zéberg-Mikkelsen, A. Baylaucq, M. Barrouhou, and C. Boned, "The Effect of Stereoisomerism on Dynamic Viscosity: A Study of Cis-Decalin and Trans-Decalin Versus Pressure and Temperature," *Physical Chemistry Chemical Physics,* vol. 5, pp. 1547-1551, 2003, doi: 10.1039/b301202f.

[234] J. T. Chen, I. M. Shiah, and H. P. Chu, "Excess Molar Volumes and Viscosities for Binary Mixtures of Propylene Glycol Monomethyl Ether with Methacrylic Acid, Benzyl Methacrylate, and 2-Hydroxyethyl Methacrylate at (298.15, 308.15, and 318.15) K," *Journal of Chemical and Engineering Data,* vol. 51, pp. 2156-2160, 2006, doi: 10.1021/je060288t.

[235] D. Dragoescu, A. Barhala, and M. Teodorescu, "Vapour Pressure and Excess Gibbs Energy of Binary 1,2-Dichloroethane + Cyclohexanone, Chloroform + Cyclopentanone and Chloroform + Cyclohexanone Mixtures at Temperatures from 298.15 to 318.15 K," *Fluid Phase Equilibria,* vol. 267, pp. 70-78, 2008, doi: 10.1016/j.fluid.2008.02.018.

[236] D. Dragoescu, A. Barhala, and M. Teodorescu, "(Vapour + Liquid) Equilibria and Excess Gibbs Free Energies of (Cyclohexanone + 1-Chlorobutane and + 1,1,1-Trichloroethane) Binary Mixtures at Temperatures from (298.15 to 318.15) K," *Journal of Chemical Thermodynamics,* vol. 41, pp. 1025-1029, 2009, doi: 10.1016/j.jct.2009.04.006.

[237] H. R. Rafiee, S. Ranjbar, and F. Poursalman, "Densities and Viscosities of Binary and Ternary Mixtures of Cyclohexanone, 1,4-Dioxane and Isooctane from T = (288.15 to 313.15) K," *Journal of Chemical Thermodynamics,* vol. 54, pp. 266-271, 2012, doi: 10.1016/j.jct.2012.05.005.

[238] W. Herz and W. Bloch, "Physical-Chemical Investigation of Compounds of the Cyclohexane Series," *Z. Phys. Chem., Stoechiom. Verwandschaftsl,* vol. 110, pp. 23-39, 1924.

[239] D. R. Caudwell, J. P. M. Trusler, V. Vesovic, and W. A. Wakeham, "Viscosity and Density of Five Hydrocarbon Liquids at Pressures up to 200 MPa and Temperatures up to 473 K," *Journal of Chemical and Engineering Data,* vol. 54, pp. 359-366, 2009, doi: 10.1021/je1008137.

[240] C.-h. Lee, D. M. Dempsey, R. S. Mohamed, and G. D. Holder, "Vapor-Liquid Equilibria in the Systems of N -Decane/Tetralin,
N-Hexadecane/Tetralin, -Decane/1-Methylnaphthalene, and
1-Methylnaphthalene/Tetralin," *Journal of Chemical and Engineering Data,* vol. 37, pp. 183-186, 1992.

[241] S. P. Verevkin, "Vapor Pressures and Enthalpies of Vaporization of a Series of 1- and 2-Halogenated Naphthalenes," *Journal of Chemical Thermodynamics,* vol. 35, pp. 1237-1251, 2003, doi: 10.1016/S0021-9614(03)00051-X.

[242] I. Mokbel, T. Guetachew, and J. Jose, "Vapor Pressures and Sublimation Pressures of 14 Polycyclic Aromatic Hydrocarbons (C_{11}-C_{18}) at Pressures in the Range from 0.5 Pa to 30 kPa," *ElData:The International Electronic Journal of Physico-Chemical Data,* vol. 2, pp. 167-180, 1995.

[243] R. Anonymous, *American Petroleum Institute Research Project 6, Carnegie-Mellon Univ.,* 1952.

[244] A. M. A. Al-Mashhadani and A. M. Awwad, "Excess Molar Volumes of an Aromatic Hydrocarbon + N-MethylPyrrolidone at 298.15 K," *Thermochimica Acta,* vol. 89, pp. 75-80, 1985.

[245] G. Guarino, O. Ortona, R. Sartorio, and V. Vitagliano, "Diffusion, Viscosity, and Refractivity Data on the Systems Dimethylformamide—Water and N-Methylpyrrolidone—Water at 5 °C," *Journal of Chemical and Engineering Data,* vol. 30, pp. 366-368, 1985, doi: 10.1021/je00041a039.

[246] A. V. Anantaraman, "Thermodynamics of Solvent Mixtures. I. Density and Viscosity of Binary Mixtures Of N -Methylpyrrolidinone – Tetrahydrofuran and Propylene Carbonate – Acetonitrile," *Canadian Journal of Chemistry,* vol. 64, pp. 46-50, 1986, doi: 10.1139/v87-078.

[247] J. R. Langan and G. A. Salmon, "Physical Properties of N-Methylpyrrolidinone as Functions of Temperature," *Journal of Chemical and Engineering Data,* vol. 32, pp. 420-422, 1987, doi: 10.1021/je00050a009.

[248] A. Henni, J. J. Hromek, P. Tontiwachwuthikul, and A. Chakma, "Volumetric Properties and Viscosities for Aqueous N-Methyl-2-Pyrrolidone Solutions from 25°C to 70°C," *Journal of Chemical and Engineering Data,* vol. 49, pp. 231-234, 2004, doi: 10.1021/je034073k.

[249] J. Águila-Hernández, A. Trejo, B. E. García-Flores, and R. Molnar, "Viscometric and Volumetric Behaviour of Binary Mixtures of Sulfolane and N-Methylpyrrolidone with Monoethanolamine and Diethanolamine in the Range 303-373 K," *Fluid Phase Equilibria,* vol. 267, pp. 172-180, 2008, doi: 10.1016/j.fluid.2008.02.023.

[250] K. R. Reddy, D. B. K. Kumar, G. S. Rao, P. Anila, and C. Rambabu, "Densities, Viscosities, Sound Speed, and IR Studies of N-Methyl-2- Pyrrolidone with Cyclohexylamine, Cyclohexanol, and Cyclohexene at Different Temperatures," *Thermochimica Acta,* vol. 590, pp. 116-126, 2014, doi: 10.1016/j.tca.2014.06.026.

[251] R. Hirawan, S. Sinha, S. A. Iwarere, J. D. Raal, P. Naidoo, and D. Ramjugernath, "Vapor-Liquid Equilibrium Data for 1-Methyl-2-Pyrrolidone + (1-Butanol Or 1-Hexene Or Water) Binary Mixtures," *Journal of Chemical and Engineering Data,* vol. 59, pp. 1643-1650, 2014, doi: 10.1021/je500092v.

[252] K. Chyliński, Z. Fraś, and S. K. Malanowski, "Vapor-Liquid Equilibrium for Propylene Glycol + 2-(2-Hexyloxyethoxy)Ethanol And 1-Methyl-2-Pyrrolidone + 1-Methoxypropan-2-ol," *Journal of Chemical and Engineering Data,* vol. 49, pp. 18-23, 2004, doi: 10.1021/je034096z.

[253] B. Blanco, S. Beltrán, J. L. Cabezas, and J. Coca, " Phase Equilibria of Binary Systems Formed by Hydrocarbons from Petroleum Fractions and the Solvents N - Methylpyrrolidone and N , N -Dimethylformamide. 1. Isobaric Vapor−Liquid Equilibria " *Journal of Chemical and Engineering Data,* vol. 42, pp. 938-942, 2002, doi: 10.1021/je970059u.

[254] K. Fischer and J. Gmehling, "Vapour-Liquid Equilibra and Heats of Mixing for Mixtures of N-Methyl Pyrrolidone-2 with C_5 or C_6 Hydrocarbons and for Hydrocarbon Mixtures," *Fluid Phase Equilibria,* vol. 119, pp. 113-130, 1996.

[255] J. K. Choi and M. J. Joncich, "Heats of Combustion, Heats of Formation and Vapor Pressures of Some Organic Carbonates Estimation of Carbonate Group Contribution to

Heat of Formation," *Journal of Chemical and Engineering Data,* vol. 16, pp. 87-90, 1971, doi: 10.1021/je60048a026.

[256] I. G. Gurevich, K. B. Gisina, V. K. Shitnikov, V. S. Dubasova, and V. L. Nikonov, "Viscosity and Density of Aproton Solvents and Electrolytes on their Bases," *Inzh.-Fiz. Zh.,* vol. 52, pp. 422-427, 1982.

[257] J. Pires, L. Timperman, J. Jacquemin, A. Balducci, and M. Anouti, "Density, Conductivity, Viscosity, and Excess Properties of (Pyrrolidinium Nitrate-Based Protic Ionic Liquid + Propylene Carbonate) Binary Mixture," *Journal of Chemical Thermodynamics,* vol. 59, pp. 10-19, 2013, doi: 10.1016/j.jct.2012.11.020.

[258] S. P. Verevkin, A. V. Toktonov, Y. Chernyak, B. Schäffner, and A. Börner, "Vapour Pressure and Enthalpy of Vaporization of Cyclic Alkylene Carbonates," *Fluid Phase Equilibria,* vol. 268, pp. 1-6, 2008, doi: 10.1016/j.fluid.2008.03.013.

[259] M. Vraneš, N. Zec, A. Tot, S. Papović, S. Dožić, and S. Gadžurić, "Density, Electrical Conductivity, Viscosity and Excess Properties of 1-Butyl-3-Methylimidazolium Bis(trifluoromethylsulfonyl)imide + Propylene Carbonate Binary Mixtures," *Journal of Chemical Thermodynamics,* vol. 68, pp. 98-108, 2014, doi: 10.1016/j.jct.2013.08.034.

[260] D. S. Wankhede, M. K. Lande, and B. R. Arbad, "Densities and Viscosities of Binary Mixtures of Paraldehyde + Propylene Carbonate at (288.15, 293.15, 298.15, 303.15, and 308.15) K," *Journal of Chemical and Engineering Data,* vol. 50, pp. 261-263, 2005, doi: 10.1021/je0496903.

[261] R. L. Thompson, J. Culp, S. P. Tiwari, O. Basha, W. Shi, K. Damodaran, K. Resnik, N. Siefert, and D. Hopkinson, "Effect of Molecular Structure on the CO_2 Separation Properties of Hydrophobic Solvents Consisting of Grafted Poly Ethylene Glycol and Poly Dimethylsiloxane Units," *Energy and Fuels,* vol. 33, pp. 4432-4441, 2019, doi: 10.1021/acs.energyfuels.9b00500.

[262] C. H. Meyers, "The Specific Volume of Superheated Ammonia Vapor," *Refrigerating Engineering,* vol. 11, pp. 345-350, 1925.

[263] I. Nagata, "Isobaric Vapor-Liquid Equilibria for the Ternary System Chloroform-Methanol-Ethyl Acetate," *Journal of Chemical and Engineering Data,* vol. 7, pp. 367-373, 1962, doi: 10.1021/je60014a013.

[264] O. Osada, M. Sato, and M. Uematsu, "Thermodynamic Properties of {xCH3OH + (1-x)H2O} with x = (1.0000 and 0.4993) in the Temperature Range from 320 K to 420 K at Pressures Up To 200 MPa," *Journal of Chemical Thermodynamics,* vol. 31, pp. 451-463, 1999.

[265] N. G. Polikhronidi, L. M. Radzhabova, A. R. Rasulov, and G. V. Stepanov, "Isochoric Heat Capacity and Coexistence Curve of Methyl Alcohol in the Neighborhood of The Critical Point," *High Temperature,* vol. 44, pp. 507-512, 2006, doi: 10.1007/s10740-006-0063-6.

[266] M. García-Mardones, I. Gascón, M. C. López, F. M. Royo, and C. Lafuente, "Viscosimetric Study of Binary Mixtures Containing Pyridinium-Based Ionic Liquids and Alkanols," *Journal of Chemical and Engineering Data,* vol. 57, pp. 3549-3556, 2012, doi: 10.1021/je300557g.

[267] V. G. Komarenko, V. G. Manzhelii, and A. V. Radtsig, "Density and Viscosity of Normal Alcohols at Low Temperatures," *Ukr. Fiz. Zh.(Ukr. Ed.),* vol. 12, p. 676, 1967.

[268] T. W. Yergovich, G. W. Swift, and F. Kurata, "Density and Viscosity of Aqueous Solutions of Methanol and Acetone from the Freezing Point to 10°C," *Journal of Chemical and Engineering Data,* vol. 16, pp. 222-226, 1971, doi: 10.1021/je60049a004.

[269] F. M. Jaeger, "Uber der Temperaturabhangigkeit der Molekularen Fteien Oberiliichenenergie Von Flussigkeiten Im Temperaturbereich Von - 80 Bis + 1650° C.," *Zeitschrift für Anorganische und Allgemeine Chemie,* vol. 101, pp. 1-214, 1917.

[270] F. E. Mckenna, H. V. Tartar, and E. C. Lingafelter, "Studies of Hemiacetal Formation in Alcohol-Aldehyde Systems. II. Refraction Studies," *Journal of the American Chemical Society,* vol. 75, pp. 604-607, 1953, doi: 10.1021/ja01099a024.

[271] T. F. Sun, J. A. Schouten, N. J. Trappeniers, and S. N. Biswas, "Measurements of The Densities of Liquid Benzene, Cyclohexane, Methanol, and Ethanol as Functions of Temperature at 0.1 Mpa," *The Journal of Chemical Thermodynamics,* vol. 20, pp. 1089-1096, 1988.

[272] G. A. Miller, "Vapor Pressure of Liquid Methanol at Low Temperatures," *Journal of Chemical and Engineering Data,* vol. 9, pp. 418-420, 1964, doi: 10.1021/je60022a040.

[273] A. Richardson, "Determination of Vapor Pressures of Alcohols and Organic Acids," *Journal of the Chemical Society,* vol. 49, pp. 761-776, 1886.

[274] T. Boublik and K. Aim, "Heats of Vaporization of Simple Non-Spherical Molecule Compounds," *Collection of Czechoslovak Chemical Communications,* vol. 37, pp. 3513-3521, 1972.

[275] S. Thomas, V. R. Bhethanabotla, and S. W. Campbell, "Total Pressure Measurements for n-Pentane-Methanol-2-Butanol at 303.15 K," *Journal of Chemical and Engineering Data,* vol. 36, pp. 374-378, 2005, doi: 10.1021/je00004a009.

[276] M. A. Villamañán and H. C. Van Ness, "Liquid-Vapor Equilibrium and Excess Gibbs Energies of 2, 5, 8-Trioxanonane+ Methanol, Or+ 1-Propanol," *Int. DATA Ser. Sel. Data Mix. Ser. A,* pp. 32-37, 1985.

[277] P. Oracz and G. Kolasinska, "Vapour-Liquid Equilibria-III. Total Vapour Pressure Measurements for Binary Mixtures of Methanol, Ethanol, 1-Propanol and 1-Butanol with Benzene, Toluene and p-Xylene at 313.15 K," vol. 35, pp. 253-278, 1987.

[278] K. Nasirzadeh, D. Zimin, R. Neueder, and W. Kunz, "Vapor-Pressure Measurements of Liquid Solutions at Different Temperatures: Apparatus for use over an Extended Temperature Range and Some New Data," *Journal of Chemical and Engineering Data,* vol. 49, pp. 607-612, 2004, doi: 10.1021/je034197x.

[279] A. Zaytseva, P. Uusi-Kyyny, J. P. Pokki, M. Pakkanen, and J. Aittamaa, "Vapor-Liquid Equilibrium for the Trans-2-Butene + Methanol, + Ethanol, + 2-Propanol, + 2-Butanol, and + 2-Methyl-2-Propanol Systems at 332 K," *Journal of Chemical and Engineering Data,* vol. 49, pp. 1168-1174, 2004, doi: 10.1021/je0341256.

[280] E. Vercher, A. V. Orchillés, P. J. Miguel, V. González-Alfaro, and A. Martínez-Andreu, "Isobaric Vapor-Liquid Equilibria for Acetone + Methanol + Lithium Nitrate at 100 kPa," *Fluid Phase Equilibria,* vol. 250, pp. 131-137, 2006, doi: 10.1016/j.fluid.2006.09.007.

[281] X. Esteve, S. K. Chaudhari, and A. Coronas, "Vapor-Liquid Equilibria for Methanol + Tetraethylene Glycol Dimethyl Ether," *Journal of Chemical and Engineering Data,* vol. 40, pp. 1252-1256, 1995, doi: 10.1021/je00022a023.

[282] J. Dong, C. Feng, and Y. Li, "Isothermal Vapor-Liquid Equilibrium for Methanol and 2,3-Dimethyl-1-Butene at 343.06 K, 353.27 K, 363.19 K, and 372.90 K," *Journal of Chemical and Engineering Data,* vol. 56, pp. 2386-2392, 2011, doi: 10.1021/je101304x.

[283] D. Ambrose, C. H. S. Sprake, and R. Townsend, "Thermodynamic Properties of Organic Oxygen Compounds XXXVII. Vapour Pressures of Methanol, Ethanol, Pentan-1-ol, And

Octan-1-ol from the Normal Boiling Temperature to the Critical Temperature," *The Journal of Chemical Thermodynamics,* vol. 7, pp. 185-190, 1975.

[284] A. R. Bazaev, I. M. Abdulagatov, E. A. Bazaev, and A. Abdurashidova, "PVT Measurements for Pure Ethanol in the Near-Critical and Supercritical Regions," *International Journal of Thermophysics,* vol. 28, pp. 194-219, 2007, doi: 10.1007/s10765-007-0158-2.

[285] L. Wang, K. Han, S. Xia, P. Ma, and F. Yan, "Measurement and Correlation of Critical Properties for Binary Mixtures and Ternary Mixtures Containing Gasoline Additives," *Journal of Chemical Thermodynamics,* vol. 74, pp. 161-168, 2014, doi: 10.1016/j.jct.2014.01.025.

[286] C. Carvajal, K. J. Tolle, J. Smid, and M. Szwarc, "Studies of Solvation Phenomena of Ions and Ion Pairs in Dimethoxyethane and Tetrahydrofuran," *Journal of the American Chemical Society,* vol. 87, pp. 5548-5553, 1965, doi: 10.1021/ja00952a005.

[287] U. Domanska, A. Sporzyński, W. C. Moollan, and T. M. Letcher, "Vapor-Liquid Equilibria of Binary Mixtures Containing Sulfolane," *Journal of Chemical and Engineering Data,* vol. 41, pp. 624-628, 1996, doi: 10.1021/je950227n.

[288] E. V. Ivanov, "To the Issue of Temperature-Dependent Behavior of Standard Molar Volumes of Components in the Binary System (Water + Tetrahydrofuran) at Ambient Pressure," *Journal of Chemical Thermodynamics,* vol. 72, pp. 37-43, 2014, doi: 10.1016/j.jct.2013.12.028.

[289] V. D. Moisejev and N. D. Antonova, "Vapor Pressure and Heat of Vaporization of Some Species of Furans," *Zh. Fiz. Khim,* vol. 44, pp. 2912-2913, 1970.

[290] W. V. Wilding and L. C. Wilson, "Experimental Results for DIPPR 1990-91 Projects on Phase Equilibria and Pure Component Properties, Vapor-Liquid and Liquid-Liquid Equilibrium Measurements on Five Binary Mixtures," *DIPPR Data Series,* vol. 2, pp. 63-115, 1994.

[291] Z. Zhang, P. Jia, and W. Li, "Vapor-Liquid Equilibrium for Ternary and Binary Mixtures of Tetrahydrofuran, Cyclohexane, and 1,2-Propanediol at 101.3 kPa"," *Journal of Chemical and Engineering Data,* vol. 61, pp. 1964-1965, 2016, doi: 10.1021/acs.jced.6b00089.

[292] E. M. Živković, D. M. Bajić, I. R. Radović, S. P. Šerbanović, and M. L. Kijevčanin, "Volumetric and Viscometric Behavior of the Binary Systems Ethyl Lactate+1,2-Propanediol, +1,3-Propanediol, +Tetrahydrofuran and +Tetraethylene Glycol Dimethyl Ether. New UNIFAC-VISCO and ASOG-VISCO Parameters Determination," *Fluid Phase Equilibria,* vol. 373, pp. 1-19, 2014, doi: 10.1016/j.fluid.2014.04.002.

[293] W. Li, Z. Zhang, B. Han, S. Hu, Y. Xie, and G. Yang, "Effect of Water and Organic Solvents on the Ionic Dissociation of Ionic Liquids," *Journal of Physical Chemistry B,* vol. 111, pp. 6452-6456, 2007, doi: 10.1021/jp071051m.

[294] A. Bhattacharjee, C. Varanda, M. G. Freire, S. Matted, L. M. N. B. F. Santos, I. M. Marrucho, and J. A. P. Coutinho, "Density and Viscosity Data for Binary Mixtures of 1-Alkyl-3- Methylimidazolium Alkylsulfates + Water," *Journal of Chemical and Engineering Data,* vol. 57, pp. 3473-3482, 2012, doi: 10.1021/je300622r.

[295] S. A. Pandit, M. A. Rather, S. A. Bhat, G. M. Rather, and M. A. Bhat, "Influence of the Anion on the Equilibrium and Transport Properties of 1-Butyl-3-methylimidazolium Based Room Temperature Ionic Liquids," *Journal of Solution Chemistry,* vol. 45, pp. 1641-1658, 2016, doi: 10.1007/s10953-016-0514-6.

[296] E. Rodil, A. Arce Jr., A. Arce, and A. Soto, "Measurements of the Density, Refractive Index, Electrical Conductivity, Thermal Conductivity and Dynamic Viscosity for Tributylmethylphosphonium and Methylsulfate Based Ionic Liquids," *Thermochimica Acta,* vol. 664, pp. 81-90, 2018, doi: 10.1016/j.tca.2018.04.007.

[297] K. R. Seddon, A. Stark, and M. J. Torres, "Chapter 4: Viscosity and Density of 1-Alkyl-3-Methylimidazolium Ionic Liquids," *ACS Symposium Series,* vol. 819, pp. 34-49, 2002, doi: 10.1021/bk-2002-0819.ch004.

[298] K. R. Harris, L. A. Woolf, M. Kanakubo, and T. Rüther, "Transport Properties of N -Butyl-N -Methylpyrrolidinium Bis(trifluoromethylsulfonyl)amide," *Journal of Chemical and Engineering Data,* vol. 56, pp. 4672-4685, 2011, doi: 10.1021/je2006049.

[299] M. Tariq, P. J. Carvalho, J. A. P. Coutinho, I. M. Marrucho, J. N. C. Lopes, and L. P. N. Rebelo, "Viscosity of (C_2-C_{14}) 1-Alkyl-3-Methylimidazolium Bis(trifluoromethylsulfonyl)amide Ionic Liquids in an Extended Temperature Range," *Fluid Phase Equilibria,* vol. 301, pp. 22-32, 2011, doi: 10.1016/j.fluid.2010.10.018.

[300] A. Ahosseini, L. R. Weatherley, and A. M. Scurto, "Viscosity and Diffusivity for the Ionic Liquid 1-Hexyl-3-Methyl-Imidazolium Bis(trifluoromethylsulfonyl)amide with 1-

Octene," *Journal of Chemical and Engineering Data,* vol. 56, pp. 3715-3721, 2011, doi: 10.1021/je1009224.

[301]   T. M. Aminabhavi and B. Gopalakrishna, "Density, Viscosity, Refractive Index, and Speed of Sound in Binary Mixtures of 2-Ethoxyethanol with n-Alkanes (C_6 to C_{12}), 2,2,4-Trimethylpentane, and Cyclohexane in the Temperature Interval 298.15–313.15 K," *Journal of Chemical and Engineering Data,* vol. 40, pp. 632-641, 1995, doi: 10.1021/je00019a022.

[302]   H. Koelbel, W. Siemes, and H. Luther, "Viscosity Relations of Hydrocarbons III. Viscosity as Function of Molar Mass of Homologous Hydrocarbons," *Brennst.-Chem,* vol. 30, pp. 362-371, 1949.

[303]   T. E. Thorpe and J. W. Rodger, "X. Bakerian Lecture : On the Relations between the Viscosity (Internal Friction) of Liquids and Their Chemical Nature," *Philosophical Transactions of the Royal Society of London,* vol. 185, pp. 397-710, 1894.

[304]   G. Knothe and K. R. Steidley, "Kinematic Viscosity of Biodiesel Components (Fatty acid Alkyl Esters) and Related Compounds at Low Temperatures," *Fuel,* vol. 86, no. 16, pp. 2560-2567, 2007.

[305]   J. N. Nayak, M. I. Aralaguppi, U. S. Toti, and T. M. Aminabhavi, "Density, Viscosity, Refractive Index, and Speed of Sound in the Binary Mixtures of Tri-N-Butylamine+ Triethylamine,+ Tetrahydrofuran,+ Tetradecane,+ Tetrachloroethylene,+ Pyridine, or+ Trichloroethylene at (298.15, 303.15, and 308.15) K," *Journal of Chemical and Engineering Data,* vol. 48, no. 6, pp. 1483-1488, 2003.

[306]   D. Wakefield and K. Marsh, "Viscosities of Nonelectrolyte Liquid Mixtures. I. N-Hexadecane+ N-Octane," *International journal of thermophysics,* vol. 8, no. 6, pp. 649-662, 1987.

[307]   D. M. Bajić, E. M. Živković, S. S. Šerbanović, and M. L. Kijevčanin, "Volumetric and Viscometric Study of Binary Systems of Ethyl Butyrate with Alcohols," *Journal of Chemical and Engineering Data,* vol. 59, pp. 3677-3690, 2014, doi: 10.1021/je5005752.

[308]   F. Hovorka, H. P. Lankblma, and S. C. Stanford, "Thermodynamic Properties of the Hexyl Alcohols . II . 1-2, 2- and 3-Hexanols and 2-Methyl-1 and -4-Pentanol," *Journal of the American Chemical Society,* vol. 60, p. 820, 1938.

[309]   S. Matsuo and T. Makita, "Viscosities of Six 1-Alkanols at Temperatures in the Range 298-348 K and Pressures up to 200 MPa," *International Journal of Thermophysics,* vol. 10, pp. 833-843, 1989, doi: 10.1007/BF00514479.

[310]   M. N. Caro, J. L. Trenzado, S. Galva, E. Romano, E. Gonzalez, R. Alcalde, and S. Aparicio, "Densities and Viscosities of Three Binary Monoglyme + 1-Alcohol Systems from (283.15 to 313.15) K," *Journal of Chemical and Engineering Data,* vol. 58, pp. 909-914, 2013.

[311]   U. Domańska and M. Królikowska, "Density and Viscosity of Binary Mixtures of {1-Butyl-3-Methylimidazolium Thiocyanate + 1-Heptanol, 1-Octanol, 1-Nonanol, or 1-Decanol}," *Journal of Chemical and Engineering Data,* vol. 55, pp. 2994-3004, 2010, doi: 10.1021/je901043q.

[312]   M. A. F. Faria, R. J. Martins, J. E. M. Cardoso, and O. E. Barcia, "Density and Viscosity of the Binary Systems Ethanol + Butan-1-ol , + Pentan-1-ol, + Heptan-1-ol, +Octan-1-ol, Nonan-1-ol, +Decan-1-ol at 0.1 MPa and Temperatures from 283.15 to 313.15 K," *Journal of Chemical and Engineering Data,* vol. 58, pp. 3405-3419, 2013.

[313]   L. H. Thomas and R. Meatyard, "Viscosity and Molecular Association IV. Association of Monohydic Alcohols and Some Hindered Phenols," *Journal of the Chemical Society,* pp. 1986-1995, 1963.

[314]   J. L. Trenzado, E. Romano, L. Segade, M. N. Caro, E. González, and S. Galván, "Densities and Viscosities of Four Binary Diethyl Carbonate + 1-Alcohol Systems from (288.15 to 313.15) K," *Journal of Chemical and Engineering Data,* vol. 56, pp. 2841-2848, 2011, doi: 10.1021/je1013476.

[315]   H. Djojoputro and S. Ismadji, "Density and Viscosity for a Binary Mixture of Cis-3-Hexenyl Formate, Butyl Acetate, Trans-2-Hexenyl Acetate, and Cis-3-Hexenyl Acetate with Ethanol at Several Temperatures," *Journal of Chemical and Engineering Data,* vol. 50, pp. 1009-1013, 2005, doi: 10.1021/je0500025.

[316]   M. K. Patwari, R. K. Bachu, S. Boodida, and S. Nallani, "Densities, Viscosities, and Speeds of Sound of Binary Liquid Mixtures of Sulfolane with Ethyl Acetate, N-Propyl Acetate, and N-Butyl Acetate at Temperature of (303.15, 308.15, and 313.15) K," *Journal of Chemical and Engineering Data,* vol. 54, pp. 1069-1072, 2009, doi: 10.1021/je800653d.

[317]   M. V. Rathnam, R. T. Sayed, K. R. Bhanushali, and M. S. S. Kumar, "Density and Viscosity of Binary Mixtures of N-Butyl Acetate with Ketones at (298.15, 303.15, 308.15, and 313.15) K," *Journal of Chemical and Engineering Data,* vol. 57, pp. 1721-1727, 2012.

[318] A. J. Batschinski, "Investigations of the Internal Friction of Fluids," *Z. Phys. Chem,* vol. 84, pp. 643-706, 1913.

[319] S. L. Lee and C. H. Tu, "Densities and Viscosities of Four Alkyl Esters with Nitromethane Systems at (293.15, 303.15, and 313.15) K," *Journal of Chemical and Engineering Data,* vol. 44, pp. 108-111, 1999, doi: 10.1021/je980207w.

[320] Q. Tian and H. Liu, "Densities and Viscosities of Binary Mixtures of Tributyl Phosphate with Hexane and Dodecane from (298.15 to 328.15) K," *Journal of Chemical and Engineering Data,* vol. 52, pp. 892-897, 2007, doi: 10.1021/je060491o.

[321] S. Fang, C.-X. Zhao, and C.-H. He, "Densities and Viscosities of Binary Mixtures of Tri-N-Butyl Phosphate + Cyclohexane, + N-Heptane at (T = (288.15, 293.15, 298.15, 303.15, and 308.15) K," *Journal of Chemical and Engineering Data,* vol. 53, pp. 2244-2246, 2008.

[322] A. Borun and A. Bald, "Conductometric Studies of 1-Ethyl-3-Methylimidazolium Tetrafluoroborate and 1-Butyl-3-Methylimidazolium Tetrafluoroborate in N,N-Dimethylformamide at Temperatures from (283.15 to 318.15) K," *Journal of Chemical and Engineering Data,* vol. 57, pp. 475-481, 2012.

[323] A. Hassein-Bey-Larouci, O. Igoujilen, A. Aitkaci, J. J. Segovia, and M. A. Villamañán, "Dynamic and Kinematic Viscosities, Excess Volumes and Excess Gibbs Energies of Activation for Viscous Flow in the Ternary Mixture {1- Propanol+ N,N-Dimethylformamide + Chloroform} at Temperatures between 293.15 K and 323.15 K," *Thermochimica Acta,* vol. 589, pp. 90-99, 2014, doi: 10.1016/j.tca.2014.05.004.

[324] M. Cocchi, M. Manfredini, D. Manzini, A. Marchetti, S. Sighinolfi, L. Tassi, A. Ulrici, M. Vignali, and P. Zannini, "Viscometric Properties and Internal Structure of N,N-Dimethylformamide + 1,2-Dimethoxyethane Binary Mixtures," *Journal of Molecular Liquids,* vol. 102, pp. 309-345, 2003.

[325] F. J. Wright, "Influence of Temperature on Viscosity of Nonassociated Liquids," *Journal of Chemical and Engineering Data,* vol. 6, pp. 454-456, 1961, doi: 10.1021/je00103a035.

[326] M. V. Rathnam, S. Mohite, and M. Nandini, "Excess Properties of Diethyl Carbonate + Ketone Binary Mixtures at Variable Temperatures: Application of PFP Theory to Excess Volumes," *Journal of Molecular Liquids,* vol. 177, pp. 229-236, 2013, doi: 10.1016/j.molliq.2012.10.038.

[327] V. A. Durov and A. Artykov, "Acoustic Spectroscopy of a Series of Alicyclic Ketones," *Journal of Physical Chemistry,* vol. 60, pp. 1855-1858, 1986.

[328] E. B. Evans, *Congr. Mondial Pet. Sect. 2,* p. 933, 1937.

[329] E. B. Evans, "The Viscosity of Hydrocarbons. Parts VII and VIII," *J. Inst. Pet. Technol,* vol. 24, p. 537, 1938.

[330] A. B. López, A. García-Abuín, D. Gómez-Díaz, M. D. La Rubia, and J. M. Navaza, "Density, Speed of Sound, Viscosity, Refractive Index and Surface Tension of N-Methyl-2-Pyrrolidone + Diethanolamine (Or Triethanolamine) from T = (293.15 to 323.15) K," *Journal of Chemical Thermodynamics,* vol. 61, pp. 1-6, 2013, doi: 10.1016/j.jct.2013.01.020.

[331] N. V. Živković, S. S. Šerbanović, M. L. Kijevčanin, and E. M. Živković, "Volumetric and Viscometric Behavior of Binary Systems 2-Butanol + PEG 200, + PEG 400, + Tetraethylene Glycol Dimethyl Ether, and + N-Methyl-2-Pyrrolidone," *Journal of Chemical and Engineering Data,* vol. 58, pp. 3332-3341, 2013, doi: 10.1021/je400486p.

[332] T. Kavitha, T. Vasantha, P. Venkatesu, R. S. Rama Devi, and T. Hofman, "Thermophysical Properties for the Mixed Solvents of N-Methyl-2-Pyrrolidone with Some of the Imidazolium-Based Ionic Liquids," *Journal of Molecular Liquids,* vol. 198, pp. 11-20, 2014, doi: 10.1016/j.molliq.2014.07.002.

[333] E. Tyunina, V. Afanas'ev, and M. Chekunova, "Viscosity and Density of Solutions of Tetraethylammonium Tetrafluoroborate in Propylene Carbonate at Different Temperatures," *Journal of Solution Chemistry,* vol. 41, pp. 307-317, 2012, doi: 10.1007/s10953-012-9793-8.

[334] AspenTech, "Aspen Plus Model of the CO_2 Capture Process by DEPG."

[335] L. L. C. Coastal Chemical Co., "Coastal AGR Solvent Bulletin."

[336] T. E. Thorpe and J. W. Rodger, "X. Bakerian Lecture. On the Relations between the Viscosity(Internal Friction) of Liquids and their Chemical Nature," *Philosophical Transactions of the Royal Society of London,* vol. 185, pp. 397-710, 1894.

[337] W. Fan, Q. Zhou, S. Zhang, and R. Yan, "Excess Molar Volume and Viscosity Deviation for the Methanol + Methyl Methacrylate Binary System at T = (283.15 to 333.15) K,"

Journal of Chemical and Engineering Data, vol. 53, pp. 1836-1840, 2008, doi: 10.1021/je800164w.

[338] F. M. Lee, L. E. Lahti, and C. E. Stoops, "Solution Properties of Urea–Alcohol–Water Mixtures," *Journal of Chemical and Engineering Data,* vol. 21, pp. 36-40, 1976, doi: 10.1021/je60068a003.

[339] M. A. Rauf, G. H. Stewart, and Farhataziz, "Viscosities and Densities of Binary Mixtures of 1-Alkanois from 15 to 55 °C," *Journal of Chemical and Engineering Data,* vol. 28, pp. 324-328, 1983, doi: 10.1021/je00033a012.

[340] G. E. Papanastasiou and I. I. Zlogas, "Physical Behavior of Some Reaction Media. 3. Density, Viscosity, Dielectric Constant, and Refractive Index Changes of Methanol + Dioxane Mixtures at Several Temperatures," *Journal of Chemical and Engineering Data,* vol. 37, pp. 167-172, 1992, doi: 10.1021/je00006a008.

[341] A. Kumar, O. Prakash, and S. Prakash, "Ultrasonic Velocities, Densities, and Viscosities of Trlethylamlne in Methanol, Ethanol, and 1-Propanol," *Journal of Chemical and Engineering Data,* vol. 26, pp. 64-67, 1981, doi: 10.1021/je00023a021.

[342] C. H. Tu, S. L. Lee, and I. H. Peng, "Excess Volumes and Viscosities of Binary Mixtures of Aliphatic Alcohols (C_1-C_4) with Nitromethane," *Journal of Chemical and Engineering Data,* vol. 46, pp. 151-155, 2001, doi: 10.1021/je0002080.

[343] Y. H. Gong, C. Shen, Y. Z. Lu, H. Meng, and C. X. Li, "Viscosity and Density Measurements for Six Binary Mixtures of Water (Methanol or Ethanol) with an Ionic Liquid ([Bmim][Dmp] or [Emim][Dmp]) at Atmospheric Pressure in the Temperature Range of (293.15 to 333.15) K," *Journal of Chemical and Engineering Data,* vol. 57, pp. 33-39, 2012, doi: 10.1021/je200600p.

[344] W. Marczak, N. Adamczyk, and M. Łężniak, "Viscosity of Associated Mixtures Approximated by the Grunberg-Nissan Model," *International Journal of Thermophysics,* vol. 33, pp. 680-691, 2012, doi: 10.1007/s10765-011-1100-1.

[345] C. Yang, W. Yu, and D. Tang, "Densities and Viscosities of Binary Mixtures of M-Cresol with Ethylene Glycol or Methanol Over Several Temperatures," *Journal of Chemical and Engineering Data,* vol. 51, pp. 935-939, 2006, doi: 10.1007/s00396-005-1441-z.

[346] C. K. Zéberg-Mikkelsen, A. Baylaucq, G. Watson, and C. Boned, "High-Pressure Viscosity Measurements for the Ethanol + Toluene Binary System," *International Journal of Thermophysics,* vol. 26, pp. 1289-1302, 2005, doi: 10.1007/s10765-005-8089-2.

[347] D. Fu, H. Wang, and L. Du, "Experiments and Model for the Surface Tension of (MDEA + [bmim][BF$_4$]) and (MDEA + [bmim][Br]) Aqueous Solutions," *Journal of Chemical Thermodynamics,* vol. 71, pp. 1-5, 2014, doi: 10.1016/j.jct.2013.11.024.

[348] A. A. Miran Beigi, M. Abdouss, M. Yousefi, S. M. Pourmortazavi, and A. Vahid, "Investigation on Physical and Electrochemical Properties of Three Imidazolium Based Ionic Liquids (1-Hexyl-3-Methylimidazolium Tetrafluoroborate, 1-Ethyl-3-Methylimidazolium Bis(trifluoromethylsulfonyl) Imide and 1-Butyl-3-Methylimidazolium methylsulfate)," *Journal of Molecular Liquids,* vol. 177, pp. 361-368, 2013, doi: 10.1016/j.molliq.2012.10.025.

[349] M. H. Ghatee and A. R. Zolghadr, "Surface Tension Measurements of Imidazolium-Based Ionic Liquids at Liquid-Vapor Equilibrium," *Fluid Phase Equilibria,* vol. 263, pp. 168-175, 2008, doi: 10.1016/j.fluid.2007.10.004.

[350] P. J. Carvalho, M. G. Freire, I. M. Marrucho, A. J. Queimada, and J. A. P. Coutinho, "Surface Tension for the 1-ALkyl-3-Methylimidazolium Bis(trifluoromethylsulfonyl)imide Ionic Liquids," *Journal of Chemical and Engineering Data,* vol. 53, pp. 1346-1350, 2008.

[351] M. G. Freire, P. J. Carvalho, A. M. Fernandes, I. M. Marrucho, A. J. Queimada, and J. A. P. Coutinho, "Surface Tensions of Imidazolium Based Ionic Liquids: Anion, Cation, Temperature and Water Effect," *Journal of Colloid and Interface Science,* vol. 314, pp. 621-630, 2007, doi: 10.1016/j.jcis.2007.06.003.

[352] J. Klomfar, M. Součková, and J. Pátek, "Surface Tension Measurements with Validated Accuracy for Four 1-Alkyl-3-Methylimidazolium Based Ionic Liquids," *Journal of Chemical Thermodynamics,* vol. 42, pp. 323-329, 2010, doi: 10.1016/j.jct.2009.09.007.

[353] M. Geppert-Rybczyńska, J. K. Lehmann, and A. Heintz, "Physicochemical Properties of Two 1-Alkyl-1-Methylpyrrolidinium Bis[(trifluoromethyl)sulfonyl]imide Ionic Liquids and of Binary Mixtures of 1-Butyl-1-Methylpyrrolidinium Bis[(trifluoromethyl)Sulfonyl]imide with Methanol or Acetonitrile," *Journal of Chemical Thermodynamics,* vol. 71, pp. 171-181, 2014, doi: 10.1016/j.jct.2013.12.009.

[354] Y. Jia-zhen, L. Jing-Bin, T. Jing, H. Mei, and others, "Study on the Density and Surface Tension of Ionic Liquid EMIBF$_4$ in Terms of Standard Addition Method," 2007.

[355] A. Muhammad, M. I. Abdul Mutalib, C. D. Wilfred, T. Murugesan, and A. Shafeeq, "Thermophysical Properties of 1-Hexyl-3-Methyl Imidazolium Based Ionic Liquids with Tetrafluoroborate, Hexafluorophosphate and Bis(Trifluoromethylsulfonyl)Imide Anions," *Journal of Chemical Thermodynamics,* vol. 40, pp. 1433-1438, 2008, doi: 10.1016/j.jct.2008.04.016.

[356] A. E. Andreatta, E. Rodil, A. Arce, and A. Soto, "Surface Tension of Binary Mixtures of 1-Alkyl-3-Methyl-Imidazolium Bis(trifluoromethylsulfonyl)imide Ionic Liquids with Alcohols," *Journal of Solution Chemistry,* vol. 43, pp. 404-420, 2014, doi: 10.1007/s10953-014-0128-9.

[357] B. J. J. Jasper and E. R. Kerr, "The Orthobaric Surface Tensions and Thermodynamic Properties of the Liquid Surfaces of a Series of 1-Alkenes, C_6 to C_{16}, and N-Decylcyclopentane, N-Decylcyclohexane and N-DecylBenzene," *Journal of American Chemical Society,* vol. 76, p. 2659, 1954.

[358] J. J. Jasper and E. V. Kring, "The Isobaric Surface Tensions and Thermodynamic Properties of the Surfaces of a Series of N-Alkanes, C_5 to C_{18}, 1-Alkenes, C_6 to C_{16}, and N-Decylcyclopentane, N-Decylcyclohexane and N-DecylBenzene " *Journal of Physical Chemistry,* vol. 59, pp. 1019-1021, 1955.

[359] J. J. Jasper, E. R. Kerr, and F. Gregorich, "The Orthobaric Surface Tensions and Thermodynamic Properties of the Liquid Surfaces of the n-Alkanes C_5 to C_{18}," *Journal of the American Chemical Society,* vol. 75, no. 21, pp. 5252-5254, 1953.

[360] A. J. Queimada, A. I. Caço, I. M. Marrucho, and J. A. P. Coutinho, "Surface Tension of Decane Binary and Ternary Mixtures with Eicosane, Docosane, and Tetracosane," *Journal of Chemical and Engineering Data,* vol. 50, pp. 1043-1046, 2005, doi: 10.1021/je050024r.

[361] L. I. Rolo, A. I. Caco, A. J. Queimada, I. M. Marrucho, and J. A. Coutinho, "Surface Tension of Heptane, Decane, Hexadecane, Eicosane, and some of their Binary Mixtures," *Journal of Chemical and Engineering Data,* vol. 47, pp. 1442-1445, 2002.

[362] H. W. D., F. E. Brown, and E. C. Davies, "The Structures of the Surfaces of Liquids, and SOlubility as Related to the Work Done by the Attraction of Two Liquid Surfaces as they Approach Each Other," *Journal of American Chemical Society,* vol. 39, pp. 354-364, 1917.

[363] M. Hennaut-Roland and M. Lek, "Methods and Equipment used at the Bureau of Physico-Chemical Standards: IV. Surface Tension of a Series of Organic Substances," *Bulletin Des Societes Chimiques Belges,* vol. 40, pp. 177-188, 1931.

[364] R. Manzoni-Ansidei, "Parachors of Branched Chain Paraffin Hydrocarbons," *Boll. Sci. Fac. Chim. Ind. Bologna,* vol. 201, 1940.

[365] O. R. Quayle, R. A. Day, and G. M. Brown, "A Study of Organic Parachors. VII. A Series of Saturated Hydrocarbons," *Journal of American Chemical Society,* vol. 66, pp. 938-941, 1944.

[366] T. W. Richards, C. L. Speyers, and E. K. Carver, "The Determination of Surface Tension with Very Small Volumes of Liquid, and the Surface Tensions of Octanes and Xylenes at Several Temperatures," *Journal of the American Chemical Society,* vol. 46, pp. 1196-1207, 1924, doi: 10.1021/ja01670a012.

[367] G. Y. Smith, "The Measurement of Boundary Tension by the Pendent-Drop Method. II," *Journal of Physical Chemistry,* vol. 48, pp. 168-172, 1944.

[368] A. I. Vogel, "Physical Properties and Chemical Constitutions IX. Aliphatic Hydrocarbons," *Journal of the Chemical Society,* pp. 133-139, 1946.

[369] J. P. Wibaut, H. Hoog, S. L. Langedijk, J. Overhoff, J. Smittenberg, N. Benninga, G. P. Bouman, H. van Dijk, W. Gaade, H. Geldof, J. Hackman, E. W. Jonker, T. Paap, and F. Zuiderweg, "Study on the Preparation and the Physical Constants of a Number of Alkanes and Cycloalkanes," *Recueil des Travaux Chimiques des Pays-Bas,* vol. 58, pp. 329-377, 1939, doi: 10.1002/recl.19390580409.

[370] A. Bagheri, A. Abolhasani, A. R. Moghadasi, A. A. Nazari-Moghaddam, and S. A. Alavi, "Study of Surface Tension and Surface Properties of Binary Systems of DMSO with Long Chain Alcohols at Various Temperatures," *Journal of Chemical Thermodynamics,* vol. 63, pp. 108-115, 2013, doi: 10.1016/j.jct.2013.04.009.

[371] J. Vijande, M. M. Piñeiro, J. García, J. L. Valencia, and J. L. Legido, "Density and Surface Tension Variation with Temperature for Heptane + 1-Alkanol," *Journal of Chemical and Engineering Data,* vol. 51, pp. 1778-1782, 2006, doi: 10.1021/je060179e.

[372] Y. V. Efremov, "Density, Surface Tension, Vapour Pressure, and Critical Parameters of Alcohols," *Russian Journal of Physical Chemistry,* vol. 40, p. 667, 1966.

[373] S. S. Katti and S. Pathak, "Surface Thermodynamic Properties of Alcohols and Related Compounds," *Journal of Chemical and Engineering Data,* vol. 14, pp. 73-76, 1969, doi: 10.1021/je60040a015.

[374] A. A. Mohammad, K. H. A. E. Alkhaldi, M. S. Altuwaim, and A. S. Al-Jimaz, "Effect of Temperature and Chain Length on the Viscosity and Surface Tension of Binary Systems of N,N-Dimethylformamide with 1-Octanol, 1-Nonanol and 1-Decanol," *Journal of Chemical Thermodynamics,* vol. 74, pp. 7-15, 2014, doi: 10.1016/j.jct.2014.03.022.

[375] W. D. Harkins and Y. C. Cheng, "The Orientation of Molecules in Surfaces. VI. Cohesion, Adhesion, Tensile Strength. Tensile Energy, Negative Surface Energy, Interfacial Tension, and Molecular Attraction," *Journal of American Chemical Society,* vol. 43, pp. 35-53, 1921, doi: 10.31046/anztla.v0i61.1336.

[376] A. I. Vogel, "Physical Properties and CHemical Constitution. XIII. Aliphatic Carboxylic Esters," *Journal of the Chemical Society,* pp. 624-644, 1948.

[377] E. R. Washburn and C. H. Shildneck, "Surface Tension Studies with N-Butyl Acetate," *Journal of the American Chemical Society,* vol. 55, pp. 2354-2357, 1933, doi: 10.1021/ja01333a020.

[378] J. L. R. Morgan and M. A. Griggs, "The Properties of Mixed Liquids III. The Law of Mixtures I," *Journal of the American Chemical Society,* vol. 39, no. 11, pp. 2261-2275, 1917.

[379] J. L. R. Morgan and F. W. Schwartz, "The Weight of a Falling Drop and the Laws of Tate VII. The Drop Weights of some of the Lower Esters, and the Surface Tensions and Molecular Weights Calculated from them," *Journal of the American Chemical Society,* vol. 33, no. 7, pp. 1041-1060, 1911.

[380] Y. Y. Yang, J. H. Deng, H. L. Yang, X. H. Zheng, G. Q. Che, and Z. Q. Huang, "Densities, Surface Tensions, and Derived Surface Thermodynamics Properties of (Trimethylbenzene + Propyl acetate, or Butyl acetate) from T = 298.15 K to 313.15 K," *Journal of Chemical Thermodynamics,* vol. 39, pp. 438-448, 2007, doi: 10.1016/j.jct.2006.07.025.

[381] Z. Li, Y. Sun, D. Zhao, Y. Zhuang, R. Wang, F. Yang, X. Liu, and Y. Chen, "Surface Tension of Binary Mixtures of (Ionic Liquid + Tributyl Phosphate)," *Journal of Chemical Thermodynamics,* vol. 132, pp. 214-221, 2019, doi: 10.1016/j.jct.2018.12.036.

[382] N. G. Tsierkezos and A. C. Filippou, "Thermodynamic Investigation of N,N-Dimethylformamide/Toluene Binary Mixtures in the Temperature Range from 278.15 to 293.15 K," *Journal of Chemical Thermodynamics,* vol. 38, pp. 952-961, 2006, doi: 10.1016/j.jct.2005.10.008.

[383] F. J. Wright, "Correlation between Surface Tension and other Physical Properties," *Journal of Applied Chemistry,* vol. 11, no. 6, pp. 193-196, 1961, doi: 10.1016/S0300-9440(98)00053-8.

[384] W. F. Seyer and C. H. Davenporteye, "The Densities and Surface Tensions of cis- and trans-Decahydronaphthalene between -30 and 180 °C," *Journal of the American Chemical Society,* vol. 63, pp. 2425-2427, 1941, doi: 10.1021/ja01854a031.

[385] G. Körösi and E. S. Kováts, "Density and Surface Tension of 83 Organic Liquids," *Journal of Chemical and Engineering Data,* vol. 26, pp. 323-332, 1981, doi: 10.1021/je00025a032.

[386] J. Timmermans and M. Hennaut-Roland, "Work of the International Bureau of Physico-Chemical Standards. VIII. Physical Constants of 20 Organic Compounds," *J. Chim. Phys.-Chim. Biol.,* vol. 34, p. 693, 1937.

[387] A. I. Vogel, "Physical Properties and Chemical Constitution. Part XV. The Phenyl Group," *Journal of the Chemical Society,* pp. 654-658, 1948.

[388] A. García-Abuín, D. Gómez-Díaz, M. D. La Rubia, A. B. López, and J. M. Navaza, "Density, Speed of Sound, Refractive Index, Viscosity, Surface Tension, and Excess Volume Of N -Methyl-2-Pyrrolidone + 1-Amino-2-Propanol {Or Bis(2-Hydroxypropyl)Amine} From T = (293.15 To 323.15) K," *Journal of Chemical and Engineering Data,* vol. 56, pp. 2904-2908, 2011, doi: 10.1021/je200121f.

[389] M. K. Bernett and W. A. Zisman, "Relation of Wettability by Aqueous Solutions to the Surface Constitution of Low-Energy Solids," *Journal of Physical Chemistry,* vol. 63, pp. 1241-1246, 1959, doi: 10.1021/j150578a006.

[390] J. A. Riddick, W. B. Bunger, and T. K. Sakano, *Organic Solvents: Physical Properties and Methods of Purification* (Properties and Methods of Purification, 4th ed.). John Wiley and Sons, New York, NY, 1986.

[391] S. Sugden, "The Variation of Surface Tension with Temperature and some Related Functions," *Journal of the Chemical Society, Transactions,* vol. 125, pp. 32-41, 1924.

[392] L. Hong, N. Siefert, R. L. Thompson, J. Culp, W. Shi, K. Resnik, and D. Hopkinson, "Solubility and Diffusivity of Syngas Components in a Hydrophobic Solvent for Pre Combustion CO_2 Capture," presented at the AIChE Annual Meeting, Orlando, Fl, 2019.

[393] B. Y. Teitelbaum, T. A. Gortalova, and E. E. Sidorova, "Politermicheskoe Issledovanie Poverkhnostnogo Natyazheniya Vodnykh Rastvorov Nizshikh Spirtov," *Zhurnal Fizicheskoi Khimii,* vol. 25, pp. 911-919, 1951.

[394] A. Bagheri and A. H. Amiri-Majed, "Surface Thermodynamics of Binary Mixtures of Aliphatic Alcohols in Heavy Water," *Journal of Chemical Thermodynamics,* vol. 51, pp. 45-50, 2012, doi: 10.1016/j.jct.2012.02.017.

[395] G. Weissenberger and F. Schuster, "Über die Molekülverbindungen der Phenole," *Monatshefte für Chemie und verwandte Teile anderer Wissenschaften* vol. 45, no. 9, pp. 437-448, 1924.

[396] M. Součková, J. Klomfar, and J. Pátek, "Measurement and Correlation of The Surface Tension-Temperature Relation for Methanol," *Journal of Chemical and Engineering Data,* vol. 53, pp. 2233-2236, 2008, doi: 10.1021/je8003468.

[397] H. Jiang, Y. Zhao, J. Wang, F. Zhao, R. Liu, and Y. Hu, "Density and Surface Tension of Pure Ionic Liquid 1-Butyl-3-Methyl- Imidazolium l-Lactate and Its Binary Mixture with Alcohol and Water," *Journal of Chemical Thermodynamics,* vol. 64, pp. 1-13, 2013, doi: 10.1016/j.jct.2013.04.015.

[398] Z. Chen, S. Xia, and P. Ma, "Measuring Surface Tension of Liquids at High Temperature and Elevated Pressure," *Journal of Chemical and Engineering Data,* vol. 53, pp. 742-744, 2008, doi: 10.1021/je700578f.

[399] H. C. Ku, C. C. Wang, and C. H. Tu, "Densities, Viscosities, Refractive Indexes, and Surface Tensions for Binary and Ternary Mixtures of Tetrahydofuran, 2-Propanol, and 2,2,4-Trimethylpentane," *Journal of Chemical and Engineering Data,* vol. 53, pp. 566-573, 2008, doi: 10.1021/je700626v.

[400] A. Villares, L. Sanz, B. Giner, C. Lafuente, and M. C. López, "Study of the Surface Tension of Chlorocyclohexane or Bromocyclohexane with some Cyclic Ethers," *Journal of Chemical and Engineering Data,* vol. 50, pp. 1334-1337, 2005, doi: 10.1021/je0500577.

[401] M. Geppert-Rybczyńska, J. K. Lehmann, J. Safarov, and A. Heintz, "Thermodynamic Surface Properties of [Bmim][NTf$_2$] or [Emim][NTf$_2$] Binary Mixtures with Tetrahydrofuran, Acetonitrile or Dimethylsulfoxide," *Journal of Chemical Thermodynamics,* vol. 62, pp. 104-110, 2013, doi: 10.1016/j.jct.2013.02.021.

[402] J. R. Brock and R. B. Bird, "Surface Tension and the Principle of Corresponding States," *AIChE Journal,* vol. 1, no. 2, pp. 174-177, 1955, doi: 10.1002/aic.690010208.

[403] J. L. Anthony, J. L. Anderson, E. J. Maginn, and J. F. Brennecke, "Anion Effects on Gas Solubility in Ionic Liquids," *The Journal of Physical Chemistry B,* vol. 109, pp. 6366-6374, 2005, doi: 10.1021/jp046404l.

[404] J. Kumełan, Á. Pérez-Salado Kamps, D. Tuma, and G. Maurer, "Solubility of CO_2 in the Ionic Liquids [bmim][CH_3SO_4] and [bmim][PF_6]," *Journal of Chemical and Engineering Data,* vol. 51, pp. 1802-1807, 2006, doi: 10.1021/je060190e.

[405] A. H. Jalili, M. Shokouhi, G. Maurer, A. T. Zoghi, J. Sadeghzah Ahari, and K. Forsat, "Measuring and Modelling the Absorption and Volumetric Properties of CO_2 and H_2S in the Ionic Liquid 1-Ethyl-3-Methylimidazolium Tetrafluoroborate," *Journal of Chemical Thermodynamics,* vol. 131, pp. 544-556, 2019, doi: 10.1016/j.jct.2018.12.005.

[406] M. Watanabe, D. Kodama, T. Makino, and M. Kanakubo, "CO_2 Absorption Properties of Imidazolium Based Ionic Liquids using a Magnetic Suspension Balance," *Fluid Phase Equilibria,* vol. 420, pp. 44-49, 2016, doi: 10.1016/j.fluid.2015.12.055.

[407] C. Moya, J. Palomar, M. Gonzalez-Miquel, J. Bedia, and F. Rodriguez, "Diffusion Coefficients of CO_2 in Ionic Liquids Estimated by Gravimetry," *Industrial and Engineering Chemistry Research,* vol. 53, pp. 13782-13789, 2014, doi: 10.1021/ie501925d.

[408] M. J. Muldoon, S. N. V. K. Aki, J. L. Anderson, J. K. Dixon, and J. F. Brennecke, "Improving Carbon Dioxide Solubility in Ionic Liquids," *Journal of Physical Chemistry B,* vol. 111, pp. 9001-9009, 2007, doi: 10.1021/jp071897q.

[409] A. H. Jalili, M. Safavi, C. Ghotbi, A. Mehdizadeh, M. Hosseini-Jenab, and V. Taghikhani, "Solubility of CO_2, H_2S, and their Mixture in the Ionic Liquid 1-Octyl-3-Methylimidazolium Bis(trifluoromethyl)sulfonylimide," *Journal of Physical Chemistry B,* vol. 116, pp. 2758-2774, 2012, doi: 10.1021/jp2075572.

[410] Z. Lei, J. Han, B. Zhang, Q. Li, J. Zhu, and B. Chen, "Solubility of CO_2 in Binary Mixtures of Room-Temperature Ionic Liquids at High Pressures," *Journal of Chemical and Engineering Data,* vol. 57, pp. 2153-2159, 2012, doi: 10.1021/je300016q.

[411] J. H. Vera and H. Orbey, "Binary Vapor-Liquid Equilibria of Carbon Dioxide with 2-Methyl-1-Pentene, 1-Hexene, 1-Heptene, and M-Xylene at 303.15, 323.15, and 343.15 K," *Journal of Chemical and Engineering Data,* vol. 29, pp. 269-272, 1984.

[412] Z. Xie, W. K. Snavely, A. M. Scurto, and B. Subramaniam, "Solubilities of CO and H_2 in Neat and CO_2-Expanded Hydroformylation Reaction Mixtures Containing 1-Octene and Nonanal up to 353.15 K and 9 MPa," *Journal of Chemical and Engineering Data,* vol. 54, pp. 1633-1642, 2009, doi: 10.1021/je900148e.

[413] H. Reamer and B. Sage, "Phase Equilibria in Hydrocarbon Systems. Volumetric and Phase Behavior of the n-Decane-CO2 System," *Journal of Chemical and Engineering Data,* vol. 8, no. 4, pp. 508-513, 1963.

[414] R. Jimenez-Gallegos, L. A. Galicia-Luna, and O. Elizalde-Solis, "Experimental Vapor−Liquid Equilibria for the Carbon Dioxide + Octane and Carbon Dioxide + Decane Systems," *Journal of Chemical and Engineering Data,* vol. 51, no. 5, pp. 1624-1628, 2006.

[415] H. Nourozieh, B. Bayestehparvin, M. Kariznovi, and J. Abedi, "Equilibrium Properties of (Carbon Dioxide + N-Decane + N-Octadecane) Systems: Experiments and Thermodynamic Modeling," *Journal of Chemical and Engineering Data,* vol. 58, no. 5, pp. 1236-1243, 2013.

[416] Z. Yun, M. Shi, and J. Shi, "High Pressure Vapor-Liquid Phase Equilibria for Carbon Dioxide - N-Octane and Carbon Dioxide - N-Nonane," *J. Gaoxiao Huaxue Gongcheng Xuebao,* vol. 9, pp. 396-399, 1995.

[417] D. Chen and W. Chen, "Phase Equilibria of N-Hexane and N-Octane in Critical Carbon Dioxide," *Huaxue Gongcheng,* vol. 20, pp. 66-69, 1992.

[418] W. L. Weng and M. J. Lee, "Vapor-Liquid Equilibrium of the Octane/Carbon Dioxide, Octane/Ethane, and Octane/Ethylene Systems," *Journal of Chemical and Engineering Data,* vol. 37, no. 2, pp. 213-215, 1992.

[419] E.-J. Choi and S.-D. Yeo, "Critical Properties for Carbon Dioxide + N-Alkane Mixtures using a Variable-Volume View Cell," *Journal of Chemical and Engineering Data,* vol. 43, no. 5, pp. 714-716, 1998.

[420] J. Yu, S. Wang, and Y. Tian, "Experimental Determination and Calculation of Thermodynamic Properties of CO_2 + Octane to High Temperatures and High Pressures," *Fluid phase equilibria,* vol. 246, no. 1-2, pp. 6-14, 2006.

[421] K. Tochigi, T. Namae, T. Suga, H. Matsuda, K. Kurihara, M. C. dos Ramos, and C. McCabe, "Measurement and Prediction of High-Pressure Vapor–Liquid Equilibria for Binary Mixtures of Carbon Dioxide + N-Octane, Methanol, Ethanol, and perfluorohexane," *The Journal of Supercritical Fluids,* vol. 55, no. 2, pp. 682-689, 2010.

[422] M. Kariznovi, H. Nourozieh, and J. Abedi, "Phase Composition and Saturated Liquid Properties in Binary and Ternary Systems Containing Carbon Dioxide, N-Decane, and N-Tetradecane," *The Journal of Chemical Thermodynamics,* vol. 57, pp. 189-196, 2013.

[423] L.-S. Wang, Z.-X. Lang, and T.-M. Guo, "Measurement and Correlation of the Diffusion Coefficients of Carbon Dioxide in Liquid Hydrocarbons under Elevated Pressures," *Fluid Phase Equilibria,* vol. 117, no. 1-2, pp. 364-372, 1996.

[424] C. Secuianu, V. Feroiu, and D. Geană, "High-Pressure Phase Equilibria in the (Carbon Dioxide + 1-Hexanol) System," *Journal of Chemical Thermodynamics,* vol. 42, pp. 1286-1291, 2010, doi: 10.1016/j.jct.2010.05.006.

[425] W. Ren, B. Rutz, and A. M. Scurto, "High-Pressure Phase Equilibrium for the Hydroformylation of 1-Octene to Nonanal in Compressed CO_2," *Journal of Supercritical Fluids,* vol. 51, pp. 142-147, 2009, doi: 10.1016/j.supflu.2009.08.003.

[426] H. S. Byun and C. Kwak, "High Pressure Phase Behavior for Carbon Dioxide-1-Butanol and Carbon Dioxide-1-OctanoI Systems," *Korean Journal of Chemical Engineering,* vol. 19, pp. 1007-1013, 2002, doi: 10.1007/BF02707225.

[427] C. Chiehming J, C. Kou-Lung, and D. Chang-Yih, "A New Apparatus for the Determination of P-x-y Diagrams and Henry's Constants in High Pressure Alcohols with Critical Carbon Dioxide," *Journal of Supercritical Fluids,* vol. 12, pp. 223-237, 1998, doi: 10.1016/s0896-8446(98)00076-x.

[428] H. Y. Chiu, R. F. Jung, M. J. Lee, and H. M. Lin, "Vapor-Liquid Phase Equilibrium Behavior of Mixtures Containing Supercritical Carbon Dioxide Near Critical Region," *Journal of Supercritical Fluids,* vol. 44, pp. 273-278, 2008, doi: 10.1016/j.supflu.2007.09.026.

[429] M. J. Lee and J. T. Chen, "Vapor-Liquid Equilibrium for Carbon Dioxide/Alcohol Systems," *Fluid Phase Equilibria,* vol. 92, pp. 215-231, 1994, doi: 10.1016/0378-3812(94)80048-0.

[430] H. S. Byun, M. Y. Choi, and J. S. Lim, "High-Pressure Phase Behavior and Modeling of Binary Mixtures for Alkyl Acetate in Supercritical Carbon Dioxide," *Journal of Supercritical Fluids,* vol. 37, pp. 323-332, 2006, doi: 10.1016/j.supflu.2005.10.007.

[431] Z. Wagner, "Vapour-Liquid Equilibrium at High Pressure in the System Containing Carbon Dioxide and Propyl Acetate," *Fluid Phase Equilibria,* vol. 110, pp. 175-182, 1995, doi: 10.1016/0378-3812(95)02752-Z.

[432] W. Shi, R. L. Thompson, M. K. Macala, K. Resnik, J. A. Steckel, N. S. Siefert, and D. P. Hopkinson, "Molecular Simulations of CO2 and H2 Solubility, CO2 Diffusivity, and Solvent Viscosity at 298 K for 27 Commercially Available Physical Solvents," *Journal of Chemical and Engineering Data,* vol. 64, pp. 3682-3692, 2019, doi: 10.1021/acs.jced.8b01228.

[433] C. Duran-Valencia, A. Valtz, L. A. Galicia-Luna, and D. Richon, "Isothermal Vapor-Liquid Equilibria of the Carbon Dioxide (CO_2)-N,N-Dimethylformamide (DMF) System at Temperatures from 293.95 K to 338.05 K and Pressures up to 12 MPa," *Journal of Chemical and Engineering Data,* vol. 46, pp. 1589-1592, 2001, doi: 10.1021/je010055w.

[434] A. Kordikowski, A. P. Schenk, R. M. Van Nielen, and C. J. Peters, "Volume Expansions and Vapor-Liquid Equilibria of Binary Mixtures of a Variety of Polar Solvents and Certain Near-Critical Solvents," *The Journal of Supercritical Fluids,* vol. 8, pp. 205-216, 1995, doi: 10.1016/0896-8446(95)90033-0.

[435] S. Vitu, J. N. Jaubert, J. Pauly, and J. L. Daridon, "High-Pressure Phase Behaviour of the Binary System {CO_2 + Cis-Decalin} from (292.75 to 373.75) K," *Journal of Chemical Thermodynamics,* vol. 40, pp. 1358-1363, 2008, doi: 10.1016/j.jct.2008.05.008.

[436] C. J. Chang, "Volume Expansion Coefficients and Activity Coefficients of High-Pressure Carbon Dioxide Dissolution in Organic Liquids at 298 k," *Journal of Chemical Engineering of Japan,* vol. 25, pp. 164-170, 1992, doi: 10.1252/jcej.25.164.

[437] M. C. Esmelindro, O. A. C. Antunes, E. Franceschi, G. R. Borges, M. L. Corazza, J. V. Oliveira, W. Linhares, and C. Dariva, "Phase Behavior of the Reactant and Products of Cyclohexane Oxidation in Compressed CO_2," *Journal of Chemical and Engineering Data,* vol. 53, pp. 2050-2055, 2008, doi: 10.1021/je800109s.

[438] Y. Feng, W. Hu, and Y. Hou, "Gas-Liquid Equilibria for Carbon Dioxide-Cyclohexane and Carbon Dioxide-Cyclohexanone Systems," *Journal of Chemical Engineering of Chinese Universities,* vol. 1, 1992.

[439] R. J. Lee and K. C. Chao, "Extraction of 1-Methylnaphthalene and M-Cresol with Supercritical Carbon Dioxide and Ethane," *Fluid Phase Equilibria,* vol. 43, pp. 329-340, 1988.

[440] C. W. Lee, C. Y. Jung, and H. S. Byun, "High Pressure Phase Behavior of Carbon Dioxide + 1-Methyl-2-Pyrrolidinone and Carbon Dioxide + 1-Ethyl-2-Pyrrolidinone Systems," *Journal of Chemical and Engineering Data,* vol. 49, pp. 53-57, 2004, doi: 10.1021/je0301545.

[441] R. Rajasingam, L. Lioe, Q. T. Pham, and F. P. Lucien, "Solubility of Carbon Dioxide in Dimethylsulfoxide and N-Methyl-2- Pyrrolidone at Elevated Pressure," *Journal of Supercritical Fluids,* vol. 31, pp. 227-234, 2004, doi: 10.1016/j.supflu.2003.12.003.

[442] M. J. Lazzaroni, D. Bush, J. S. Brown, and C. A. Eckert, "High-Pressure Vapor-Liquid Equilbria of Some Carbon Dioxide + Organic Binary Systems," *Journal of Chemical and Engineering Data,* vol. 50, pp. 60-65, 2005, doi: 10.1021/je0498560.

[443] S. Tian, Y. Hou, W. Wu, S. Ren, and K. Pang, "Physical Properties of 1-Butyl-3-Methylimidazolium Tetrafluoroborate/ N -Methyl-2-Pyrrolidone Mixtures and the Solubility of CO_2 In the System at Elevated Pressures," *Journal of Chemical and Engineering Data,* vol. 57, pp. 756-763, 2012, doi: 10.1021/je200886j.

[444] M. R. Bohloul, A. Vatani, and S. M. Peyghambarzadeh, "Experimental and Theoretical Study of CO_2 Solubility In N-Methyl-2-Pyrrolidone (NMP)," *Fluid Phase Equilibria,* vol. 365, pp. 106-111, 2014, doi: 10.1016/j.fluid.2013.12.019.

[445] E. E. Isaacs, F. D. Otto, and A. E. Mather, "Solubility of Hydrogen Sulfide and Carbon Dioxide in Propylene Carbonate Solvent," *Canadian Journal of Chemical Engineering,* vol. 55, p. 751, 1977.

[446] X. Gui, Z. Tang, and W. Fei, "CO_2 Capture with Physical Solvent Dimethyl Carbonate at High Pressures," *Journal of Chemical and Engineering Data,* vol. 55, pp. 3736-3741, 2010, doi: 10.1021/je1002708.

[447] F. Murrieta-Guevara, A. Romero-Martinez, and A. Trejo, "Solubilities of Carbon Dioxide and Hydrogen Sulfide in Propylene Carbonate, N-Methylpyrrolidone and Sulfolane," *Fluid Phase Equilibria,* vol. 44, pp. 105-115, 1988, doi: 10.1016/0378-3812(88)80106-7.

[448] Y. P. Zubchenko, S. F. Shakhova, T. Wei, L. I. Titel'man, and L. K. Kaplan, "Phase Equilibria and Volume Relations in the System Propylene Carbonate + Carbon Dioxide," *Russian Journal of Physical Chemistry,* vol. 44, pp. 2044-2047, 1971.

[449] E. R. Shenderei, Y. D. Zelvenskii, and F. P. Ivanovskii, "Solubility of CO_2 in Methanol at Low Temperatures and High Pressure," *Khim. Prom.,* vol. 4, pp. 328-331, 1959.

[450] M. Yorizane, S. Sadamoto, H. Masuoka, and Y. Eto, "Solubility of Gases in Methanol at High Pressures," *Kogyo Kagaku Zasshi,* vol. 72, pp. 2174-2177, 1969.

[451] W. Weber, S. Zeck, and H. Knepp, "Gas Solubilities in Liquid Solvents at High Pressures : Apparatus and Results for Binary and Ternary Systems of N_2, CO_2 , and CH_3OH," *Fluid Phase Equilibria,* vol. 18, pp. 253-278, 1984.

[452] T. E. Chang and W. Rousseau, "Solubilities of Carbon Dioxide in Methanol and Methanol-Water at High Pressures: Experimental Data and Modeling," *Fluid Phase Equilibria,* vol. 23, pp. 243-258, 1985.

[453] J. H. Hong and R. Kobayashi, "Vapor-Liquid Equilibrium Studies for the Carbon Dioxide-Methanol System," *Fluid Phase Equilibria,* vol. 41, pp. 269-276, 1988.

[454] J. Im, W. Bae, J. Lee, and H. Kim, "Vapor-Liquid Equilibria of the Binary Carbon Dioxide - Tetrahydrofuran Mixture System," *Journal of Chemical and Engineering Data,* vol. 49, pp. 35-37, 2004, doi: 10.1021/je0202228.

[455] D. Kodama, T. Yagihashi, T. Hosoya, and M. Kato, "High Pressure Vapor-Liquid Equilibria for Carbon Dioxide+Tetrahydrofuran Mixtures," *Fluid Phase Equilibria,* vol. 297, pp. 168-171, 2010, doi: 10.1016/j.fluid.2010.04.018.

[456] V. A. Toussaint, E. Kühne, A. Shariati, and C. J. Peters, "Solubility Measurements of Hydrogen in 1-Butyl-3-Methylimidazolium Tetrafluoroborate and the Effect of Carbon Dioxide and a Selected Catalyst on the Hydrogen Solubility in the Ionic Liquid," *Journal of Chemical Thermodynamics,* vol. 59, pp. 239-242, 2013, doi: 10.1016/j.jct.2012.12.013.

[457] J. Kumełan, Á. Pérez-Salado Kamps, D. Tuma, and G. Maurer, "Solubility of the Single Gases H_2 and CO in the Ionic Liquid [bmim][CH_3SO_4]," *Fluid Phase Equilibria,* vol. 260, pp. 3-8, 2007, doi: 10.1016/j.fluid.2006.06.010.

[458]   J. Kumełan, Á. Pérez-Salado Kamps, D. Tuma, and G. Maurer, "Solubility of H_2 in the Ionic Liquid [bmim][PF_6]," *Journal of Chemical and Engineering Data,* vol. 51, pp. 11-14, 2006, doi: 10.1021/je050362s.

[459]   S. Raeissi and C. J. Peters, "Understanding Temperature Dependency of Hydrogen Solubility in Ionic Liquids, Including Experimental Data in [bmim][Tf_2N]," *AIChE Journal,* vol. 58, pp. 3553-3559, 2012, doi: 10.1002/aic.13742.

[460]   Z. Lei, C. Dai, Q. Yang, J. Zhu, and B. Chen, "UNIFAC Model for Ionic Liquid-CO (H_2) Systems: An Experimental and Modeling Study on Gas Solubility," *AIChE Journal,* vol. 60, no. 12, pp. 4222-4231, 2014, doi: 10.1002/aic.

[461]   S. Raeissi, A. M. Schilderman, and C. J. Peters, "High Pressure Phase Behaviour of Mixtures of Hydrogen and the Ionic Liquid Family [$C_n$mim][Tf_2N]," *Journal of Supercritical Fluids,* vol. 73, pp. 126-129, 2013, doi: 10.1016/j.supflu.2012.09.003.

[462]   X. Liu, M. He, N. Lv, H. Xu, and L. Bai, "Selective Absorption of CO_2 from H_2, O_2 and N_2 by 1-Hexyl-3-Methylimidazolium Tris(Pentafluoroethyl)Trifluorophosphate," *Journal of Chemical Thermodynamics,* vol. 97, pp. 48-54, 2016, doi: 10.1016/j.jct.2016.01.013.

[463]   J. Kumełan, D. Tuma, and G. Maurer, "Partial Molar Volumes of Selected Gases in Some Ionic Liquids," *Fluid Phase Equilibria,* vol. 275, pp. 132-144, 2009, doi: 10.1016/j.fluid.2008.09.024.

[464]   M. F. Friedrich, S. Kokolakis, M. Lucas, and P. Claus, "Measuring Diffusion and Solubility of Slightly Soluble Gases in [C_nMIM][NTf_2] Ionic Liquids," *Journal of Chemical and Engineering Data,* vol. 61, pp. 1616-1624, 2016, doi: 10.1021/acs.jced.5b00990.

[465]   V. I. Sokolov and A. A. Polyakov, "Solubility of H_2 in N-Decane, N-Tetradecane, 1-Hexane, 1-Octene, Isopropyl Benzene, 1-Methyl Naftalene and Decalin," *Zh. Prikl. Khim,* vol. 50, pp. 1403-1405, 1977.

[466]   E. Brunner, "Solubility of Hydrogen in 10 Organic Solvents at 298.15, 323.15, and 373.15 K," *Journal of Chemical and Engineering Data,* vol. 30, pp. 269-273, 1985, doi: 10.1021/je00041a010.

[467]   K. J. Kim, T. R. Way, K. T. Feldman, and A. Razani, "Solubility of Hydrogen in Octane, 1-Octanol, and Squalane," *Journal of Chemical and Engineering Data,* vol. 42, pp. 214-215, 1997, doi: 10.1021/je960268z.

[468]   E. Brunner, "Solubility of Hydrogen in Alcohols," *Bunsengesellschaft fur Physikalische Chemie,* vol. 83, no. 7, pp. 715-721, 1979.

[469]   X. Lu, Z. Wu, and Y. Hou (Y.C. Hou), "Solubilities of N_2, H_2, Ar in 1-Octanol at High Pressure," *Fluid Phase Equilibria,* vol. 92, pp. 139-148, 1994, doi: 10.1016/0378-3812(94)80045-6.

[470]   M. S. Wainwright, T. Ahn, D. L. Trimm, and N. W. Cant, "Solubility of Hydrogen in Alcohols and Esters," *Journal of Chemical and Engineering Data,* vol. 32, pp. 22-24, 1987, doi: 10.1021/je00047a006.

[471]   IUPAC. "IUPAC Solubility Data Series." srdata.nist.gov/solubility (Accessed 12-Oct-2020).

[472]   T. Tsuji, K. Sue, T. Hiaki, and N. Itoh, "Solid-Liquid Equilibrium and Hydrogen Solubility of Trans-Decahydronaphthalene + Naphthalene and Cis-Decahydronaphthalene + Naphthalene for a New Hydrogen Storage Medium in Fuel Cell System," *Fluid Phase Equilibria,* vol. 257, pp. 183-189, 2007, doi: 10.1016/j.fluid.2007.01.029.

[473]   M. Herskowttz, J. Wlsnlak, and L. Skladman, "Hydrogen Solubility in Organic Liquids," *Journal of Chemical and Engineering Data,* vol. 28, pp. 164-166, 1983, doi: 10.1021/je00032a009.

[474]   T. N. Tyvina, V. V. Fokina, and A. A. Polyakov, "Phase and Volume Relationships in the Systems Carbon Monoxide -Cyclohexanone and Hydrogen - Cyclohexanone," *Journal of Applied Chemistry of the USSR,* vol. 58, pp. 393-396, 1985.

[475]   J. Yao, H. M. Sebastian, H. M. Lin, and K. C. Chao, "Gas-Liquid Equilibria in Mixtures of Hydrogen and 1-Methylnaphthalene," *Fluid Phase Equilibria,* vol. 1, no. 4, pp. 293-304, 1977, doi: 10.1016/0378-3812(77)80012-5.

[476]   M. S. Shaharun, H. Mukhtar, and B. K. Dutta, "Solubility of Carbon Monoxide and Hydrogen in Propylene Carbonate and Thermomorphic Multicomponent Hydroformylation Solvent," *Chemical Engineering Science,* vol. 63, pp. 3024-3035, 2008, doi: 10.1016/j.ces.2008.02.035.

[477]   K. Bezanehtak, G. B. Combes, F. Dehghani, N. R. Foster, and N. S. Wales, "Vapor - Liquid Equilibrium for Binary Systems of Carbon Dioxide + Methanol , Hydrogen + Methanol , and Hydrogen + Carbon Dioxide at High Pressures," vol. 60, pp. 161-168, 2002, doi: 10.1021/je010122m.

[478] C. Descamps, C. Coquelet, C. Bouallou, and D. Richon, "Solubility of Hydrogen in Methanol at Temperatures From 248. 41 to 308. 20 K," *Thermochimica Acta,* vol. 430, pp. 1-7, 2005, doi: 10.1016/j.tca.2004.12.001.

[479] J. Vila, P. Ginés, E. Rilo, O. Cabeza, and L. M. Varela, "Great Increase of the Electrical Conductivity of Ionic Liquids in Aqueous Solutions," *Fluid Phase Equilibria,* vol. 247, pp. 32-39, 2006, doi: 10.1016/j.fluid.2006.05.028.

[480] D. Almantariotis, S. Stevanovic, O. Fandiño, A. S. Pensado, A. A. H. Padua, J. Y. Coxam, and M. F. Costa Gomes, "Absorption of Carbon Dioxide, Nitrous Oxide, Ethane and Nitrogen by 1-Alkyl-3-Methylimidazolium ($C_n$mim, n = 2,4,6) Tris(pentafluoroethyl) Trifluorophosphate Ionic Liquids (eFAP)," *Journal of Physical Chemistry B,* vol. 116, pp. 7728-7738, 2012, doi: 10.1021/jp304501p.

[481] C. Black, G. G. Joris, and H. S. Taylor, "The Solubility of Water in Hydrocarbons," *The Journal of Chemical Physics,* vol. 16, no. 5, pp. 537-543, 1948, doi: 10.1063/1.1746932.

[482] I. G. Economou, J. L. Heidman, C. Tsonopoulos, and G. M. Wilson, "Mutual Solubilities of Hydrocarbons and Water: III. 1-Hexene, 1-Octene, C_{10}-C_{12} Hydrocarbons," *AIChE Journal,* vol. 43, pp. 535-546, 1997, doi: 10.1002/aic.690430226.

[483] Q. Wang and K. C. Chao, "Vapor-Liquid and Liquid-Liquid Equilibria and Critical States of Water + N-Decane Mixtures," *Fluid Phase Equilibria,* vol. 59, pp. 207-215, 1990, doi: 10.1016/0378-3812(90)85035-9.

[484] V. V. Filippov, N. P. Markuzin, and V. P. Sazonov, "Liquid-Vapor and Liquid-Liquid-Vapor Equilibrium in the Systems Nitromethane + Water and Water + Hexyl Alcohol," *Journal of Applied Chemistry of the USSR,* vol. 50, pp. 1321-1324, 1977.

[485] Y. Marcus, "Structural Aspects of Water in 1-Octanol," *Journal of Solution Chemistry,* vol. 19, pp. 507-517, 1990, doi: 10.1007/BF00650383.

[486] O. Iulian, L. Hamplea, and I. Sandulescu, "Isothermal Vapor-Liquid-Equilibria of Water Plus N, N-Dimethyl-Formamide Systems," *Revue Roumaine De Chimie,* vol. 40, pp. 7-11, 1995.

[487] E. P. Sokolova and A. G. Morachevskii, "Dynamic Properties of Methyl Ethyl Ketone and Water and Cyclohexanone and Water Systems," *Vestn. Leningr. Univ. Fiz. Khim.,* vol. 22, pp. 98-106, 1967.

[488] S. P. Christensen and M. E. Paulaitis, "Phase Equilibria for Tetralin-Water and 1-Methylnaphthalene-Water Mixtures at Elevated Temperatures and Pressures," *Fluid Phase Equilibria,* vol. 71, pp. 63-83, 1992, doi: 10.1016/0378-3812(92)85005-S.

[489] O. Noll, K. Fischer, and J. Gmehling, "Vapor−Liquid Equilibria and Enthalpies of Mixing for the Binary System Water + N -Methyl-2-Pyrrolidone in the Temperature Range 80−140 °C," *Journal of Chemical and Engineering Data,* vol. 41, pp. 1434-1438, 1996, doi: 10.1021/je960175h.

[490] S. Y. Lam and R. L. Benoit, "Some Thermodynamic Properties of the Dimethylsulfoxide–Water and Propylene Carbonate–Water Systems at 25 °C," *Canadian Journal of Chemistry,* vol. 52, pp. 718-722, 1974, doi: 10.1139/v74-113.

[491] I. Mokbel, H. Kasehgari, E. Rauzy, and J. Jose, "Static Measurements of the Total Vapor Pressure of Water + Methanol Mixtures at Temperatures between 243 and 313 K," *ElData:The International Electronic Journal of Physico-Chemical Data,* vol. 1, pp. 135-138, 1995.

[492] N. Yarym-Agaev and A. A. Koliushko, "Designing the Phase-Diagram of 2-Component System under the Absence of Experimental Data on Equilibrium Data Composition," *Zhurnal Fizicheskoi Khimii,* vol. 64, no. 9, pp. 2349-2353, 1990.

[493] J. Matouš, J. P. Novak, J. Šobr, and J. Pick, "Phase Equilibria in the System Tetrahydrofuran (1)-Water (2)," *Collection of Czechoslovak Chemical Communications,* vol. 37, pp. 2653-2663, 1972.

[494] V. A. Shnitko and V. B. Kogan, "Liquid-Vapor Equilibrium in the Systems Tetrahydrofuran-Water and Tetrahydrofuran-Ethylene Glycol and a Method for Dehydration of Tetrahydrofuran," *J. Appl. Chem. USSR,* vol. 4, pp. 1236-1242, 1968.

[495] K. H. Smith, S. Chen, and N. S. Siefert, "Modular CO_2 Capture Processes for Integration with Modular Scale Gasification Technologies: Literature Review and Gap Analysis for Future R & D," in "NETL Technical Report Series," DOE/NETL, Pittsburgh, PA, 2020.

[496] O. I. Abiodun, A. Jantan, A. E. Omolara, K. V. Dada, N. A. E. Mohamed, and H. Arshad, "State-of-the-Art in Artificial Neural Network Applications: A Survey," *Heliyon,* vol. 4, p. e00938, 2018, doi: 10.1016/j.heliyon.2018.e00938.

[497] D. J. Livingston, *Artificial Neural Networks: Methods and Applications* (Methods in Molecular Biology). Humana Press, 2009.

[498] W. Duch and N. Jankowski, "New Neural Transfer Functions," *Applied Mathematics and Computer Science,* vol. 7, pp. 639-658, 1997.

[499] N. Jankowski and W. Duch, "Transfer Functions: Hidden Possibilities for Better Neural Networks," *9th European Symposium on Artificial Neural Networks,* vol. 7, pp. 81-94, 2001.

[500] W. S. Mcculloch and W. Pitts, "A Logical Calculus of the Ideas Immanent in Nervous Activity," *Bulletin of Mathematical Biology,* vol. 52, no. 1/2, pp. 99-115, 1990.

[501] B. FIllion, "Modeling of Soybean Oil Hydrogenation Process," University of Pittsburgh, 2001.

[502] D. E. Rumelhart, G. E. Hinton, and R. J. Williams, "Learning Representations by Back-Propagating Errors," *Nature,* vol. 323, pp. 533-536, 1986, doi: 10.1038/323533a0.

[503] K. I. Funahashi, "On the Approximate Realization of Continuous Mappings by Neural Networks," *Neural Networks,* vol. 2, pp. 183-192, 1989, doi: 10.1016/0893-6080(89)90003-8.

[504] K. Hornik, M. Stinchcombe, and H. White, "Multilayer Feedforward Networks are Universal Approximators," *Neural Networks,* vol. 2, pp. 359-366, 1989, doi: 10.1016/0893-6080(89)90020-8.

[505] R. Lemoine, B. Fillion, A. Behkish, A. E. Smith, and B. I. Morsi, "Prediction of the Gas-Liquid Volumetric Mass Transfer Coefficients in Surface-Aeration and Gas-Inducing Reactors Using Neural Networks," *Chemical Engineering and Processing: Process Intensification,* vol. 42, pp. 621-643, 2003, doi: 10.1016/S0255-2701(02)00211-8.

[506] A. Behkish, R. Lemoine, L. Sehabiague, R. Oukaci, and B. I. Morsi, "Prediction of the Gas Holdup in Industrial-Scale Bubble Columns and Slurry Bubble Column Reactors Using Back-Propagation Neural Networks," *International Journal of Chemical Reactor Engineering,* vol. 3, 2005, doi: 10.2202/1542-6580.1193.

[507] A. Quesada. "5 Algorithms to Train a Neural Network." https://www.neuraldesigner.com/blog/5_algorithms_to_train_a_neural_network (Accessed 10-May-2021).

[508] H. Yu and B. M. Wiliamowski, "Levenberg-Marquardt Training," in *Industrial Electornics Handbook*, vol. 5, 2nd ed.: CRC Press, 2011.

[509] T. N. Cheema, M. A. Z. Raja, I. Ahmad, S. Naz, H. Ilyas, and M. Shoaib, "Intelligent Computing with Levenberg–Marquardt Artificial Neural Networks for Nonlinear System of COVID-19 Epidemic Model for Future Generation Disease Control," *European Physical Journal Plus,* vol. 135, 2020, doi: 10.1140/epjp/s13360-020-00910-x.

[510] D. M. Hawkins, S. C. Basak, and D. Mills, "Assessing Model Fit by Cross-Validation," *Journal of Chemical Information and Computer Sciences,* vol. 43, pp. 579-586, 2003, doi: 10.1021/ci025626i.

[511] I. T. Nabney, *Netlab: Algorithms for Pattern Recognition* (Advances in Pattern Recognition). London: Springer Science & Business Media, 2002.

[512] T. Boublík, "Hard-Sphere Equation of State," *The Journal of Chemical Physics,* vol. 53, pp. 471-472, 1970, doi: 10.1063/1.1673824.

[513] G. A. Mansoori, N. F. Carnahan, K. E. Starling, and T. W. Leland, "Equilibrium Thermodynamic Properties of the Mixture of Hard Spheres," *The Journal of Chemical Physics,* vol. 54, pp. 1523-1525, 1971, doi: 10.1063/1.1675048.

[514] A. Tihic, G. M. Kontogeorgis, N. Von Solms, and M. L. Michelsen, "A Predictive Group-Contribution Simplified PC-SAFT Equation of State: Application to Polymer Systems," *Industrial and Engineering Chemistry Research,* vol. 47, pp. 5092-5101, 2008, doi: 10.1021/ie0710768.

[515] W. A. Burgess, D. Tapriyal, I. K. Gamwo, Y. Wu, M. A. McHugh, and R. M. Enick, "New Group-Contribution Parameters for the Calculation of PC-SAFT Parameters for Use at Pressures to 276 MPa and Temperatures to 533 K," *Industrial and Engineering Chemistry Research,* vol. 53, pp. 2520-2528, 2014, doi: 10.1021/ie4034973.

[516] W. G. Chapman, K. E. Gubbins, G. Jackson, and M. Radosz, "New Reference Equation of State for Associating Liquids," *Industrial and Engineering Chemistry Research,* vol. 29, pp. 1709-1721, 1990.